

PHASE RELATIONS, ELEMENT DISTRIBUTIONS, AND GEOCHEMISTRY OF
METAMORPHIC ROCKS FROM THE EASTERN ARUNTA BLOCK, N.T.

Stephen K. Dobos
B.Sc.(Hons) Sydney

Thesis submitted for the degree of.
Doctor of Philosophy

School of Earth Sciences,
Macquarie University,
North Ryde, N.S.W.

June, 1978

To Donna

TABLE OF CONTENTS

ABSTRACT

v

CHAPTER 1: GENERAL INTRODUCTION

1.1 Aims of Investigation	1
1.2 Location	2
1.3 Previous Investigations	4
1.4 Outline of Thesis	5
1.5 Conventions Used in this Thesis	6

CHAPTER 2: GEOLOGICAL SETTING AND GEOCHRONOLOGY

2.1 Brief Review of the Geology of the Arunta Block	8
2.2 Geology of the Jervois Range Area	12
2.3 Granitic Rocks in the Jervois Range Area	14
2.4 Geochronology of the Jervois Range Area	16
2.5 Geology of the Valley Bore Area	21
2.6 Geochronology of the Valley Bore Area	23

CHAPTER 3: AMPHIBOLITES IN THE JERVOIS RANGE AREA

3.1 Petrography	24
3.2 Phase Relations	26
3.3 Composition and Element Distribution between Hornblende and Chlorite	31
3.4 Actinolite Pseudomorphs in Samples of Metagabbro	39
3.5 Parent-Rock Source of the Jervois Range Amphibolites	41

CHAPTER 4: STAUROLITE-BEARING ROCKS IN THE JERVOIS RANGE AREA

4.1 Petrography	44
4.2 Phase Relations	47
4.3 Composition and Element Distribution between Minerals in the Staurolite-Bearing Rocks	60

CHAPTER 5: PELITIC SCHISTS IN THE JERVOIS RANGE AREA

5.1	Petrography	85
5.2	Phase Relations	88
5.3	Mineral Compositions and Distribution of Elements between Minerals in the Metapelitic Schists	91
5.4	AFM Topologies and Reactions	112
5.5	Bulk-Rock Geochemistry	125

CHAPTER 6: CHLORITE-QUARTZ⁺GARNET SCHISTS

6.1a	Petrography of the Jervois Range Schists	131
6.1b	Comparison of the Jervois Range Schists with a Chlorite-Garnet Schist from Broken Hill, N.S.W.	135
6.2	Phase Relations	136
6.3	Composition of, and Element Distribution between, Chlorite and Garnet	139
6.4	Mineral Reactions in Chlorite-Quartz ⁺ Garnet Schists	147
6.5	Geochemistry	159
6.6	Origin of the Chlorite-Quartz ⁺ Garnet ⁺ Magnetite Schists	164

CHAPTER 7: MAGNESIAN CORDIERITE-RICH ENCLAVES IN PHLOGOPITE
SCHIST FROM THE VALLEY BORE AREA, EASTERN HARTS
RANGE, N.T.

7.1	Field Occurrence and Petrography	179
7.2	Phase Relations	182
7.3	Temperature-Pressure Conditions of Formation	184
7.4	Mineralogy of the Cordierite	189
7.5	The Distribution of Mg and Fe between Coexisting Minerals in the Cordierite-Rich Enclaves	192

CHAPTER 8: GARNET, GEDRITE AND CORDIERITE-BEARING GNEISS IN
THE VALLEY BORE AREA (IRINDINA CK.)

8.1	Field Occurrence	197
8.2	Phase Relations	198

8.3	Temperature-Pressure Conditions of Metamorphism of the Garnet-Gneiss	203
8.4	The Distribution of Elements between Phases in the Garnet Gneiss	205

CHAPTER 9: CORDIERITE-GEDRITE STABILITY UNDER HIGH-PRESSURE
HYDROUS CONDITIONS--AN EVALUATION

9.1	Introduction	215
9.2	Aluminium in Gedrite	216
9.3	Gedrite Site Occupancy Relations	220
9.4	Gedrite-Cordierite Relations	222
9.5	Water in Cordierite	224
9.6	Cordierite-Gedrite-Kyanite-Quartz Divariant Stability Field	225
9.7	Discussion	227
9.8	Conclusions	232

CHAPTER 10: ULTRAMAFIC AND CALC-SILICATE GRANULITES AT MT
MARY IN THE VALLEY BORE AREA

10.1	Introduction	234
10.2	Phase Assemblages in the Mt Mary Granulites	235
10.3	Mineral Compositions in the Ultramafic Granulite	235
10.4	Mineral Compositions in the Calc-Silicate Granulite	238
10.5	Temperature-Pressure Conditions of Metamorphism at Mt Mary	240

CHAPTER 11: SUMMARY AND CONCLUSIONS

11.1	Brief Summary of Major Conclusions Drawn from Chapters 2 to 6, Jervois Range Area	243
11.2	Brief Summary of Major Conclusions Drawn from Chapters 7 to 10, Valley Bore Area	246
11.3	Comparison of Metamorphic Pressure-Temperature Conditions between the Jervois Range and Valley Bore Areas	247

BIBLIOGRAPHY

250

APPENDIX

Facies nomenclature and analytical methods used in this
thesis; bulk-rock analyses and brief petrographic
descriptions of rocks discussed in the text

272

Abstract

The Jervois Range area, northeastern Arunta Block, N.T., underwent a single, prograde, low-pressure regional metamorphism, accompanied by granite emplacement, dated at 1850 m.y. Subsequent emplacement of alaskitic and large pegmatitic bodies, dated at 1700 m.y., resulted in the retrograde hydration of cordierite.

Metamorphic grades in the Jervois Range area range from the uppermost greenschist facies, characterized by the assemblage chlorite + andalusite + muscovite, to the middle of the amphibolite facies, characterized by the appearance of sillimanite. Characteristic metapelitic assemblages in the lower amphibolite facies include cordierite + chlorite + biotite, cordierite + andalusite + biotite, staurolite + almandine + andalusite, and almandine + chlorite + quartz.

Using the compositions of naturally-occurring minerals, realistic metamorphic reactions have been inferred for the prograde breakdown of muscovite + chlorite, and the retrograde hydration of cordierite + biotite. Naturally-occurring reactions and assemblages may differ markedly from those proposed on theoretical grounds.

Chlorite-quartz-garnet and other naturally-occurring assemblages in the system $\text{SiO}_2\text{-Al}_2\text{O}_3\text{-FeO-MgO-H}_2\text{O}$ may be derived by the isochemical metamorphism of parent-rocks of appropriate bulk-composition. These parent-rocks may have been formed originally either by the halmyrolytic alteration of volcanoclastic sediments, or by the deposition of sediments rich in authigenic chamosite. Because of their relatively simple bulk-composition, mineral compositions in chlorite-quartz-garnet schists may be used to infer realistic, multi-variant garnet-forming reactions.

P-T conditions of prograde metamorphism in the Jervois Range area appear to have been 2-3 kb at 480-580°C. These values are consistent with metamorphic assemblages found in the northeastern Arunta Block to the west of the Jervois Range area.

Metamorphic rocks in the Valley Bore area, eastern Harts Range, N.T., belong to the upper amphibolite and lower granulite facies, temperatures of metamorphism ranging from 620 to 820°C and pressures varying from 6 to 10 kb. These higher temperatures and relatively higher pressures are consistent with those inferred for rocks in the Strangways Range area, 100 km to the west of the Valley Bore area.

These contrasting metamorphic conditions in the two areas are unlikely to have been formed under a single geothermal gradient, and the two areas may be parts of two distinct metamorphic "belts", each with its own geothermal gradient.

Naturally-occurring assemblages indicate that the correct calibration of the cordierite-garnet geothermometer-beobarometer is of the form proposed by Hensen and Green (1971, 1972, 1973). Calculations and natural parageneses indicate that there is no convincing evidence to support a modification of the cordierite-gedrite kyanite-quartz divariant stability field experimentally derived by Green and Vernon (1972).

I hereby state that, except where otherwise acknowledged, the work embodied in this thesis is my own, and that no part of it has been previously submitted for academic qualification at any university or institution.

A handwritten signature in cursive script, appearing to read "S. K. Dobos", written in black ink.

Stephen K. Dobos

Acknowledgements

I wish to thank Petrocarb Exploration N.L., Central Pacific Minerals N.L. and their staff, especially Mr. George Teague, for financial and logistic support in the field. To Lindsay Johannsen, without whose help I would not have been able to visit the Valley Bore area, I extend my thanks.

I have learnt much from discussions with Drs L. P. Black, T. H. Green, B. J. Hensen, S. E. Shaw, I. M. Threadgold, and S. Y. Wass. In particular, the often heated arguments with Dr. R. H. Flood on the significance of instrumental analyses will never be forgotten. For all their help, I express my appreciation.

Thanks go to Dr. I. R. Plimer and to my colleagues G. J. Corbett, M. J. Gole and G. S. Teale for comparative samples used in this thesis. To Mr. N. G. Ware, who taught me how to use the T.P.D. electron microprobe at A.N.U., to Mr. D. Oliver, who lettered most of the diagrams in this thesis, and to others who in their own way contributed to this work, I express my gratitude.

I am indebted to Professor P. B. Hostettler, who allowed me time to complete this thesis. I am greatly indebted to the typist, Mrs. A. Coates, for cheerfully clawing her way through the manuscript, and for attending to items of grammar and punctuation which escaped my attention.

I am grateful to my wife Donna for her help in the preparation of this thesis, for her patience, and for sharing the first years of our married life with metamorphic rocks.

Finally, I am extremely grateful to my supervisor, Associate Professor R. H. Vernon, for suggesting the area studied in this work, for arranging financial support for field work, for continued discussions and guidance, and for the painstaking way in which he helped improve the manuscript. I am happy to express my gratitude in saying that, without his patience and encouragement, this thesis would not have been written.

CHAPTER 1: GENERAL INTRODUCTION

1.1 Aims of Investigation

The major aim of this investigation is to examine in some detail the phase-relations, the distribution of elements between phases, the elemental abundances, and the origins of selected mafic and pelitic rocks in the eastern Arunta Block with a view to ascertaining the temperatures, pressures and compositional parameters accompanying their formation. This is done in the light of much new experimental, thermodynamic and mineral-chemical data, and attempts are made to evaluate and reconcile experimental, theoretical and observed data, where these differ.

Special attention is paid to naturally occurring chlorite-garnet⁺quartz⁺staurolite⁺andalusite assemblages, as these fall almost precisely in the simple system $\text{FeO-MgO-Al}_2\text{O}_3\text{-SiO}_2\text{-H}_2\text{O}$. This greatly simplifies the phase-relations, and, with the help of detailed chemical analyses and thermodynamic data, an attempt is made to formulate a set of realistic sliding mineral equilibria. Regionally metamorphosed rocks in this particular compositional system pose a problem as to the nature of their parental rock-type. In the absence of unambiguous evidence of large-scale metasomatism, an attempt is made to present pre-metamorphic, sedimentary rocks of appropriate bulk chemical composition as probably parental rock-types.

To date, the easternmost exposures of the Arunta Block have

received only cursory examination. A secondary aim of this investigation is to interpret and integrate the petrology of the metamorphic rocks in this area with the geology of the better-known central and western Arunta Block.

More specifically, certain regions within the Arunta Block contain aluminous schists and gneisses, in which the Al_2SiO_5 polymorphs are andalusite and sillimanite, whereas in others they are kyanite and sillimanite. Part of the above aims is (i) to determine whether, in the areas under investigation, these assemblages represent slight perturbations of the geothermal gradient about the Al_2SiO_5 triple point in P-T space, or whether they were produced by significantly different geothermal gradients; (ii) to determine the relationship of the metamorphic events in the areas studied to those inferred for other parts of the Arunta Block.

1.2 Location

The Arunta Block extends as a tectonic unit for some 1000 km across southern Northern Territory, Australia, between latitudes 20° and 24°S . It is bounded to the west and northwest by the Gibson and Great Sandy Deserts, and to the east and southeast by the Simpson Desert. (See fig. 1.) The areas studied represent the best exposed eastern parts of the Arunta Block and are:

- (i) the Jervois Range area, 266 km northeast of Alice Springs (lat. $22^\circ 39'\text{S}$, long. $136^\circ 16'\text{E}$; Huckitta sheet: Australia 1:250,000 Geological Series Map No. SF 55-11

The Arunta Block N.T.

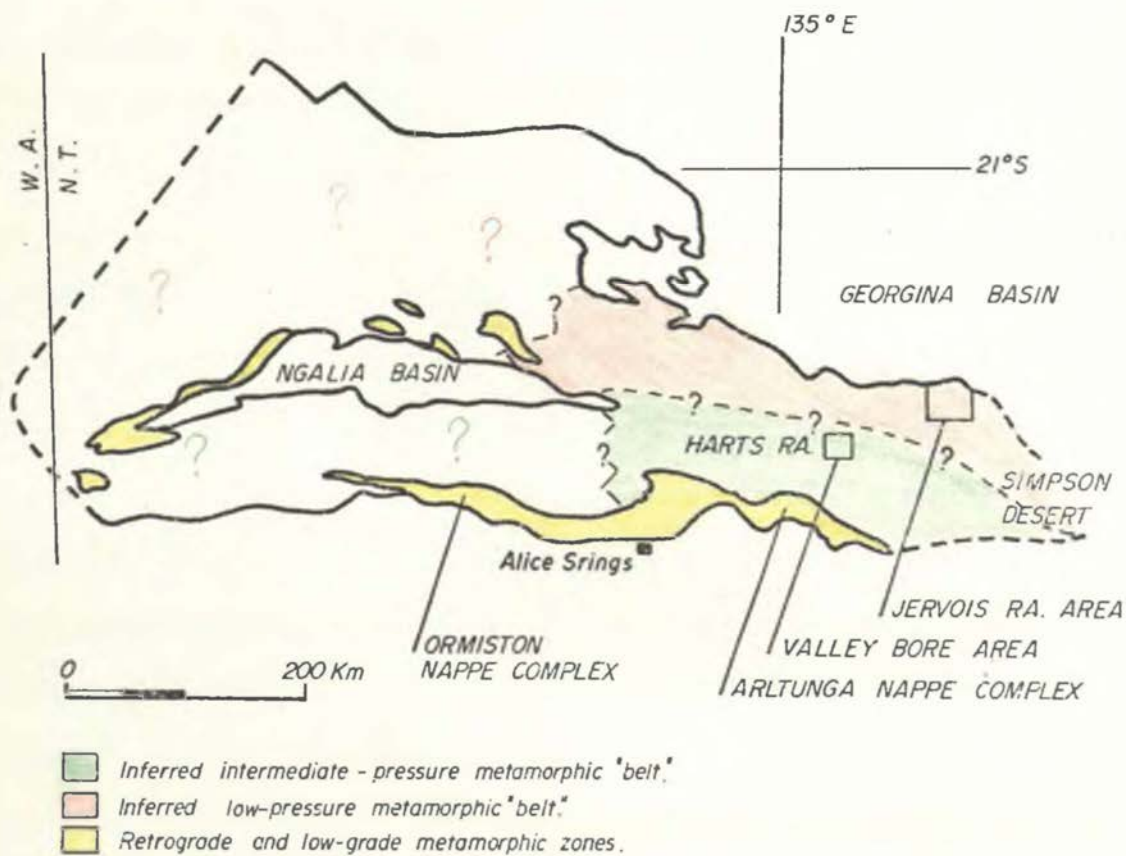
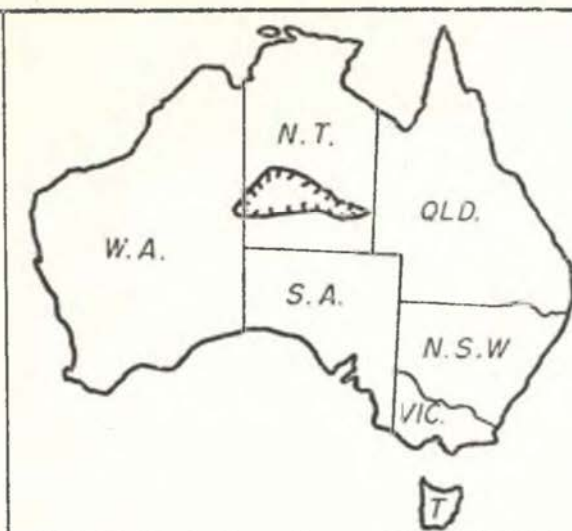


FIGURE 1: Locality map of the Arunta Block, N.T. showing location of the Jervois Range and Valley Bore areas. The inferred metamorphic "belts" are based on Ferman and Shaw (1973).

Northern Territory) and

(ii) the Valley Bore area (lat. $23^{\circ}3'S$, long. $135^{\circ}9'E$; Illogwa Creek sheet: Australia 1:250,000 Geological Series Map No. SF 53-15 Northern Territory) which lies on the eastern flank of the Harts Range, about 100 km WSW of the Jervois Range area.

Because of its remote location, the Valley Bore area posed logistical problems, resulting in much less detailed sampling than in the Jervois Range area, where a small mining camp was situated.

1.3 Previous Investigations

The earliest geological reports on the Proterozoic rocks of the Jervois Range area were rather superficial unpublished reports dealing with the ores and economics of the sulphide deposits at the Jervois Mine. Other reconnaissance surveys and reports prior to 1963, together with older radiometric dates, are adequately summarized in the handbook accompanying the Huckitta Geological Map (Smith, 1963). Robertson (1959) mapped the surface workings and adjacent rocks at the Jervois Mine, and Morgan (1959) prepared a descriptive petrographic report based on samples collected by Robertson (1959). Catley (1965) reported on exploratory drilling and geophysical work carried out around the mine area. He concluded that the sulphides were syngenetic, metamorphosed along with the surrounding rocks, and modified by metasomatism during subsequent granite emplacement. Many recent exploration reports exist, but these are all adequately covered by Shaw and Stewart, Warren et al.

and Watson in Knight (1975).

The Valley Bore area was first mapped by Joklik (1955) as part of a thesis dealing with mica mineralization in the Harts Range area. Subsequent mapping and reconnaissance work are described in the notes accompanying the Illogwa Creek Geological Map (Shaw and Milligan, 1969). A large-scale regional metamorphic, structural and Bouguer anomaly map of central Australia has been compiled by Forman and Shaw (1973), and the notes to this map contain much useful information regarding the broader tectonic aspects of the Arunta Block. These notes also contain a summary of major metamorphic assemblages in a series of ACF and AFM diagrams, and the bibliography covers the majority of geological work carried out on tectonics and regional structures in central Australia prior to 1973.

Professor A. F. Wilson and co-workers of the University of Queensland are engaged in an ongoing project of metamorphic and geochemical studies in the Strangways Range area, 100 km west of the Harts Range. The Bureau of Mineral Resources, Geology and Geophysics, Canberra, is also engaged in a mapping, tectonic and geochronologic project covering various regions of the Arunta Block. Although various published and unpublished papers have appeared as a result of these projects, none have dealt specifically with the petrology or radiometric dating of the two areas under investigation in this thesis.

1.4 Outline of Thesis

To provide the necessary geological setting for this

investigation, the following chapter begins with an outline of the geology and geochronology of the Arunta Block as a whole, and then of the Jervois Range and Valley Bore areas in particular.

Subsequent chapters deal in turn with specific rock-types selected from the Jervois Range and Valley Bore areas. Each of these chapters discusses the petrography, mineral parageneses, and distribution of elements between phases in order to give a close estimate of metamorphic conditions producing them. Some of these chapters end with an examination of element abundances within the selected rock-types, to infer possible parent-rock compositions.

Several chapters evaluate and compare recent experimental and theoretical work with naturally occurring metamorphic assemblages; these follow chapters in which such experimental and theoretical data are utilized.

The concluding chapter attempts to synthesize metamorphic conditions in the eastern Arunta Block in early Proterozoic times. This synthesis is integrated with the presently-known geology of the Arunta Block, and the sequence of major events is summarized.

Mineral assemblages, selected petrographic descriptions, and major and trace element analyses or rocks referred to in the text are tabulated in the appendix at the end of the thesis.

1.5 Conventions Used in this Thesis

- (i) Igneous rock names are used in the sense of Streckeisen et al. (1973).

(ii) $\underline{Mg} = (\text{atomic } Mg^{2+} / (Mg^{2+} + Fe^{2+})) \times 100$

(iii) The distribution coefficient K_D is used in the following

sense: $K_{D \text{ A-B}}^{Y-Z} = (X_A^Y / X_B^Y) / (X_A^Z / X_B^Z)$ which is equivalent to

$(X_A^Y / (1 - X_A^Y)) / (X_A^Z / (1 - X_A^Z))$, where X_A^Y is the mole fraction of

component A in phase (mineral) Y; e.g. $K_{D \text{ Mg-Fe}}^{\text{cord-gt}} =$

$(X_{Mg^{2+}}^{\text{cord}} / X_{Fe^{2+}}^{\text{cord}}) / (X_{Mg^{2+}}^{\text{gt}} / X_{Fe^{2+}}^{\text{gt}})$.

(iv) "FeO" in electron microprobe analyses represents total iron expressed as FeO.

(v) "r" and "R" are the correlation coefficient and the coefficient of multiple correlation respectively. In general, as the absolute value of these coefficients increases (to a limit of 1.00), changes in the values of the dependent variable are increasingly "accounted for" by changes in the independent variable(s). At the same time, estimated values of the dependent variable become more reliable.

(vi) The oxidation ratio (O.R.) is defined as:

$\text{molecular } 2Fe_2O_3 \times 100 / (2Fe_2O_3 + FeO)$.

(vii) Sample numbers are the last three digits of catalogue numbers in the reference collection of the School of Earth Sciences, Macquarie University (#6801 to 6999).

CHAPTER 2: GEOLOGICAL SETTING AND GEOCHRONOLOGY

2.1 Brief Review of the Geology of the Arunta Block

The Arunta Block consists mainly of an extensive complex of early-Proterozoic (possibly older) sedimentary and igneous rocks, which have been subjected to complex deformation and metamorphism (Shaw and Stewart, in Knight, 1975). These events, accompanied by frequent intrusions of granitic and mafic rocks and by migmatization, differ in number, age and intensity from place to place within the Arunta Block. Therefore, the geochronological history of the Arunta Block is complex, as younger tectonic and metamorphic events commonly partially or totally obscure the radiometric ages of older events. As a consequence, much of the early K/Ar dating in the Arunta Block is suspect because of inadequate geological control. Rb/Sr ages must also be interpreted with caution.

Current geochronological research in the Arunta Block, essentially by Black (1974, 1975), has shown that the earliest-known widespread event was a metamorphic episode dated at about 1800 m.y. Most of the granulite facies rocks in the Arunta Block have been attributed to this event. A second widespread metamorphic episode is dated at about 1700 m.y. and is responsible for retrograde metamorphism (and commonly radiometric resetting) of many of the previously formed granulite facies rocks. This second metamorphism produced mainly amphibolite facies rocks, but locally attained the

granulite facies. Migmatization and the emplacement of mafic rocks have been dated at between 1200 and 1100 m.y. Granite emplacement is more frequent, ages ranging from 1800 to 1100 m.y. Finally, the Alice Springs Orogeny, dated at about 350 m.y. (Forman et al., 1967; Stewart, 1971), caused widespread retrogression of high-grade rocks along two east-west belts within the Arunta Block.

As an example of the complexity of the geochronology, some workers have dated seven metamorphic events in the Strangways Range area (A. F. Wilson, pers. comm. 1976). Some of these events were retrograde, and two produced granulite facies grades. As a result of this complexity, large-scale correlation of events is difficult and chronostratigraphic correlation at best tentative. The most realistic attempts so far are summarized by Shaw and Stewart (in Knight, 1975).

A compilation of metamorphic mineral parageneses by Forman (Forman and Shaw, 1973) shows that four main regional metamorphic belts extend east-west across the Arunta Block. "Belt" is used here in a general, descriptive sense. The belts are:

(i) A low-pressure metamorphic belt, exposed in the east in the Jervois Range area, extends west almost to the Western Australian border. This belt contains rocks varying in metamorphic grade from the lower-greenschist to the lower-granulite facies. Depending on grade, metapelitic rocks contain andalusite or sillimanite. Although several narrow kyanite-bearing zones are exposed in part of this belt (e.g.

southeast of Reynolds Range), they represent localized areas of retrogression (R. G. Warren, pers. comm. 1976).

(ii) An inferred higher-pressure metamorphic belt is exposed in the Valley Bore area and extends due west to the Strangways Range area. The rocks in this belt vary in grade from greenschist to granulite facies, and metapelitic rocks contain kyanite or sillimanite.

(iii) A narrow, well-defined, low-grade (retrograde) metamorphic belt extends along the southern edge of the Arunta Block, corresponding with the Arltunga Nappe Complex in the east and the Ormiston Nappe Complex in the west.

(iv) A less well-defined, low-grade (retrograde) metamorphic belt extends along the northern edge of the Ngalia Basin.

The metamorphism of both of these low-grade belts has been attributed to the mid-Carboniferous Alice Springs Orogeny (Forman and Shaw, 1973).

Work by Vernon (1972), Green and Vernon (1974) and Woodford and Wilson (1976) has shown that kyanite- and sillimanite-bearing assemblages in the Strangways Range area were formed as a result of high-pressure, granulite facies metamorphism. Conditions are estimated at 800°C and 9-10 kb. Based on the relative disposition of the Al_2SiO_5 polymorphs in P,T space (Holdaway, 1971; Anderson et al., 1977), pressure conditions for these assemblages must lie at least several kilobars above those experienced by rocks in the northern low-pressure belt. This raises several questions:

(i) Are the kyanite-sillimanite assemblages in the Valley Bore area representative of similar high pressures, or do they represent a P-T gradient, with minor local variations, passing much closer to the Al_2SiO_5 triple point than that of the Strangways Range area?

(ii) Are the high-grade, sillimanite-bearing assemblages west of the Strangways Range also representative of high-pressure metamorphic conditions?

(iii) If two belts representing differing metamorphic pressures exist, what are the metamorphic, structural, and time relations between them?

As the Jervois Range and Valley Bore areas are the best eastern exposures of the andalusite-sillimanite and kyanite-sillimanite metamorphic belts, respectively, this investigation aims (in part) to answer the first of the above questions.

2.2 Geology of the Jervois Range Area

The metamorphic rocks in the Jervois Range area are the best-preserved, easternmost exposures of the Arunta Block. They are overlain by moderately-dipping sedimentary rocks of the upper Proterozoic - lower Cambrian Mopunga Group, which forms the Jervois Range, as shown on the map accompanying the thesis.

The metamorphic rocks in this area are broadly divisible into five compositional types:

- (i) pelitic, ferro-pelitic and magnesio-ferro-pelitic schists and gneisses;
- (ii) orthoamphibolites and rocks of related mafic composition;
- (iii) silicic metavolcanic rocks and felspathic schists and gneisses;
- (iv) quartzites and magnetite quartzites;
- (v) carbonate and calc-silicate rocks.

This sequence has been tentatively correlated with the Lander Rock and Mount Stafford Beds in the Reynolds Range area by R. G. Warren (pers. comm. 1973). They may also correlate with the "upper sequence" exposed in the Harts Range area (Shaw and Stewart, in Knight, 1975).

In outcrop, the carbonate and calc-silicate rocks occur both as continuous, thin beds and as discontinuous, thinner lenses within the predominating metapelitic schists and magnetite quartzites. West of Jervois Range, the orthoamphibolites and metavolcanic rocks

occur as sills or lava flows within the schists and quartzites. East of the Jervois Range, the metamorphosed mafic rocks occur as stocks with sill-like offshoots, intrusive into the metasedimentary sequence.

The area has undergone three phases of deformation, namely:

- (i) extensive, tight, isoclinal folding (F_1), producing a well-defined foliation (S_1) which coincides with, or lies at small angles to bedding or lithological layering (S_0);
- (ii) a second deformation, resulting in complex, steeply-plunging to vertical, asymmetrical, similar and isoclinal folds. As a consequence, S_1 poles define a peripheral girdle to F_2 fold-axes. In places, F_2 folding has resulted in the formation of a new schistosity (S_2) axial-plane to folds in S_1 foliation.
- (iii) a third minor deformation, probably associated with the emplacement of granitic rocks, has superimposed crenulations on S_1 and S_2 .

2.3 Granitic Rocks in the Jervois Range Area

Three granitic outcrops (each $< 5 \text{ km}^2$) occur east of the Jervois Range and two more (equally small) occur to the west. These small exposures are sufficiently unaltered to enable blasted samples to be used for thin-sectioning, chemical analysis and radiometric dating. Large areas of granitic outcrop are shown on the Huckitta geological map as occurring some 15 km east of the Jervois Range. However, detailed field work has shown that some of these are non-existent, and the others are too intensely weathered for petrographic and geochemical analysis.

The small granitic bodies are intrusive into the metamorphic sequence. In the eastern exposures, they have caused slight contact metamorphism of the metagabbroic rocks. Contacts with metapelitic rocks are not exposed at the eastern localities. The western granitic bodies occur as isolated outcrops on a small plain. The metamorphic rocks in this region belong to the lower-amphibolite facies, and metapelitic schists contain andalusite. Contacts between granitic and lower-amphibolite facies rocks are not exposed; however, blocks of sillimanite-bearing gneiss occur within and adjacent to these granitic bodies. The gneissic blocks are up to 20 x 40 m in outcrop, and are commonly cut by quartz-felspar and microgranitic veins. The mode of occurrence and the higher metamorphic grade of the gneissic rocks suggest that they were brought up to the present level of exposure by the diapiric emplacement of the granitic bodies.

Petrographic and chemical data (presented in the appendix) strongly suggest that these granitic rocks are of the I-type, as defined by Chappell and White (1974). That is, they were derived by partial melting of a predominantly igneous source with little, if any, previous crustal history. An I-type origin is also favoured by the absence of cordierite, garnet, sillimanite and kyanite from the granitic rocks. In addition, these granites are associated with small deposits of copper, tungsten and molybdenum minerals, similar to those associated with I-type granites in eastern Australia (Chappell and White, 1974; White and Chappell, 1976).

2.4 Geochronology of the Jervois Range Area

Geochronological work on the Jervois Range granitic and metapelitic rocks was done in collaboration with Dr. L. P. Black of the Bureau of Mineral Resources, Geology and Geophysics. The results presented in table 1 are the latest geochronological data from the Jervois Range area and are as yet unpublished.

Taken individually, the four granitic rocks, 801-804, show a limited scatter of points along the isochrons. This is especially restricted in sample 803, giving rise to large errors. Combining the chemically similar pair (801 and 802) and combining the spatially related pair (803 and 804), the errors are reduced, and a consistent total-rock age of 1850 ± 15 m.y. is obtained. As expected, this age is much older than the 1400 m.y. age for the Jervois Granite determined by the K/Ar method (Hurley et al., 1961), but agrees with the 1840 m.y. age determined by the Rb/Sr method for the same rock by Wilson et al. (1960). Since the granites intrude the metamorphic rocks, 1850 ± 15 m.y. must represent the minimum age of the metamorphism in the Jervois Range area. This age agrees well with that of the Arunta Orogeny (Forman et al., 1967), which gave rise to granulite facies metamorphism in the Harts and Strangways Ranges, and has been dated at 1860 m.y. (Woodford and Wilson, 1976).

The second set of consistent total-rock ages, at about 1700 m.y., was obtained from an alaskite stock (805), two large but separate pegmatites (806 and 807), and a quartz-muscovite-biotite

SAMPLE	DESCRIPTION	TOTAL ROCK AGE IN MILLION YRS.	$\frac{87\text{Sr}}{86\text{Sr}}$ INITIAL RATIO	MODEL FIT	MINERAL AGE	COMMENTS
801	"Jervois Granite" biotite granodiorite	1850 \pm 80	0.698 \pm 0.006	2	1580 biotite	minor feldspar alteration and recrystallization of minute muscovite
801 + 802	"Jervois Granite" + "Jinka Granite"	1830 \pm 30	0.6935 \pm 0.002	4		802 similar to 801; occurs 20 km west of Jervois Range
803	slightly foliated biotite granodiorite	1480 \pm 530	0.708 \pm 0.013	2		slight feldspar alteration; very limited spread of data points
804	lineated hornblende-biotite granite	1680 \pm 250	0.715 \pm 0.022	1	1510 \pm 23 feldspar	slight feldspar alteration; very limited spread of data points
803 + 804		1870 \pm 40	0.699 \pm 0.002	3		two outcrops are several kilometers apart
805	alaskite	1590 \pm 140		1	1490 \pm 10 feldspar	feldspars relatively unaltered; muscovite appears primary
806	tourmaline pegmatite "Samarkand" prospect	1680 \pm 60		2	1708 muscovite	feldspar unaltered
807	tourmaline pegmatite "Jericho" prospect	1680 \pm 30	0.714 \pm 0.015	2	1695 muscovite	feldspar unaltered
808	biotite micro-granite dyke				1700 musco. 1535 biot.	insufficient data point spread for total rock age
809	quartz - muscovite - biotite schist	1660 \pm 50	0.711 \pm 0.011	1		schist occurs adjacent to #807 - "Jericho" pegmatite

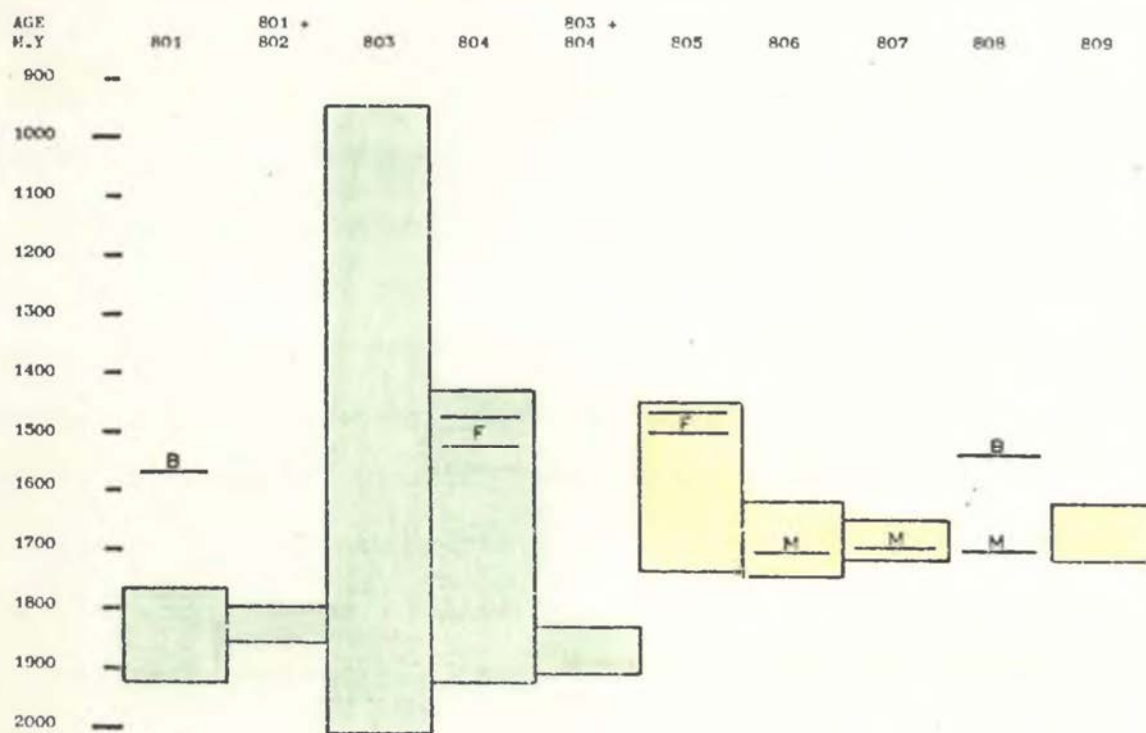


TABLE 1: Rb/Sr Radiometric Age Determinations on Rocks from the Jervois Range Area, N.T.

schist adjacent to pegmatite 807. This age is in agreement with muscovite ages of samples 806, 807 and 808. Although the second widespread metamorphic event in the Arunta Block is also dated at about 1700 m.y., there is no evidence for a second prograde metamorphism in the Jervois Range area. Instead, in the area under study, this age is taken to represent a thermal event associated with the emplacement of alaskite and large pegmatite bodies.

At distances of up to two kilometres from the alaskite and pegmatite intrusions, the metamorphic ages of micaceous schists have been obscured, whereas adjacent to these bodies the radiometric ages have been completely reset (e.g. sample 809). In addition, these intrusions may explain the local retrograde alteration of cordierite in pelitic schists, and the apparent recrystallization, to fine muscovite aggregates, of the alteration products of feldspars in granitic and metamorphosed mafic igneous rocks.

The younger feldspar and biotite ages (1480 to 1580 m.y.) may represent a second and much weaker thermal event that reset the ages of these minerals only. However, it is more likely that these younger ages represent the time difference between crystallization and the attainment of blocking temperatures (that is, the temperature below which a mineral can no longer exchange Rb and Sr with its surroundings). The normal sequence of Rb/Sr ages measured in rocks from orogenic belts is total-rock age > K-feldspar age > muscovite age > biotite age. However, inversions in this order are common and depend partly on grain size, in that coarse-grained

minerals tend to have higher blocking temperatures than do fine-grained ones. As an example, the difference in time between crystallization and attainment of blocking temperatures of fine-grained micas in rocks from the Grenville orogenic belt in Canada is approximately 150 m.y. (Moorbath in Gass et al., 1972).

The four granitic rocks taken in pairs (801 and 802; 803 and 804) have sufficiently low $^{87}\text{Sr}/^{86}\text{Sr}$ initial ratios to be consistent with an I-type origin. However, this fact alone is not sufficient proof of such an origin, as recent work has shown that S- and I-type bodies may have overlapping initial $^{87}\text{Sr}/^{86}\text{Sr}$ ratios (Flood and Shaw, 1977).

The sequence of events in the Jervois Range area may be summarized as follows:

- (i) deposition of sediments; emplacement of mafic and silicic sills and flows;
- (ii) metamorphism and deformation of the sedimentary/igneous pile;
- (iii) 1850 m.y. emplacement of granitic bodies, probably at the end of the metamorphism; minor deformation; age corresponds with the end of the Arunta Orogeny, which is the first widespread metamorphic and tectonic event in the Arunta Block;
- (iv) 1700 m.y. thermal event, associated with the intrusion of alaskite and large pegmatite bodies; local partial to complete resetting of previous metamorphic ages in mica schists; local retrograde alteration of cordierite in metapelitic rocks; recrystallization of feldspar alteration products to fine muscovite aggregates; age corresponds to the second widespread metamorphic event in the Arunta Block;
- (v) 1580-1480 m.y. attainment of blocking temperatures in biotite and K-feldspar, or a second, much weaker, thermal event;

(vi)

the Jervois Range area has escaped the radiometric masking effects of all subsequent tectonic and metamorphic events observed elsewhere in the Arunta Block, including the Alice Springs Orogeny.

2.5 Geology of the Valley Bore Area

The Valley Bore area, on the eastern flank of the Harts Range, is the northern part of a large structural dome some 30 km across. This structure was first named the Entia Dome by Joklik (1955), but is currently shown on geological maps as the Huckitta Anticline. The apex of this large structure (also its geographic centre) is referred to as the Inkamulla Dome. A smaller, parasitic dome, entirely within the Huckitta Anticline, occurs some 8 km southeast of the Inkamulla Dome, and is known as the Huckitta Dome. Granodiorite stocks (thought to be diapiric; Joklik, 1955) are exposed at the centres of the Inkamulla and Huckitta Domes, and are named accordingly.

An east-west traverse across the Valley Bore area crosses the Brady, Irindina, Bruna and Entia Gneisses on both limbs of the dome, and also the Riddock Amphibolite to the west. With the exception of the Cadney Gneiss, which is not exposed in the Huckitta Anticline, the Valley Bore area contains all the major metamorphic units exposed in the Harts Range area. Brief descriptions of these formations, based on the work of Joklik (1955) are as follows:

Brady Gneiss: quartz-plagioclase-biotite-muscovite-almandine gneiss, locally sillimanite-bearing; in outcrop the unit is prominently differentiated into mica-rich and mica-poor layers; stratigraphically and structurally, this is the uppermost unit in the Valley Bore area.

Irindina Gneiss: quartz-plagioclase-biotite-almandine gneiss, locally sillimanite- and/or muscovite-bearing; the large percentage of biotite in this unit gives rise to well-defined schistosity.

Bruna Gneiss: quartz-plagioclase-microcline-biotite gneiss, with porphyroblasts of microperthitic microcline or bluish-grey plagioclase; locally smaller amphibole and almandine porphyroblasts may also be present.

Entia Gneiss: quartz-microcline-plagioclase gneiss with minor biotite and muscovite; locally may contain sillimanite and garnet; this unit also contains enclaves of quartz-muscovite-biotite-kyanite schist, in which the kyanite may be partly or wholly replaced by fine-grained, muscovite-rich aggregates; this is the lowermost stratigraphic unit in the Valley Bore area.

The quartzo-felspathic nature of these gneissic rocks suggests that they were largely derived from igneous rocks of rhyolitic to dacitic compositions (or their volcanoclastic equivalents). Representative analyses of these gneisses, listed in Joklik (1955), show marked similarities to the average analyses of rhyolitic and rhyodacitic rocks listed by Nockolds (1954). In particular, the Entia Gneiss is chemically almost identical to the "average calc-alkali rhyolite", and the Brunu Gneiss strongly resembles the "average rhyodacite". Application of the major-element discriminant function of Shaw (1972) to these analyses confirms the igneous parentage of the Entia and Brunu Gneisses.

The four units described all show minor compositional and textural variations across and along strike, though they remain predominantly quartzo-felspathic. In addition, all these gneisses contain lenses and discontinuous layers of rocks of widely differing bulk compositions. In the Valley Bore area, these include clinozoisite-hornblende-corundum rocks, biotite-kyanite-corundum schists, quartz-epidote rocks, gedrite-bearing gneisses, cordierite-bearing gneisses, pegmatites, and metamorphosed, mafic igneous rocks.

2.6 Geochronology of the Valley Bore Area

Although work is currently in progress to date rocks from the Huckitta Anticline, no radiometric ages are yet available from the metamorphic rocks in the Valley Bore area. However, a sample of the Cadney Gneiss (which overlies the Brady Gneiss), from 50 km southwest of the Valley Bore area, has been dated at 1720 ± 25 m.y. (Armstrong and Stewart, 1975). This Rb/Sr age represents the commencement of retention of radiogenic ^{87}Sr by the Proterozoic metamorphic units in the eastern and southeastern Arunta Block. It is the minimum age of the metamorphic rocks in the Valley Bore area and may be interpreted either as the age of the only high-grade metamorphic event in the area, or as the resetting of the age of a previous metamorphic episode by a subsequent, high-grade, metamorphic event.

Numerous pegmatites intrude all the rocks in the Harts Range area. One was dated at about 400 m.y. by Wilson et al. (1960). This date agrees with an age of 357 m.y. determined for the retrograde metamorphism of the Irindina Gneiss in the same area by Hurley et al. (1961). Stewart (1971) and Armstrong and Stewart (1975) have shown that the Cadney Gneiss occurring close to the Arltunga Nappe Complex is retrogressed to the greenschist facies, and its Rb/Sr age is reset to about 350 m.y. Ages between 340 and 400 m.y. correspond to the age of the Alice Springs Orogeny, which Black (1975) considers was sufficiently intense to produce local melting below the Huckitta Dome. It is yet to be determined whether the Inkamulla and Huckitta Granodiorites were emplaced during this orogeny.

CHAPTER 3: AMPHIBOLITES IN THE JERVOIS RANGE AREA

3.1 Petrography

West of the Jervois Range, metamorphosed mafic rocks occur as deformed and boudinaged sills and flows within the predominantly felsic and pelitic metasediments. They vary in thickness from several metres to over one kilometre, and are commonly cut by fine veinlets of quartz or quartz and adularia. In the hand specimen, these rocks are typically fine-grained and slightly foliated, and some are "spotted" with plagioclase crystals or crystal aggregates up to 15 mm in diameter. East of the Jervois Range, rocks of similar composition occur as stocks, small sills and dykes. These are coarse-grained and massive.

Field evidence and the petrography of these rocks (see appendix, table 2) indicate that they are orthoamphibolites: that is, essentially plagioclase-hornblende assemblages representing metamorphosed basalts and gabbros. Textural studies in thin-section indicate that the large, typically euhedral, plagioclase crystals or crystal aggregates in "spotted" amphibolites are relics of basalt phenocrysts.

Relict plagioclase in both metabasalts and metagabbros commonly contains aggregates of fine white mica ("sericite"), and, in addition, may also contain much larger laths or rosettes of muscovite. In some samples, such as 814 and 818, the replacement

of plagioclase by white mica is extensive, leaving only microscopically small areas of optically clear plagioclase. This implies either

- (i) the large-scale alteration of bulk composition (including the addition of potassium) during weathering, burial, or metamorphism; or
- (ii) the redistribution of elements within the basalt or gabbro during weathering, burial or metamorphism, by processes which, on a large scale, do not alter the bulk-rock composition (e.g. Smith, 1968).

A third possibility is that samples such as 818 (with 3.14% K_2O) represent potassium-rich metagabbros or metabasalts. While this would obviate the need for the addition or redistribution of potassium, it does not explain the alteration of plagioclase. Nor is there any evidence of relict K-felspar. In addition, such potassium-rich rocks would plot well above the tholeiite-alkali-olivine-basalt dividing line on an $Na_2O + K_2O$ versus SiO_2 diagram, whereas the Jervois Range rocks plot on or below this line (see table 2 in appendix).

The following observations establish a time relation between chemical alteration or element redistribution and metamorphism:

- (i) relict plagioclase contains relatively large grains of white mica;
- (ii) clay alteration products are absent from both relict and metamorphic (non-relict) plagioclase grains;
- (iii) both relict and metamorphic plagioclase contain small inclusions of epidote, hornblende and biotite;

- (iv) white mica inclusions are absent from metamorphic plagioclase.

The following facts must also be added:

- (v) inclusions of white mica, epidote, hornblende and biotite within plagioclase phenocrysts in basalts are not known;
- (vi) post-metamorphic, low-temperature surface processes cannot lead to the crystallization of white mica from the alteration of feldspar;
- (vii) the formation of epidote, hornblende and biotite inclusions in plagioclase must have taken place under metamorphic conditions.

The above points indicate that bulk-rock alteration or element redistribution in these metamorphosed mafic rocks took place prior to or during metamorphism. Consequently, any former clay-rich alteration products in plagioclase were recrystallized to white mica during metamorphism. Potassium-rich alteration products in the former basalt groundmass could account for minor biotite and the potassium content of hornblende in the amphibolites.

3.2 Phase Relations

The highest-grade mineral parageneses in amphibolites from the Jervois Range area are as follows:

plagioclase - hornblende \pm magnetite
plagioclase - hornblende - quartz \pm magnetite
plagioclase - hornblende - clinopyroxene
plagioclase - hornblende - quartz - chlorite \pm magnetite.

Minor amounts of epidote, ilmenite or sphene, and biotite may occur in all of the above assemblages. Microprobe analysis confirms that the amphibole is hornblende with $Al_2O_3 > 6\%$ by weight. Coexisting

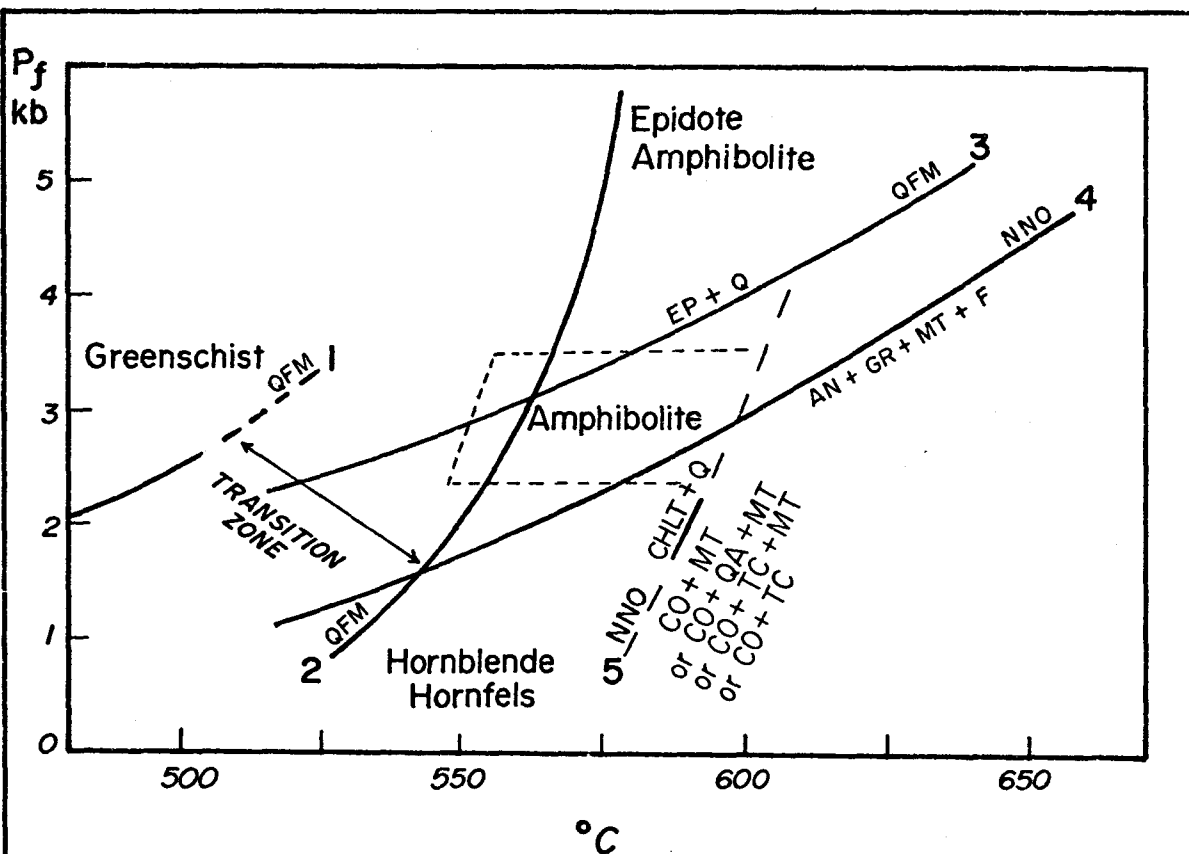
plagioclase varies from An₂₅ to An₅₈. Hence, these mineral parageneses belong to the amphibolite facies of regional metamorphism. (A discussion of facies nomenclature employed in the thesis is given in the appendix.)

There is no clear-cut textural evidence to suggest that epidote or chlorite in these amphibolites is retrograde. Even where these minerals are present in the same rock, evidence of retrogression is equivocal. Therefore, they have been included in the main assemblage. The amounts of epidote and chlorite in these amphibolites being minor, the conditions of formation of these rocks are inferred to lie close to the transition zone - amphibolite facies boundary at about 3 kb (see fig. 2).

The bulk composition of amphibolite 812 (see appendix, table 2) closely corresponds to that used by Liou et al. (1974) to determine experimentally the physical conditions involved in greenschist to amphibolite transitions. The experiments indicate that, at f_{O_2} defined by the quartz-fayalite-magnetite buffer, the transition to amphibolite is complete at 550°C, 2kb and 570°C, 4kb. However, direct comparison is possible only if the natural assemblage were formed under f_{O_2} conditions similar to the QFM buffer.

Unfortunately, at temperatures below 600°C, the magnetite_{ss} - ilmenite_{ss} oxygen barometer of Buddington and Lindsley (1964) is difficult to use in natural assemblages, where X_{usp} and X_{hae} are small, for the following reasons:

- (i) small errors in analysis produce large errors in the computed value of f_{O_2} ;



- Curve 1: greenschist to transition zone boundary - Liou et al. (1974)
 Curve 2: transition zone to amphibolite facies boundary - Liou et al. (1974)
 Curve 3: reaction curve : epidote (Ps 25) + quartz anorthite + grossularite + magnetite + fluid at the QFM buffer - Liou (1973), Holdaway (1972)
 Curve 4: reaction curve : epidote (Ps 25) + quartz anorthite + grossularite + magnetite + fluid at the NNO buffer - Liou (1973), Holdaway (1972)
 Curve 5: upper stability limit of chlorite + quartz at the NNO buffer. Reactant chlorite compositions may range from clinochlore through pycnochlorite and brunsvigite to daphnite. The reaction products with increasing chlorite Mg are: cordierite + magnetite, cordierite + orthoamphibole + magnetite, cordierite + talc + magnetite, cordierite + talc; all include a fluid phase. At f_{O_2} below the QFM buffer, iron-rich chlorite + quartz react to garnet_{ss} + orthoamphibole + cordierite; in the Mg-free system, the products are cordierite + magnetite; as before, all include a fluid product. Synthesized from Turnock, (1960); Fawcett and Yoder, (1966); Akella and Winkler, (1966); Hsu, (1968); Hsu and Burnham, (1969); Fleming and Fawcett, (1976); James et al., (1976); Velde, (1973).

FIGURE 2: Experimentally defined P_f , T conditions of greenschist, transition zone and amphibolite facies. The enclosed area indicates probable conditions of formation of the Jervois Range amphibolites.

- (ii) strictly, the presence of small amounts of Cr and Mn in both phases indicates that the magnetite-ilmenite pair is no longer divariant in T and f_{O_2} ;
- (iii) the computed values of X_{usp} and X_{hae} are strongly dependent on the method used to "discard" components such as Mg and Ca.

Applying the computational method of Anderson (1968) to a magnetite-ilmenite pair in a Jervois Range amphibolite results in $X_{usp} = 0.0006\%$ and $X_{hae} = 0.61\%$, yielding $f_{O_2} \ll 10^{-55}$ atm. on the curves of Powell and Powell (1977). This value falls outside the stability field of magnetite at 500°C (Buddington and Lindsley, 1964), and may indicate disequilibrium between ilmenite and magnetite at temperatures over 500°C . However, oxide pairs from 22 pelitic schists in the Jervois Range area also give similar low values, so that it is more likely that the points outlined above are responsible for the geologically unreasonable values. (At 600°C , $f_{O_2} = 10^{-55}$ atm., most Fe-bearing silicates would be unstable.)

Assuming that the magnetite and ilmenite in the amphibolite were stable, and equilibrated under the same conditions as the silicate phases, $\log f_{O_2}$ must lie between -20 and -15 atm. at 600°C (Rumble, 1973, fig. 2), so that the work of Liou et al. (1974) is broadly applicable. Allowing for the presence of both chlorite and epidote in minor quantities, this sets a lower limit of about 540°C as the temperature of formation of these amphibolites at 3 kb. These conditions are in agreement with the fact that amphibolites with

minor chlorite and epidote belong to neither the low-pressure greenschist to amphibolite facies transition zone (plagioclase-actinolite-chlorite; Miyashiro, 1961; Seki, 1961; Shiraki, 1971) nor to the intermediate-pressure transition zone (albite-epidote-hornblende ⁺ almandine; Fyfe and Turner, 1966; Turner, 1968).

The presence of minor amounts of chlorite or epidote in plagioclase-hornblende assemblages is strongly dependent on bulk composition, as well as P, T, and f_{O_2} . The stability of both of these minerals is increased towards higher temperatures by bulk compositions rich in Al_2O_3 . On a plot of molecular $(Al_2O_3) - (FeO - Fe_2O_3 + MgO) - (CaO + Na_2O)$, chlorite-bearing amphibolites, such as sample 816, are significantly richer in Al_2O_3 than are the bulk compositions used in the experiments of Liou et al. (1974). Consequently, chlorite-bearing amphibolites may represent metamorphosed, altered basalts. For appropriate bulk compositions, stability fields for the assemblages (calcic)-plagioclase-hornblende-chlorite-quartz and (calcic)-plagioclase-hornblende-epidote-quartz may exist within the amphibolite facies proper.

The upper temperature limit of the formation of chlorite-bearing amphibolites is marked by the upper stability limit of the assemblage chlorite + quartz. However, chlorite would normally break down before reaching this limit by multiphase reactions involving plagioclase, amphibole and quartz (if present). This limit has been determined experimentally for chlorite compositions varying in Mg and Al content at $590^\circ C$, $P_{H_2O} = 2 \text{ kb}$, and f_{O_2} defined by the

nickel-nickel oxide buffer (Fleming and Fawcett, 1976; James et al., 1976), as shown in fig. 2.

Hornblendes from all the amphibolites in the Jervois Range area have a similar pleochroic scheme with Z = bluish-green, and, on this basis, probably share the same upper temperature limit of formation (Miyashiro, 1958; Shido, 1958; Binns, 1965).

3.3 Composition and Element Distribution between Hornblende and Chlorite

Representative electron microprobe analyses of hornblendes in amphibolites from the Jervois Range area are listed in table 2. The assumption that all iron is FeO leads to errors, and various recalculation schemes have been proposed to evaluate minimum Fe³⁺ contents of hornblendes. The method of Stout (1972) to calculate minimum Fe³⁺ content presupposes that all Na is found in the A site and, also, that the seven M sites are fully occupied. The method described below is based on only two facts: namely, that seven cation sites cannot contain more than seven cations, and that the crystal structure must be electrically neutral (charge balance). Calculations are based on 23 oxygens in the amphibole structure (assuming negligible F), which allows for the two hydrogens in the hydroxyl radical ($22\text{O}^{2-} + 2\text{OH}^- = 23\text{O}^-$) and overcomes the effects of poor H₂O determinations in classical analysis (Robinson et al., 1971; Binns, 1965).

Based on the normal amphibole structure, the number of cation sites per 23 oxygens is as follows (Robinson et al., 1971; Stout,

SAMPLE	821		825		816	
	HORNBLLENDE	CHLORITE	HORNBLLENDE	CHLORITE	HORNBLLENDE	CHLORITE
SiO ₂	44.61	25.43	40.56	25.94	41.41	24.55
TiO ₂	.26	.11	1.12	.18	.39	.00
Al ₂ O ₃	11.80	21.39	10.33	18.49	14.53	20.98
Cr ₂ O ₃	.14	.00	.00	.00	.00	.00
FeO	17.44	23.06	26.20	32.20	21.50	29.43
MnO	.00	.22	.00	.14	.42	.23
MgO	10.29	17.21	4.73	10.65	6.46	12.79
CaO	11.87	.00	11.31	.00	11.27	.00
Na ₂ O	.95	.00	1.20	.00	1.53	.00
K ₂ O	.16	.00	1.77	.00	.33	.00
TOTAL	97.52	87.42	97.22	87.60	97.84	87.98
CATIONS PER No. OXYGENS	23	28	23	28	23	28
Si	6.6494	5.3150	6.4586	5.6849	6.3146	5.2851
Ti	.0291	.0173	.1341	.0297	.0447	
Al	2.0729	5.2689	1.9386	4.7757	2.6113	5.3230
Cr	.0165					
Fe	2.1739	4.0306	3.4889	5.9014	2.7418	5.2983
Mn		.0389		.0260	.0542	.0419
Mg	2.2865	5.3622	1.1228	3.4794	1.4685	4.1046
Ca	1.8956		1.9296		1.8413	
Na	.2745		.3705		.4523	
K	.0304		.3595		.0642	
TOTAL	15.4288	20.0329	15.8026	19.8971	15.5929	20.0529
Mg	51.3	57.1	23.3	37.1	34.9	43.7
Al ^{iv}	1.3505	2.6850	1.5414	2.3151	1.6854	2.7149
Al ^{vi}	.7223	2.5839	.3972	2.4606	.9259	2.6081
K _D chlt-hbl Mg-Fe	1.26		1.94		1.45	
COEXISTING PLAG. % An	54.5		24.8		31.8	
SUM OF OCT. CATIONS	7.1239	xxxxxx	7.0726	xxxxxx	7.0764	xxxxxx
Al ^{iv} - Al ^{vi} - 2Ti - Cr - Na - K	0.2486	xxxxxx	0.1460	xxxxxx	0.1536	xxxxxx

TABLE 2: Microprobe analyses of coexisting chlorite and hornblende in amphibolites from the Jervois Range area.

1972):

- (i) 8 tetrahedral T sites which may be occupied by Si or Al;
- (ii) 5 small octahedral M sites (2XM(1), 2XM(2), 1XM(3)) which may be occupied by Al, Fe^{3+} , Cr, Ti, Fe^{2+} , Mg or Mn;
- (iii) 2 larger octahedral M sites (2XM(4)) which may be occupied by Ca, Na, Fe^{2+} , Mg or Mn;
- (iv) 1 large A site, which may be partly or wholly vacant, may contain Na or K.

This leads to the theoretical formula $\text{A}_{0-1}\text{M}_7\text{T}_8\text{O}_{22}(\text{OH})_2$, although a small "fraction" of some M sites may be vacant.

A first constraint for a hornblende formula is that the sum of possible octahedral cations excluding Na + K cannot exceed 7, as there are only 7 suitable sites available. Thus:

$$\text{Al}^{\text{VI}} + \text{Fe}^{3+} + \text{Cr} + \text{Ti} + \text{Fe}^{2+} + \text{Mg} + \text{Mn} + \text{Ca} \leq 7 \text{ (Eqn. 1)}$$

(Because this is a calculation of the minimum Fe^{3+} in hornblende, it does not preclude Na entering M(4).)

A second constraint is imposed by the requirements of charge balance. Aluminium substitution in the T sites may take place in one of two ways:

(i) $\text{Mg Si (M,T)} \rightleftharpoons \text{Al Al}$; and

(ii) $\square \text{ Si (A,T)} \rightleftharpoons \text{Na Al}$.

As a result, the charge deficiency of tetrahedral Al not compensated by the substitution of tri- or tetravalent cations for divalent cations in the M sites is made up by Na (+K) in the A site. In common hornblende, where (Na + K) is usually less than one, this

leads to the statement of the second constraint:

$$\text{Al}^{\text{IV}} - \text{Al}^{\text{VI}} - 2\text{Ti} - \text{Fe}^{3+} - \text{Cr} = (\text{Na} + \text{K}) \text{ in A site, or}$$

$$\text{Al}^{\text{IV}} - \text{Al}^{\text{VI}} - 2\text{Ti} - \text{Fe}^{3+} - \text{Cr} - \text{Na} - \text{K} = 0 \quad (\text{Eqn. 2})$$

The numerical value for these two constraints listed in table 2 is too high to be due to errors in analysis alone. The oxidation of some Fe^{2+} to Fe^{3+} reduces the above figures, and iteration may be used to arrive at values of 7 and 0, respectively. This yields a minimum Fe^{3+} content consistent with the structure of amphiboles, and, for low values of the oxidation ratio, does not greatly affect the number of other cations calculated from microprobe analyses.

For the amphiboles listed in table 2, the calculations yield the following:

	<u>821</u>	<u>825</u>	<u>816</u>
Fe_2O_3	3.38	1.85	2.04
FeO	14.40	24.53	19.66
Fe^{3+}	.3760	.2206	.2329
Fe^{2+}	1.7803	3.2510	2.4945
O.R.	17.44	6.35	8.54
<u>Mg</u>	56.0	25.6	36.9
$K_D^{\text{chl-hbl}}$	1.05	1.71	1.33
$K_D^{\text{Mg-Fe}}$			

Although various maximum Fe^{3+} contents may be calculated (Stout, 1972), these depend on the number and proportion of sites assumed to be vacant. Since hornblendes in amphibolites are not usually rich in Fe^{3+} (Shido and Miyashiro, 1959; Grapes et al., 1977), these minimum calculated values probably lie close to the actual values.

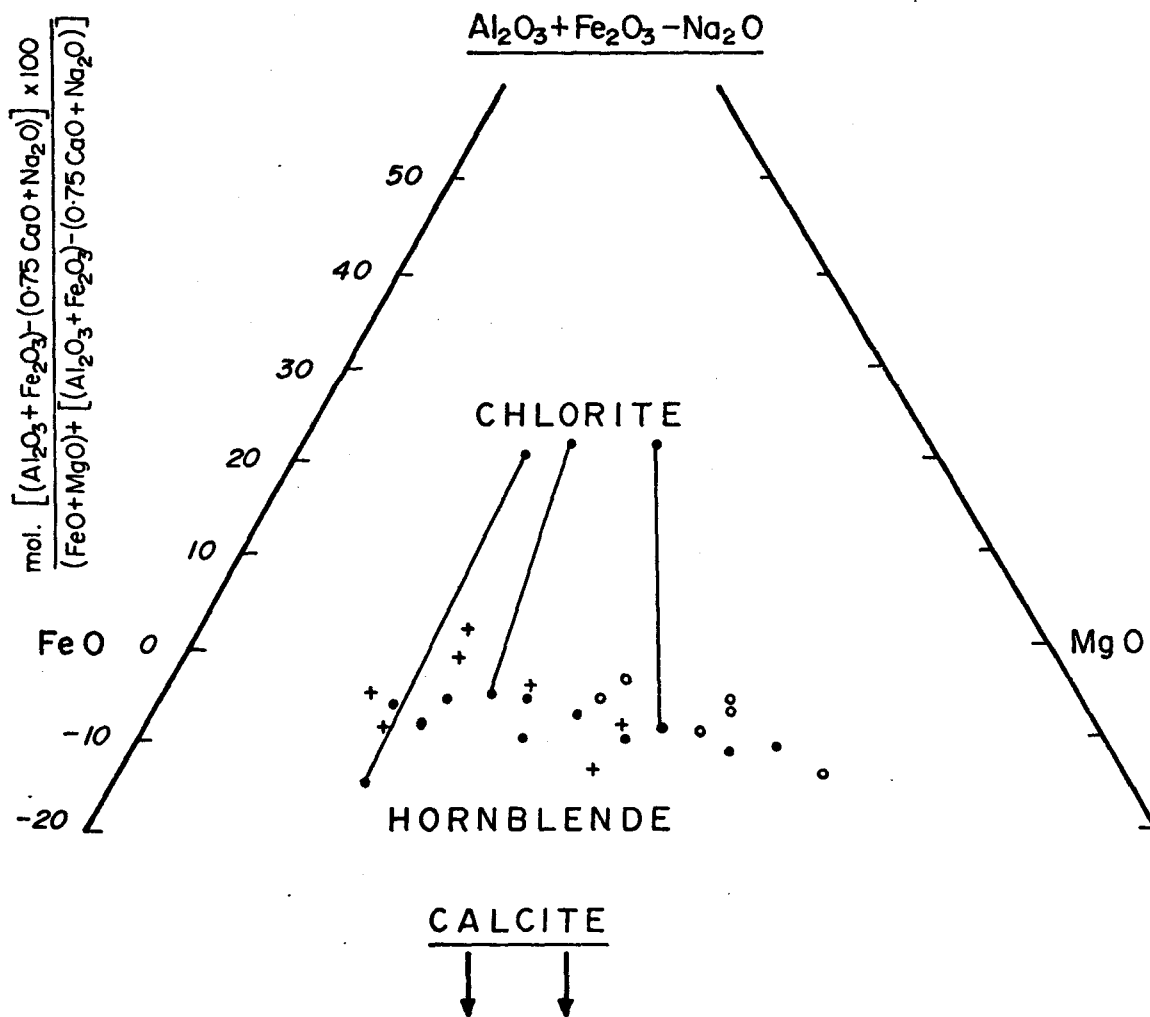
In a full mafic compositional system of 12 components (Si-Ti-Al-Fe-Mn-Mg-Ca-Na-K-O-H-C) and five intensive "variables" (P, T, f_{H_2O} , f_{O_2} and f_{CO_2}), the compositions of 9 coexisting phases at equilibrium are fully specified (in theory) by the values of the intensive variables. If a fixed oxidation ratio is assumed, and the fluid-phase components are not perfectly mobile, the independent variables reduce to P, T and X_{CO_2} , yielding 2 degrees of compositional freedom for a 9-phase assemblage. (This model assumes $P_s = P_f$, with the chemical potentials of H_2O and CO_2 dependent on P, T and X_{CO_2} ; Greenwood, 1967). As the number of phases (minerals) decreases, the compositions of the remaining phases become increasingly dependent on the bulk composition of the system. In addition, the composition of a multicomponent phase becomes functionally dependent on the compositions of the other coexisting phases.

In general, this means that the compositions of plagioclase and hornblende in amphibolites are dependent on the bulk composition of the amphibolite, as well as on the values of P and T. Qualitative examples are given by Engel and Engel (1962), Binns (1965), and Bard (1970). However, since metamorphosed, unaltered basalts have a relatively restricted compositional field, broad compositional limits may be defined for hornblende as a function of metamorphic conditions (Leake, 1971). In a general way, a plot of hornblende Al^{VI} versus Si may be used to discriminate probable, broad pressure conditions of formation (Raase, 1974, fig. 1). On this basis,

hornblendes from the Jervois Range amphibolites fall below the 5 kb line, in the field containing the Zone A hornblendes from the Broken Hill area (Binns, 1965), and the Zone B hornblendes from the Abukuma plateau (Shido and Miyashiro, 1959). On the basis of Ti^{4+} content, the Jervois hornblendes fall into the lower amphibolite facies (Raase, 1974, fig. 2), but, because of the constraints of bulk composition and alteration already mentioned, this fact alone does not constitute proof of such a metamorphic grade.

Hornblendes from the Jervois Range amphibolites, corrected for minimum Fe^{3+} , are tschermakititic to ferrotschermakititic hornblendes on the basis of Al^{IV} and $Na + K$ (Deer, Howie and Zussman, 1962, vol. 2, fig. 71). On the basis of Al^{IV} and $(Al^{VI} + Fe^{3+} + Ti)$, they are slightly more pargasitic. A plot of these hornblendes on the "epidote" diagram (fig. 3) of Harte and Graham (1975) shows marked similarities to hornblendes from Zone A of Binns (1965) in the Broken Hill area, and to hornblendes from Zone B in the Abukuma area (Shido, 1958; Shido and Miyashiro, 1959). Although the Broken Hill samples represent a somewhat higher grade (sillimanite in metapelitic rocks), all these hornblendes were formed under low-pressure, amphibolitie facies conditions.

The phases plagioclase and hornblende dominate the mineral assemblages of amphibolites, and account for most of the chemical components in both number and quantity. As a consequence, the distribution of elements between these two minerals is not greatly affected by minor amounts of other phases. As an example, Grapes



- hornblende and chlorite from the Jervois Range amphibolites; hornblendes have been corrected for minimum Fe^{3+} by the method outlined in the text.
- + Zone A hornblendes from Broken Hill amphibolites (Binns, 1965)
- Zone B hornblendes from amphibolites in the Abukuma Plateau area (Shido, 1958; Shido and Miyashiro, 1959).

FIGURE 3: Hornblende and chlorite analyses from the Jervois Range amphibolites plotted on the "epidote" diagram of Harte and Graham (1975).

et al. (1977) have observed the compositional dependence of hornblende on plagioclase in amphibolites from the Hidaka Metamorphic Belt (see also Leake, 1965). Therefore, a general relation is expected between hornblende Mg and anorthite content of coexisting plagioclase. (The Al_2O_3 content of hornblende varies with the Mg value of that mineral (Robinson et al., 1971).)

Regression on 12 such mineral pairs in Jervois Range amphibolites yields the following relations:

$$\begin{aligned} \text{hornblende } \underline{Mg} &= 33.55 \ln \text{ plag An} - 28.49 \ln \text{ hbld } Al^{3+} \\ &\quad - 59.81 \qquad R = .957 \qquad (\text{Eqn. 3}) \end{aligned}$$

$$\begin{aligned} \text{plagioclase An} &= 36.94 \ln \text{ hbld } \underline{Mg} + 7.47 \ln \text{ hbld } Al^{3+} \\ &\quad - 99.22 \qquad R = .927 \qquad (\text{Eqn. 4}) \end{aligned}$$

where $Al^{3+} = \text{hornblende } (Al^{IV} + Al^{VI})$.

These relations represent the compositional control of bulk chemistry on the mineral phases, and are part of a family of such relations for differing P, T (and f_{H_2O} ?) domains.

Three coexisting chlorite-hornblende pairs from different amphibolites were analysed, and the results are presented in table 2. Although the chlorites are ripidolitic, with subequal aluminium contents, they coexist with plagioclase varying in composition from An25 to An55. The Mg values of chlorites vary, reflecting the bulk composition of the host rock as indicated by hornblende Mg. The distribution coefficient $K_{D_{Mg-Fe}}^{chl-hbl}$ also varies from 1.26 to 1.94, or, if minimum Fe^{3+} contents are assumed, from 1.05 to 1.71. Although the chlorite-hornblende pairs were formed under similar conditions,

the variation in K_D is expected, due to

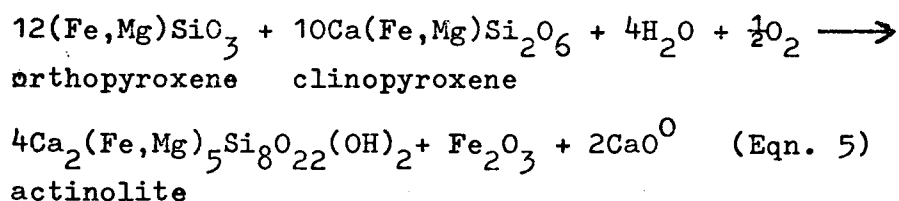
- (i) non-ideal solid solution in both minerals,
- (ii) different bulk compositions, which influence the M site occupancies in hornblende, in turn affecting the distribution of Fe and Mg between the two phases.

The position of hornblende coexisting with chlorite (as compared to hornblendes from chlorite-free amphibolites), on the "epidote" plot of figure 3, further suggests the stability of minor amounts of chlorite in these rocks under lower-amphibolite facies conditions.

3.4 Actinolite Pseudomorphs in Samples of Metagabbro

Microprobe analysis has confirmed the actinolitic composition of pseudomorphs after igneous pyroxenes in several samples of Jervois Range metagabbro. Sample 820 contains large aggregates of actinolite with $Al_2O_3 = 1.09\%$ and $Mg = 69.1$; elsewhere in the same sample a pseudomorph after pyroxene is made up of actinolite with $Al_2O_3 = 4.67\%$ and $Mg = 62.1$. Sample 811 contains actinolite with $Al_2O_3 = 2.17\%$ and $Mg = 64.9$. Metagabbros in which the plagioclase is little altered and probably relict, and in which mafic minerals have been replaced by actinolite, require explanation.

If, during metamorphism, most of the plagioclase in a gabbro remains unaltered (metastable), then the mafic minerals must undergo hydration reactions with little felspar interaction. Such a reaction, simplified and written to conserve silica, could be:



Other reactions may be written to conserve calcium or iron, the role of O_2 may be changed, and olivine may also be used as a reactant. The calcium and iron products (depending on f_{O_2}) may combine with Al and Si (from the breakdown of minor amounts of feldspar) to give epidote or chlorite, which are present in minor amounts in some of these rocks. Such reactions can produce actinolite with only minimal alteration of feldspars, resulting in relict plagioclase and actinolite pseudomorphs.

The conditions under which such reactions may take place are unknown. It is unlikely that progressive regional metamorphism first produced actinolite pseudomorphs which were later rimmed by hornblende. It is possible that the gabbro first underwent low-grade burial metamorphism, during which actinolite pseudomorphs after pyroxene were produced. Subsequent sharp changes in P and T, caused by prograde amphibolite facies metamorphism, could have caused the crystallization of blue-green hornblende rimming actinolite. This implies non-equilibrium between the two amphiboles. Grapes (1975) describes similar occurrences from Japan, and attributes hornblende rims on actinolite to new conditions of metamorphism imposed on the assemblages of a previous metamorphic episode.

An alternate explanation is also possible. Prograde metamorphism of gabbro to amphibolite facies conditions may have

produced fine hornblende reaction rims on pyroxene, leaving the bulk of the pyroxene and the plagioclase unaltered. Subsequent retrograde metamorphism may then have pseudomorphed the relict pyroxene by reactions similar to equation 5. Unfortunately, there is insufficient textural evidence to decide between the two alternatives.

3.5 Parent-Rock Source of the Jervois Range Amphibolites

Recent work on the petrology and composition of island-arc and orogenic systems has characterized the composition of basaltic rocks in these environments, relative to ocean-floor and continental areas (Jakes and Gill, 1970; Jakes and White, 1971, 1972; Miyashiro, 1974; Ringwood, 1974; Miyashiro and Shido, 1975; and many others). As a result, many chemical tests have been proposed to discriminate between these regional (source) types, including the use of isotopes and rare-earth elements (e.g. Pearce and Cann, 1971; Floyd and Winchester, 1975; Pearce, 1975; Pearce, Gorman and Birkett, 1975).

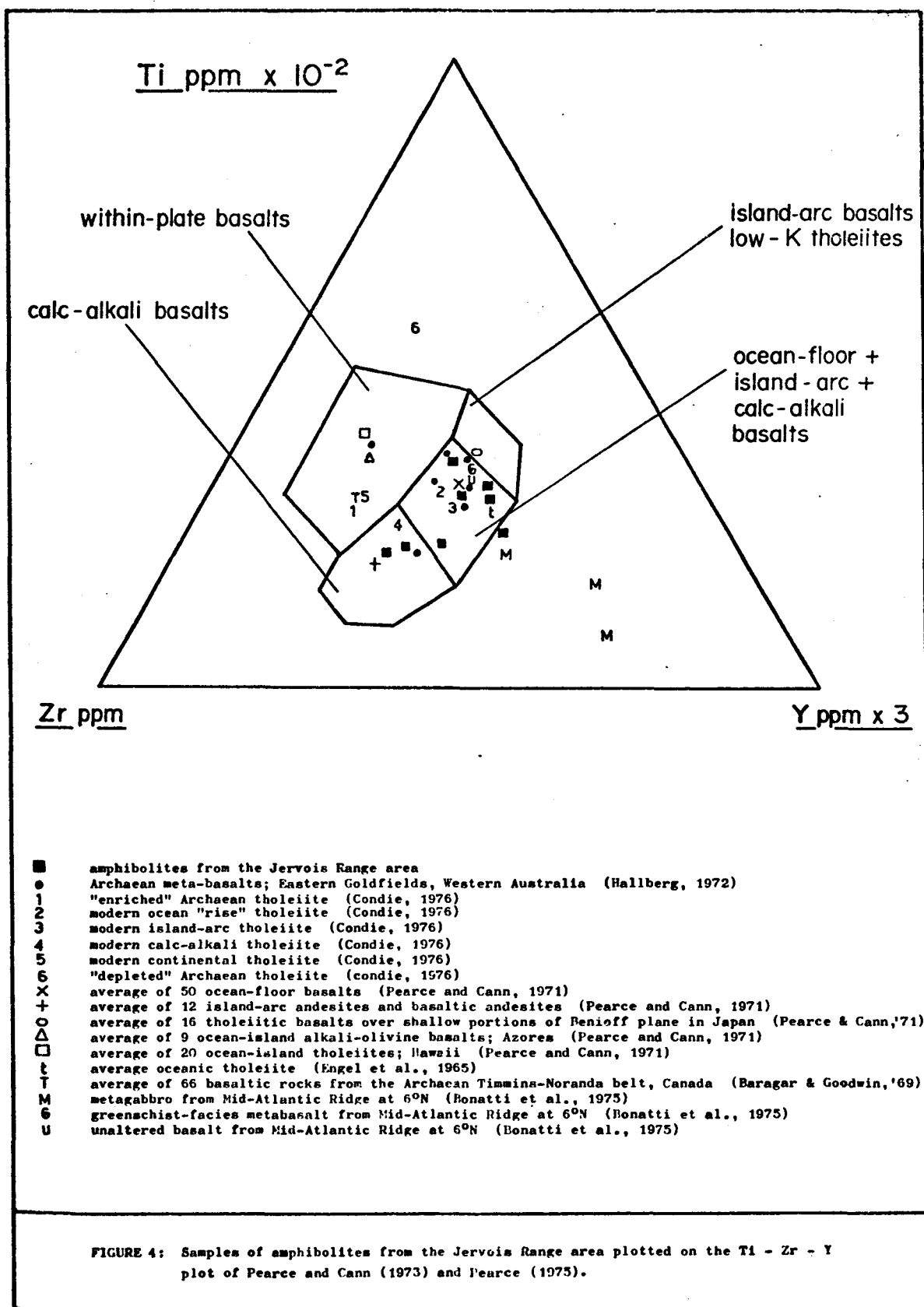
However, the usefulness of such chemical discriminants is very limited when applied to metamorphosed basalts, due to the possibility, even probability, that many of these were chemically altered prior to and during metamorphism (e.g. Vallance, 1965, 1967, 1969; Smith, 1968; Jolly and Smith, 1972; Jolly, 1972; Barron, 1976). Smith and Smith (1976) recently tested these discriminant methods using an outcrop of basalt which had undergone weathering and burial. They concluded that, of all the proposed discriminant functions, the Ti-Zr-Y plot of Pearce and Cann (1971) was the least affected by

burial metamorphism, and thus the most likely to give meaningful results when applied to metamorphic rocks. This further implies that, at least for the outcrop tested, Ti, Zr and Y behave coherently during element redistribution and alteration.

The bulk-rock modification and probable introduction of potassium, described in section 3.1, render the K-Ti-P plot of Pearce et al. (1975) ambiguous. On such a plot, the Jervois Range amphibolites are scattered from within the "oceanic" field, through the "continental" field, towards the potassium apex.

Resorting to the Ti-Zr-Y plot (fig. 4), the Jervois Range amphibolites fall within the fields of calc-alkali and island-arc basalts. The one point falling outside these fields is a plagioclase-rich metagabbro, and this follows the Y enrichment trend described by Bonatti et al. (1975) for plagioclase-rich ocean-floor gabbro.

The similarity of the Jervois Range amphibolites to many Archaean metabasalts from Western Australia (Hallberg, 1972), and to island-arc basaltic andesites (Pearce and Cann, 1971) suggests island-arc or oceanic (as opposed to continental) origins for the parent basalts and gabbros. In this respect, they are similar to mafic granulites in the Strangways Range area, N.T. (Wilson, 1975). Interpretations of parent-rock sources, based on chemical evidence alone, must be accepted with caution. In some instances (Green, 1973; Vallance, 1974) even fresh basalts are not successfully discriminated by these tests and, in addition, other types of rock alteration may well exist in which Ti, Zr and Y do not behave coherently.



CHAPTER 4: STAUROLITE-BEARING ROCKS IN THE JERVOIS RANGE AREA

4.1 Petrography

In the Jervois Range area, staurolite-bearing rocks occur as relatively narrow (< 10 m) lens-shaped units, in a sequence of predominantly pelitic and quartz-rich metasediments characterized by high total-iron content. Compositional variations across this sequence are rapid, and the rocks range from magnetite-garnet rocks containing minor quartz, through magnetite-quartzites, andalusite- and cordierite-bearing magnetite schists, to muscovite-magnetite schists with subordinate quartz.

This sequence, the "mine sequence", crops out in the shape of a letter "j", and represents the hinge and one limb of a large, vertically dipping, isoclinal fold with axial plane oriented north-south. Although the outcrop of the mine sequence is about 1 km wide (see map accompanying the thesis) weathering is so intense that aluminous and ferromagnesian minerals in these rocks are unsuitable for chemical analysis. Fortunately, diamond drill core is available from several localities in this sequence, and analytical data for pelitic rocks in the Jervois Range area are based on samples from these cores.

Brief petrographic descriptions of key staurolite-bearing assemblages, together with photomicrographs and bulk-rock analyses, are presented in the appendix (appendix table 3, et seq.). With

the exception of andalusite and chlorite in some assemblages, textural studies do not indicate that any of the minerals listed do not belong to the parageneses presented in the descriptions.

In sample 826, andalusite is commonly rimmed, or completely replaced by, muscovite-rich aggregates, which may contain minor amounts of chlorite and opaque minerals. However, the same rock also contains small andalusite grains (rounded, < 1.0 mm, and containing elliptical inclusions of biotite), without any sign of alteration, in chlorite-rich layers. In the Jervois Range area there is no conclusive textural or isotopic evidence to support a metamorphic episode prior to the one around 1850 m.y. Hence, the andalusite referred to above is not a relic of a previous metamorphism, and may have belonged to one of two metamorphic assemblages, namely:

- (i) a highest-grade paragenesis of quartz-muscovite-biotite-andalusite-garnet-staurclite-chlorite-magnetite; or
- (ii) a lower-grade assemblage formed prior to the attainment of (i) above, but still part of the same prograde metamorphic episode (see Turner, 1968, p.79).

This author strongly favours the first alternative, owing partly to the existence of similar assemblages inferred to be stable parageneses by J. Green (1963), Albee (1968), Guidotti (1974), Froese and Gasparrini (1975) and Ghent (1975). Although the alteration of andalusite may have taken place during the peak of metamorphism, the fine-grained, decussate nature of the muscovite aggregates

suggests a lower-temperature, retrograde process. Evidence of metasomatic activity exists in an adjacent unit of tourmaline-garnet-biotite gneiss, which itself is cut by veins of quartz and microscopic veins of muscovite. Elsewhere in the mine sequence, microscopic veins of quartz \pm adularia \pm chlorite \pm calcite are common.

In samples 828 to 832, textural criteria are consistent with (but not always proof of) the fact that the small amounts of chlorite present are retrograde in origin, or at least formed after the highest-grade paragenesis. Multiphase, multicomponent, chlorite-forming retrograde reactions commonly result in part, or complete, alteration of biotite, though chlorite may also replace other phases, such as muscovite and quartz (see sample 829). In these rocks, retrograde chlorite is usually characterized by one or more of the following:

- (i) in sections perpendicular to cleavage, alteration of biotite commonly results in an aggregate of thin, tapering ("spindle"-shaped) chlorite laths, the grain boundaries of which are commonly curved, and not parallel to biotite (001). Muscovite laths and opaque grains may also be intergrown with the chlorite. Such textures are characteristic of altered biotite in granitic rocks, and are developed to various extents in samples 828 to 832.
- (ii) the retrograde alteration of biotite to chlorite is commonly accompanied by the breakdown of other ferromagnesian phases, especially garnet, to chlorite rims or pseudomorphs

(as in sample 829).

(iii) retrograde chlorite is commonly fine-grained and occurs in radiating or decussate aggregates which cross-cut the foliation defined by muscovite and biotite belonging to the highest-grade paragenesis.

The abundant chlorite in samples 826 and 827 exhibits none of the above three characteristics. Intergrowths with biotite are parallel, commonly coarse-grained, and generally extend over the entire length of the biotite grain. Within the intergrowth, chlorite-biotite grain boundaries along (001) are not curved. These intergrowths do not resemble the retrograde alteration of biotite; rather, they appear to be stable analogues of similar intergrowths between muscovite and biotite (e.g. in sillimanite-bearing schists from the Broken Hill area). In addition, idioblastic biotite and chlorite grain relations suggest the attainment of textural equilibrium (see photomicrographs in the appendix).

In conclusion, petrographic evidence indicates that (1) chlorite is part of the highest-grade parageneses in samples 826 and 827, and, in addition, (2) andalusite is not precluded from the paragenesis of sample 826.

4.2 Phase Relations

The highest-grade staurolite-bearing parageneses in the Jervois Range area are as follows:

staurolite-garnet-andalusite-chlorite-biotite-muscovite-
quartz (6)

staurolite-garnet-andalusite-chlorite-quartz (7)

staurolite-garnet-andalusite-biotite-muscovite-quartz (8)

staurolite-garnet-biotite-muscovite-quartz (9)

All of these parageneses contain magnetite, and may also contain ilmenite and trace amounts of apatite and chalcopyrite. Paragenesis (7) includes trace amounts of muscovite and biotite, and paragenesis (8) may also include albite.

Three simplistic arguments are often used to argue against the stability of some of the above paragenesis.

(i) Firstly, paragenesis (6), together with magnetite, ilmenite and vapour, comprises a ten-phase assemblage which does not appear to be in equilibrium.

(ii) Secondly, parageneses (6) to (8) cannot be successfully plotted as normal "three-phase" assemblages on the AFM projection of J. Thompson (1957).

Bulk-rock analyses of representative staurolite-bearing samples (see appendix table 3) yield the following average values: ZnO = 0.08%, MnO = 0.44%, CaO = 0.27%, Na₂O = 0.76%. The manganese and zinc content of these rocks are respectively 2 to 7 and 2 to 18 times the values quoted for average "geosynclinal" shales (Turekian and Wedepohl, 1961).

Since zinc is strongly partitioned into staurolite, manganese and calcium (the latter in the absence of other calcic phases) are strongly partitioned into garnet, and sodium (in the absence of feldspar) is partitioned into muscovite, these minor elements must be counted as components when applying the phase rule. Hence, a

ten-phase assemblage in the system Si-Ti-Al-Fe-Mn-Zn-Mg-Ca-Na-K-H-O has a variance of four, and may exist, at equilibrium, for a range of values of P, T, f_{H_2O} , and f_{O_2} . The presence of appreciable Ca, Mn and Zn cannot be shown on an AFM diagram, which is a projection in the system SiO_2 - Al_2O_3 -FeO-MgO- K_2O - H_2O (SAFMKH). Garnet and staurolite, when "stabilized" by these minor components, cannot be part of the simple AFM projection if the latter already contains three phases which, for practical purposes, do not contain these minor elements.

(iii) A third argument raised against the stability of paragenesis (7) is that it is essentially free of Na, K and Ca, and belongs to the compositional system SiO_2 - Al_2O_3 -FeO-MgO- H_2O (SAFMH). Such compositions do not represent sedimentary rocks, so that the assemblage has been metasomatically derived. Since the alteration of biotite to chlorite is a common retrograde reaction, and could be accompanied by the metasomatic removal of potassium from the bulk rock, it is inferred that the chlorite of paragenesis (7) is retrograde. This whole argument is based on generalities, and it will be shown in chapter 6 that sediments within the system SAFMH, though not common, do exist.

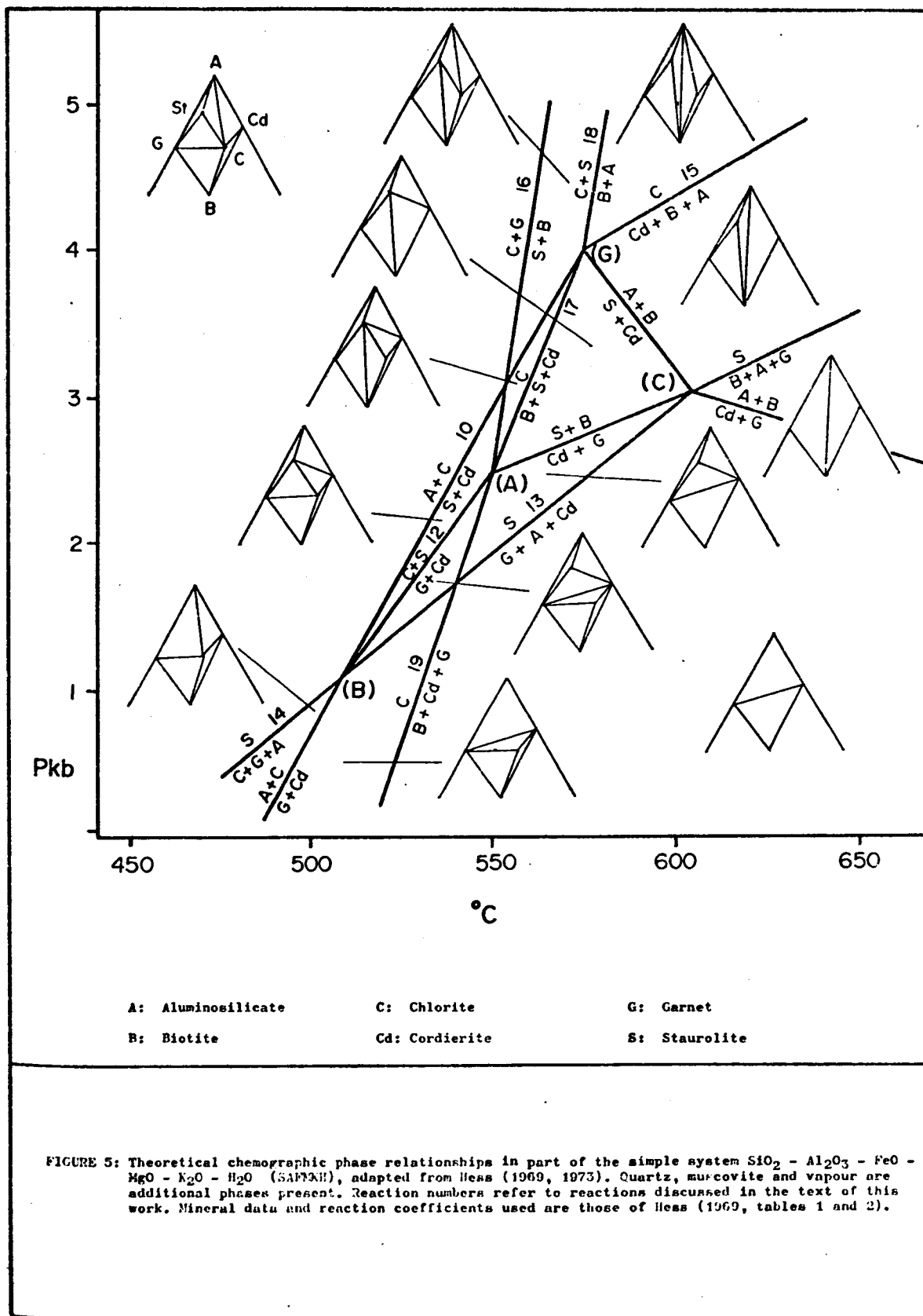
The chemographic relations in P_f , T space between quartz, chlorite, cordierite, biotite, andalusite and its polymorphs, and essentially Na-free muscovite, Zn-free staurolite, and Mn-Ca-free garnet, have been deduced by various workers in the simple system SAFMKH. A petrogenetic grid in this system was first proposed by

Albee (1965b), and has since been refined by Hess (1969, 1973), A. Thompson (1976, II fig. 7), and Kephezinskas and Khlestov (1977, fig. 4a). The latter four grids are configurationally similar, but the positions of the invariant points and the slopes of the univariant (discontinuous) reactions vary from grid to grid. These differences arise due to

- (i) uncertainties in the positions of the first few invariant points plotted,
- (ii) differences in the assumed compositions of some of the participating phases, and
- (iii) uncertainties in the values of entropy and molar volume of some of the participating phases (Korzhinskii, 1959).

The semi-quantitatively calibrated petrogenetic grid of Hess (1969) is presented in figure 5 to indicate possible chemographic relations in the Jervois Range rocks. Relevant experimentally determined reaction curves and stability fields are plotted in figure 6.

The coexistence of chlorite + quartz in some of the staurolite-bearing assemblages (as well as others to be discussed in chapter 6), may be used to set an upper limit for the temperature of formation of such assemblages in the Jervois Range area. The stability limit for chlorite + quartz has been investigated in the system SAMH by Fawcett and Yoder (1966), Velde (1973), Chernosky (1975), and indirectly by Seifert (1973). In the system SAFH it has been investigated by Turnock (1960), Hsu (1968), and James et al.



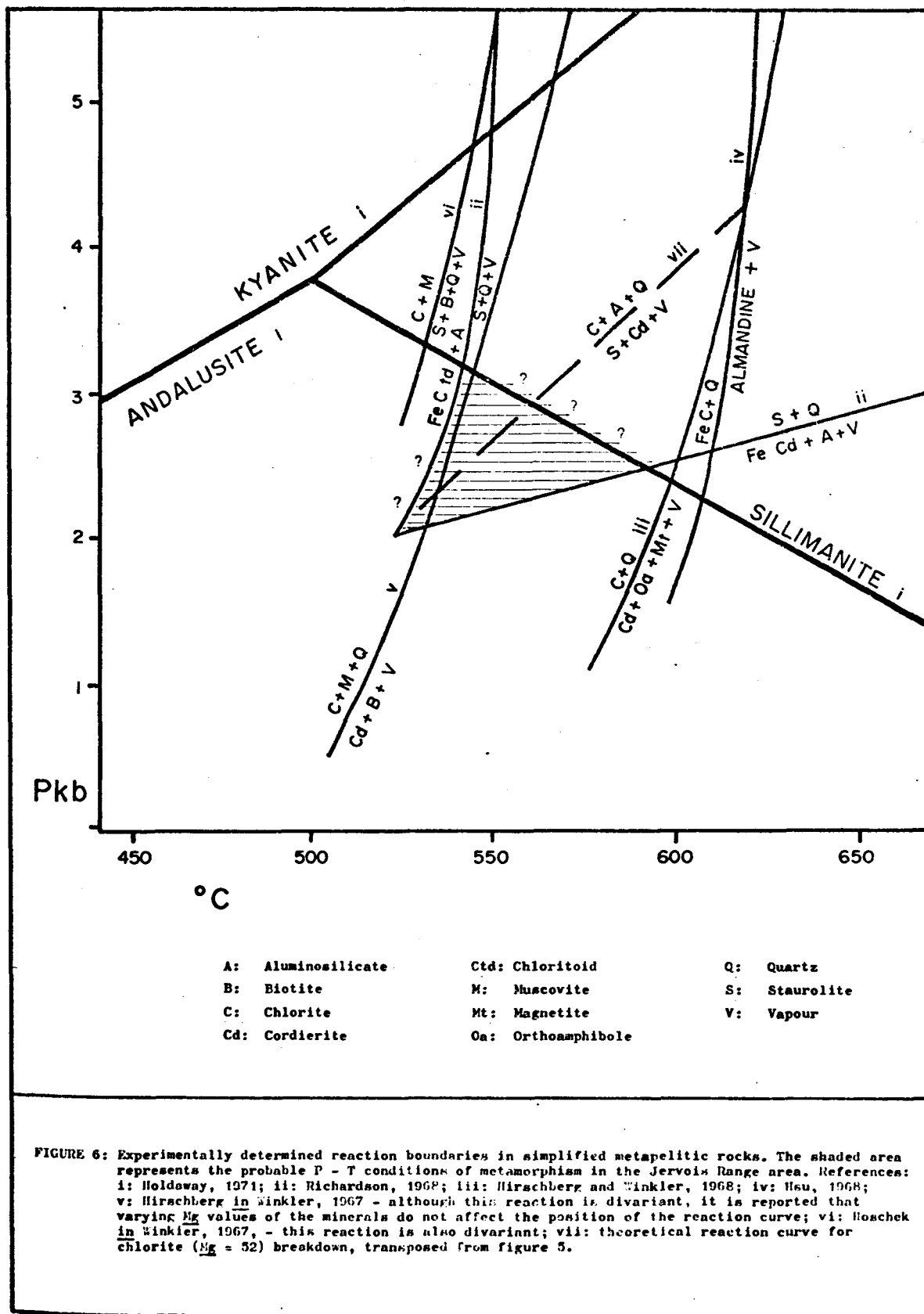


FIGURE 6: Experimentally determined reaction boundaries in simplified metapelitic rocks. The shaded area represents the probable P - T conditions of metamorphism in the Jervois Range area. References: i: Holdaway, 1971; ii: Richardson, 1968; iii: Hirschberg and Winkler, 1968; iv: Hsu, 1968; v: Hirschberg in Winkler, 1967 - although this reaction is divariant, it is reported that varying Mg values of the minerals do not affect the position of the reaction curve; vi: Hoeschek in Winkler, 1967, - this reaction is also divariant; vii: theoretical reaction curve for chlorite (Mg = 52) breakdown, transposed from figure 5.

(1976). In the more complex system SAFMH, the upper stability of chlorite + quartz has been determined by Akella and Winkler (1966), and in greater detail by Fleming and Fawcett (1976).

A synthesis of these investigations indicates that, in the SAMH system, the chlorite stable to the highest temperature in the presence of quartz (to 590°C at 2 kb P_{H_2O}) has the composition $Mg_{9.72}Al_{4.56}Si_{5.72}O_{20}(OH)_{16}$, corresponding to clinocllore (Deer et al., 1963). At lower temperatures, the assemblage Al-poor chlorite + quartz reacts to chlorite + talc + quartz, and the assemblage Al-rich chlorite + quartz reacts to chlorite + cordierite + quartz; with rising temperature, the resultant chlorites approach clinocllore in composition. In the SAFMH system ($Mg \div 50$), the composition of chlorite stable to the highest temperature in the presence of quartz (505°C, 2 kb P_{H_2O}) has been calculated from the data of Fleming and Fawcett as $(Mg,Fe)_{9.96}Al_{4.07}Si_{5.97}O_{20}(OH)_{16}$, assuming no oxidation at the NNO buffer. Mirroring reactions in the SAMH system, at temperatures of around 540°C, Al-poor Fe-Mg chlorite + quartz reacts to chlorite + talc + magnetite + quartz or chlorite + magnetite + quartz, and Al-rich Fe-Mg chlorite + quartz reacts to chlorite + cordierite + quartz, the chlorites approaching pycnochlorite-brunsvigite as the temperature rises towards 595°C.

In the SAFH system, the chlorite stable at the highest temperatures in the presence of quartz is daphnite, of approximate composition $Fe_{9.5}Al_5Si_{5.5}O_{20}(OH)_{16}$, assuming no oxidation. The upper thermal stability of daphnite + quartz is quoted as 600°C at

2 kb P_{H_2O} , on the NNO buffer, by Turnock (1960) and Hsu (1968). James et al. (1976) suggest that at these temperatures the above assemblage may be metastable, and that the stable limit may be as low as 530°C at 2 kb P_{H_2O} (NNO). This is in agreement with the trend of chlorite stability limits in the absence of quartz at 2 kb P_{H_2O} (NNO), and the projection of McOnie et al (1975) indicates that daphnite breaks down to Fe-cordierite + magnetite_{ss} + quartz at 540°C under these conditions.

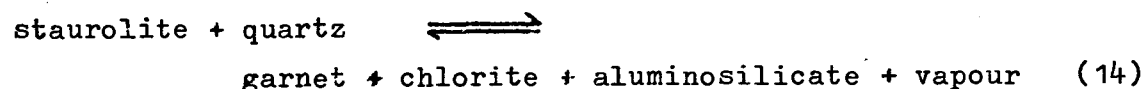
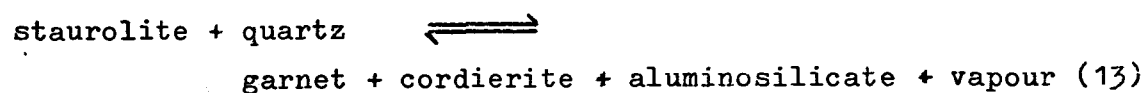
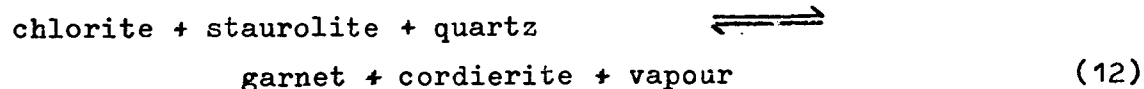
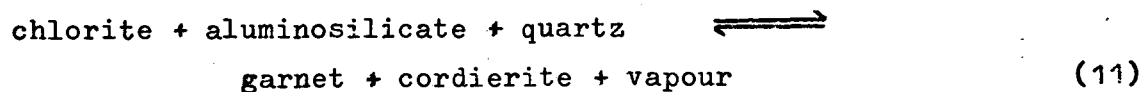
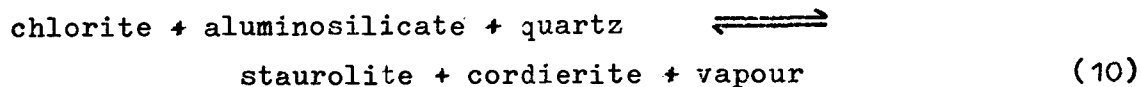
With increasing Mg, the breakdown of the most stable chlorites with quartz at 2 kb P_{H_2O} , NNO buffer, yields the following assemblages: Fe-cordierite + magnetite, cordierite + orthoamphibole + magnetite, cordierite + talc + magnetite, cordierite + talc. At f_{O_2} defined by the QFM buffer, iron-rich chlorite + quartz react to garnet_{ss} + orthoamphibole + cordierite; all products include a vapour phase.

Akella and Winkler (1966) reacted chlorite (Mg = 62, Al = 5.36 per 28 oxygens) + quartz to orthoamphibole + cordierite + vapour at 562°C, P_{H_2O} = 2 kb, f_{O_2} around the QFM buffer. Although this temperature is lower than the 595°C obtained by Fleming and Fawcett (1976), it may be explained, at least in part, by the 10% seeding of the runs with natural ferrogedrite (with Na_2O = 2%). In addition, the natural chlorite used also contained small amounts of sodium and calcium, which stabilized their particular orthoamphibole, relative to pure, synthetic orthoamphibole. Note that the relation $x_{Mg}^{oa} < x_{Mg}^{chl} < x_{Mg}^{crd}$ must hold; the more aluminous starting chlorite in the experiments of Akella and Winkler (1966) does not affect the

orthoamphibole-forming reaction, as it would have reacted to clinochlore + cordierite before producing orthoamphibole (Fleming and Fawcett, 1976, fig. 5).

Hence, for all chlorites, the stable coexistence of chlorite + quartz indicates temperatures of formation below 595°C at 2 kb $P_{\text{H}_2\text{O}}$ at f_{O_2} defined by the NNO buffer, whilst the stability of daphnite + quartz may indicate temperatures of equilibration as low as 530°C . Increasing the pressure by 1 kb raises the chlorite + quartz stability by 25°C for Fe-free compositions (Fawcett and Yoder, 1966). Applying an empirical least-squares curvature extrapolation derived from the data of Akella and Winkler (1966) to the data of Fleming and Fawcett (1976) yields a limit of 612°C at 4 kb $P_{\text{H}_2\text{O}}$ (NNO) for chlorite ($\text{Mg} \div 50$) + quartz. Increasing f_{O_2} lowers the stability limit of Fe-bearing chlorite + quartz, whereas decreasing f_{O_2} to QFM or even to MI values does little in the SAFH system (Turnock, 1960, fig. 40).

Neglecting magnetite and ilmenite, and trace amounts of muscovite and biotite ("accounted for" by Fe^{3+} , Ti, Na and K) the 6 phase paragenesis (7) quartz-chlorite-staurolite-garnet-andalusite-(vapour) is 4-variant in the system SAFMH + Mn + Zn + Ca (see analysis, sample 827, appendix table 3). Although the phase rule allows the stable coexistence of this assemblage, it does not prove that the phases are all in equilibrium. Several reactions in the system SAFMH are predicted by petrogenetic grids (fig. 5) which are of relevance to the "K-free" assemblage of sample 827; they are:



If, in an assemblage between 510 and 600°C, the reactants of reaction (10) (chlorite + aluminosilicate + quartz) are stable, then, according to figure 5, reactions (12) and (13), proposed by Ganguly (1968), need not be considered. Note that this argument is not complicated by "extra" components, as these are not normally strongly partitioned into chlorite or aluminosilicate.

The stability of aluminosilicate + chlorite + quartz precludes the formation of cordierite by reactions (10) to (13) on the petrogenetic grid of figure 5. Even if the tie line between aluminosilicate and chlorite were broken to yield stauroilite + cordierite by reaction (10), sample 827 (paragenesis 7) would not contain cordierite, unless the composition of chlorite coexisting with cordierite and stauroilite were more iron-rich than $\text{Mg} = 47$. (The bulk composition of sample 827 falls on the Fe-side of the tie line Fe-stauroilite-chlorite ($\text{Mg} = 47$) on a corrected AFM plot.) If different phase compositions and thermochemical data were to position reaction curves (12) and (13) on the higher-pressure side of reaction

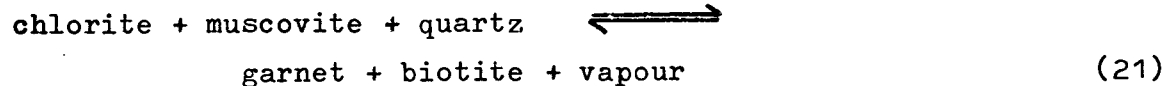
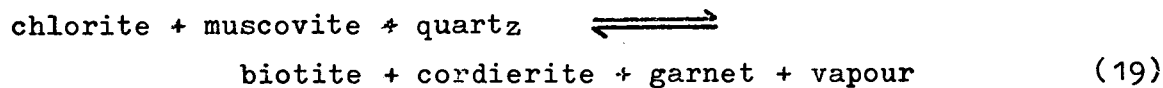
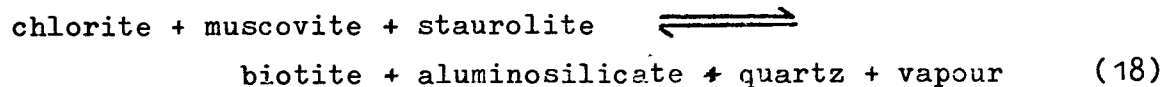
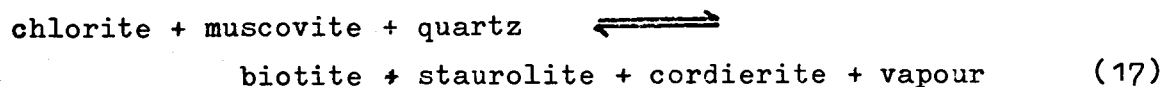
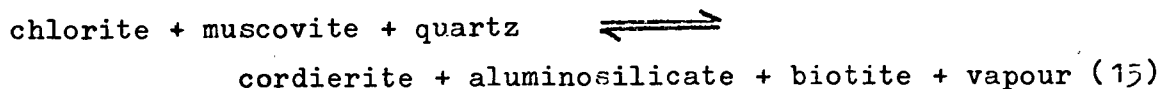
(10) in a chemographic analysis, staurolite could still be stabilized by appreciable amounts of zinc, moving reaction curves (12) and (13) to higher temperatures, and shifting the formation of cordierite to higher grades.

For reaction (10), the four grids of Hess (1969, 1973), A. Thompson (1976) and Kephezinskas and Khlestov (1977) indicate P_{H_2O} from 2.7 to 3.8 kb at 550°C and 3.7 to 5 kb at 600°C; unfortunately reaction (10) has not been experimentally investigated. Reaction (13) has been experimentally determined in the system SAFH by Richardson (1968), and at higher pressures by Ganguly (1972); the results are plotted in figure 6.

The stability field of the "K-free" paragenesis (7) must lie in the stability field of chlorite + andalusite + quartz. In addition, this stability field must also lie wholly within the stability fields of the appropriate Mn-Ca-bearing garnet + quartz + magnetite and that of the appropriate zincian staurolite + magnetite + quartz. These latter fields must be larger than those involving "pure" (Ca-Mn-free) garnet and "pure" (Zn-free) staurolite (e.g. Hsu, 1968, fig. 13), but the extent of enlargement of the appropriate fields is not known as a function of the concentration of the minor elements.

The addition of K and Na to the system SAFMH + Mn + Ca + Zn yields the same variance of 4 for the assemblage: quartz-chlorite-garnet-staurolite-andalusite-biotite-muscovite-(vapour) (paragenesis (6)). Some of the more relevant chlorite-consuming reactions proposed in the

system SAFMKH are as follows (fig. 5):



Reaction (15) has been experimentally investigated by Hirschberg and Winkler (1968) and reaction (20) by Hoschek (1969). Reaction (16) has been proposed by Carmichael (1970) and reaction (21) by J. Thompson and Norton (1968) and Hollister (1969a). Reactions (15) and (20) have often been quoted as marking the beginning of the amphibolite facies, and the consequent "incompatibility" of muscovite + chlorite in this facies. Even in the simple system SAFMKH, reaction (20) is divariant (sliding), and of little use in marking the "incompatibility" of muscovite + chlorite (or of marking the beginning of amphibolite facies conditions, unless P-T bands are accepted as facies boundaries (Turner, 1968)). Reactions (15) and (16) are univariant only in the simple system SAFMKH, and, even in the experiments of Hirschberg and Winkler (1968), the muscovite contained

Na and Fe^{3+} , and the chlorite concentrate contained Fe^{3+} , Mn and Ca. The sliding reactions (20) and (21) are of more general applicability in natural systems, and do not preclude the stability of chlorite + muscovite in parts of the amphibolite facies. Winkler (1976, p.77, 221) now acknowledges that muscovite + chlorite may be stable within his "medium grade".

With the same provisos as before, the stability of chlorite + andalusite + quartz implies (fig. 5) that P-T conditions for cordierite formation by reactions (17) and (19) had not been attained in the Jervois Range area. The addition of Na, Mn, Ca and Zn as components of phases participating in reactions (15), (16) and (18) increases the variance of these reactions, so that, in certain natural assemblages, the coexistence of chlorite + muscovite + quartz in rocks of the amphibolite facies need not be considered metastable. Parageneses such as (6) and (8) are not rare (J. Green, 1963; Albee, 1968; Guidotti, 1974; Froese and Gasparri, 1975; Ghent, 1975), although bulk compositions appropriate to paragenesis (7) are uncommon.

The small number of staurolite-bearing samples in the Jervois Range area (largely limited by the drill core available), and the lack of lower-grade equivalents of the rocks preclude the proposal of reactions leading to parageneses (6) to (9), especially since the role of chloritoid is uncertain.

The probable stability field of the Jervois Range staurolite-bearing rocks is indicated in figure 6. The field is poorly defined

because of

- (i) uncertainties in the location of the andalusite-sillimanite boundary,
- (ii) uncertainties in the (enlarged) stability field of Mn-Ca-bearing almandine-pyrope,
- (iii) uncertainties in the (enlarged) stability field of zincian staurolite.

Based on the composition of the garnet rims in paragenesis (7) ($X_{Fe} = 0.86$, $X_{Mg} = 0.09$, $X_{Mn} = 0.03$, $X_{Ca} = 0.02$), the Al content of the chlorite, and the fact that fibrolite occurs in nearby areas, the conditions of formation of these rocks are inferred at approximately 570°C at 2.75 kb P_{H_2O} . Note that the upper pressure-limit is largely controlled by the position of the andalusite-sillimanite boundary. At these conditions, the work of Ganguly (1972) indicates $-\log f_{O_2}$ values between 16 and 18 for the assemblage staurolite + magnetite + quartz in the SAFH system. However, the partitioning of zinc (and, to a much lesser extent, magnesium) into staurolite must increase the stability field of the above assemblage with respect to f_{O_2} . For reasons explained in chapter 3, the almost pure coexisting magnetite and ilmenite in these rocks cannot be used to refine f_{O_2} (or T) values in the Jervois Range assemblages.

4.3 Composition and Element Distribution between Minerals in the

Staurolite-Bearing Rocks

For a closed system (excepting a vapour phase), the phase rule determines the relationships between intensive variables, components

and phases (minerals). For certain metamorphic rocks, the intensive variables correspond to the "imposed" variables T , P , f_{H_2O} and f_{O_2} , though each of the latter two may be buffered by the mineral assemblage under certain conditions.

Taking as an example the assemblage cordierite-garnet-sillimanite-quartz (no vapour) in the SAFM system, the variance of 2 is accounted for by T and P , the "limiting" case of Goldschmidt's mineralogical phase rule. If the variance of an assemblage increases, and each extra degree of freedom is accounted for by additional imposed variables such as f_{H_2O} , the assemblage remains limiting. Two important characteristics of a limiting assemblage are:

- (i) the composition of each of the phases is uniquely determined by the particular set of values of the imposed variables; as these change, the compositions of some (or all) of the phases change accordingly. These compositional changes are referred to as sliding reactions (simple reactions of J. Thompson and Norton, 1968);
- (ii) the compositions of each of the phases is independent of the bulk composition of the assemblage.

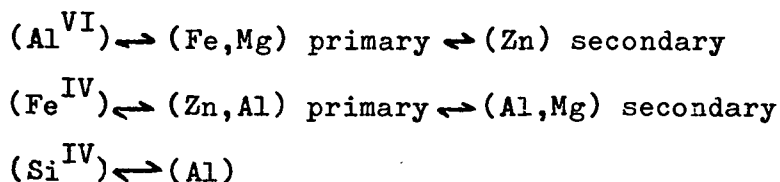
Comparison of mineral compositions between two assemblages from different areas is best made on (preferably identical) limiting assemblages, for then the differences in mineral compositions reflect differences in imposed conditions of P , T etc., and not the largely undetermined effects of bulk composition. The Jervois Range rocks are best compared to assemblages in the upper staurolite zone of the

Rangely Quadrangle, Maine (Guidotti, 1974), as is done later in this chapter. Guidotti's study gives full analyses of the coexisting minerals, rather than Fe/Mg values only. However, his assemblages contain plagioclase (An 17.5) and graphite, and are devoid of magnetite, and andalusite is not inferred as a stable phase. Guidotti's assemblage muscovite-quartz-plagioclase-staurolite-biotite-chlorite-garnet-ilmenite-graphite-(vapour) is trivariant if Mn is counted as a component, implying one degree of compositional freedom if f_{H_2O} is buffered by the assemblage.

Coexisting minerals in samples from each of the parageneses (6) to (9) have been analysed; representative analyses are presented in tables 3 to 6.

Staurolite

Staurolite structural formulae were based on 46 oxygens, using the formula of Smith (1968), namely: $Fe \leq 4 \quad Al \sim 18 \quad Si \sim 8 \quad O_{44} \quad (OH) \sim 4$. Principal component analysis of natural staurolites (Griffen and Ribbe, 1973) has confirmed this formula, and indicated the following substitution schemes:



In contrast to the suggestion of Juurinen (1956) that half the iron ions in staurolite are in the ferric state, Schreyer and Chinner (1966) suggested that Fe^{3+} in classical staurolite analyses is

SAMPLE 826 PARAGENESIS (6)

STAUKROLITE - GARNET - ANDALUSITE - CHLORITE - MUSCOVITE - BIOTITE - QUARTZ GNEISS

	<u>STAUKROLITE</u>		<u>GARNET</u>		<u>BIOTITE</u>	<u>MUSCOVITE</u>	<u>CHLORITE</u>	
	core	rim	core	rim			(prim)	(sec)
SiO ₂	26.06	25.92	36.20	36.77	35.44	46.33	21.82	24.50
TiO ₂	.21	.32	.00	.29	1.00	.00	.00	.00
Al ₂ O ₃	53.79	53.93	19.80	19.87	18.72	34.93	22.50	17.29
FeO	14.12	13.76	31.22	39.24	21.37	1.77	31.50	37.72
MnO	.00	.00	9.65	1.31	.00	.00	.00	.18
ZnO	1.49	1.25	.00	.00	.00	.00	.00	.00
MgO	1.17	1.23	1.17	2.10	10.11	1.16	10.59	6.61
CaO	.00	.00	1.93	.29	.12	.00	.00	.00
Na ₂ O	.00	.00	.00	.00	.27	.87	.00	.00
K ₂ O	.00	.00	.00	.00	9.04	9.87	.00	.00
TOTAL	96.84	96.41	99.97	99.87	96.07	94.93	86.41	86.30
CATIONS PER No. OXYGENS	46	46	12	12	22	22	28	28
Si	7.3914	7.3633	2.9856	3.0125	5.3928	6.1863	4.8664	5.6639
Ti	.0448	.0684		.0179	.1144			
Al	17.9806	18.0559	1.9246	1.9186	3.3572	5.4969	5.9140	4.7108
Fe	3.3492	3.2689	2.1533	2.6885	2.7194	.1976	5.8750	7.2924
Mn			.6741	.0909				.0352
Zn	.3120	.2622						
Mg	.4947	.5209	.1438	.2565	2.2934	.2309	3.5208	2.2780
Ca			.1705	.0255	.0196			
Na					.0797	.2252		
K					1.7547	1.6811		
TOTAL	29.5727	29.5396	8.0519	8.0104	15.7312	14.0180	20.1762	19.9803
Mg	12.87	13.74	6.26	8.71	45.75		37.42	23.80
X _{Fe}			68.54	87.82				
X _{Mg}			4.58	8.38				
X _{Mn}			21.46	2.97				
X _{Ca}			5.42	0.83				
Al ^{iv}					2.6072	1.8137	3.1336	2.3361
Al ^{vi}					.7500	3.6832	2.7804	2.3747

TABLE 3: Microprobe analyses of minerals in paragenesis (6).

SAMPLE 827 PARAGENESIS (7)

STAUKROLITE-GARNET-ANDALUSITE-CHLORITE-QUARTZ GNEISS with trace MUSCOVITE and
BIOTITE

	<u>STAUKROLITE</u>		<u>GARNET</u>		<u>BIOTITE</u>	<u>MUSCOVITE</u>	<u>CHLORITE</u>
	core	rim	core	rim			
SiO ₂	25.49	26.29	36.71	36.62	37.11	46.28	22.54
TiO ₂	.29	.34	.00	.00	1.32	.00	.10
Al ₂ O ₃	54.08	53.70	20.27	20.07	18.58	36.05	22.92
Cr ₂ O ₃	.00	.00	.00	.14	.00	.00	.00
FeO	13.98	13.77	36.00	38.31	21.37	1.93	30.06
MnO	.14	.00	3.19	1.52	.00	.00	.00
ZnO	1.38	1.32	.00	.00	.00	.00	.00
MgO	1.44	1.47	2.05	2.31	8.65	.68	11.19
CaO	.00	.00	1.65	.75	.37	.00	.00
Na ₂ O	.00	.00	.00	.00	.29	.79	.00
K ₂ O	.00	.00	.00	.00	8.53	9.58	.00
TOTAL	96.80	96.89	99.87	99.72	96.22	95.31	86.81
CATIONS							
PER No.	46	46	12	12	22	22	28
OXYGENS							
Si	7.2380	7.4326	2.9990	3.0004	5.5943	6.1411	4.9472
Ti	.0619	.0723			.1496		.0165
Al	18.0981	17.8925	1.9516	1.9380	3.3010	5.6327	5.9288
Cr				.0091			
Fe	3.3197	3.2556	2.4595	2.6250	2.6941	.2142	5.5175
Mn	.0337		.2207	.1055			
Zn	.2893	.2755					
Mg	.6096	.6195	.2497	.2821	1.9439	.1345	3.6613
Ca			.1444	.0658	.0598		
Na					.0848	.2032	
K					1.6403	1.6216	
TOTAL	29.6503	29.5480	8.0249	8.0259	15.4678	13.9523	20.0713
Mg	15.51	15.99	9.22	9.70	41.91		39.89
X _{Fe}			80.00	85.27			
X _{Mg}			8.12	9.16			
X _{Mn}			7.18	3.43			
X _{Ca}			4.70	2.14			
Al ^{iv}					2.4057	1.8589	3.0528
Al ^{vi}					.8953	3.7788	2.8760

TABLE 4: Microprobe analyses of minerals in paragenesis (7).

SAMPLE 830 PARAGENESIS (8)

STAUROLITE-GARNET-ANDALUSITE-BIOTITE-MUSCOVITE-QUARTZ GNEISS

	<u>STAUROLITE</u>	<u>GARNET</u>		<u>BIOTITE</u>	<u>MUSCOVITE</u>	<u>CHLORITE</u>
		core	rim			(sec)
SiO ₂	26.34	36.63	36.53	34.53	46.33	26.02
TiO ₂	.18	.00	.00	1.35	.30	.00
Al ₂ O ₃	54.06	20.45	20.36	20.07	35.48	19.88
FeO	11.82	34.47	34.91	24.17	2.08	34.28
MnO	.00	5.84	6.06	.00	.00	.52
ZnO	3.51	.00	.00	.00	.00	.00
MgO	.79	1.50	1.62	7.13	.66	6.17
CaO	.00	1.04	.39	.00	.00	.00
Na ₂ O	.00	.00	.00	.25	.87	.00
K ₂ O	.00	.00	.00	8.72	9.44	.00
<u>TOTAL</u>	<u>96.70</u>	<u>99.93</u>	<u>99.87</u>	<u>96.22</u>	<u>95.16</u>	<u>86.87</u>
CATIONS PER No. OXYGENS	46	12	12	22	22	28
Si	7.4711	2.9997	2.9981	5.3053	6.1615	5.8056
Ti	.0384			.1537	.0300	
Al	18.0716	1.9737	1.9693	3.6342	5.5611	5.2277
Fe	2.8037	2.3606	2.3960	3.1056	.2313	6.3963
Mn		.4051	.4213			.0983
Zn	.7350					
Mg	.3340	.1831	.1982	1.6331	.1308	2.0522
Ca		.0912	.0343			
Na				.0745	.2243	
K				1.7090	1.6015	
<u>TOTAL</u>	<u>29.4538</u>	<u>8.0134</u>	<u>8.0172</u>	<u>15.6154</u>	<u>13.9405</u>	<u>19.5801</u>
<u>Mg</u>	10.64	7.20	7.64	34.46		24.29
X _{Fe}		77.65	78.56			
X _{Mg}		6.02	6.50			
X _{Mn}		13.33	13.81			
X _{Ca}		3.00	1.13			
Al _{iv}				2.6947	1.8385	2.1944
Al _{vi}				.9395	3.7226	3.0333

TABLE 5: Microprobe analyses of minerals in paragenesis (8).

SAMPLE 828 PARAGENESIS (9)

STAUKROLITE - GARNET - BIOTITE - MUSCOVITE - QUARTZ GNEISS

	<u>STAUKROLITE</u>		<u>GARNET</u>		<u>BIOTITE</u>	<u>MUSCO.</u>
	core	rim	core	rim		
SiO ₂	26.56	26.23	36.36	36.52	34.74	45.78
TiO ₂	.12	.00	.11	.00	.93	.00
Al ₂ O ₃	54.13	53.96	19.90	20.23	19.46	35.48
Cr ₂ O ₃	.00	.00	.11	.00	.00	.00
FeO	15.62	15.80	40.15	39.13	25.74	2.49
MnO	.00	.00	.76	1.63	.00	.00
ZnO	.58	.46	.00	.00	.00	.00
MgO	.82	.86	1.20	1.29	6.23	.70
CaO	.00	.00	1.42	1.10	.00	.00
Na ₂ O	.00	.00	.00	.00	.00	.42
K ₂ O	.00	.00	.00	.00	9.08	10.36
<u>TOTAL</u>	<u>97.83</u>	<u>97.31</u>	<u>100.01</u>	<u>99.90</u>	<u>96.18</u>	<u>95.23</u>
CATIONS						
PER No.	46	46	12	12	22	22
OXYGENS						
Si	7.4630	7.4165	2.9941	3.0014	5.3866	6.1253
Ti	.0254		.0069		.1084	
Al	17.9255	17.9812	1.9313	1.9595	3.5561	5.5948
Cr			.0072			
Fe	3.6704	3.7360	2.7649	2.6894	3.3376	.2786
Mn			.0530	.1135		
Zn	.1203	.0960				
Mg	.3435	.3625	.1473	.1580	1.4400	.1396
Ca			.1253	.0969		
Na						.1090
K					1.7959	1.7982
<u>TOTAL</u>	<u>29.5481</u>	<u>29.5922</u>	<u>8.0299</u>	<u>8.0187</u>	<u>15.6246</u>	<u>14.0155</u>
<u>Mg</u>	8.56	8.84	5.06	5.55	30.14	
X _{Fe}			89.46	87.95		
X _{Mg}			4.77	5.17		
X _{Mn}			1.71	3.71		
X _{Ca}			4.06	3.17		
Al ^{iv}					2.6134	1.8747
Al ^{vi}					.9427	3.7201

TABLE 6: Microprobe analyses of minerals in paragenesis (9).

generated by oxidation during grinding. The absence of Fe^{3+} in staurolites has been confirmed (at least for some samples) by Mössbauer spectroscopy (Bancroft et al., 1967; Smith, 1968), so that all iron in the listed analyses is taken to be in the ferrous state.

A ternary atomic plot of all staurolite analyses from the Jervois Range samples (n=47) yielded the following average result:

$$\text{Si}^{4+} = 25.17 \quad (s = 0.35)$$

$$\text{Al}^{3+} = 60.80 \quad (s = 0.47)$$

$$\text{Fe}^{2+} + \text{Mg}^{2+} + \text{Zn}^{2+} = 14.03 \quad (s = 0.37)$$

This close clustering is not affected by either staurolite Mg (8.23 to 15.98; weighted average of 12.10, $s = 2.86$) or ZnO content (0.77 to 3.67%; weighted average of 1.69%, $s = 1.19$). There is little compositional zoning in staurolite; increases in Mg and decreases in Zn from core to rim are slight, and compositional differences in apparent interpenetration-twin zones (sample 827) are negligible.

The strong partitioning of Zn into staurolite, and the increase in partitioning with decrease in modal staurolite (Guidotti, 1974) is illustrated by sample 830, which contains approximately 1% modal staurolite: bulk rock $\text{ZnO} = 0.027\%$, staurolite $\text{ZnO} = 3.51\%$ (a "concentration factor" of 129). In samples 826 to 828, where staurolite is abundant, the concentration factor is much smaller (e.g. sample 826 - bulk rock $\text{ZnO} = 0.21\%$, staurolite $\text{ZnO} \approx 1.3\%$, giving a concentration factor of only 6.2).

Garnet

In the Jervois Range staurolite-bearing rocks, garnet constitutes

from 5% of the total volume of the rock (sample 829), up to 20% (samples 826 and 827). In general, the small garnets are manganese-rich, and in some samples show little compositional zoning (sample 830 - bulk rock MnO = 0.40%; garnet diameters up to 0.6 mm, average MnO content ~ 6.0 %). The larger garnets of samples 826 and 827 are normally zoned, with Mn and Ca describing symmetrical, bell-shaped distribution curves (figure 7). The Ca curve is flattened relative to the Mn curve, and there is a slight upturn in both curves at 220 μm from the edges. Fe, Mg and Mg all describe similar but upturned curves, that of Mg and Mg being flattened relative to Fe (figure 7). There is a slight downturn in these curves at 220 μm from the rims of the grain; these curves, as a whole, are similar to figure 8 of Hollister (1969a). Although the Mn content of garnets in samples 828 and 830 rises, and Fe in 828 falls, from core to rim, Mg and Mg rise in all the garnets considered in this chapter.

The garnets listed in tables 3 to 6 contain less octahedral Al and more cubic divalent ions than required by the ideal aluminosilicate garnet formulae. If these garnets conform to the ideal structural formulae, then an approximate Fe^{3+} content may be calculated by varying the oxidation ratio to yield a total of 8 cations per 12 oxygens. When the garnet rims are recalculated this way, the sum of octahedral ions closely approaches 2 and the sum of cubic co-ordinated ions approaches 3 (the average deviations are 0.0011 and -0.0072 respectively). The resultant garnet oxidation ratios range from 2.02 to 2.89 or, alternatively, the percentage of andraditic end-member

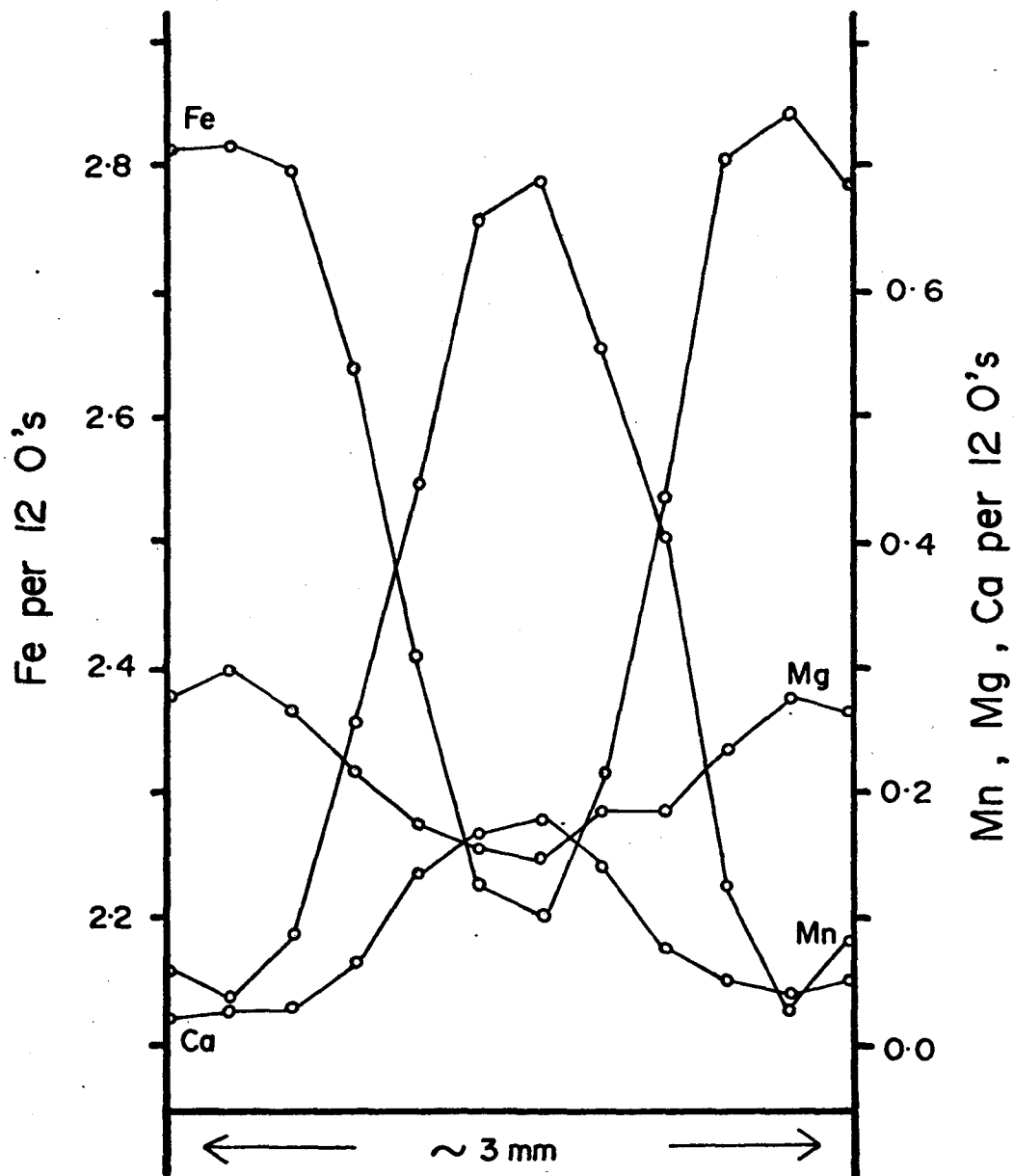


FIGURE 7: Garnet zoning in sample 826. Element concentrations are shown as the number of cations per 12 oxygen - formula.

varies from 2.71 to 3.78%.

Chlorite

The primary chlorites of samples 826 and 827 are pseudo-thuringites, with Al contents very close to the maximum to be expected in rocks that also contain andalusite (6 per 20 cations; Albee, 1962). In Al content, they are very similar to chlorites from the upper staurolite zone of the Rangely Quadrangle (Guidotti, 1974) but they are richer in iron ($\text{Mg} = 37.5$ and 39.9 for the Jervois chlorites as against ~ 50 for the Rangeley chlorites).

Samples 830 and 826 also contain minor retrograde chlorite. In sample 826 this chlorite is confined to a few, microscopically narrow zones which may represent solution channels along cracks. Optically, these retrograde chlorites have first-order gray interference colours, in contrast with the primary chlorites which have deep, anomalous blue interference colours. Microprobe analysis confirms that they are chemically distinct, being richer in silica and iron ($\text{Mg} = 23.8$ for sample 826 and 24.3 for sample 830) than the primary chlorites.

To test for chemical equilibrium between chlorite and the other minerals of paragenesis (6) in sample 826, 19 different chlorites, from different areas of the sample, and in contact with different minerals, were analysed. This yielded an average Mg of 37.43 , with a standard deviation of 0.81 . These analyses were then used with 10 biotite analyses to generate all possible K_D 's, as proposed by Deb and

Saxena (1976). The results confirm what has already been inferred from textural studies, and what may also be inferred from the close clustering and approximately normal distribution of chlorite Mg's, namely, that the chlorite is part of the equilibrium paragenesis.

Muscovite

Analysed muscovites in these rocks are lower in Al and Na, and higher in Mg and Fe, than those in the upper staurolite zone of Guidotti (1974). Their structural formulae also indicate silicon in excess of 6 per 22 oxygens. This celadonitic substitution agrees well with the ferromagnesian nature of some of these rocks, and, since bulk compositions are generally low in sodium, the paragonite content of muscovites (in the absence of albite or plagioclase) is not a function of P and T, but of bulk composition. Since the muscovites are not "saturated" with an amount of Na appropriate to their conditions of formation, they cannot be used as a semi-quantitative geothermometer as proposed by Guidotti and Sassi (1976).

Biotite

The biotites in samples 826 and 827, though similar in Al content and Mg to those described by Guidotti (1974), appear to co-exist with less magnesian chlorite. Whereas the difference in Mg between these two minerals in sample 827 is only 2%, and may be explained by modest amounts of analytical error and oxidation in chlorite, the difference in sample 826 is 8.3%, and is less easily

dismissed. The problem is that, according to Guidotti (1974, p.479) "Only such chlorites of probably retrograde origin (all with the lowest observed Mg/Fe values) have Mg/Fe values less than that of the associated biotite." This is true for the demonstrably retrograde chlorite in sample 826 ($\text{Mg} = 23.8$). However, the primary chlorite, though more magnesian ($\text{Mg} = 37.5$) than the retrograde chlorite, is also less magnesian than the biotite ($\text{Mg} = 45.8$). Since the primary chlorite is in apparent textural equilibrium, and fulfils the criteria of Deb and Saxena (1976) for apparent chemical equilibrium, it would appear that the criterion of Guidotti (1974) need not always apply. A similar relationship has been observed (for more magnesian rocks) in a cordierite-chlorite-biotite assemblage by Guidotti et al. (1975a).

Possible Topologies in the simple SAFMKH System

The bulk compositions and phases of parageneses (6) to (9) are plotted on a corrected AFM projection in figure 8. Bearing in mind that only trace amounts of biotite and muscovite exist in paragenesis (7), figure 8 indicates a possible bulk compositional control on biotite composition. For similar P, T conditions, this is probable if the assemblages buffer f_{O_2} and/or $f_{\text{H}_2\text{O}}$, so that with a variance of 4 they are no longer limiting parageneses.

It has been pointed out previously that appreciable Zn, Mn and Ca may stabilize assemblages "forbidden" in the simple SAFMKH system (e.g. staurolite + biotite in the presence of garnet + chlorite; Albee, 1965b, 1968, 1972). However, neither chlorite nor biotite

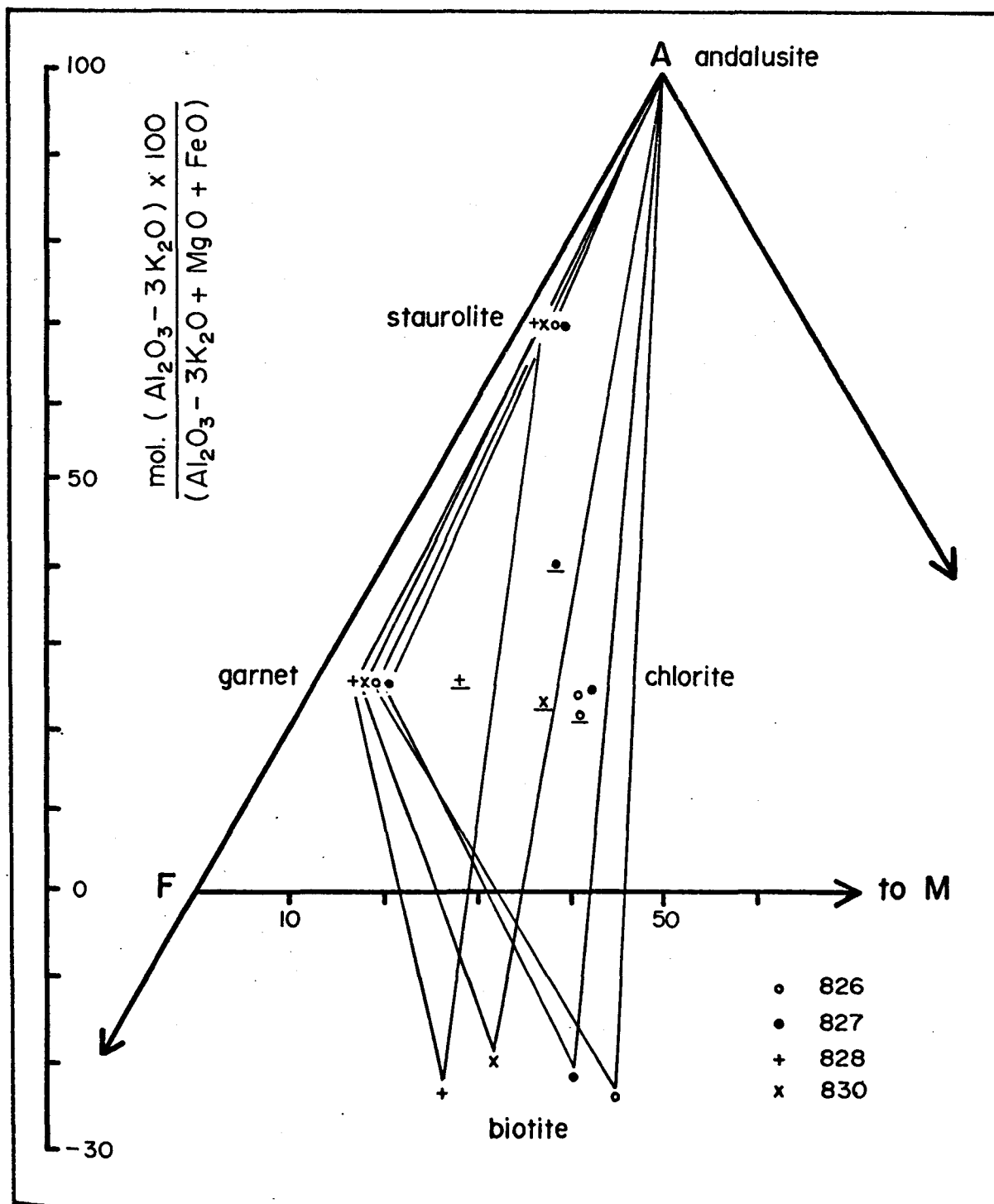


FIGURE 8: AFM plot of samples 826, 827 (only trace biotite), 828 and 830. Bulk compositions are shown underlined and have been corrected for magnetite.

is stabilized by extra components (apart from "normal" amounts of Ti in biotite etc.), so that the assemblage andalusite-chlorite-biotite-quartz-muscovite-(vapour) may be rigorously plotted on an AFM projection. Accepting that chlorite is not retrograde in parageneses (6) and (7), and that it may be less magnesian than biotite, two possible AFM topologies are presented in figure 9. The other stability fields plotted in these projections are conjectural in the pure SAFMKH system, although they are compatible with the topology of Hess (1969) for Fe-rich bulk compositions lying on the low-T side of reaction (10) in figure 5.

With respect to reaction (16) and paragenesis (9), the relative stability of Mn-Ca-stabilized garnet-chlorite versus Zn-stabilized staurolite-biotite cannot be evaluated with the data presented here. (Paragenesis (9) is 6-variant in the system SAFMKH-Mn-Ca-Zn-Na).

AFM diagrams proposed for lower-amphibolite facies conditions show stable chlorite compositional fields from about $Mg = 60$ to 100 (except those of Guidotti et al., 1975). If chlorite + biotite is also stable on the Fe side of an andalusite-biotite tie-line, as in the Jervois Range rocks, then, for certain conditions, figure 9 implies a miscibility gap in chlorite compositions. This problem cannot be resolved on present data, and more intense sampling will be carried out if further drill core becomes available.

The Distribution of Elements between Phases

For a given set of intensive variables, the distribution of Mg and Fe between two minerals (A and B) at equilibrium is given by:

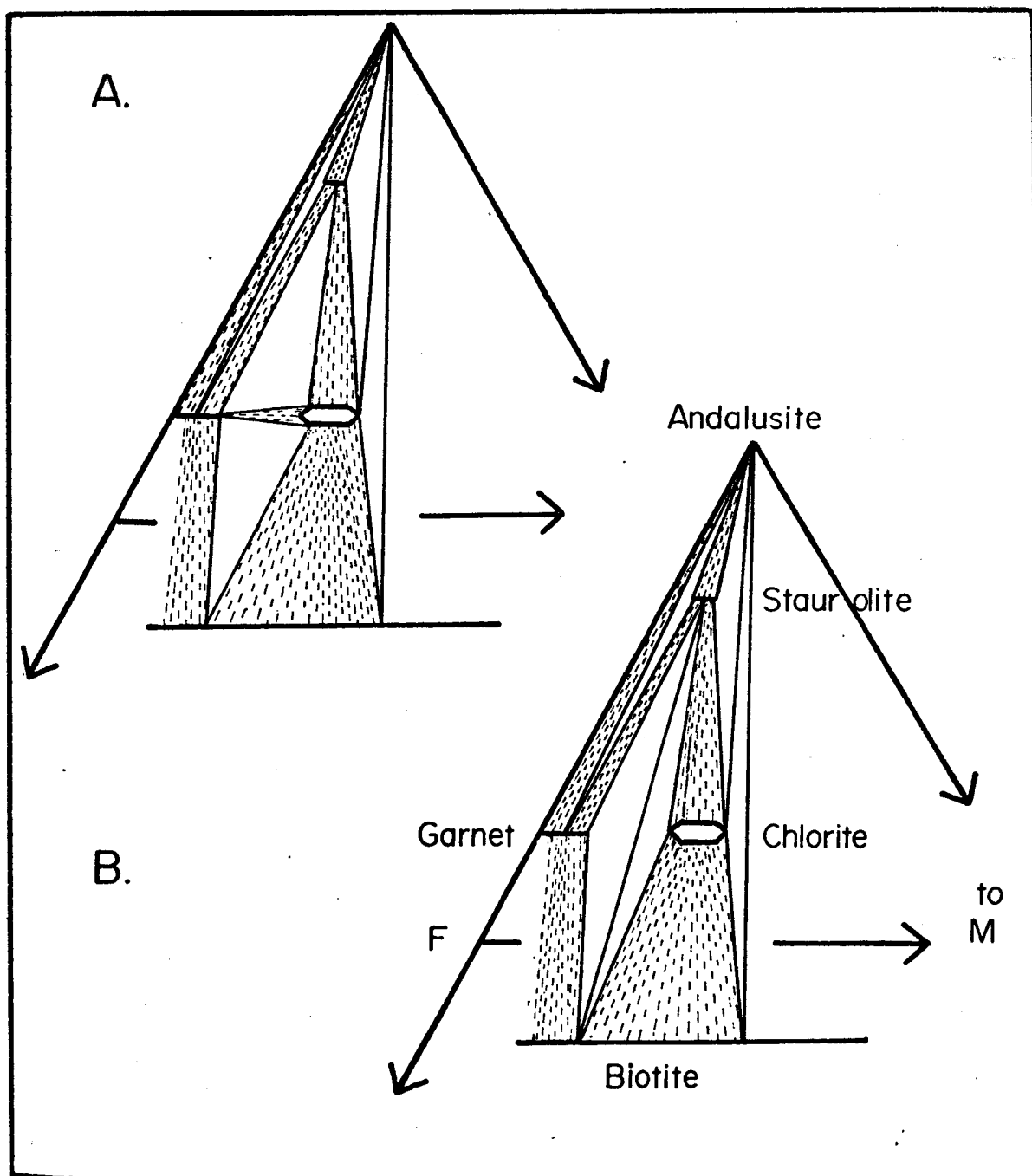


FIGURE 9: Two possible simplified AFM topologies for staurolite - bearing rocks from the Jervois Range area, inferred from assemblages (6) to (9) inclusive. Quartz, muscovite and vapour are possible additional phases. The presence of additional chemical components in garnet and staurolite permits the stable coexistence of more than three phases depicted on the AFM diagram. The coexistence of chlorite with more magnesian biotite is discussed in the text.

$$K = \frac{X_{Mg}^A X_{Fe}^B}{X_{Fe}^A X_{Mg}^B} \times \frac{Y_{Mg}^A Y_{Fe}^B}{Y_{Fe}^A Y_{Mg}^B} \left(= \frac{a_{Mg}^A a_{Fe}^B}{a_{Fe}^A a_{Mg}^B} \right)$$

$$= K_{D_{Mg-Fe}}^{A-B} \times K_{Y_{Mg-Fe}}^{A-B} \quad (\text{eqn. 22})$$

where X_{Mg}^A refers to the mole fraction $Mg/(Mg+Fe)$ in mineral A, Y_{Mg}^A is the activity coefficient of Mg in phase A, and K_D is the distribution coefficient. When all the activity coefficients are equal to one (or practically so) for all compositions of phases A and B, then $K_D \equiv K$ for the range of P, T for which $K_Y = 1$. The value of K_D is then purely a function of the imposed variables, and independent of bulk composition, which implies that the solid solutions are ideal ($\Delta H^{EM} = \Delta S^{EM} = \Delta V^{EM} \equiv 0$).

The non-ideal behaviour of Fe-Mg silicate phases may arise from one or more of the following "end-member" causes.

1: Non Ideality of Mixing

(i) In a phase in which all Fe-Mg mixing takes place in identical (or nearly so) crystal sites ("one-site" mixing), atomic interactions may be such that mixing is not ideal, implying that the partial molar enthalpy is not independent of composition ($\Delta H^{EM} \neq 0$).

(ii) In a one-site phase, and also in multi-site phases where each site may exhibit ideal mixing, long and short range ordering decreases the entropy of the Fe-Mg distribution, so that $\Delta H^{EM} \neq 0 \neq \Delta S^{EM}$. Cases (i) and (ii) imply that K_D is not independent of the compositions of both phases (i.e. K_D is no longer constant for

fixed P, T).

2: Effects of other Components

Two special cases arise, namely:

(i) If a third element, Z, substitutes for both Fe and Mg in one or both phases, and Z does not discriminate between Fe and Mg, then K_D will not change. This perfect dilution implies that Fe and Mg are substituted by Z in the same initial ratios in which they existed before dilution.

(ii) If a third element Z substitutes only for, say, Fe in one or both phases, then, using $Fe = Fe + Z$ in calculating K_D , the distribution coefficient will not change. Unfortunately, for significant concentrations of Z, cases (i) and (ii) are not common, so that the presence of one or more extra exchangeable species in one or both phases will affect the value of K_D . Kretz (1961) gives a more formal evaluation of this problem.

In the general case, K_Y will not only vary with composition, but also with the imposed variables of P, T, etc., so that K_D is rarely exactly equal to K.

Since at equilibrium

$$\ln K = -\Delta G^0/RT \quad (\text{eqn. 23})$$

we have:

$$\left(\frac{\partial \ln K}{\partial T}\right)_P = \frac{\Delta H^0}{RT^2} \quad (\text{eqn. 24})$$

$$\left(\frac{\partial \ln K}{\partial P}\right)_T = \frac{-\Delta V^0}{RT} \quad (\text{eqn. 25})$$

Equation (24) indicates that the most useful geothermometers will be those coexisting mineral pairs which undergo large enthalpy changes on Fe-Mg exchange. Fe-Mg exchange between two silicate phases, in which both elements are octahedrally coordinated, will, in general, involve low enthalpy changes. In such cases, K (or K_D) will vary only slightly with temperature, so that small analytical errors, and the possible effects of other exchangeable elements, will lead to large errors in estimated temperature of equilibration. In garnet, the divalent cations are in 8-fold cubic coordination, so that at low temperatures and pressures almandine is intrinsically more stable than pyrope. In the normal spinels the divalent cations are in 6-fold octahedral coordination, but their atomic environment differs from a silicate structure. In staurolite, iron is in 4-fold tetrahedral coordination (Smith, 1968), although limited Fe-Mg substitution occurs on the octahedral Al site. Any of these three minerals, when paired with an octahedrally coordinated silicate, will exhibit much larger enthalpy changes with temperature for the exchange reaction.

Equation (25) indicates that the behaviour of K with pressure is dependent on the volume change of the reaction involved. Fe end-member silicates have larger molar volumes than do the corresponding Mg end-members. However, the exchange reaction is antipathetic in that as Fe is replaced by Mg in one phase its molar volume decreases, but the accompanying substitution of Mg by Fe in the other phase increases its molar volume by a similar amount. In general, as Fe-Mg silicates

do not exhibit large excess volumes of mixing, Fe-Mg exchange reactions are practically independent of moderate changes in pressure, so that, for fixed f_{O_2} , K (or K_D) may be taken as a function of temperature and composition (or temperature alone if both phases form ideal solid solutions).

The behaviour of distribution coefficients and their use as geothermometers has been well documented (Ramberg and De Vore, 1951; Kretz, 1958, 1961, 1963; Mueller, 1961; Saxena, 1968a, b, 1969a, b; Albee, 1965c; Sen and Chakraborty, 1968; Saxena and Hollander, 1969; Ganguly and Kennedy, 1974; and others).

With respect to garnet, the more recent works emphasize two facts:

- (i) K_D 's are functions of the Mg/Fe ratios and Mn and Ca contents of garnets;
- (ii) with zoned garnets, microprobe analyses of rim compositions should be used when calculating K_D 's.

Strong zoning in garnets reduces the applicability of many of the earlier works based on analyses of garnet concentrates. Even where the Mg/Fe ratio does not change from core to rim, the bulk Mn and Ca content of strongly zoned garnets is much higher than that of the garnet rims, with which the rest of the minerals in the assemblage are in equilibrium.

Since the number of staurolite-bearing samples from the Jervois Range area is limited, and similar assemblages from different parts of the area are unavailable, the partitioning of Fe and Mg between

phases in these rocks must be compared with similar assemblages from other areas. Since Guidotti (1974) lists full microprobe analyses for similar assemblages, a comparison of the above rocks with those from the Rangeley Quadrangle was attempted.

To allow for non-ideal mixing of Fe and Mg in garnet, and to allow for the effects of Ca and Mn on K_D , the method of Ganguly and Kennedy (1974) was adapted for use with the data of Guidotti (1974), using the equation:

$$\ln K_D = a + b(x_{Fe}^{gt} - x_{Mg}^{gt}) + c(x_{Mn}^{gt} + 2x_{Ca}^{gt}) \quad (\text{eqn. 26})$$

The relative effects on $\ln K_D$ of Mn and Ca are taken from equation 5 of Ganguly and Kennedy (1974). Equation (26) treats garnet_{ss} as a simple mixture of four end-member components, and is regressed on the data pairs of biotite, chlorite and staurolite coexisting with garnet in the assemblages of Guidotti (1974) from the upper staurolite zone. The following points must be taken into account:

- (i) garnet solid solution may depart significantly from a simple mixture model (Guggenheim, 1967);
- (ii) the different coefficients of equation (26) for the various mineral pairs are derived by regression from data that are compositionally closely clustered. Application of equation (26) to compositions outside the range used to derive the coefficients may lead to errors in estimated K_D 's;
- (iii) equation (26) requires that the minerals paired with garnet be ideal solutions for Fe-Mg mixing;
- (iv) equation (26) also requires that, if any other compositional

effects vary K_D (e.g. Al content of biotite), then this variable must be kept constant.

The coefficients of the estimating equations derived from Guidotti's data are presented in table 7. The signs of the coefficients are the same as those of Ganguly and Kennedy (1974, eqn. 5), and are consistent with the explanation of Dallmeyer (1974; note reciprocal K_D is used here) for garnet substitution. The observed and estimated K_D 's are in general agreement (table 7). The differences become less pronounced when viewed against the observed range of K_D 's in the data of Guidotti (1974), especially when the small compositional range of those minerals is considered against the much larger range in the Jervois assemblages.

When recast in the form $K_{D_{Mg-Fe}}^{gt-bio}$ and corrected for Mn and Ca (relative effects based on Ganguly and Kennedy, 1974) using the data of Albee (1965c), the observed distribution coefficients fall between 0.15 and 0.27. Although the higher values are consistent with staurolite-zone rocks, the lower figures fall below those appropriate for the garnet zone (Albee, 1965c). This situation accentuates the problems associated with the rigorous use of K_D 's as geothermometers, namely, the very approximate nature of the compositional corrections, and possibly the largely undetermined effects of varying f_{O_2} on K_D .

Multivariate linear regression methods used to evaluate K_D as a function of temperature and composition (e.g. Saxena, 1969b, still suffer from several drawbacks:

SAMPLE No. (PARAGENESIS)	K_D $\frac{\text{bio-gt}}{\text{Mg-Fe}}$	K_D $\frac{\text{chlt-gt}}{\text{Mg-Fe}}$	K_D $\frac{\text{stlt-gt}}{\text{Mg-Fe}}$	K_D $\frac{\text{bio-stlt}}{\text{Mg-Fe}}$
826 (6)	<u>8.84</u> 5.70	<u>6.28</u> 3.61 R 3.27	<u>1.67</u> 0.98	<u>5.29</u>
827 (7)	<u>6.72</u> 6.00	<u>6.18</u> 4.26	<u>1.77</u> 1.11	<u>3.79</u>
830 (8)	<u>6.36</u> 7.92	* * R 3.88	<u>1.44</u> 1.56	<u>4.42</u>
829 (9)	<u>7.34</u> 8.10	* *	<u>1.65</u> 1.23	<u>4.45</u>
Range of K_D 's from the data of Guidotti (1974)	<u>7.20</u> to <u>8.18</u>	<u>8.22</u> to <u>9.51</u>	<u>1.49</u> to <u>1.78</u>	<u>4.28</u> to <u>5.13</u>

Numbers underlined represent observed K_D 's. Values immediately below these (not underlined) are predicted from the regression equations below, derived from the data of Guidotti (1974), based on the method of Ganguly and Kennedy (1974). Values prefixed by "R" are for secondary (retrograde) chlorite.

$$\ln K_D^{\text{bio-gt}} = 2.8514(x_{\text{Fe}}^{\text{gt}} - x_{\text{Mg}}^{\text{gt}}) + 4.7123(x_{\text{Mn}}^{\text{gt}} + 2x_{\text{Ca}}^{\text{gt}}) - 0.7425$$

R = 0.974

$$\ln K_D^{\text{chlt-gt}} = 5.6750(x_{\text{Fe}}^{\text{gt}} - x_{\text{Mg}}^{\text{gt}}) + 11.5056(x_{\text{Mn}}^{\text{gt}} + 2x_{\text{Ca}}^{\text{gt}}) - 3.7571$$

R = 0.953

$$\ln K_D^{\text{stlt-gt}} = 0.1436(x_{\text{Fe}}^{\text{gt}} - x_{\text{Mg}}^{\text{gt}}) + 4.1509(x_{\text{Mn}}^{\text{gt}} + 2x_{\text{Ca}}^{\text{gt}}) - 0.3273$$

R = 0.752

gt - garnet; bio - biotite; chlt - chlorite; stlt - staurolite.

TABLE 7: Comparison of observed K_D 's in staurolite-bearing rocks from the Jervois Range area with those observed and predicted from the Rangeley Quadrangle, Maine, taking garnet solid-solution to be a "simple mixture" of four end-member components.

- (i) the relationship of K_D to composition need not be linear for any or all components in either or both phases;
- (ii) where data from several areas are used, it becomes difficult to account accurately for differences in physical conditions between the areas;
- (iii) use of older, mineral concentrate data introduces errors with respect to the real compositions of garnet rims in zoned grains.

The distribution coefficients between primary chlorite and garnet appear to be consistent with lower amphibolite facies conditions (Kamineni, 1976; note use of reciprocal K_D). However, since biotite is probably close to an ideal Fe-Mg solid solution for fixed Al and Ti content (Mueller, 1972), the coexistence of some chlorites with less magnesian biotite, and others with more magnesian biotite, implies strong non-ideality for chlorite solid solutions. This, in turn, reduces the significance of similar K_D values for chlorites with different compositions coexisting with garnet. A similar relationship has been observed by Albee (1965a), who noted that at garnet $Mg = 9$, $K_{D_{Mg-Fe}}^{chl-gt}$ varied from 7.5 at chlorite $Mg = 36$ to 12.3 at chlorite $Mg = 55$, within the kyanite zone in the Lincoln Mountain Quadrangle.

Use of garnet analyses corrected for andradite component in table 7 does little to alter the numerical values of the distribution coefficients. However, differing f_{O_2} conditions between the Jervois Range (+ magnetite + ilmenite) and Rangeley Quadrangle (+ graphite)

assemblages may account for some of the differences between the observed and predicted K_D 's. In general, element partitioning between phases from the two areas suggests similar temperatures of metamorphism.

The bulk-rock geochemistry of these rocks will be discussed at the end of the next chapter.

CHAPTER 5: PELITIC SCHISTS IN THE JERVOIS RANGE AREA

5.1 Petrography

The rocks discussed in this chapter range from magnetite-free, muscovite-rich schists, through muscovite-biotite schists, to andalusite- and cordierite-bearing schists and gneisses. Most of these assemblages vary considerably in their magnetite content, and magnetite-quartz gneisses containing biotite and chlorite are also included here. Although the bulk-rock compositions of many of these rocks are high in FeO, much of this component is contained in magnetite, so that the Fe-Mg silicates have intermediate to high Mg values. As a result, garnets in these assemblages are Mn-rich, and owe their stability to high Mn contents of the rocks.

With the exception of sample 855 from the mine sequence, the cordierite in these rocks occurs as rounded, or commonly deformed, ovoid poikiloblasts up to 20 mm in length. The inclusions in the "cordierite" consist of numerous rounded or ovoid quartz grains (average length about 0.03 mm), and, in some samples, the poikiloblasts also contain larger, idioblastic chlorite or biotite inclusions, as well as magnetite and other opaque oxide grains. The "cordierite" in these poikiloblasts has been entirely retrogressed to very fine, felted aggregates of chlorite and white mica ("pinitite"), commonly exhibiting a yellowish-brown tinge in plane-polarized light. In some samples (e.g. 870) the retrograde products are rich

in chlorite and contain (hydrated?) iron oxides, giving the poikiloblasts a dark, green-brown colour. In these cases, the poikiloblasts are repeatedly zoned, with alternating chlorite-rich and chlorite-poor zones commonly separated by thin bands rich in iron oxides.

Whereas the volume of biotite altered to chlorite in rocks that do not contain retrogressed cordierite is quite small (in many rocks almost negligible), the volume of biotite altered to chlorite in rocks that do contain retrogressed cordierite poikiloblasts is large. In many of the latter rocks, the alteration to chlorite is complete.

Some assemblages contain what appears to be idioblastic primary chlorite (see chapter 4). This primary chlorite has grayish-brown interference colours, contrasting sharply with the retrograde chlorite (replacing biotite and/or garnet), which has bluish-purple interference colours, and which is also much darker green in plane-polarized light. However, in rocks in which the colour difference is not marked, textural criteria indicate that "both" chlorites are retrograde. In such rocks, where chlorite of one colour occurs in, or adjacent to, solution channels and cracks, later differential oxidation of one generation of chlorite may be responsible for the colour variation.

In some rocks, chlorite also occurs in veins, together with adularia, and, less commonly, calcite. This chlorite is darker still in plane-polarized light, and is generally more iron-rich than

the retrograde chlorite, although, in several rocks, microprobe analysis has shown that retrograde and vein chlorite are similar in composition.

Surface samples, and many taken from shallow depths in drill cores, commonly exhibit part or complete alteration of magnetite ("martitisation"; Ramdohr, 1969) and may be accompanied by the accumulation of haematite and limonite along mica cleavage and grain boundaries. (The bulk-rock compositions of such samples cannot be reliably plotted on an AFM diagram, since the total Fe^{2+} in silicates cannot be evaluated.) Rocks in which Fe-Mg silicates have been altered (oxidized) were not subjected to analysis.

Sillimanite ("fibrolite") occurs in several localities west of the Jervois Range, in quartz-muscovite-biotite-magnetite schists, with or without andalusite. The sillimanite has preferentially nucleated in muscovite, and, to a lesser extent, in adjacent quartz grains, and only small amounts of sillimanite occur in biotite. Where present, andalusite shows no evidence of replacement by sillimanite or any other mineral formed in the sillimanite-forming reaction.

Brief petrographic descriptions of selected, analysed rocks appear in the appendix (appendix table 4 et seq.), together with abbreviated microprobe data for those samples not specifically listed in the text.

5.2 Phase Relations

The pelitic rocks and quartz-magnetite gneisses discussed here, plus the rocks of chapters 4 and 6, occur in five major outcrop units in the Jervois Range area. Within each of these units, and especially in the "mine sequence", where drill core has provided unweathered material, there is great variation in both the thickness and bulk composition of the individual horizons. Extensive weathering precludes the detailed mapping of mineral assemblages, and thin horizons or lenses (< 1 m) cannot be traced over any considerable distance.

Examination of five drill cores, extending some 200 m along strike in the Jervois Mine area, shows that most units less than 10 m in maximum thickness occur as interbedded lens-shaped bodies rather than as continuous thin beds. Even some of the thicker units (up to 40 m in thickness) occur as a series of large-scale, discontinuous lenses, and many of these contain smaller lenses of contrasting bulk composition.

The silicate assemblages in this chapter represent bulk compositions lying within, and to the magnesian side of, the join andalusite - biotite. They are found over a larger area, and represent a larger temperature range, than the staurolite-bearing assemblages of the previous chapter. The highest-grade parageneses observed (or inferred in the case of retrogressed cordierite) in the Jervois Range area are as follows:

chlorite-muscovite-quartz	(27)
chlorite-andalusite-biotite-muscovite-quartz	(28)
biotite-muscovite-quartz	(29)
biotite-andalusite-muscovite-quartz	(30)
biotite-chlorite-muscovite-quartz	(31)
cordierite-biotite-muscovite-quartz	(32)
cordierite-biotite-andalusite-muscovite-quartz	(33)
cordierite-biotite-chlorite-muscovite-quartz	(34)
sillimanite-biotite-muscovite-quartz	(35)
sillimanite-biotite-(andalusite)-muscovite-quartz	(36)

All of the above parageneses may contain varying amounts of magnetite, with or without ilmenite, and may also contain garnet if the bulk-rock MnO content exceeds 0.3%. Minor amounts of plagioclase are present in some of the parageneses, and apatite may form up to 3.2% of some rocks (e.g. sample 865, containing 1.19% P_2O_5). Trace amounts of ferroan gahnite may be present in rocks in which $ZnO > 0.2\%$. However, if the rock is rich in chlorite and/or magnetite and/or garnet, no gahnite is present, as the Zn is then contained in zinc-bearing chlorite (Fron del and Ito, 1975; see also Guidotti, 1974, table 7), zinc-bearing garnet (Guidotti, 1974, tables 11A, B, C), and possibly, in a franklinite component of magnetite. Trace amounts of zircon may be present in some rocks, and recrystallized detrital tourmaline (as distinct from

metasomatically introduced tourmaline, as discussed in chapter 4) may form up to 8% of some thin (2m), muscovite-rich units.

Less common assemblages include muscovite \pm quartz \pm garnet, without magnetite or biotite or chlorite, and the muscovite-free quartz-magnetite-garnet \pm chlorite \pm biotite rocks, which grade compositionally into magnetite-quartzites.

Parageneses (28) and (30) imply that, in the SAFMKH system of figure 5, the tie line staurolite-chlorite has been broken by reaction (18). If, as was suggested in the previous chapter, the chlorite field is split into two regions, then biotite + andalusite may be stable without breaking the staurolite-chlorite tie line (fig. 9). At pressures above the invariant point (Gt) in figure 5, where chlorite + aluminosilicate are still stable, staurolite may be stabilized to the higher-temperature side of reaction curve (18) by significant amounts of Zn.

Paragenesis (33) lies to the higher-temperature side of reaction curve (15) (fig. 5). However, information regarding the compositional control of mineral assemblages is lost in schematic analyses that hold mineral compositions invariant. Since in a real system the variance of reaction (15) is increased by Na and Ti in the micas, paragenesis (33) may be stable under the same conditions at which chlorite is still stable (e.g. A. Thompson, 1976, fig. 1C).

5.3 Mineral Compositions and Distribution of Elements between Minerals in the Metapelitic Schists

Introduction

Parageneses (28), (33) and (34) are limiting assemblages (in the sense of Albee, 1965c) in the simple system SAFMKH. Strictly, however, the presence of Mn (in the absence of garnet), Ti (in the absence of ilmenite and rutile), Ca (in the absence of garnet and plagioclase) and Na (in the absence of feldspar) gives these parageneses several degrees of compositional freedom. As a consequence, the compositions of minerals from several identical parageneses, even within relatively small domains such as 5 m of drill core, need not be identical, even if f_{H_2O} and f_{O_2} are assumed to be externally buffered, and thus constant, over the whole domain.

Another consequence of the presence of these minor components is illustrated by sample 870, in which the assemblage cordierite-andalusite-biotite-chlorite-muscovite-quartz occurs. This assemblage, with vapour, is univariant in the simple system SAFMKH. For this assemblage to be stable over a range of P and T in the simple system, the phase rule demands that the sample be divided into domains of (mosaic) equilibrium, each of which must contain at least one less mineral than the total assemblage. In the thin sections examined, cordierite (retrogressed, as described previously) is not in contact with andalusite, and three compositional domains may be inferred (each containing muscovite + quartz), namely:

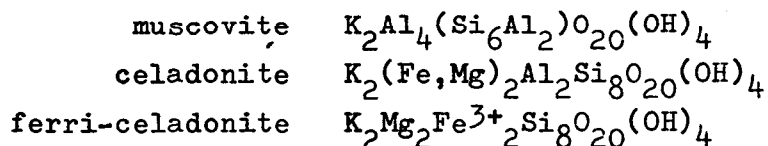
- (i) andalusite-biotite-chlorite
- (ii) biotite-chlorite
- (iii) cordierite-biotite-chlorite

However, in the real system, the partitioning of Mn (in the absence of garnet) into chlorite, and Na (in the absence of feldspar) into muscovite (see table 16) removes the necessity of invoking mosaic equilibrium to satisfy the constraints of the phase rule in the simple system. This is consistent with the uniformity of the composition of the primary chlorite and unaltered biotite in all the above "domains".

Microprobe analyses of minerals of representative parageneses are presented in tables 8 to 17.

Muscovite

Employing the terminology of Guidotti and Sassi (1976), limited octahedral and tetrahedral substitutions in muscovite may be described in the pseudoternary system:



Parameters that increase with increasing celadonite content in muscovite may be defined as follows (Guidotti and Sassi, 1976, p.103):

$$\begin{aligned} si &= Si - 6 \\ mf &= Mg + Fe^{2+} \\ a &= 6 - \sum Al \end{aligned}$$

If the coupled octahedral-tetrahedral substitution in muscovite is

SAMPLE 874 PARAGENESIS (28)

CHLORITE-BIOTITE-MUSCOVITE-ANDALUSITE-QUARTZ SCHIST

	<u>CHLORITE</u>	<u>BIOTITE</u>	<u>MUSCOVITE</u>
SiO ₂	22.66	35.21	45.39
TiO ₂	.12	1.41	.18
Al ₂ O ₃	22.88	19.74	35.64
FeO	28.78	22.26	2.50
MnO	.20	.00	.00
MgO	11.75	8.14	.57
CaO	.00	.10	.00
Na ₂ O	.00	.17	.88
K ₂ O	.00	9.20	9.74
<u>TOTAL</u>	<u>86.39</u>	<u>96.23</u>	<u>94.90</u>
CATIONS			
PER No.	28	22	22
OXYGENS			
Si	4.9684	5.3670	6.0865
Ti	.0198	.1616	.0182
Al	5.9123	3.5462	5.6324
Fe	5.2771	2.8375	.2803
Mn	.0371		
Mg	3.8405	1.8497	.1139
Ca		.0163	
Na		.0502	.2288
K		1.7888	1.6660
<u>TOTAL</u>	<u>20.0552</u>	<u>15.6173</u>	<u>14.0261</u>
<u>Mg</u>	42.12	39.46	
Al ^{iv}	3.0316	2.6330	1.9135
Al ^{vi}	2.8807	.9132	3.7189

TABLE 8: Microprobe analyses of minerals in paragenesis (28).

PARAGENESIS (29)

MUSCOVITE-BIOTITE-QUARTZ±GARNET SCHISTS

SAMPLE 853					SAMPLE 875	
	CHLORITE alt.bio.	MUSCOVITE	GARNET core	GARNET rim	BIOTITE	MUSCOVITE
SiO ₂	23.66	47.04	35.73	35.76	35.45	45.74
TiO ₂	.18	.00	.39	.00	1.47	.43
Al ₂ O ₃	19.33	34.38	21.25	20.59	19.42	34.82
FeO	35.24	2.11	30.54	31.93	20.37	2.34
MnO	1.23	.00	9.52	9.53	.00	.00
MgO	6.60	1.15	1.22	1.32	10.10	.69
CaO	.00	.00	1.15	.68	.00	.08
Na ₂ O	.00	1.14	.00	.00	.17	.76
K ₂ O	.00	9.25	.00	.00	8.77	9.95
TOTAL	86.24	95.07	99.80	99.81	95.75	94.81
CATIONS PER No. OXYGENS	28	22	12	12	22	22
Si	5.4250	6.2590	2.9313	2.9515	5.3678	6.1419
Ti	.0310		.0241		.1674	.0434
Al	5.2236	5.3913	2.0546	2.0028	3.4656	5.5104
Fe	6.7573	.2348	2.0953	2.2039	2.5794	.2628
Mn	.2389		.6615	.6662		
Mg	2.2560	.2281	.1492	.1624	2.2798	.1381
Ca			.1011	.0601		.0115
Na		.2941			.0499	.1979
K		1.5700			1.6939	1.7043
TOTAL	19.9318	13.9773	8.0171	8.0469	15.6038	14.0103
Mg	25.03		6.65	6.86	46.92	
X _{Fe}			69.68	71.26		
X _{Mg}			4.96	5.25		
X _{Mn}			22.00	21.54		
X _{Ca}			3.36	1.94		
Al ^{iv}	2.5750	1.7410			2.6322	1.8581
Al ^{vi}	2.6486	3.6503			.8334	3.6523

TABLE 9: Microprobe analyses of minerals in paragenesis (29).

PARAGENESIS (30)

ANDALUSITE-BIOTITE-MUSCOVITE-QUARTZ+GARNET SCHISTS

	SAMPLE 833			SAMPLE 856			SAMPLE 871		
	CHLORITE	MUSCOVITE	CHLORITE	BIOTITE	GARNET	GARNET	CHLORITE	BIOTITE	MUSCOVITE
	alt.bio.		alt.bio.		core	rim	alt.bio.		
SiO ₂	25.05	45.90	23.03	34.40	35.71	36.05	26.05	35.01	46.57
TiO ₂	.00	.45	.16	1.59	.00	.00	.00	1.70	.26
Al ₂ O ₃	22.40	34.88	22.51	20.34	20.67	20.71	19.88	20.94	34.95
FeO	23.24	2.54	30.83	23.32	32.58	33.48	26.13	20.23	2.32
MnO	.44	.00	.25	.00	7.30	6.17	.22	.00	.00
MgO	14.92	.64	10.73	7.96	2.14	2.02	14.28	9.33	.73
CaO	.00	.00	.00	.00	1.58	1.57	.00	.21	.00
Na ₂ O	.00	.69	.00	.23	.00	.00	.00	.36	.92
K ₂ O	.00	9.81	.00	8.50	.00	.00	.00	8.22	9.73
TOTAL	86.05	94.91	87.31	96.34	99.98	100.00	86.56	96.00	95.48
CATIONS PER No. OXYGENS	28	22	28	22	12	12	28	22	22
Si	5.3237	6.1519	5.0484	5.2496	2.9296	2.9503	5.5826	5.2668	6.1927
Ti		.0454	.0264	.1825				.1923	.0260
Al	5.6105	5.5096	5.7637	3.6582	1.9985	1.9975	5.0243	5.7126	5.4773
Fe	4.1304	.2847	5.6517	2.9761	2.2352	2.2913	4.6859	2.5451	.2560
Mn	.0792		.0464		.5072	.4277	.0400		
Mg	4.7269	.1279	3.5064	1.8108	.2617	.2464	4.5650	2.0924	.1447
Ca					.1389	.1377		.0338	
Na		.1793		.0681				.1050	.2372
K		1.6772		1.6546				1.5774	1.6504
TOTAL	19.8707	13.9760	20.0430	15.5999	8.0711	8.0509	19.9014	15.5254	13.9863
Mg	53.37		38.29	37.83	10.48	9.71	49.35	45.12	
X _{Fe}					71.12	73.84			
X _{Mg}					8.33	7.94			
X _{Mn}					16.14	13.78			
X _{Ca}					4.42	4.44			
Al ^{iv}	2.6763	1.8481	2.9516	2.7504			2.4174	2.7332	1.8073
Al ^{vi}	2.9342	3.6615	2.8121	.9078			2.6069	.9794	3.6700

TABLE 10: Microprobe analyses of minerals in paragenesis (30).

PARAGENESIS (31)

CHLORITE-BIOTITE-MUSCOVITE-QUARTZ-GARNET SCHISTS

SAMPLE 846				SAMPLE 850				SAMPLE 873			
CHLORITE	CHLORITE	GARNET	GARNET	CHLORITE	CHLORITE	MUSCOVITE	GARNET	GARNET	CHLORITE	MUSCOVITE	
primary	alt.bio.	core	rim	primary	alt.bio.		core	rim	primary		
SiO ₂	24.17	24.31	36.61	36.77	25.54	23.98	46.12	36.45	36.31	23.64	45.89
TiO ₂	.15	.00	.00	.00	.00	.00	.00	.11	.10	.00	.26
Al ₂ O ₃	22.66	19.92	20.60	20.54	20.29	20.16	34.99	20.32	19.98	22.84	35.09
FeO	22.74	29.03	26.72	27.12	23.65	27.17	2.72	19.41	16.88	27.24	2.07
MnO	.38	1.26	10.81	10.42	1.19	1.51	.00	18.51	22.58	.15	.00
MgO	16.89	11.22	2.74	2.93	15.40	13.07	.44	2.45	1.92	12.26	.50
CaO	.00	.00	2.54	2.18	.00	.00	.00	2.64	1.83	.00	.98
Na ₂ O	.00	.00	.00	.00	.00	.00	.30	.00	.00	.00	.95
K ₂ O	.00	.00	.00	.00	.00	.00	10.48	.00	.00	.00	9.97
TOTAL	86.99	85.74	100.02	99.96	86.07	85.89	95.05	99.89	99.80	86.13	94.91
CATIONS PER No. OXYGENS	28	28	12	12	28	28	22	12	12	28	22
Si	5.0829	5.4062	2.9695	2.9801	5.4717	5.2834	6.1867	2.9678	2.9894	5.1374	6.1486
Ti	.0237							.0067	.0062		.0262
Al	5.6162	5.2209	1.9692	1.9619	5.1231	5.2548	5.5317	1.9499	1.9280	5.8498	5.5410
Fe	3.9992	5.3989	1.8142	1.8381	4.2372	5.0061	.3051	1.3216	1.1558	4.9506	.2319
Mn	.0677	.2373	.7426	.7153	.2159	.2818		1.2765	1.5659	.0276	
Mg	5.2950	3.7196	.3313	.3540	4.9184	4.2928	.0880	.2974	.2344	5.9718	.1198
Ca			.2207	.1893				.2303	.1605		.0115
Na							.0780				.2468
K							1.7933				1.7040
TOTAL	50.0847	19.9829	8.0457	8.0387	19.9663	20.0989	13.9828	8.0502	8.0402	19.9372	14.0298
Mg	56.97	40.79	15.45	16.15	53.72	46.16		18.37	16.86	44.51	
X _{Fe}			58.36	59.36				42.28	37.09		
X _{Mg}			10.66	11.43				9.51	7.52		
X _{Mn}			23.89	23.10				40.84	50.24		
X _{Ca}			7.10	6.11				7.37	5.15		
Al ^{iv}	2.9171	2.5938			2.5283	2.7166	1.8133			2.8626	1.8514
Al ^{vi}	2.6991	2.6271			2.5948	2.5182	3.7184			2.9872	3.6896
COMP. COEX. FELSPAR										An: 44.58 Ab: 53.76 Or: 1.66	

TABLE 11: Microprobe analyses of minerals in paragenesis (31).

PARAGENESIS (32)

CORDIERITE-BIOTITE-MUSCOVITE-QUARTZ SCHISTS

	SAMPLE 837		SAMPLE 838	
	<u>CHLORITE</u>	<u>BIOTITE</u>	<u>BIOTITE</u>	<u>MUSCOVITE</u>
	alt.bio.			
SiO ₂	24.42	36.07	37.54	46.01
TiO ₂	.26	1.27	1.28	.39
Al ₂ O ₃	22.93	20.07	19.85	34.66
FeO	21.54	17.82	13.46	2.46
MnO	.40	.20	.00	.00
MgO	16.27	11.73	14.34	1.15
CaO	.00	.00	.00	.00
Na ₂ O	.00	.40	.18	.79
K ₂ O	.00	8.48	9.24	9.72
<u>TOTAL</u>	<u>85.82</u>	<u>96.04</u>	<u>95.89</u>	<u>95.18</u>
CATIONS				
PER No.	28	22	22	22
OXYGENS				
Si	5.1653	5.3659	5.4767	6.1489
Ti	.0414	.1421	.1404	.0392
Al	5.7161	3.5188	3.4130	5.4591
Fe	3.8102	2.2169	1.6422	.2749
Mn	.0717	.0252		
Mg	5.1302	2.6013	3.1187	.2291
Ca				
Na		.1154	.0509	.2047
K		1.6092	1.7195	1.6570
<u>TOTAL</u>	<u>19.9349</u>	<u>15.5948</u>	<u>15.5614</u>	<u>14.0129</u>
<u>Mg</u>	57.38	53.99	65.51	
Al ^{iv}	2.8347	2.6341	2.5233	1.8511
Al ^{vi}	2.8814	.8847	.8897	3.6080

TABLE 12: Microprobe analyses of minerals in paragenesis (32).

SAMPLE 855 PARAGENESIS (33)

CORDIERITE-ANDALUSITE-BIOTITE-MUSCOVITE-QUARTZ SCHIST

	<u>CHLORITE</u>	<u>BIOTITE</u>	<u>MUSCOVITE</u>	<u>CORDIERITE</u>
	alt.bio.			
SiO ₂	23.06	35.79	45.48	47.58
TiO ₂	.00	1.54	.00	.00
Al ₂ O ₃	23.40	19.25	35.69	33.18
FeO	23.66	19.87	2.22	7.20
MnO	.43	.00	.00	.86
MgO	15.36	10.82	.97	8.29
CaO	.00	.00	.00	.00
Na ₂ O	.00	.41	.88	.78
K ₂ O	.00	8.60	9.72	.00
<u>TOTAL</u>	<u>85.91</u>	<u>96.28</u>	<u>94.96</u>	<u>97.89</u>
CATIONS				
PER No.	28	22	22	18
OXYGENS				
Si	4.9463	5.3725	6.0857	4.9311
Ti		.1738		
Al	5.9154	3.4056	5.6284	4.0527
Fe	4.2441	2.4944	.2484	.6240
Mn	.0781			.0755
Mg	4.9115	2.4213	.1935	1.2808
Ca				
Na		.1193	.2283	.1567
K		1.6484	1.6591	
<u>TOTAL</u>	<u>20.0954</u>	<u>15.6337</u>	<u>14.0434</u>	<u>11.1208</u>
<u>Mg</u>	53.64	49.26		67.24
Al ^{iv}	3.0537	2.6275	1.9143	1.0689
Al ^{vi}	2.8617	.7781	3.7141	2.9838

TABLE 13: Microprobe analyses of minerals in paragenesis (33).

PARAGENESIS (34)?

CORDIERITE-CHLORITE-BIOTITE-MUSCOVITE-QUARTZ SCHISTS

SAMPLE 854				SAMPLE 859	
	<u>CHLORITE</u>	<u>"CHLORITE"</u>	<u>MUSCOVITE</u>	<u>CHLORITE</u>	<u>BIOTITE</u>
	primary?	alt.bio.		primary?	
SiO ₂	25.99	28.12	45.81	23.45	35.70
TiO ₂	.25	.33	.25	.16	1.65
Al ₂ O ₃	22.29	20.63	34.12	23.09	20.01
FeO	14.54	17.27	2.84	25.34	19.76
MnO	.43	.72	.00	.37	.00
MgO	22.52	17.28	1.07	14.13	9.66
CaO	.00	.00	.00	.00	.00
Na ₂ O	.00	.38	1.27	.00	.00
K ₂ O	.00	1.59	9.56	.00	9.00
<u>TOTAL</u>	<u>86.02</u>	<u>86.05</u>	<u>94.92</u>	<u>86.54</u>	<u>95.78</u>
CATIONS					
PER No.	28	28	22	28	22
OXYGENS					
Si	5.2788	5.8355	6.1597	5.0302	5.3823
Ti	.0382	.0515	.0253	.0258	.1871
Al	5.3356	4.9795	5.4070	5.8374	3.5554
Fe	2.4697	2.9971	.3194	4.5457	2.4913
Mn	.0740	.1266		.0672	
Mg	6.8186	5.3457	.2145	4.5184	2.1711
Ca					
Na		.1529	.3311		
K		.4209	1.6397		1.7308
<u>TOTAL</u>	<u>20.0149</u>	<u>19.9097</u>	<u>14.0967</u>	<u>20.0247</u>	<u>15.5180</u>
<u>Mg</u>	<u>73.41</u>	<u>64.08</u>		<u>49.85</u>	<u>46.57</u>
Al ^{iv}	2.7212	2.1645	1.8403	2.9698	2.6177
Al ^{vi}	2.6144	2.8150	3.5667	2.8676	.9377

TABLE 14: Microprobe analyses of minerals in paragenesis (34)?
Textural criteria with respect to chlorite in these
samples are ambiguous.

SAMPLE 857 PARAGENESIS (34)

CORDIERITE-CHLORITE-BIOTITE-MUSCOVITE-QUARTZ SCHIST

	CHLORITE	CHLORITE	CHLORITE	CHLORITE	BIOTITE	MUSCOVITE	"MUSCOV."
		alt.bio.	alt.crd.	in veins			alt.crd.
SiO ₂	26.78	26.96	28.74	26.71	37.91	45.71	48.08
TiO ₂	.00	.13	.00	.00	1.35	.42	.00
Al ₂ C ₃	23.16	21.02	22.75	20.22	19.53	34.18	30.63
FeO	15.40	20.26	21.43	26.89	13.43	3.01	3.82
MnO	.60	.71	.76	1.10	.00	.00	.00
MgO	20.33	16.76	12.16	10.79	14.68	1.17	2.80
CaO	.00	.00	.00	.00	.00	.00	.10
Na ₂ O	.00	.00	.00	.00	.20	.78	.00
K ₂ O	.00	.00	.00	.00	9.04	9.63	8.67
<u>TOTAL</u>	<u>86.27</u>	<u>85.84</u>	<u>85.84</u>	<u>85.71</u>	<u>96.14</u>	<u>94.90</u>	<u>94.10</u>
CATIONS PER No. OXYGENS	28	28	28	28	22	22	22
Si	5.4258	5.6416	5.9878	5.8123	5.5068	6.1454	6.4768
Ti		.0205			.1475	.0425	
Al	5.5302	5.1840	5.5862	5.1857	3.3435	5.4158	4.8628
Fe	2.6093	3.5454	3.7338	4.8935	1.6314	.3384	.4303
Mn	.1030	.1258	.1341	.2027			
Mg	6.1404	5.2283	3.7767	3.5002	3.1789	.2345	.5623
Ca							.0144
Na					.0563	.2033	
K					1.6751	1.6515	1.4898
<u>TOTAL</u>	<u>19.8087</u>	<u>19.7456</u>	<u>19.2186</u>	<u>19.5944</u>	<u>15.5395</u>	<u>14.0314</u>	<u>13.8364</u>
<u>Mg</u>	<u>70.18</u>	<u>59.59</u>	<u>50.29</u>	<u>41.70</u>	<u>66.09</u>		
Al ^{iv}	2.5742	2.3584	2.0122	2.1877	2.4392	1.8546	1.5252
Al ^{vi}	2.9560	2.8256	3.5740	2.9980	.8503	3.5612	3.3396

TABLE 15: Microprobe analyses of minerals in paragenesis (34).

SAMPLE 870

ANDALUSITE-CORDIERITE-CHLORITE-BIOTITE-MUSCOVITE-QUARTZ SCHIST

	<u>CHLORITE</u>	<u>"CHLORITE"</u>	<u>BIOTITE</u>	<u>MUSCOVITE</u>
		altd. crd.		
SiO ₂	24.21	27.74	37.38	46.22
TiO ₂	.10	.00	1.32	.32
Al ₂ O ₃	23.24	24.94	20.07	35.21
FeO	21.02	21.31	16.29	2.08
MnO	.49	.68	.00	.00
MgO	16.89	9.70	12.38	.56
CaO	.00	.00	.00	.00
Na ₂ O	.00	.63	.23	1.27
K ₂ O	.00	1.21	8.53	9.12
<u>TOTAL</u>	<u>85.95</u>	<u>86.21</u>	<u>96.10</u>	<u>94.78</u>
CATIONS PER No. OXYGENS	28	28	22	22
Si	5.1034	5.8046	5.4762	6.1705
Ti	.0159		.1458	.0321
Al	5.7736	6.1505	3.4745	5.5399
Fe	3.7055	3.7290	2.0011	.2322
Mn	.0875	.1205		
Mg	5.3076	3.0258	2.7110	.1114
Ca				
Na		.2556	.0655	.3287
K		.3230	1.5983	1.5531
<u>TOTAL</u>	<u>19.9935</u>	<u>19.4090</u>	<u>15.4724</u>	<u>13.9679</u>
<u>Mg</u>	58.88	44.79	57.53	
Al ^{iv}	2.8966	2.1954	2.5238	1.8295
Al ^{vi}	2.8770	3.9551	.9507	3.7104

TABLE 16: Microprobe analyses of minerals in sample 870. For a discussion of its paragenesis, see text, page 91.

MINERALS IN GARNET-BEARING, MUSCOVITE-FREE SCHISTS

SAMPLE 847				SAMPLE 862		SAMPLE 863	
CHLORITE	CHLORITE	GARNET	GARNET	BIOTITE	GARNET	CHLORITE	GARNET
	alt.bio.	core	rim		rim		rim
SiO ₂	25.33	27.83	36.74	40.50	36.01	26.18	36.96
TiO ₂	.00	.00	.12	1.35	.23	.00	.13
Al ₂ O ₃	22.39	18.76	20.41	13.60	19.35	18.53	19.73
FeO	18.58	22.54	23.47	13.14	16.69	23.78	15.83
MnO	.43	.81	11.99	.59	23.61	4.42	22.40
MgO	19.27	15.96	2.93	17.31	1.53	12.95	1.37
CaO	.00	.00	4.04	.00	2.56	.00	3.57
Na ₂ O	.00	.00	.00	.46	.00	.00	.00
K ₂ O	.00	.00	.00	8.82	.00	.00	.00
TOTAL	86.00	85.90	99.70	95.77	99.98	85.68	99.99
CATIONS PER No. OXYGENS	28	28	12	22	12	28	12
Si	5.2586	5.8964	2.9744	5.9227	2.9688	5.7244	3.0156
Ti			.0073	.1485	.0143		.0080
Al	5.4782	4.6844	1.9474	2.3440	1.8801	4.7751	1.8972
Fe	3.2257	3.9937	1.5890	1.6070	1.1507	4.3483	1.0801
Mn	.0756	.1454	.8222	.0731	1.6487	.8186	1.5480
Mg	5.9637	5.0409	.3536	3.7736	.1880	4.2212	.1666
Ca			.3504		.2261		.3121
Na				.1304			
K				1.6453			
TOTAL	20.0018	19.7608	8.0443	15.6446	8.0767	19.8876	8.0276
Mg	64.90	55.80	18.20	70.13	14.04	49.26	11.26
X _{Fe}			51.01		35.81		34.77
X _{Mg}			11.35		5.85		5.36
X _{Mn}			26.39		51.31		49.83
X _{Ca}			11.25		7.04		10.05
Al ^{iv}	2.7414	2.1036		2.0773		2.2756	
Al ^{vi}	2.7368	2.5808		.2667		2.4995	

Sample 847: "chloritized" garnet-biotite-chlorite-quartz-magnetite schist

Sample 862: garnet-quartz-magnetite schist with minor biotite

Sample 863: chlorite-garnet-quartz-magnetite schist

TABLE 17: Microprobe analyses of minerals in garnet-bearing, muscovite-free schists.

ideal, the relation between these parameters is: $si = mf = \frac{1}{2}a$
(or $si = a - mf$). The regression relations between these parameters
for 19 primary muscovites taken from parageneses (6) to (9) and
(27) to (34) are as follows:

$$si = 0.1463 mf + 0.0914 \quad r = 0.237 \quad (\text{eqn } 37)$$

$$si = 0.3932 a - 0.0360 \quad r = 0.751 \quad (\text{eqn } 38)$$

$$mf = 0.6329 a + 0.1287 \quad r = 0.745 \quad (\text{eqn } 39)$$

$$si = 0.6764 a - 0.4475 mf + 0.0216 \quad R = 0.893 \quad (\text{eqn } 40)$$

The departures of the regression relations from the ideal relations
are comparable in magnitude with those of the muscovites of Guidotti
(1974), and may be ascribed to a combination of the factors listed
below:

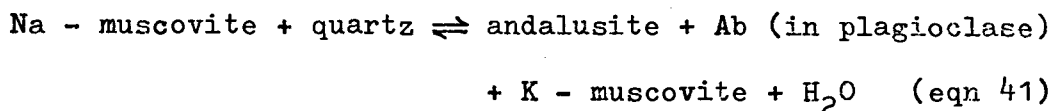
- (i) microprobe analytical errors (see appendix; also Reed
and Ware, 1975);
- (ii) the assumption that all Fe recorded is Fe^{2+} ;
- (iii) the presence of Ti, which allows the octahedral
substitution $AlAl \rightleftharpoons (Mg,Fe)Ti$; accounting for Ti
content does not significantly alter the relations,
possibly because some Ti recorded ($K_{\alpha} = 4.51 \text{ KeV}$)
may be due to the presence of Ba ($L_{\alpha} = 4.47 \text{ keV}$);
- (iv) the presence of elements not sought during analysis,
such as Ba (up to 5227 ppm in the bulk rock), Rb (up
to 1286 ppm), Cs, Li and V (especially in rocks low
in magnetite but high in vanadium).

The average Si, Al and Fe+Mg contents (based on 220's) of 8
muscovites from andalusite-bearing limiting assemblages are 6.147,

5.560 and 0.392, respectively. The Si value agrees well with that of Al-saturated muscovites (6.144) from the upper-staurolite zone of Guidotti (1973, fig. 3), whereas the Al value is lower, and the Fe+Mg value higher, than the corresponding values of 5.678 and 0.158 respectively. If negligible analytical errors are assumed, the differences may be explained by higher f_{O_2} conditions in the Jervois Range area, leading to ferri-celadonite substitution, as distinct from celadonite substitution in the graphite-bearing rocks of Guidotti (1973, 1974).

Although the average Na+K content of primary muscovite from the Jervois Range area (1.880; $s = 0.042$) is similar to that of the upper-staurolite zone in the Rangeley Quadrangle (1.890; $s = 0.048$, Guidotti, 1974, table 8A), the paragonite contents of the former vary from 5 to 19%, whereas those of the latter are approximately constant at 23.5%. As expected, Al- and Na-saturated rocks (containing albite or plagioclase, with or without andalusite) have muscovites with the highest paragonite contents (16 to 19% in the Jervois Range area), but even these figures cannot be used as a direct measure of temperature of formation for the following reasons:

- (i) to overcome bulk-compositional controls, the paragonite contents of muscovites should be compared between identical, limiting assemblages, with similar plagioclase compositions;
- (ii) the paragonite content of muscovite is not a single-valued function of temperature alone, even in limiting assemblages. The reaction



either buffers $f_{\text{H}_2\text{O}}$, or its equilibrium is determined by the externally controlled $f_{\text{H}_2\text{O}}$ (Guidotti and Sassi, 1976, pp. 128-129).

In the Jervois Range area the discontinuous nature of compositional units, plus the sampling difficulties already mentioned, preclude rigorous T and $f_{\text{H}_2\text{O}}$ studies based on muscovite composition. In broad terms, if $f_{\text{H}_2\text{O}}$ is assumed to have been similar in the Rangeley and Jervois areas, temperatures of muscovite formation in the Jervois area are consistent with upper-garnet to transition zone conditions in the Rangeley area (Guidotti and Sassi, 1976, fig. 7).

Biotite

The average properties of 12 biotites from the sillimanite-free assemblages of this chapter are tabulated below. To avoid the effects of gross bulk compositional control, low-Al biotites from assemblages devoid of muscovite (e.g. 862) are not included

	Range	Average	Std. Devn.
<u>Mg</u>	37.83 - 66.09	50.12	9.62
Al/220's	3.21 - 3.71	3.49	0.14
Al ^{iv} /220's	2.47 - 2.75	2.61	0.09
Al ^{vi} /220's	0.73 - 0.98	0.88	0.07
Ti/220's	0.14 - 0.19	0.17	0.02

It must be pointed out that some of the biotite analyses in tables 8 to 17 are of the centres of grains partly altered (marginally) to chlorite. Although the analysed areas may appear to be optically "fresh", there is no guarantee that the analyses

represent the equilibrium compositions of biotites at the highest grade. The same proviso also applies to analyses of optically unaltered biotite laths in rocks in which many of the laths are partly altered to chlorite, even though the centres of the latter may be similar in composition to the former.

Although drawn from seven different parageneses, the data yield the following relationships:

$$\text{Al} = -0.0098 \text{ Mg} + 3.9835 \quad (r = -0.67) \quad (\text{eqn. 42})$$

$$\text{Al}^{\text{iv}} = -0.008 \text{ Mg} + 3.010 \quad (r = -0.83) \quad (\text{eqn. 43})$$

$$\text{Ti} = -0.0013 \text{ Mg} + 0.2351 \quad (r = -0.66) \quad (\text{eqn. 44})$$

These relations probably arise from crystallochemical controls, but as yet are poorly understood (Dallmeyer, 1974; Sobolev, 1972).

There is no significant correlation between Al^{vi} and Mg , in agreement with the findings of Guidotti et al. (1975b) in the Rangeley, Rumford and Old Speck Mountain Quadrangles, Maine.

Garnet

Garnets in these rocks occur as dodecahedra or trapezohedra with diameters less than 2 mm, typically about 1 mm. The cores commonly contain subangular ovoid inclusions of quartz, generally less than 0.05 mm in length. In some specimens, the garnet is partly or completely pseudomorphed by chlorite, and, in these rocks, the biotite is also commonly altered to chlorite. Without exception, all garnets are manganese-rich, and exhibit the following compositional characteristics:

	Range	Average	Std. Devn.
X_{Fe} core	39.2 - 71.1	53.91	11.17
X_{Fe} rim	34.8 - 73.8	49.95	13.52
X_{Mn} core	16.1 - 43.8	30.85	9.88
X_{Mn} rim	13.8 - 51.5	35.87	13.10
X_{Mg} core	5.0 - 11.4	9.01	1.92
X_{Mg} rim	5.3 - 12.3	8.49	2.57
X_{Ca} core	1.8 - 11.3	6.22	2.81
X_{Ca} rim	1.9 - 10.1	5.85	2.31

(based on 9 core and 12 rim analyses, where

$X_{Fe} = Fe/(Fe+Mn+Mg+Ca)$ in atomic %, etc.)

Chemical zoning in these small, Mn-rich garnets is not pronounced, the greatest variation between core and rim compositions being exhibited by the Mn-profile of reverse-zoned garnets partly pseudomorphed ("resorbed") by chlorite. The Mn-enrichment of the rims of partly pseudomorphed garnets results from the strong affinity of the relatively large Mn^{2+} ion for the cubic coordination sites of the garnet. As the garnet breaks down, most of the Mn is not liberated, but remains in the garnet rim, displacing Fe and Mn. As the reaction proceeds, the Mn diffuses further into the garnet. This diffusion process has been documented and discussed by de Bethune et al. (1975), Loomis (1975), Grant and Weiblen (1971) and Mueller and Schneider (1971).

Chlorite

The primary chlorites in these rocks are ripidolitic, with an average Mg value of 59.05 ($s = 9.95$). A few samples, from slightly lower-grade areas to the west of the Jervois Range, contain chlorites which fall outside the ripidolite boundary (e.g. sample 874). As discussed in the previous chapter, this reflects the wider compositional range of chlorite in the presence of quartz at lower temperatures.

In the molecular projection Al_2O_3 -FeO-MgO, the primary chlorites are always more magnesian than the coexisting biotites, although the difference is commonly less than 5%. Where secondary chlorite is also present (i.e. altered biotite) it is less magnesian than primary chlorite, although it may be more or less aluminous. Chlorite flakes in retrogressed cordierite appear to be less magnesian than those replacing biotite (e.g. table 15). However, the former are minute in size, intimately intergrown with white mica, and are commonly accompanied by equally fine-grained opaque oxide grains. As a consequence, their analyses are not reliable.

The Distribution of Fe^{2+} and Mg^{2+} between Coexisting Phases

It is commonly accepted that the Mg values of coexisting ferromagnesian minerals in metapelitic rocks decrease in the following order: cordierite > chlorite > biotite > chloritoid > staurolite > garnet (Albee, 1965a, b, 1972; Fox, 1971, Hess, 1969;

Hensen, 1971; A. Thompson, 1976). The above relation holds for primary chlorite + biotite pairs from assemblages described in this chapter, but an inverse relationship exists for samples 826 and 827 of the previous chapter, i.e. $\text{Mg chlorite} < \text{Mg biotite}$.

Such contrasting relations are not unique to chlorite-biotite pairs. The relation $\text{Mg chloritoid} < \text{Mg staurolite}$, contradictory to that listed above, has been documented by Rumble (1970), Schreyer and Chinner (1966), and Petrov (1969). A similar set of contradictory relations also exists for metamorphic and igneous olivine-orthopyroxene pairs (e.g. Saxena, 1969a; Wood, 1975, etc.).

For such pairs, the distribution coefficient K_D can take on values both less and greater than 1, depending on the composition of the system, even at the same temperature. Graphically, this means that some or all of the nest of K_D curves on a Roozeboom diagram may cross the straight diagonal $K_D = 1$. This implies that the solid solution in one or both minerals is strongly non-ideal, and this in turn can be largely attributed to order-disorder phenomena; compare fig. 12 of Saxena (1973) with figs. 2 and 3 of Grover and Orville (1969).

In contrast, mineral pairs exhibiting near-ideal solid-solution properties have a nest of K_D curves lying on only one side of the diagonal $K_D = 1$, implying that K_D is consistently less or greater than 1, irrespective of composition.

Hence $K_{D_{Mg-Fe}}^{chl t-bio}$ values both less and greater than 1 in the Jervois Range rocks may be explained by the non-ideal behaviour of chlorite solid-solution, because, for similar Al and Ti content, Fe-Mg mixing in biotite is probably nearly ideal (Mueller, 1972).

Chlorite and biotite Mg values in samples 826 and 874 are similar, yet their $K_{D_{Mg-Fe}}^{chl t-bio}$ values are less and greater respectively than 1. This suggests that the concentration of other elements substituting in the octahedral Mg and Fe sites may influence the value of K_D . The non-ideal behaviour of Al substitution for Fe and Mg is demonstrated by equations 45 and 46 which were empirically derived from the six analysed biotite-chlorite pairs described in this and the preceding chapter.

$$K_{D_{Mg-Fe}}^{chl t-bio} = 24.8172 X_{Al^{vi}}^{chl t} - 0.0012 \underline{Mg}^{chl t} - 4.8494$$

$$R = 0.86 \quad (eqn 45)$$

$$K_{D_{Mg-Fe}}^{chl t-bio} = 18.5024 X_{Al^{vi}}^{chl t} + 4.8258 X_{Al^{vi}}^{bio} - 4.1342$$

$$R = 0.92 \quad (eqn 46)$$

(where $X_{Al^{vi}}$ is the atomic fraction $Al^{vi}/(Al^{vi}+Mg+Fe)$).

Listed below are the observed K_D 's from the upper staurolite zone in the Rangeley Quadrangle (Guidotti, 1974), and those predicted for these rocks by equations 45 and 46.

Observed	Predicted (45)	Predicted (46)
1.16	1.19	1.11
1.12	1.30	1.29
1.13	1.25	1.24
1.13	1.32	1.32

The significance of the differences between the two sets of values is hard to assess, owing to the small number of samples available, though the values do suggest similar temperatures of formation.

This approach to the comparison of distribution coefficients from two different areas metamorphosed under similar physical conditions should be further refined and tested, but will require much larger sample sizes, and a wide range of chlorite and biotite compositions to make the derived relations quite general.

For biotite-garnet pairs, $K_{D_{Mg-Fe}}^{bio-gt}$, as defined in table 7, page 82, is equal to 9.25 for sample 856. This is higher by 0.41 than the highest value derived from the staurolite-bearing rocks of chapter 4, and is higher by 1.07 than the highest value derived from the supper-staurolite zone rocks of Guidotti (1974). In the light of the factors that control the value of $K_{D_{Mg-Fe}}^{bio-gt}$ (discussed in chapter 4), these discrepancies cannot suggest any temperature difference between sample 856 and the staurolite-bearing rocks of

the previous chapter. In addition, the much higher Mn content of garnet in sample 856 may also be responsible for the discrepancy, if garnet departs significantly from simple-mixture behaviour at this high-Mn composition. Other biotite-garnet pairs (e.g. 862) cannot be compared, as in these cases the octahedral Al content of biotite is markedly different from those used in chapter 4 to derive the defining equation (e.g. 0.2667 as against the average of 0.8812 in samples 826 to 829). As pointed out by Dallmeyer (1974), variations in biotite octahedral aluminium and titanium will significantly alter Fe-Mg distribution coefficients between biotite and other ferromagnesian minerals.

5.4 AFM Topologies and Reactions

Introduction

With the aid of microprobe analyses, the inferred sequence of prograde AFM topologies is plotted in figures 10 to 12. The following points need emphasis:

- (i) Because of the discontinuous nature of both the rock compositional units and usable outcrop, figs. 10 to 12 were inferred from groupings of assemblages, and not by the location in the field of any well-defined reaction boundaries. The inferred isograd which marks the boundary between the two topologies in figs. 10 and 11 is plotted on the accompanying map.
- (ii) Because many of these rocks contain abundant magnetite, plotting bulk compositions on AFM diagrams requires some

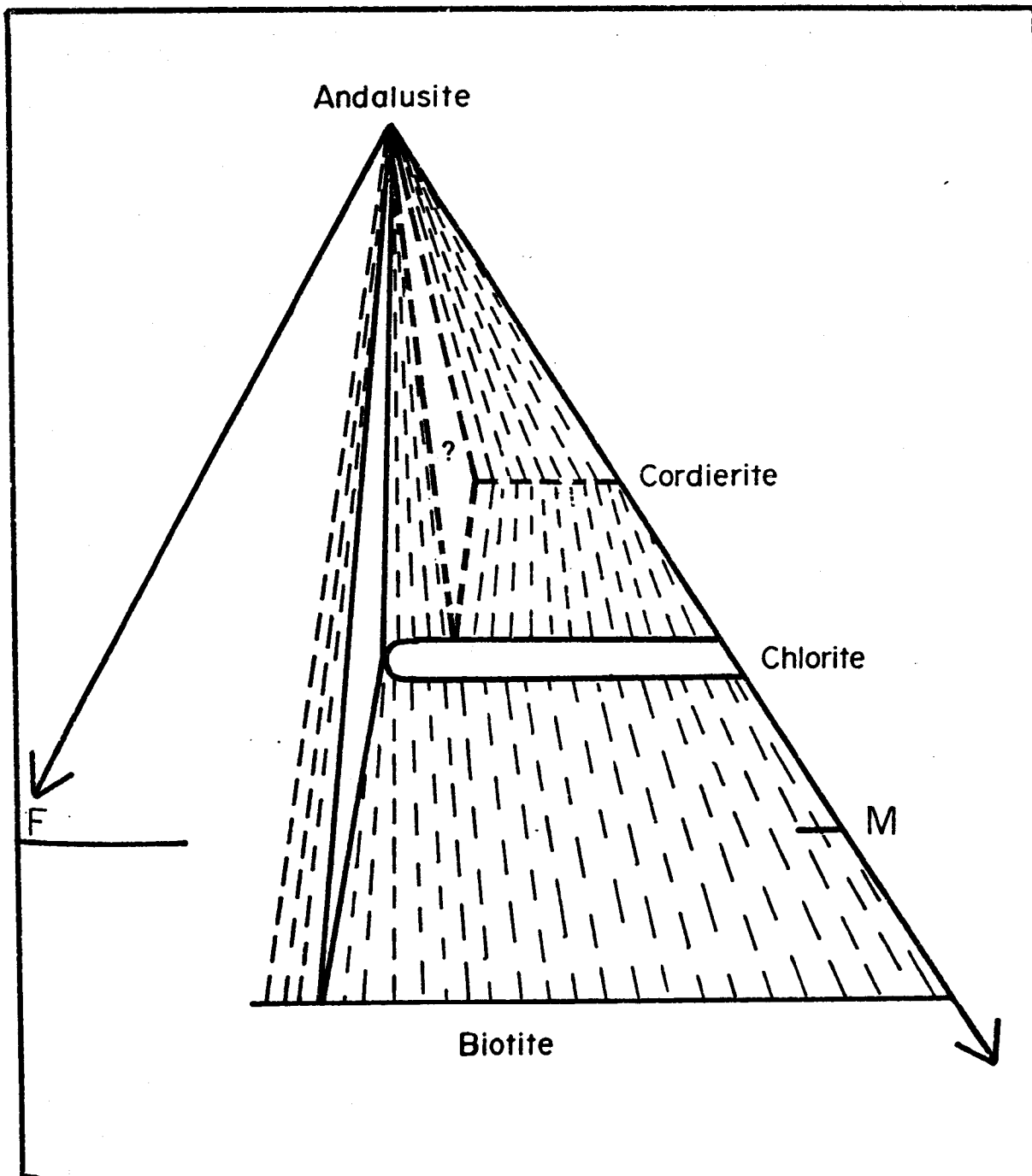


FIGURE 10: Inferred AFM topology for the lowest - grade metapelitic rocks in the Jervois Range area. Owing to the absence of rocks of appropriate bulk composition, the stability of cordierite in this zone has not been confirmed.

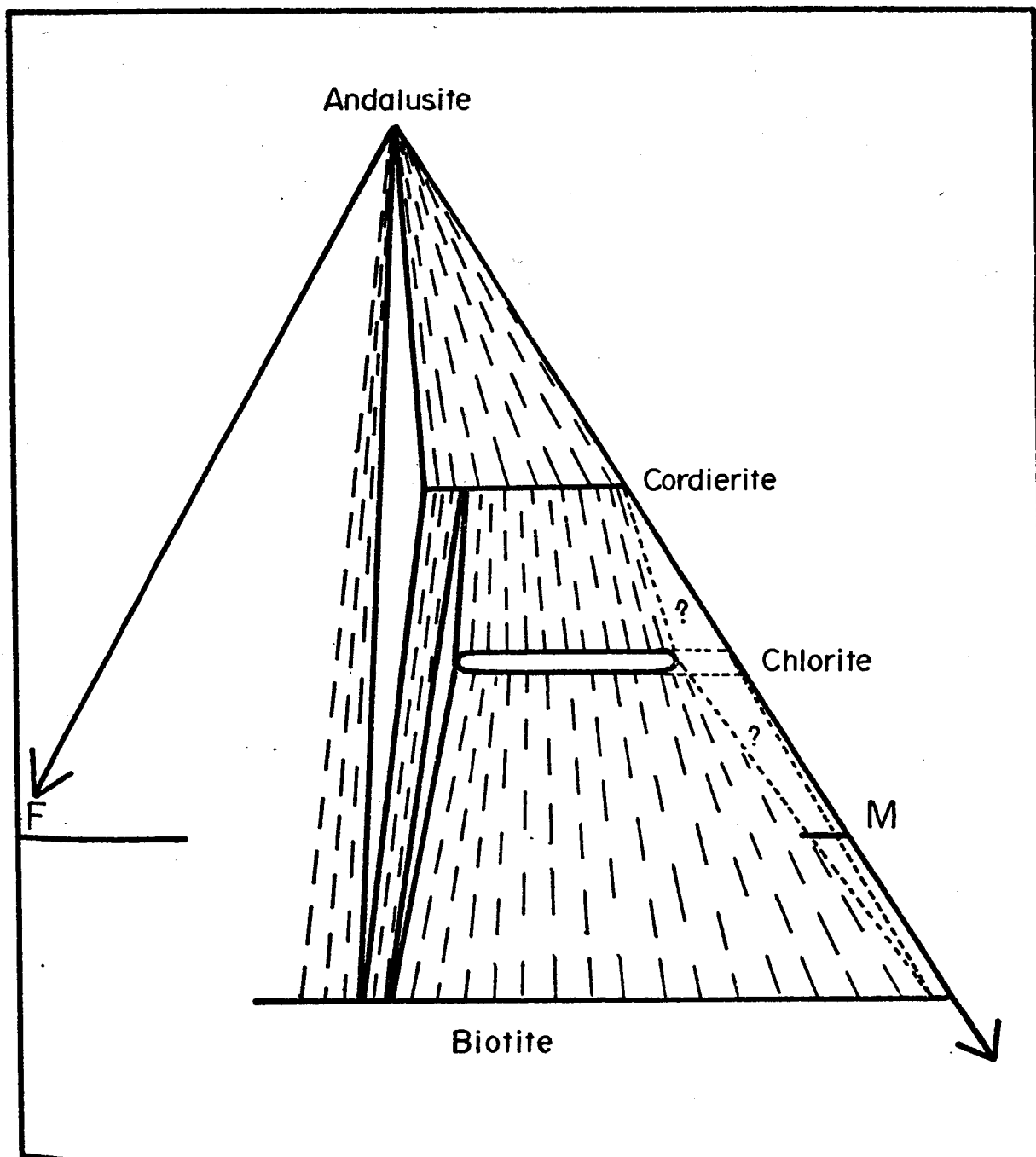


FIGURE 11: Inferred AFM topology for medium - grade metapelitic rocks in the Jervois Range area. The assemblage Mg - rich cordierite - Mg - rich chlorite - Mg - rich biotite has not been confirmed in this zone.

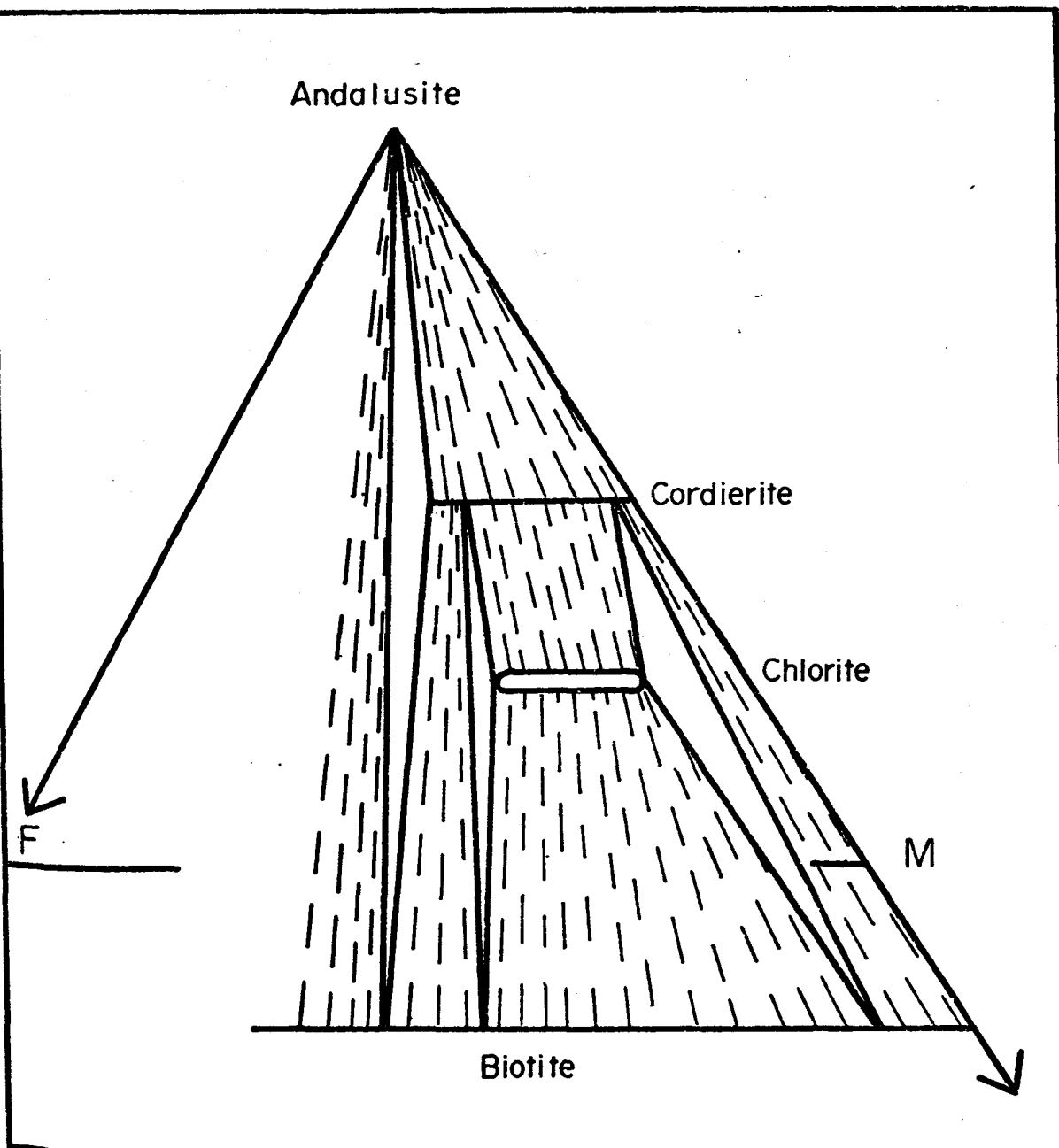


FIGURE 12: Inferred AFM topology for the highest - grade meta-pelitic rocks in the mine sequence, east of the Jervois Range. This topology corresponds to the magnesian half of those presented in figure 9, representing lower to middle amphibolite facies conditions. In the highest - grade area to the west of Jervois Range, sillimanite is the stable aluminosilicate, and chlorite may not be an equilibrium phase.

care. The use of uncorrected FeO values from analyses causes points to be plotted too far towards the F corner, commonly plotting outside the appropriate mineral stability fields. In unweathered rocks, the silicate bulk FeO is easily calculated by assuming all Fe_2O_3 to be contained in magnetite, yielding the correction formula:

$$\text{mol. FeO}_{\text{silicates}} = \text{mol. FeO}_{\text{total}} - \text{mol. Fe}_2\text{O}_3_{\text{total}}$$

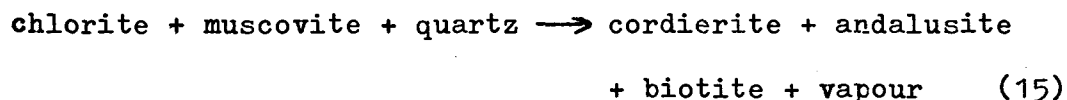
For weathered rocks (resulting in "martitization" of magnetite), the FeO component of the oxide phases is partly or completely oxidized, so that use of the above correction formula yields plotted points that are too Mg-rich, which again may fall outside the appropriate mineral stability fields.

- (iii) The AFM topologies are for the ideal system SAFMKH, and real rock compositions containing extra components (the excess components of Korzhinskii, 1959) may depart significantly from them. As an example, disregard the Mn content of sample 870. The observed paragenesis andalusite-cordierite-biotite-chlorite-muscovite-quartz-(vapour) is then univariant in the system SAFMKH, and, since such univariant assemblages at equilibrium are unlikely to be found in nature, mosaic equilibrium may be invoked to explain its stability. The three potential domains contain the assemblages andalusite-chlorite-biotite, muscovite-chlorite-biotite, and cordierite-biotite-chlorite, as explained previously. However,

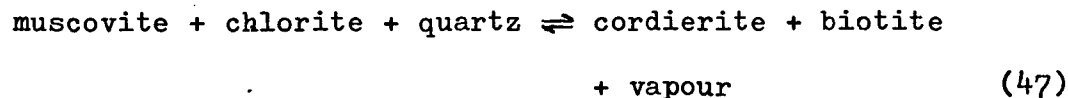
these are not common to any one of the AFM diagrams, implying that the assemblages are not in equilibrium or that the AFM topology is incorrect. These problems are simply and logically solved if excess components in real rocks are taken into account.

Prograde Reactions Involving the Breakdown of Chlorite

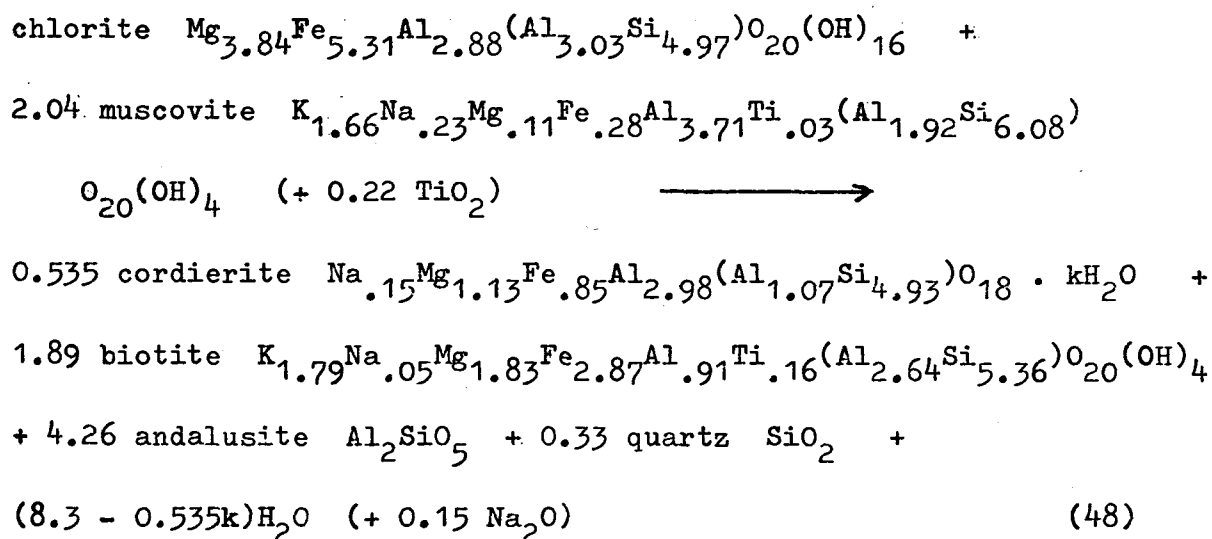
The reactions inferred from the natural assemblages are a consequence of the shrinking of the chlorite compositional field by reaction with muscovite, the frequently quoted reaction being:



Initially, the cordierite stability field is extended towards the iron end-member. Once the assemblage andalusite-cordierite-biotite becomes stable, the chlorite stability field is further reduced by the continuous, divariant reaction



Using real mineral compositions from samples 855 and 874, and deriving $K_D^{\text{cord-bio}}$ from the former, a more realistic equivalent to $K_D^{\text{Mg-Fe}}$ reaction (15) can be calculated. The constraints for this calculation are that the reaction be closed to all the components in the SAFMKH system, so that stoichiometry is maintained within the minerals for the elements Si, Al, Fe, Mg and K. For 1 mole of chlorite, the reaction is:



Unlike reaction 15, the quartz in this reaction is a product, and the coefficients differ markedly from those commonly used to set up Schreinemakers grids (see Hess, 1969, table 2). The sodium liberated in reaction 48 indicates that the reaction in nature is not univariant, consistent with the fact that, as a result of reactions with chlorite, the remaining muscovite becomes more paragonitic. The titanium consumed in reaction 48 must come from ilmenite and/or magnetite, again indicating that real prograde reactions are likely to be complex, involving all or nearly all minerals in an assemblage.

Sillimanite-bearing Assemblages

From the available evidence (only two "fibrolite"-bearing samples being available, both free of chlorite) it cannot be inferred whether any chlorite is stable at the conditions of the andalusite to sillimanite transition. The appearance of "fibrolite" is not due to the breakdown reaction of muscovite + quartz (unless the K-felspar product has been metasomatically removed); nor does

the textural evidence support a simple polymorphic pseudomorphous reaction of andalusite to sillimanite. The petrographic evidence available does not indicate any particular mechanism of fibrolite formation.

Retrograde Reactions

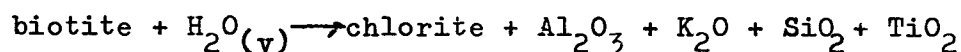
The retrogression of almost all the cordierite-bearing rocks throughout the Jervois Range area has already been described in the first section of this chapter. Several observations merit attention:

- (i) For a series of rocks of fixed biotite content, the greater the volume of (altered) cordierite, the greater is the amount of biotite altered to chlorite. This suggests a correlation between the two alteration mechanisms.
- (ii) Rocks devoid of cordierite show little if any biotite alteration. Exceptions are restricted mainly to thin compositional units (of the order of 1 to 2 m thick) which lie adjacent to cordierite-rich rocks.
- (iii) In many cordierite-rich rocks, large grains of biotite, not in contact with any other grains of biotite have been completely replaced by chlorite, without any observable change in grain shape or volume; this implies at least a local, near iso-volumetric reaction.
- (iv) With the exception of water vapour, there is no evidence to date to suggest widespread introduction (or removal) of components into these rocks.

The following subsection is an attempt to explain these

observations by considering a possible reaction system which leaves the bulk-compositions virtually intact, requiring a minimum of metasomatism. Consider that the retrogression is caused simply by the addition of water to the rocks during the waning stage of metamorphism.

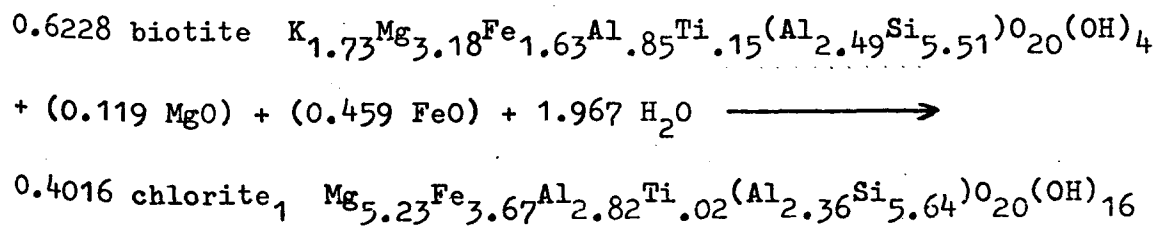
At the site of single biotite grains, the following reaction may be proposed:

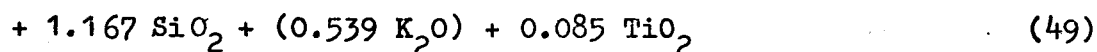


There are two drawbacks associated with the above, rather simplistic, reaction:

- (i) the product components must either form new aluminosilicate minerals within, or adjacent to, the chlorite; no such minerals are observed, so that diffusion away from this reaction site has to be postulated;
- (ii) molar volume calculations show that the amount of chlorite produced from the Mg and Fe available in a biotite grain is insufficient to pseudomorph that biotite grain completely.

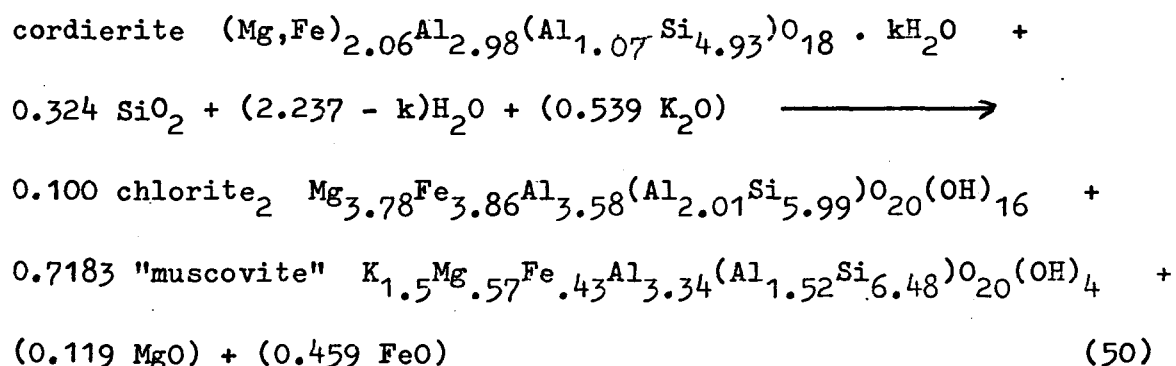
Using slightly simplified, but realistic mineral formulae from an appropriate sample (857, table 15), a different reaction may be written to conserve Al at this reaction site:





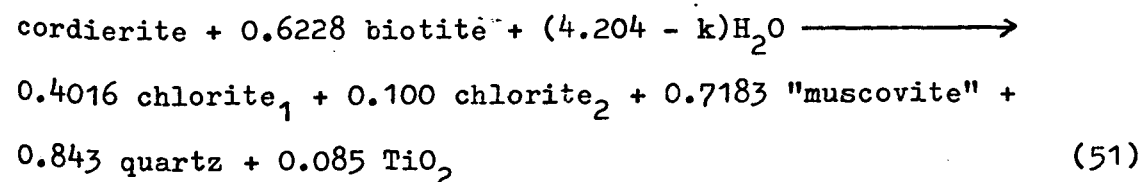
Reaction 49 produces the same volume of chlorite as the volume of biotite consumed (within the errors of approximate molar volumes calculated from density data in Deer, Howie and Zussman, 1963).

At the cordierite site, a reaction may be written to conserve Al, again using slightly simplified formulae for chlorite and muscovite from sample 855, and, in the case of cordierite, from sample 855:



In this reaction also, the volume change of cordierite + quartz reacting to "pinite" (chlorite₂ + "muscovite") is very small, and silica is readily available, since the cordierite poikiloblasts contain abundant quartz inclusions.

Addition of reactions 49 and 50 results in the simultaneous breakdown of cordierite and biotite by simple hydration involving no net change in bulk composition:



Using molar volumes (in cm³) of 306 for biotite, 433 for both

chlorites and 282 for "muscovite", reaction 51 not only allows the complete replacement of biotite grains by chlorite, but produces virtually no change in the volume of the rock; $\Delta V_{51} = +3.9\%$. The very approximate nature of the phyllosilicate molar volumes used suggests that the net reaction may involve no volume change at all, or even that the volume change may be slightly negative. Reaction 51 also explains the observation that, in most cordierite-bearing rocks, the amount of chloritized biotite is proportional to the amount of retrogressed cordierite.

Several details arise regarding reaction (51). Minute amounts of sodium in biotite have been treated as potassium, and equally minute amounts of sodium in cordierite have been ignored. This sodium may react with existing muscovite during the reaction, or may even combine with excess aluminium to form albite. No evidence for these possibilities has yet been found in the Jervois Range rocks, and, because the amounts of sodium are so minute, the evidence may not be forthcoming on further microprobe analysis. The titanium released from biotite may form rutile, or may combine with excess iron to form ilmenite; thin needles of these minerals have been observed in the retrograde chlorite.

Reaction 51 as written, using the analyses from table 15, requires a cordierite that is more iron-rich than would be expected to coexist with biotite with $Mg = 66$. This may have arisen as a consequence of the rather uncertain analyses of "muscovite" and chlorite in the ultra-fine grained "pinite", so that, in the actual rock, the coefficients of reaction 51 may have been slightly

different. In addition, neglecting the effects of possible oxidation during the hydration, and the treatment of all Fe in "muscovite" as ferrous iron, may have made the cordierite (in the calculation) more iron-rich than it would have been in the actual rock. However, these details do not alter the conclusions drawn from reaction 51.

A more important point is that, in several rocks, the biotite is altered, whereas biotite inclusions in retrogressed cordierite do not appear to have undergone alteration. If, during the initial stages of hydration, the biotite is "shielded" by the cordierite from the "vapour" phase, no reaction may take place. However, once the "vapour" comes into contact with a cordierite-biotite grain boundary, the reaction should occur. Some of the biotite inclusions contain minute leaves of chlorite along cleavage planes, and these extend, or are inferred to extend, to biotite/cordierite grain boundaries. Examination of biotite-cordierite boundaries (perpendicular to (001) of biotite) under high magnification commonly reveals minute rims of what appears to be white mica, or, less commonly, chlorite, about 0.002 mm wide. It is thus possible that the biotite inclusions were shielded from access to water by the cordierite itself, in the absence of a network of cordierite/quartz grain boundaries connecting the biotite inclusions to the rims of the cordierite porphyroblasts. In such cases, when water did get to the inclusions along grain boundaries of the cordierite breakdown products, the amount of biotite breakdown was controlled mainly by the amount of unaltered cordierite present. Hence, if at

this stage little fresh cordierite remained, only a small amount of biotite breakdown could occur.

Reaction 51 requires the diffusion of potassium from the biotite breakdown site towards the cordierite breakdown site, and the complementary diffusion of iron and magnesium in the opposite direction. These components diffused along their respective activity gradients, not as neutral species, but probably as charged ions. Reaction 51 is similar to an ionic reaction documented by Fisher (1970), which also involved the complementary diffusion of K and (Mg+Fe).

Reaction 51 thus closely approximates a possible natural reaction, and demonstrates that the assemblages seen in the Jervois Range rocks probably arose as a result of a simple, retrograde hydration, involving little or no large-scale migration of non-volatile components. A possible source of water and the cause of the retrograde episode could well be the second period of emplacement of granitic bodies towards the end of, or after the main metamorphic event. From the data in table 1, chapter 2, the retrograde event is assigned an age of 1680 ± 30 m.y.

5.5 Bulk-Rock Geochemistry

Major Elements

The metapelitic rocks of this chapter, and the staurolite-bearing rocks of chapter 4 have been divided into two groups, namely:

- (i) the first, iron-rich group, in which each sample has $\text{FeO or Fe}_2\text{O}_3 \geq 6\%$ or $\text{FeO} + \text{Fe}_2\text{O}_3 \geq 10\%$; this group contains 32 samples;
- (ii) the second group, containing all the metapelitic rocks listed in appendix tables 3 to 7; this includes all the rocks of group one, and, in addition, the more aluminium-rich and iron- and manganese-poor schists.

The sample size is 53.

Although low in aluminium content, the iron-rich samples 862 and 864 are included in groups one and two as they represent particular compositional variants co-deposited with the pelitic sediments, in the same sense as sample 865, which is low in iron, but is abnormally rich in aluminium (32.95% Al_2O_3) compared with the more "normal" metapelites.

Averages, standard deviations and ranges of the component oxides are listed in table 18. These figures are unweighted with respect to volume, and are not to be taken to represent the "average" metapelitic rock in the Jervois Range area. A half matrix of linear correlation coefficients is also presented in table 18 for the group one rocks. The addition of the extra rocks of group two

BULK-ROCK GEOCHEMICAL DATA - JERVOIS RANGE AREA METAPELITIC ROCKS

GROUP ONE ROCKS; SAMPLE SIZE 32

GROUP TWO ROCKS; SAMPLE SIZE 53

	mean	std. dev.	lowest	smpl.	highest	smpl.	mean	std. dev.	lowest	smpl.	highest	smpl.
SiO ₂	56.19	8.56	35.29	(862)	71.12	(828)	56.51	8.14	29.96	(826)		
TiO ₂	.55	.22	.13	(862,4)	.83	(856)	.60	.20			.85	(826,33)
Al ₂ O ₃	13.09	5.06	2.65	(862)	20.19	(838)	15.81	5.64			32.95	(865)
Fe ₂ O ₃	12.44	11.66	1.37	(855)	52.54	(862)	9.13	9.92				
FeO	6.73	3.14	2.08	(834)	11.69	(847)	6.03	3.86	.47	(865)		
MnO	.76	1.13	.09	(839)	5.37	(863)	.58	.94	.03	(872)		
MgO	2.52	1.18	.45	(862)	5.58	(855)	2.54	1.16				
CaO	.77	.76	.09	(831)	3.50	(849)	1.04	1.48			8.21	(878)
Na ₂ O	.51	.56	.01	(862,4)	2.82	(832)	.66	.62			2.96	(837)
K ₂ O	2.96	1.79	.02	(847)	5.54	(838)	3.61	1.95			8.74	(865)
P ₂ O ₅	.29	.31	.02	(828)	1.20	(849)	.24	.28				
H ₂ O ⁺	2.68	1.56	.56	(862)	8.37	(836)	2.70	1.33				

HALF - MATRIX OF LINEAR CORRELATION COEFFICIENTS OF GROUP ONE ROCKS

	SiO ₂	TiO ₂	Al ₂ O ₃	Fe ₂ O ₃	FeO	MnO	MgO	CaO	Na ₂ O	K ₂ O	P ₂ O ₅	H ₂ O ⁺	Totl.
SiO ₂	1	.30	.34	-.84	.04	-.23	-.16	-.52	.19	.20	-.72	-.03	.08
TiO ₂		1	.96	-.67	-.52	-.52	.30	-.34	.10	.88	-.47	.51	.25
Al ₂ O ₃			1	-.71	-.48	-.63	.29	-.41	.11	.91	.52	.50	.30
Fe ₂ O ₃				1	.02	.49	-.27	.44	-.19	-.56	.63	-.32	-.25
FeO					1	.02	.20	.23	.04	-.57	.33	-.42	.03
MnO						1	-.18	.24	-.30	-.67	.14	.30	.46
MgO							1	.31	-.15	.20	.22	.48	.19
CaO								1	.13	-.34	.83	-.12	.20
Na ₂ O									1	.06	-.04	-.07	.10
K ₂ O										1	-.36	.57	.30
P ₂ O ₅											1	-.16	.14
H ₂ O ⁺												1	.30
Totl.													1

Bulk - rock total = 0.889SiO₂ + 0.103TiO₂ + 0.921Al₂O₃ + 0.884Fe₂O₃ + 0.850FeO
+ 0.839MnO + 0.932MgO + 1.031CaO + 0.661Na₂O + 0.872K₂O + 0.785P₂O₅ + 0.882H₂O⁺
+ 11.524 (R = 0.971)

TABLE 18: Bulk - rock geochemical data for metapelitic rocks from the Jervois Range area. Rocks belonging to group one have either FeO or Fe₂O₃ > 6%, or FeO + Fe₂O₃ > 10%; these include all the rocks listed in appendix tables 4 and 5, plus samples 828, 830, 831 and 832, listed in appendix table 3. Blanks in the group two table above indicate that the lowest and/or highest values are those listed under group one.

lowers the correlation of all the significant element pairs, and with the exception of Al-K ($r = 0.83$) the absolute values of the correlation coefficients fall below 0.7.

Allowing for the effect of differing water content, comparison of the two averages with the average geosynclinal and platform shales compiled by Wedepohl (1969) and listed in appendix table 7 shows that the Jervois Range rocks are lower in titanium and calcium (especially compared with platform shales), and that sodium is lower than that of the average geosynclinal shale. In addition, the group one average is richer in iron and manganese by factors of 3 and 8.4, respectively, and, for the group two average, the factors are 2.3 and 6.4. Both group averages are lower in silica, calcium and sodium, and higher in iron, manganese and potassium than the average greywacke compiled by Pettijohn (1963), although individual units (e.g. 837, appendix table 6) may be similar. Comparison with pelagic clays is ruled out by the coarse-grained, clastic nature of many of the massive quartzites, and by the preservation in the field of a range of macroscopic structures attributable to turbidites.

Major element analyses of these rocks, coupled with field evidence, suggest that they are the metamorphic equivalents of fine-grained pelitic sediments, locally iron- and manganese-enriched, probably deposited as part of a flysch sequence (Selley, 1970; Shaw and Stewart, 1973).

The strong negative correlation of ferric oxide (practically all contained in magnetite) with silica is explained by the principle of closure, resulting from the fact that, as modal magnetite increases,

modal silicates must decrease. For group two rocks, $r_{\text{Fe}^{3+}\text{-Si}} = -0.67$. The strong positive correlation between aluminium, potassium and titanium, taken in pairs, arises from the fact that these elements are common to both muscovite and biotite, and the micas constitute the major aluminosilicate phases in these rocks. The correlation shows that most of the titanium is contained in micas, not in magnetite. This is further borne out by magnetite analyses, in which TiO_2 is commonly less than 0.1%, and by the moderate negative correlation with Fe_2O_3 . For group two rocks, $r_{\text{Ti-K}} = 0.57$, $r_{\text{Ti-Al}} = 0.69$, $r_{\text{Al-K}} = 0.83$, $r_{\text{Fe}^{3+}\text{-Ti}} = -0.61$.

The positive correlation between phosphorous and calcium indicates that a large proportion of calcium in phosphorous-rich rocks is contained in apatite. Since the metapelitic rocks in the Jervois Range area are commonly plagioclase-deficient, and, since the apatite-rich rocks are rich in magnetite (commonly true for iron-rich sedimentary silicate rocks; James, 1966), the correlation between calcium and phosphorous drops markedly when the relatively iron-poor rocks of group two are included. (For group two rocks, $r_{\text{Ca-P}} = 0.22$).

Trace Elements

Several of the samples in appendix tables 4 to 7 contain cross-cutting veinlets of quartz⁺calcite⁺chlorite⁺fluorite up to 2 mm in thickness. Though care was taken in preparing such samples for bulk-rock analysis, six samples with very high Ba content (1159 to 5227 ppm) probably indicate that

- (i) the quartz⁺calcite⁺chlorite⁺fluorite veining is responsible for the metasomatic introduction of Ba; and
- (ii) some veining was not detected during sample preparation.

These samples do not appear to have anomalous values for other trace elements except uranium (samples 852 and 859), but, because of the uncertainty, are not used in any discussion.

Similarly, two samples are high in rubidium (830 and 853), although their Ba content appears to be normal.

Barium in group one rocks varies from 1067 ppm to below the practical detection limit. Most values fall in the range of 200 to 800 ppm, with an average of 501 ppm for 28 samples. Inclusion of group two rocks changes the average to 519 ppm. Mica-rich rocks are the richest in barium content, explaining the high correlation coefficients for Ba-K (0.76 for both groups). The range of Ba contents above corresponds well to the range observed in pelitic sediments, and values below 830 ppm may also be common to greywackes (Wedepohl, 1969). Note that the barium content of these rocks is generally inconsistent with a deep-sea clay origin.

The rubidium content of group one rocks varies from less than 10 to 433 ppm, with an average value of 257 ppm. The K/Rb ratio varies from 19 to 280, with an average of 104. For group two, the range of Rb content is increased to 625 ppm with an average of 277 ppm, and the K/Rb ratio is raised to an upper limit of 485 with an average of 120. The low Rb content of samples 863 and 847 is a consequence of their very low mica content, and the resultant low K content.

Although the Rb content of these rocks falls within the range compiled for shales (Wedepohl, 1969, 37-K-1), the work of Leask (1967) suggests that the K/Rb ratios are anomalously low compared with a mean ratio of 270 for Precambrian argillites. This suggests that the source rocks for the pelitic sediments were themselves enriched in Rb relative to K, as compared with more "normal" source rocks, or that, during sedimentation, there existed some chemical process which enriched the sediments in Rb relative to K. One possible Rb-enriching process is discussed in section 6 of the next chapter.

The bulk compositions of samples such as 862 and 864 correspond to those of sedimentary iron-formations (Appel, 1974; James, 1966), and the bulk compositions of the more aluminous metapelitic rocks in the Jervois Range area are bracketed by these on the one hand, and the more "normal" metapelitic rocks on the other. Possible origins for the iron component of these iron-rich metapelites will be discussed in section 6 of the next chapter.

CHAPTER 6: CHLORITE-QUARTZ⁺GARNET SCHISTS

6.1a Petrography of the Jervois Range Schists

Chlorite-quartz rocks, with or without garnet, occur within the mine sequence (chapter 4), although one 2 m-wide unit has been found southwest of the Jervois Range. They have three typical modes of occurrence:

- (i) Thin bands of chlorite (up to 4 mm), commonly with quartz and magnetite, alternate with equally thin bands of predominantly quartz, muscovite-biotite, muscovite-chlorite, epidote, biotite-spessartine, and K-felspar-magnetite. These layered rocks occur in beds that never exceed 20 cm in thickness and have been found only in the northern part of the mine sequence.
- (ii) Beds of chlorite schist, up to 60 cm in thickness, occur throughout the mine sequence. These schists contain little quartz and magnetite, and in several localities are almost monomineralic (Morgan, 1959). In outcrop, the contact of these beds with muscovite-bearing metapelites is marked by strongly weathered biotitic layers some 2 cm in thickness. However, no drill-core of this material has been located by the author.
- (iii) Chlorite-quartz-magnetite⁺-schists occur in lenses up to

20 m long and 12 m thick at the centres. They are best exposed in two localities: one at the northern and one at the southern end of the mine sequence. In addition, drill cores of these assemblages from elsewhere in the mine sequence are available. In the northern exposure, the lens contains quartz-poor and quartz-rich beds, and, whereas some of these contain numerous garnet porphyroblasts up to 5 mm in diameter, others contain far fewer garnets (up to 15 mm in diameter), and still others contain no garnet at all. The southern exposure, though still containing quartz-rich bands, is mineralogically more homogeneous, and all but pure quartz layers contain garnet. The garnet crystals are not uniformly distributed, and layers containing up to 70% porphyroblasts are common. Some of the porphyroblasts are elongate, and reach a length of 6 cm; all of them have well developed crystal faces.

The rocks to be discussed are from the third type of occurrence. However, both the exposures, and, to a lesser extent, the available drill core, are extensively weathered. Blasting at both sites produced somewhat fresher material, which provided the least altered samples for bulk-rock and electron-microprobe analysis. Petrographic descriptions of these rocks appear in the appendix.

Banding and Schistosity

In relatively garnet-poor domains, the schistosity is defined by the parallel alignment of chlorite laths. Alternating chlorite-

rich and quartz-rich bands, each ranging in thickness from 1 mm to over 20 mm, define a compositional layering that is almost parallel to the schistosity. In garnet-rich domains, the schistosity is less well developed, and wraps around the garnet porphyroblasts.

Garnet Porphyroblasts

The garnet porphyroblasts in the relatively quartz-rich rocks from the northern exposure are poikiloblastic, with inclusions of magnetite octahedra and angular to subangular quartz grains and grain aggregates. The sizes and shapes of the quartz inclusions in the garnet and the quartz grains in the matrix are similar, with two exceptions. First, the grain boundaries between quartz and the ends of chlorite laths in sections perpendicular to [001] in the matrix are commonly sutured or "saw-toothed", whereas the grain boundaries between quartz inclusions and garnet are generally planar or curvilinear. Second, the poikiloblastic garnet crystals contain a greater proportion of elongate quartz fragments than does the chlorite-quartz matrix.

Many of the poikiloblastic garnet crystals have "ragged" boundaries against the matrix in the quartz-rich rocks. However, where parts of such poikiloblasts extend into chlorite layers deficient in quartz, crystal faces are present. Even though many of these poikiloblasts have ragged boundaries against the quartz-rich matrix under high magnification, the poikiloblasts may show idioblastic (rhombododecahedral) crystal shapes under low magnification.

In chlorite-rich, quartz-poor rocks, garnet/chlorite grain boundaries are planar and sharp.

Garnet Alteration

There is no textural evidence to suggest that the chlorite in the matrix is not in chemical equilibrium with the garnet. Although garnet has altered to chlorite in a few of these rocks, this is only very local, and the amount of garnet altered is minute. The secondary (retrograde) chlorite so formed is optically different from, and chemically more iron-rich than, the primary chlorite of the matrix.

Veining of Garnet Porphyroblasts

Several of the quartz-rich rocks contain garnet grains veined by quartz and chlorite similar in composition to the matrix chlorite. However, these veins have not replaced garnet. Rather, they have filled dilatation cracks in the garnet. The two garnet "halves" across some of these cracks may exhibit perfect interlocking outlines. However, this feature is not generally developed where the filling is quartz alone.

Retrograde Alteration of Biotite

Sample 887 contains isolated flakes of biotite in the chlorite matrix. A few of these have undergone retrograde alteration, resulting in spindle-shaped laths of chlorite replacing only the biotite. As described in chapter 4, the secondary chlorite is texturally and optically distinct from the primary chlorite, and the compositional difference between the two chlorites is shown in table 21.

6.1b Comparison of the Jervois Range Schists with a Chlorite-Garnet Schist from Broken Hill, N.S.W.

Several chlorite-garnet⁺quartz schists outcrop in the Precambrian Willyama Complex around Broken Hill, N.S.W. One of these is relatively well-known to Australian hard-rock petrologists and mineralogists on account of the common occurrence of perfectly-formed garnet porphyroblasts, commonly exceeding 10 cm in diameter.

Since this outcrop occurs in the Thackaringa-Pinnacles Retrograde Shear Zone, several workers have inferred that the uncommon bulk-composition of the chlorite-garnet schist has resulted from the metasomatic removal of Ca, Na and K from a high-grade, mafic parent rock, and the contemporaneous retrogression of the parent-rock matrix to chlorite. By analogy, it might be reasoned by these workers that the chlorite-quartz⁺-garnet rocks in the Jervois Range area were also formed in this way. However, as will be discussed in section 6 of this chapter, the occurrence of the chlorite-garnet assemblage in a retrograde shear zone at Broken Hill does not automatically require the addition or removal of any chemical components other than H₂O and CO₂.

Two observations indicate that the garnet in the chlorite-garnet schist at Broken Hill is not a relic phase from a higher-grade assemblage:

- (i) Inclusions in the garnet porphyroblasts comprise chlorite, quartz and magnetite, and not high-grade mafic minerals such as pyroxene, amphibole, cordierite or biotite which

would be present in the hypothetical parent rock.

- (ii) If the garnets were relics from a more common, higher-grade assemblage, then the intense metasomatism postulated by these workers might be expected to alter the garnet to chlorite.

Vernon and Ransom (1971) and Chenhall (1973) have shown that, in many parts of the retrograde shear-zones around Broken Hill, retrogression has been from the lower granulite to the lower amphibolite facies. Hence it may be more realistically inferred that both the chlorite and garnet nucleated and grew under conditions of the lower amphibolite facies. It is still to be shown whether or not the retrogression was accompanied by metasomatic addition or removal of components other than H_2O and CO_2 .

Consequently, it cannot be reasoned by analogy with the Broken Hill chlorite-garnet schist that the Jervois Range chlorite-quartz⁺-garnet schists are retrograde. All that can be inferred from the Broken Hill occurrence is that the chlorite and garnet both grew under conditions of the lower amphibolite facies (see next section).

6.2 Phase Relations

The inferred mineral parageneses in the Jervois Range area are as follows:

chlorite-quartz⁺-magnetite (52)

chlorite-quartz-garnet⁺-magnetite (53)

chlorite-garnet⁺-magnetite (54)

These assemblages may include minor amounts of biotite and ilmenite

or rutile, and all contain at least trace amounts of apatite and zircon. Biotite may occur in increasing proportions to yield transitional assemblages between these and the more "normal" muscovite-bearing metapelitic rocks. Assemblage (54) does exist as a rock unit in its own right, but is more commonly found in layers or domains within much larger chlorite-quartz-garnet bodies. Assemblages (53) and (54) also occur in the chlorite-garnet schist in the Thackaringa Pinnacles Retrograde Shear Zone, where both assemblages may contain small amounts of labradorite or andalusite, and commonly minor amounts of biotite.

These rocks are not unique to the Jervois Range and Broken Hill areas, nor are the mineral assemblages unique to the bulk-compositional system implied by them (i.e. $\text{SiO}_2\text{-Al}_2\text{O}_3\text{-FeO-MgO(-MnO-Fe}_2\text{O}_3)\text{-H}_2\text{O}$; see also appendix tables 8 and 9). Based on bulk-composition, the staurolite- and andalusite-bearing chlorite-garnet-quartz schist (sample 827), discussed in chapter 4, also belongs here. Localities and parageneses of similar rocks, and their higher-grade metamorphic equivalents, are listed in table 19. Most of the regionally-metamorphosed rocks occur in Precambrian terrains.

Two points arise from the peculiar bulk-composition of these rocks:

- (i) First, assemblages (52) to (54) are multivariant, commonly with five degrees of freedom. Since both garnet and chlorite undergo a series of solid substitutions, assemblage (53) may represent a wide range of bulk-compositions within the system $\text{SiO}_2\text{-Al}_2\text{O}_3\text{-FeO-MgO(-MnO-CaO)-}$

METAMORPHIC ROCKS WITH BULK-COMPOSITIONS FALLING ESSENTIALLY IN THE SYSTEM $\text{SiO}_2 - \text{Al}_2\text{O}_3 - \text{FeO} - \text{MgO} - \text{H}_2\text{O}$

(CHLORITE - RICH ROCKS AND THEIR HIGHER GRADE EQUIVALENTS)

chlorite-garnet-quartz-(magnetite)	Copperfield, Western Australia, this work, sample 890.
chlorite-garnet-plagioclase-(magnetite-quartz)	Broken Hill, New South Wales, this work, sample 893; Chenhall, 1973; Vernon and Ransom, 1971; Vernon, 1969.
chlorite-garnet-(magnetite)	Perdignano, Italy, this work, sample 894, Emiliani and Venturelli, 1972.
chlorite-quartz-rutile, chlorite-garnet-talc	Sofala, New South Wales, Barron, 1976, table 3, p 614, # 46187, 46265. (1,2)
chlorite-garnet-quartz	Frenchman's Cap, Tasmania, Spry, 1963, table 1, p 127, # 8. (3)
chlorite-garnet-(quartz-biotite-staurolite)	Colobrières, France, Caruba et al., 1975, table 5, p 161, "unaltered rock". (4)
chloritoid-chlorite-andalusite-(muscovite-quartz)	Yahagi Mura, Japan, Seki, 1954, in Iwao, 1973, table 3, p 464, # 7. (5)
staurolite-sillimanite-quartz	Takanuki, Japan, Urano and Kanisawa, 1965, in Iwao, 1973, table 4, p 465, # St(1). (6)
chlorite-garnet-quartz ⁺ (biotite-magnetite), chlorite-cordierite-gedrite-cummingtonite-garnet-andalusite ⁺ (biotite-magnetite)	Khetri, Rajasthan, India, Lal and Shukla, 1975, table 1, p 181, # 392, 472, 564A. (7,8,9)
spessartine-chlorite-quartz-(muscovite)	Venn-Stavelot Massif, France, Kramm, 1976, table 1, p 141, # OT4 (10)
chlorite-garnet-cordierite-gedrite-(biotite-quartz-magnetite), cordierite-gedrite-garnet-biotite-(magnetite)	Koolanooka, Western Australia, this work, samples 891, 892.
anthophyllite-garnet-quartz-(biotite), cordierite-hypersthene-quartz-garnet-sillimanite-(biotite)	Strangways Range, Northern Territory, Vernon pers. comm. and 1972. (11)
cordierite-hypersthene-quartz-(biotite)	Karnatka, India, Iyer and Kutty, 1975, table 2, p 129, # 8. (12)
olivine-cordierite-garnet-gedrite-(biotite-chlorite-magnetite)	Harz Mts. Germany, Abraham and Schreyer, 1973, table 1, p 280, # EH3. (13)
talc-garnet-kyanite-quartz	western Tasmania, Raheim and Green, 1974, table 1, p 223, # 71-310. (14)
cordierite-gedrite-garnet-quartz-(chlorite-biotite-magnetite)	Front Ra. Colorado, U.S.A., Gable and Sims, 1969, table 2, p 26, # 1,6. (15,16)
cordierite-garnet-sillimanite-quartz-(staurolite-biotite-magnetite), cordierite-garnet-gedrite-quartz- (biotite-magnetite), cordierite-gedrite-biotite	Fishtail Lake, Ontario, Canada, Lal and Moorhouse, 1969, table 7, p 157, # 1-1, 112, 80. (17,18,19)
enstatite-cordierite-sillimanite-quartz	Beitbridge, Rhodesia, Chinner and Sweatman, 1968, table 1, p 1055, # 5. (20)
cordierite-orthopyroxene-(biotite-chlorite), orthopyroxene-garnet-(spinel-biotite-magnetite), orthopyroxene- spinel-magnetite-(biotite-gedrite)	Quairading, Western Australia, Davidson and Mathison, 1974, table 9, p 283, # 1,5,6. (21,22,23)
cordierite-orthopyroxene-sapphirine-(phlogopite)	Namaqualand, South Africa, Clifford et al., 1975, table 3, p 353, # a. (24)
gedrite-sapphirine-orthopyroxene-spinel-sillimanite-corundum-(phlogopite-plagioclase-magnetite), cordierite- gedrite-garnet-sillimanite-kyanite-quartz-spinel-(phlogopite-höbhomite-magnetite)	Strangways Ra. Northern Territory, Woodford and Wilson, 1976a, table 1, p 420, # 122,419.(25,26)
chlorite-corundum-(cordierite-sapphirine-muscovite-rutile)	Mt. Painter, South Australia, Oliver and Jones, 1965.

TABLE 19: Metamorphic rocks with bulk compositions falling essentially in the system $\text{SiO}_2 - \text{Al}_2\text{O}_3 - \text{FeO} - \text{MgO} - \text{H}_2\text{O}$ ($\text{MnO} - \text{FeO} - \text{CaO}$). The minerals listed in the above assemblages need not all be in equilibrium, and those in brackets are generally subordinate in volume. Most of the analyses have been reproduced in appendix tables 9, 10, and 11, and are cross-referenced by the last set of numbers (in brackets).

H₂O.

- (ii) Second, phase relations in this system cannot be applied indiscriminately to the normal pelitic system SAFMKH.

As an example, assemblage (53), chlorite-quartz-garnet, exists at the same temperature and pressure conditions as assemblage (33), cordierite-andalusite-biotite-(muscovite-quartz), for a wide range of chlorite compositions. On an AFM diagram (fig. 12) depicting assemblage (33), chlorites more magnesian than Mg = 40 cannot coexist with garnet, because of the presence of muscovite, which reacts with chlorites (Mg 40 to 60) to form biotite, andalusite and cordierite. In the absence of muscovite, chlorite-quartz-garnet assemblages are stable to the upper thermal limit of chlorite+quartz, where they react to form cordierite-gedrite⁺-garnet assemblages (Fleming and Fawcett, 1976; Lal and Shukla, 1975; Lal and Moorhouse, 1969; Gable and Sims, 1969).

6.3 Composition of, and Element Distribution between, Chlorite and Garnet

Chlorite compositions in these rocks (tables 20 to 22) fall in the corundophilite and ripidolite fields, being lower in silica content than would be expected for chlorites approaching their upper thermal stability limits in the presence of quartz (Fleming and Fawcett, 1976). Since all the silica-bound Al, Mg and Fe in chlorite-quartz rocks is contained in chlorite, bulk-compositional variations are reflected in the compositions of chlorites, and seemingly homogeneous rocks may be compositionally "banded". A modest example

CHLORITE-QUARTZ-GARNET SCHISTS

PARAGENESIS (53)				PARAGENESIS (52)		PARAGENESIS (53)		
SAMPLE 879				SAMPLE 881		SAMPLE 882		
CHLORITE	GARNET	GARNET		CHLORITE	CHLORITE	CHLORITE	GARNET	GARNET
nr. gt.	core	rim				nr. gt.	core	rim
SiO ₂	24.21	36.91	36.89	22.33	22.80	21.59	36.18	36.36
TiO ₂	.16	.20	.00	.11	.14	.11	.00	.00
Al ₂ O ₃	22.34	20.56	20.76	22.91	21.89	23.36	20.36	20.44
Cr ₂ O ₃	.00	.00	.00	.12	.00	.12	.00	.00
FeO	24.82	21.37	29.53	28.35	27.70	30.40	32.04	35.42
MnO	.28	17.07	7.58	.13	.21	.13	8.14	4.39
MgO	14.13	.99	2.27	11.91	13.18	10.07	1.62	1.84
CaO	.00	2.77	2.81	.00	.00	.00	1.64	1.48
TOTAL	85.94	99.87	99.84	85.86	85.92	85.78	99.98	99.93
CATIONS PER No. OXYGENS	28	12	12	28	28	28	12	12
Si	5.2059	3.0094	2.9912	4.9214	5.0070	4.8234	2.9693	2.9778
Ti	.0259	.0123		.0182	.0231	.0185		
Al	5.6615	1.9757	1.9839	5.9508	5.6655	6.1507	1.9693	1.9729
Cr				.0209		.0212		
Fe	4.4633	1.4571	2.0024	5.2252	5.0871	5.6797	2.1990	2.4259
Mn	.0510	1.1788	.5206	.0243	.0391	.0246	.5658	.3045
Mg	4.5294	.1203	.2744	3.9131	4.3148	3.3538	.1982	.2246
Ca		.2367	.2441				.1442	.1299
TOTAL	19.9370	7.9903	8.0166	20.0739	20.1366	20.0719	8.0458	8.0356
Mg	50.37	7.63	12.05	42.82	45.89	37.13	8.27	8.47
X _{Fe}		48.67	65.84				70.77	78.64
X _{Mg}		4.02	9.02				6.38	7.28
X _{Mn}		39.39	17.12				18.21	9.87
X _{Ca}		7.91	8.03				4.64	4.21
Al ^{iv}	2.7941			3.0786	2.9930	3.1766		
Al ^{vi}	2.8674			2.8722	2.6725	2.9741		

TABLE 20: Microprobe analyses of minerals in parageneses (52) and (53) from the northern exposure in the mine sequence.

CHLORITE-QUARTZ-GARNET±MINOR BIOTITE SCHISTS

SAMPLE 887					SAMPLE 889				
CHLORITE	CHLORITE	BIOTITE	GARNET	GARNET	CHLORITE	CHLORITE	GARNET	GARNET	
	alt.bio.		core	rim	near gt.		core	rim	
SiO ₂	21.96	21.48	36.86	36.55	36.57	22.30	22.23	36.80	36.89
TiO ₂	.09	.06	1.18	.00	.00	.00	.00	.00	.00
Al ₂ O ₃	24.73	21.82	19.42	20.85	20.39	22.92	22.79	20.57	20.82
FeO	28.78	37.89	20.41	36.33	36.58	30.28	30.39	33.01	38.55
MnO	.09	.24	.05	2.84	3.02	.00	.00	6.25	.16
MgO	10.47	4.87	9.12	1.98	2.03	10.26	10.30	1.30	2.58
CaO	.00	.00	.00	1.41	1.40	.00	.00	2.10	.81
Na ₂ O	.00	.00	.18	.00	.00	.00	.00	.00	.00
K ₂ O	.00	.00	8.88	.00	.00	.00	.00	.00	.00
TOTAL	86.12	85.91	96.10	99.96	99.99	85.76	85.71	100.03	99.81
CATIONS									
PER No.	28	28	22	12	12	28	28	12	12
OXYGENS									
Si	4.8215	4.9798	5.5401	2.9794	2.9881	4.9659	4.9589	3.0030	2.9976
Ti	.0149	.0105	.1334						
Al	6.3992	5.9619	3.4400	2.0031	1.9635	6.0153	5.9915	1.9783	1.9939
Fe	5.2844	7.3460	2.5654	2.4766	2.4996	5.6389	5.6692	2.2527	2.6197
Mn	.0167	.0471	.0064	.1961	.2090			.4320	.0110
Mg	3.4269	1.6831	2.0434	.2406	.2473	3.4060	3.4252	.1581	.3125
Ca				.1231	.1226			.1836	.0705
Na			.0525						
K			1.7025						
TOTAL	19.9636	20.0284	15.4837	8.0189	8.0301	20.0261	20.0448	8.0077	8.0052
Mg	39.34	18.64	44.34	8.85	9.00	37.66	37.66	6.56	10.66
X _{Fe}				81.56	81.20			74.43	86.93
X _{Mg}				7.92	8.03			5.22	10.37
X _{Mn}				6.46	6.79			14.27	0.36
X _{Ca}				4.05	3.98			6.07	2.34
Al ^{iv}	3.1785	2.0202	2.4599			3.0341	3.0411		
Al ^{vi}	3.1607	2.9417	.9801			2.9812	2.9504		

TABLE 21: Microprobe analyses of minerals in paragenesis (53). Note difference in composition between primary and retrograde (altered biotite) chlorite.

CHLORITE-QUARTZ-GARNET SCHISTS

	<u>SAMPLE 885</u>			<u>SAMPLE 886</u>			
	<u>CHLORITE</u>	<u>CHLORITE</u>	<u>GARNET</u>	<u>CHLORITE</u>	<u>CHLORITE</u>	<u>GARNET</u>	<u>GARNET</u>
	near gt.			near gt.	core		rim
SiO ₂	24.14	23.79	36.95	22.23	22.01	36.41	36.32
TiO ₂	.10	.21	.19	.00	.00	.00	.00
Al ₂ O ₃	21.04	20.47	20.88	23.33	23.53	20.32	20.80
Cr ₂ O ₃	.00	.10	.15	.00	.00	.00	.00
FeO	29.05	29.56	32.18	28.02	28.63	34.81	39.36
MnO	.00	.20	5.03	.00	.18	5.53	.85
MgO	12.18	11.97	1.96	11.76	11.46	1.66	2.52
CaO	.00	.00	2.69	.00	.00	1.37	.28
<u>TOTAL</u>	<u>86.51</u>	<u>86.30</u>	<u>100.03</u>	<u>85.34</u>	<u>85.81</u>	<u>100.10</u>	<u>100.13</u>
CATIONS PER No. OXYGENS	28	28	12	28	28	12	12
Si	5.2774	5.2476	2.9908	4.9139	4.8603	2.9828	2.9628
Ti	.0164	.0348	.0116				
Al	5.4210	5.3215	1.9918	6.0779	6.1237	1.9619	1.9997
Cr		.0174	.0096				
Fe	5.3110	5.4528	2.1783	5.1797	5.2871	2.3848	2.6851
Mn		.0374	.3448		.0337	.3837	.0587
Mg	3.9695	3.9361	.2365	3.8752	3.7725	.2027	.3064
Ca			.2333			.1202	.0245
<u>TOTAL</u>	<u>19.9953</u>	<u>20.0476</u>	<u>7.9967</u>	<u>20.0467</u>	<u>20.0773</u>	<u>8.0361</u>	<u>8.0372</u>
<u>Mg</u>	<u>42.77</u>	<u>41.93</u>	<u>9.79</u>	<u>42.80</u>	<u>41.65</u>	<u>7.83</u>	<u>10.24</u>
X _{Fe}			72.78			77.14	87.33
X _{Mg}			7.90			6.56	9.97
X _{Mn}			11.52			12.41	1.91
X _{Ca}			7.80			3.89	.80
Al ^{iv}	2.7226	2.7524		3.0861	3.1397		
Al ^{vi}	2.6984	2.5691		2.9918	2.9840		

TABLE 22: Microprobe analyses of minerals in paragenesis (53)

is shown by the two analyses of chlorite in sample 881 (table 20), taken just 3 mm apart. The maximum manganese content of the chlorites appears to be 0.3% MnO, and no sensible difference in MnO content between the cores and rims of chlorite laths has been detected at these low levels. In rocks containing garnet, chlorite adjacent to garnet rims either contains no detectable manganese, or else contains less manganese than chlorite grains 7 mm away from the garnet.

Many of the garnet porphyroblasts in the Jervois Range chlorite-rich rocks have manganese-rich cores (up to 40% spessartine content in sample 879), and some of these show the characteristic Rayleigh fractionation curve for Mn content between the cores and rims. For example, the garnet porphyroblasts of sample 887 are almost identical in zoning to the curves depicted in figure 7. However, zoning is less well developed in poikiloblasts rich in quartz inclusions, some of which are hardly zoned at all and have zoning profiles resembling those of small garnet crystals from the Broken Hill rock described previously (fig. 13). Garnet rims in rocks from the northern locality are richer in manganese than those from the southern locality and drill core. Although bulk-composition partly controls the spessartine content of garnet rims, the difference between the range of compositions (9 to 17% versus 7 to 0.4% spessartine contents, tables 20 to 22) also reflects a slight increase in metamorphic grade in the southern part of the mine sequence.

Kamineni (1976) has shown that a plot of 15 coexisting chlorite-

Fe
CATIONS per
12 OXYGENS

Mn, Mg, Ca
CATIONS per
12 OXYGENS

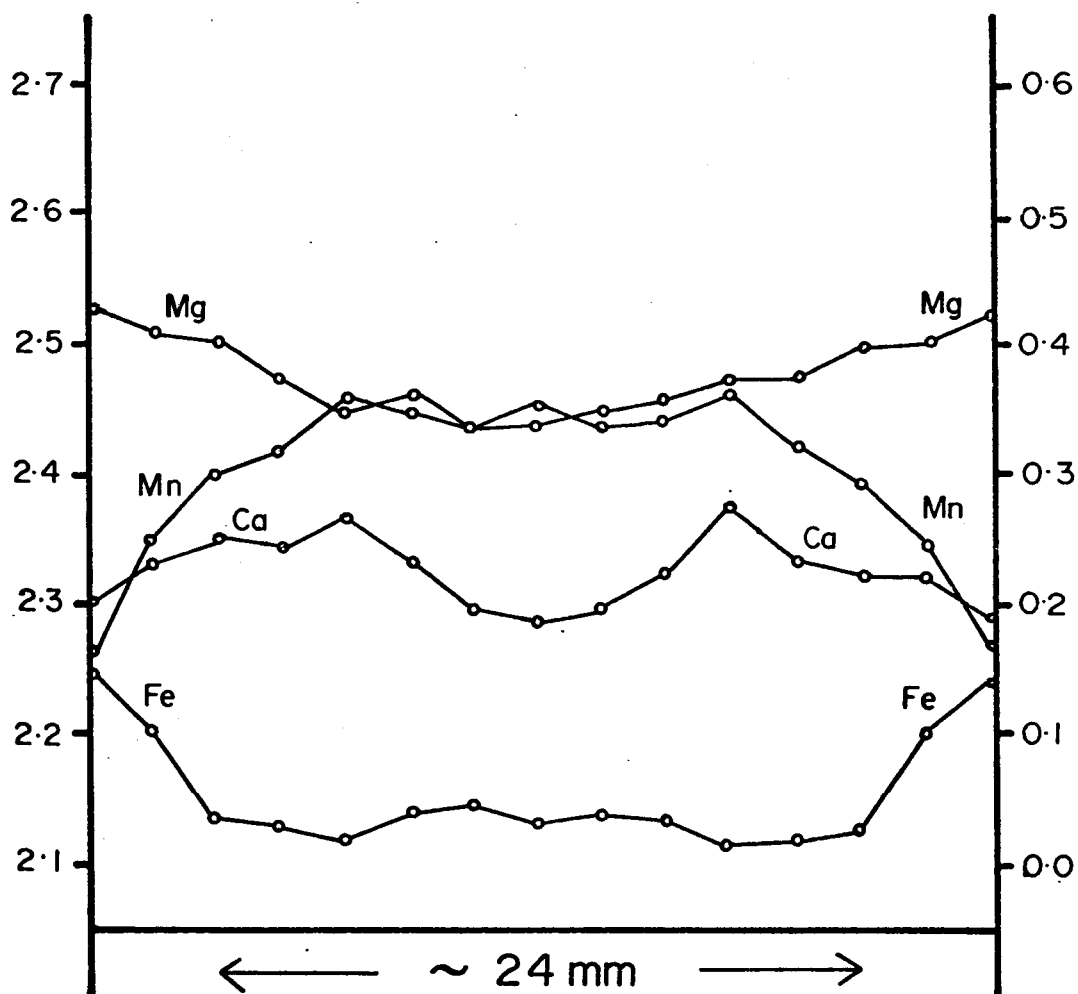


FIGURE 13: Garnet zoning in sample 893, a chlorite - garnet - magnetite - quartz schist from the Thackaringa - Pinnacles Retrograde Shear Zone, Broken Hill, N.S.W. Element concentrations are shown as the number of cations per 12 oxygen - formula. The vertical scales are identical to those of figure 7 to facilitate comparison.

garnet pairs, formed under epidote-amphibolite facies conditions, define a trend approximating a constant $K_D^{\text{chlt-gt}}_{\text{Mg-Fe}}$ value on a linear plot of chlorite Mg versus garnet Mg. He obtained a range of distribution coefficients between 5.38 and 14.29, with an average of 8.59, but used whole-garnet analyses and not rim compositions to derive these figures.

The compositions of 8 coexisting chlorite-garnet rims from the Jervois Range area, and one each from the Broken Hill, Copperfield (W.A.) and Koolanooka (W.A.) areas (studied here for comparison) also plot on a well-defined trend that may be approximated by

$$\text{Mg}^{\text{gt}} = 15.21 \ln \text{Mg}^{\text{chlt}} - 46.33; r = 0.89 \quad (\text{eqn. 55})$$

These K_D values range from 5.06 to 7.41, with an average of 6.33.

This well-defined trend may appear strange in the light of the compositional controls of K_D 's discussed in chapters 4 and 5.

However, reference to table 23 shows that these garnet-chlorite pairs occur in a relatively restricted compositional field. Consequently, compositions outside this field will probably not plot on this trend (e.g. high Mg pairs in fig. 1 of Kamineni, 1976).

Since the precise variation of $K_D^{\text{chlt-gt}}_{\text{Mg-Fe}}$ with temperature has not been determined, and since compositional correction factors have not been formulated, all that can be said of the mineral-pairs studied here is that they formed under broadly similar conditions of temperature. By comparison with the data of Albee (1965a) and Kamineni (1967), temperatures of formation appropriate to lower-amphibolite facies conditions may be inferred for these rocks.

The data of table 23 do not lend themselves to treatment by the

smpl.	X_{Al}^{vi} chl.	Mg chl.	Mg gt.	X_{Fe}^{viii} gt.	X_{Mg}^{viii} gt.	X_{Mn}^{viii}	X_{Ca}^{viii}	$K_{D_{Mg-Fe}}^{chl-gt}$	$\ln K_D$
879	.2418	50.36	12.05	.6584	.0902	.1712	.0803	7.4074	2.0025
882	.2477	37.12	8.47	.7864	.0728	.0987	.0421	6.3786	1.8522
885	.2253	42.77	9.79	.7278	.0790	.1152	.0780	6.8856	1.9294
886	.2484	42.79	10.24	.8733	.0997	.0191	.0080	6.5533	1.8800
887	.2699	39.33	9.00	.8120	.0803	.0679	.0389	6.5576	1.8806
889	.2479	37.65	10.65	.8693	.1037	.0036	.0234	5.0634	1.6220
827	.2386	39.89	9.70	.8527	.0916	.0343	.0214	6.1772	1.8209
826	.2283	37.42	8.71	.8782	.0838	.0297	.0083	6.2803	1.8374
890	.2321	38.68	9.29	.8266	.0847	.0130	.0757	6.1548	1.8173
891	.2292	35.79	8.12	.7891	.0697	.0868	.0543	6.3117	1.8424
893	.2238	52.24	15.63	.7461	.1382	.0501	.0665	5.9056	1.7759

Since a plot of chlorite Mg versus garnet Mg for the above samples, excluding samples 889 and 893, almost defines a straight line, it might be inferred that the above chlorite - garnet pairs (excepting 889 and 893) equilibrated under similar conditions of temperature. If this is the case, then the variation in K_D is largely due to compositional variations in the minerals. Consequently, a regression of the type used in chapter 4 was attempted to define the controls on K_D (as in table 7.) with the following results:

$$\text{Excluding 889 and 893, } \ln K_{D_{Mg-Fe}}^{chl-gt} = -1.5994(X_{Fe}^{gt} - X_{Fe}^{gt}) - 0.7191(X_{Mn}^{gt} + 2X_{Mn}^{gt}) + 3.1453$$

$$(R = 0.9583)$$

Although this relation is well defined, the coefficients of the garnet compositional terms are negative, and this is not consistent with the relation derived from the data of Guidotti (1974). Furthermore, there is little if any field evidence to indicate appreciable temperature differences between sample 889 and samples 887 and 886. This suggests that the above relation may be largely spurious. In fact, inclusion of samples 889 and 893 yields the relation:

$$\ln K_{D_{Mg-Fe}}^{chl-gt} = 0.4969(X_{Fe}^{gt} - X_{Mg}^{gt}) + 0.9781(X_{Mn}^{gt} + 2X_{Ca}^{gt}) + 1.3363$$

$$(R = 0.6583)$$

This relation is consistent with that in table 7, but is not as well defined as the one above it. Hence many more samples from a single, small area are required to more properly evaluate the relative effects of mineral composition and temperature on K_D .

TABLE 23: Comparative table of garnet and chlorite compositional parameters from rocks inferred to have been formed under similar temperature conditions.

method used in chapter 4. Since, in these rocks, variations of octahedral aluminium in chlorite are too great to be ignored, and since a wider range of chlorite Mg values is present here, larger errors may result from the possible non-ideal behaviour of Fe-Mg substitution in chlorite. Several regression techniques were applied to the data in table 23, but the correlations were generally poor and no self-consistent relations that improved the trend of equation 55 could be found. Regression on all the possible variables for such a small sample-size would lead to possible spurious relations (e.g. the negative coefficients of the Fe-Mg and Ca-Mn terms in the first relation in table 23). The author is currently attempting to obtain many more chlorite-garnet-bearing samples, in order to bracket more closely the compositional effects on K_D , and ascertain its temperature dependence more accurately.

6.4 Mineral Reactions in Chlorite-Quartz⁺-Garnet Schists

The bulk-compositions of these rocks belong essentially to the system $\text{SiO}_2\text{-Al}_2\text{O}_3\text{-FeO-MgO-H}_2\text{O}$, with minor amounts of MnO-CaO-TiO_2 (appendix table 8). For all practical purposes, the four minerals chlorite, quartz, garnet and magnetite comprise all the phase assemblages of these rocks. As will be shown in part 6 of this chapter (and consistent with the observations of part 1), these rocks were derived by the isochemical metamorphism of sediments of the appropriate bulk-composition, involving large-scale mass transfer of no components other than H_2O and possibly CO_2 . On this basis, inferences can be made concerning realistic mineral reactions in

chlorite-quartz⁺-garnet rocks, based on observed mineral compositions and mass-balance constraints.

The occurrence (in the lower-grade northern exposure) of some garnet-free chlorite-quartz schists relatively poor in MnO leads to two conclusions:

- (i) Under conditions of the lower greenschist facies, the mineral assemblage of all the rocks considered here would essentially be chlorite-quartz-magnetite, with very minor amounts of calcite/dolomite/ankerite, ilmenite/rutile, and white mica. As a consequence of this, the bulk-rock (silicate) composition may be corrected for magnetite content by subtraction of mol. Fe_2O_3 from mol. FeO (although a potential source of error applies to those rocks in which the magnetite has been oxidized during weathering). The remaining FeO, together with all the MgO and Al_2O_3 , must reside in chlorite, so that the approximate composition of the "initial" or low-grade chlorite can be calculated from the corrected bulk-composition. Even in samples with relatively Mn-rich chlorites (e.g. 879, 881), microprobe analyses of co-existing magnetite show little if any Mn ($\ll 0.2\%$ MnO). Hence, to a first approximation, manganese also resides in the "initial" chlorite.
- (ii) The nucleation and growth of garnet with increasing metamorphic grade appears to be favoured in rocks in which the initial chlorite is:

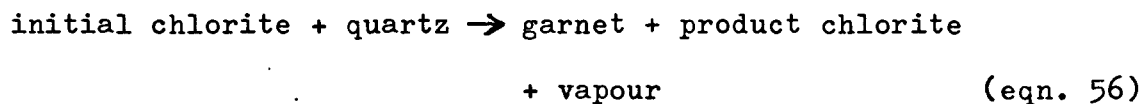
- (a) Mn-rich; and
- (b) relatively Fe-rich.

Thus sample 881, with only 0.25% MnO, and with chlorite $Mg \div 44.5$, contains no garnet. An Fe-rich chlorite-quartz assemblage will react to form an Fe-rich garnet with increasing metamorphic grade (Hsu, 1968), and the composition of the remaining chlorite must become more magnesian.

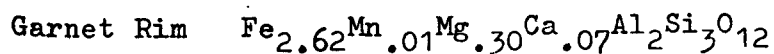
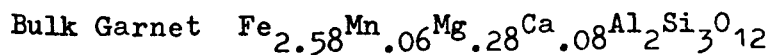
Three samples were selected to study the formation of garnet from chlorite+quartz. Analysis of samples adjacent to the three selected indicates that, to a first approximation, each multi-variant garnet-forming reaction may be considered to be isochemical within the domain of the sample. (1) Sample 879, from the northern exposure, contains abundant garnet porphyroblasts with diameters ranging from 1.5 to 2.5 mm, with an average value of about 2 mm. (2) Sample 882 (also from the northern exposure) contains relatively few garnet porphyroblasts (about one per 125 cm^3 of rock). These are all about 8 mm in diameter, and appear to be homogeneously distributed throughout the particular horizon. (3) Sample 889, from the higher-grade southern exposure, contains a garnet porphyroblast, 2.6 cm diameter, in a volume of rock of 220 cm^3 . Within the small domain (1.8 m long by 0.4 m wide) from which it was taken, the garnet crystals are all of approximately the same size, and appear to be uniformly distributed.

All these garnets are zoned, more or less following Rayleigh fractionation curves, and it is assumed that, as these garnets grew, the compositions of their rims were in equilibrium with their chlorite-

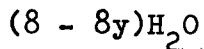
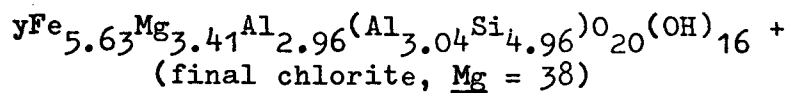
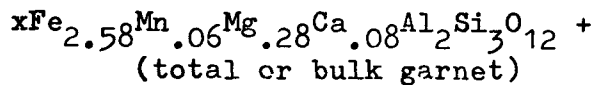
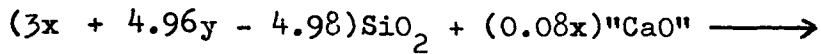
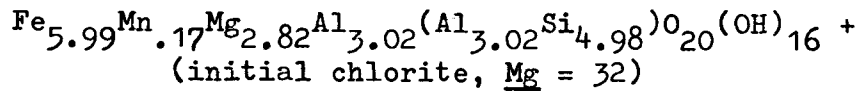
quartz matrices (Hollister, 1966, 1969a; Kretz, 1973). This pre-supposes restricted or no diffusion in garnet, and much less restricted diffusion in the matrix (but still sufficiently restricted to maintain low-compositional gradients for Fe, Mg and Mn in samples such as 886, table 22). With the further assumption of negligible or no oxidation or reduction during the garnet-forming reaction, mass balance in a closed system enables (in theory) the compositional variations of the products to be followed as the following reaction proceeds:



Since any point within the garnet was once a rim, "garnet" in equation 56 refers to the bulk-composition of all the garnet within any of the specified "rims". Thus, by taking successive points along a garnet profile, it is possible (in theory) to follow the reaction as the garnet grew; since the initial chlorite and garnet compositions can be (approximately) calculated. The total or bulk-composition of any garnet within any specified "rim" is approximated by the composition of the "rim", since the volume of the outer section of any sized garnet is much greater than the volume of the initial, Mn-rich nucleus. As an example, the bulk-composition of one large porphyroblast from sample 889 was calculated from microprobe data, and checked against the XRF analysis of half that garnet, giving excellent agreement, as shown by the following formulae:



The net garnet-forming reaction for sample 889 (using the true bulk-garnet composition and the observed final chlorite composition from table 21) is thus approximated by:



(eqn. 57)

Equation 57, even without solving for x and y, indicates the net reaction that has taken place to form garnet in sample 889. A graphical representation of equation 57 is easily made (fig. 14), requiring only the plotting of garnet core and rim analyses, together with final (observed) and initial (calculated) chlorite compositions, for an approximation. Equation 57, together with similar equations for samples 879 and 882, indicates little change in the Al content of chlorite as the reaction proceeds. Therefore, figure 14 depicts compositional changes in garnet and chlorite in the top half of the FeO-MnO-MgO triangle. In this figure, the crosses represent initial compositions, and, as reactions proceed, the compositions of the bulk garnets move towards the arrowheads, which closely correspond to observed rim compositions.

In general, there will be no unique solution for x and y that exactly balances all the elements in equation 57, although, with

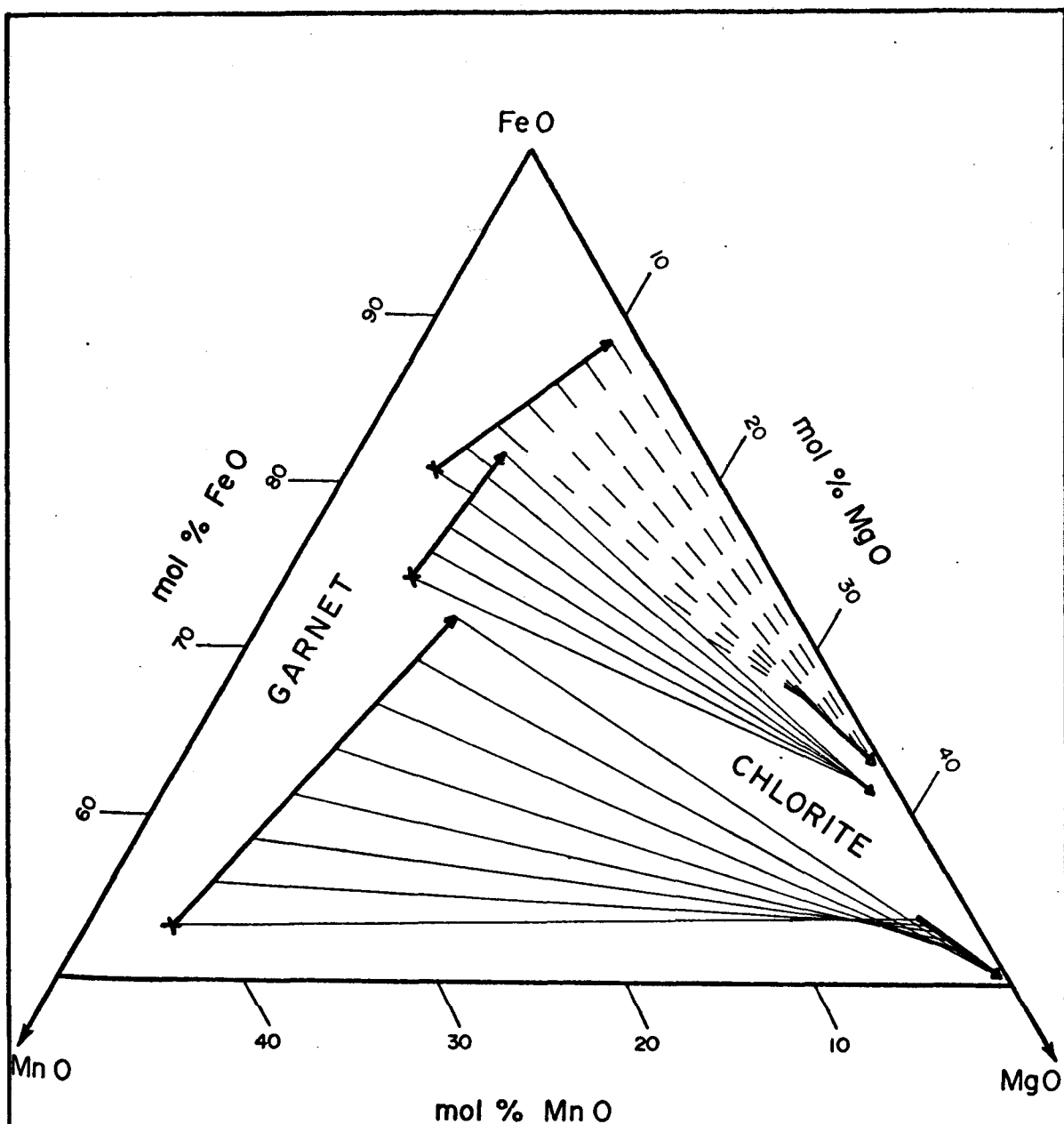


FIGURE 14: The reaction of chlorite + quartz to garnet, projected on the FeO apex of the molecular FeO - MnO - MgO triangular plot. Upper set of tie lines: sample 889; middle set of tie lines: sample 882; lower set of tie lines: sample 879. Initial garnet compositions (i.e. cores) are plotted as crosses; as the reaction proceeds, garnet and chlorite compositions move towards the arrowheads, which represent observed chlorite and garnet rim compositions. The observed garnet rim compositions closely approximate the bulk compositions of the garnet crystals. For further explanation, see text.

minor "adjustments" to the initial chlorite composition, unique values may be calculated. This arises from the approximations made and from sampling errors. One sampling error, applicable to all rocks with large porphyroblasts, is that the analysed sample may contain a garnet/matrix ratio slightly different from that produced by the actual reaction. This leads to errors in the calculation of the initial chlorite composition.

A further complication arises if the chlorite composition in the sample is heterogeneous. In this case, the composition of the equilibrium chlorite and garnet rim is controlled by relative element diffusion rates as well as bulk-composition, and the garnet-forming reaction may not have taken place iso-chemically within the compositional domain represented by the sample.

It is possible that the real reaction was accompanied by redox reactions, so that equation 57 is not complete. The source of Ca is not known; if it came from decarbonation of minor calcite, there is no problem, but if it came from the breakdown of dolomite or ankerite, or from an aluminous phase such as epidote, equation 57 is not complete. The roles of magnetite and ilmenite as sources for Mn and Ti have been ignored, and, if these minerals enter the reaction, then the Fe/Mg ratio will change. Perhaps the most important detail is that of magnetite correction. If any of the magnetite has been oxidized, then the silicate FeO is difficult to determine exactly, and the problem is aggravated

by oxidation on grinding.

Despite these details, equation 57 is a realistic approximation of the probable multivariant garnet-forming reaction. It is most easily applied to rocks in which the garnet crystals are all of approximately the same size, and show the normal, bell-shaped zoning profile. Figure 14 makes clear two points concerning these garnet-forming reactions:

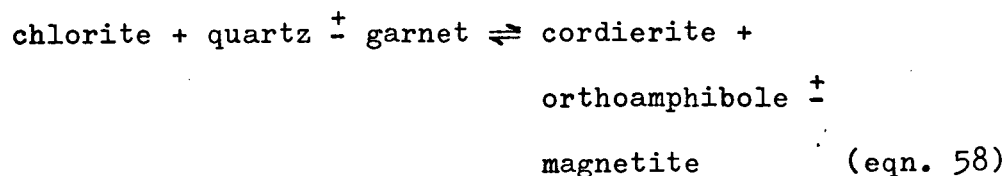
- (i) in such a multivariant assemblage, the pyrope content of garnet is as much determined by the initial chlorite composition as it is by the temperature and pressure under which it crystallized;
- (ii) increasing the Mn content will cause increasingly more magnesian chlorite to react to garnet.

It is therefore possible to explain why a more magnesian chlorite exists with garnet in the lower-grade, Mg-rich and Mn-rich northern mine sequence than in the southern, higher-grade, Fe-rich, Mn-poor area.

With increasing metamorphic grade, and under appropriately low f_{O_2} conditions (Hsu, 1968), garnet would become poorer in Mn and richer in Mg as further chlorite reacts. At these temperatures, coexisting magnetite/ilmenite pairs cannot be used to estimate T and f_{O_2} , as explained in chapter 3.

The garnet-forming reaction is terminated at the upper stability limit of intermediate-Mg chlorite+quartz, where, in

the absence of potassium-bearing phases, the remaining chlorite reacts to form a gedrite-cordierite⁺quartz-bearing assemblage. This is illustrated by two samples from Koolanooka, W.A., analysed by the author (tables 24 and 25 respectively). Both samples, especially 891, are very similar to chlorite-quartz-garnet rocks in bulk-composition (see figs. 15 and 16 and appendix table 9). The experimental work of Hsu and Burnham (1969), and Fleming and Fawcett (1976), also indicates that the upper stability limit of intermediate-Mg chlorite+quartz is bounded by cordierite- and orthoamphibole-forming reactions. However, it is not possible to state whether garnet enters the reaction, or whether it remains refractory, possibly exchanging Fe and Mg with the mineral assemblage being formed. Textural evidence from samples 891 and 892 is not conclusive (see descriptions in appendix), and accurate mass balance equations cannot be set up, since it is not known whether magnetite enters the reaction. Nor is there any lower-grade equivalent to indicate the composition of the reacting chlorite. Thus the inferred reaction is:



This reaction is similar to that inferred by Lal and Shukla (1975) for quartz-bearing, chlorite-rich rocks in the Khetri Copper Belt, India.

CORDIERITE-GARNET-GEDRITE-CHLORITE-QUARTZ-MAGNETITE HORNFELS

	<u>GARNET</u>	<u>GARNET</u>	<u>CORDIERITE</u>	<u>GEDRITE</u>	<u>CHLORITE</u>
	core	rim			prob.ret.
SiO ₂	36.50	36.53	47.49	42.32	22.88
TiO ₂	.00	.16	.00	.18	.00
Al ₂ O ₃	21.05	20.76	32.45	13.91	21.93
Cr ₂ O ₃	.00	.00	.00	.12	.00
FeO	35.19	35.00	11.55	32.16	31.22
MnO	2.74	3.91	.14	.87	.00
MgO	2.92	1.79	6.41	6.87	9.66
CaO	1.52	1.94	.00	.25	.00
Na ₂ O	.00	.00	.45	1.20	.00
<u>TOTAL</u>	<u>99.92</u>	<u>100.09</u>	<u>98.49</u>	<u>97.88</u>	<u>85.69</u>
CATIONS PER No. OXYGENS	12	12	18	23	28
Si	2.9606	2.9753	4.9665	6.5349	5.1235
Ti		.0098		.0209	
Al	2.0112	1.9928	3.9995	2.5314	5.7876
Cr				.0147	
Fe	2.3870	2.3840	1.0101	4.1529	5.8465
Mn	.1882	.2697	.0124	.1138	
Mg	.3531	.2173	.9993	1.5814	3.2247
Ca	.1321	.1693		.0414	
Na			.0912	.3593	
<u>TOTAL</u>	<u>8.0332</u>	<u>8.0182</u>	<u>11.0790</u>	<u>15.3507</u>	<u>19.9823</u>
<u>Mg</u>	12.89	8.35	49.71	27.58	35.55
X _{Fe}	78.00	78.41			
X _{Mg}	11.54	7.15			
X _{Mn}	6.15	8.87			
X _{Ca}	4.32	5.57			
Al ^{iv}				1.4651	2.8765
Al ^{vi}				1.0663	2.9111

TABLE 24: Microprobe analyses of minerals in sample 891 from Koolanooka, W.A. Chlorite is abundant and probably retrograde (see text).

CORDIERITE-GARNET-GEDRITE-BIOTITE-MAGNETITE HORNFELS

	<u>GARNET</u>	<u>GARNET</u>	<u>CORDIERITE</u>	<u>GEDRITE</u>	<u>BIOTITE</u>	<u>CHLORITE</u>
	core	rim				retrograde
SiO ₂	36.79	36.83	48.42	51.11	33.89	25.23
TiO ₂	.00	.00	.00	.00	1.07	.00
Al ₂ O ₃	20.87	20.86	32.71	9.86	17.71	20.41
FeO	37.22	37.72	8.50	23.60	26.21	26.26
MnO	.16	.20	.00	.00	.00	.00
MgO	3.51	3.44	8.39	13.02	8.95	14.18
CaO	.75	.94	.00	.00	.39	.00
Na ₂ O	.00	.00	.36	.28	.36	.00
K ₂ O	.00	.00	.00	.00	7.73	.00
<u>TOTAL</u>	<u>99.30</u>	<u>99.99</u>	<u>98.38</u>	<u>97.87</u>	<u>96.31</u>	<u>86.08</u>
CATIONS PER No. OXYGENS	12	12	18	23	22	28
Si	2.9875	2.9784	4.9908	7.3901	5.2633	5.4491
Ti					.1250	
Al	1.9973	1.9881	3.9735	1.6802	3.2415	5.1952
Fe	2.5276	2.5510	.7327	2.8537	3.4041	4.7430
Mn	.0110	.0137				
Mg	.4249	.4147	1.2892	2.8064	2.0721	4.5655
Ca	.0653	.0814			.0649	
Na			.0719	.0785	.1084	
K					1.5314	
<u>TOTAL</u>	<u>8.0136</u>	<u>8.0273</u>	<u>11.0581</u>	<u>14.8089</u>	<u>15.8107</u>	<u>19.9528</u>
<u>Mg</u>	14.39	13.98	63.76	49.58	37.84	49.05
X _{Fe}	83.45	83.34				
X _{Mg}	14.03	13.55				
X _{Mn}	.36	.45				
X _{Ca}	2.16	2.66				
Al ^{iv}				.6099	2.7367	2.5509
Al ^{vi}				1.0703	.5048	2.6443

TABLE 25: Microprobe analyses of minerals in sample 892 from Koolanooka, W.A. The trace amounts of chlorite are retrograde.

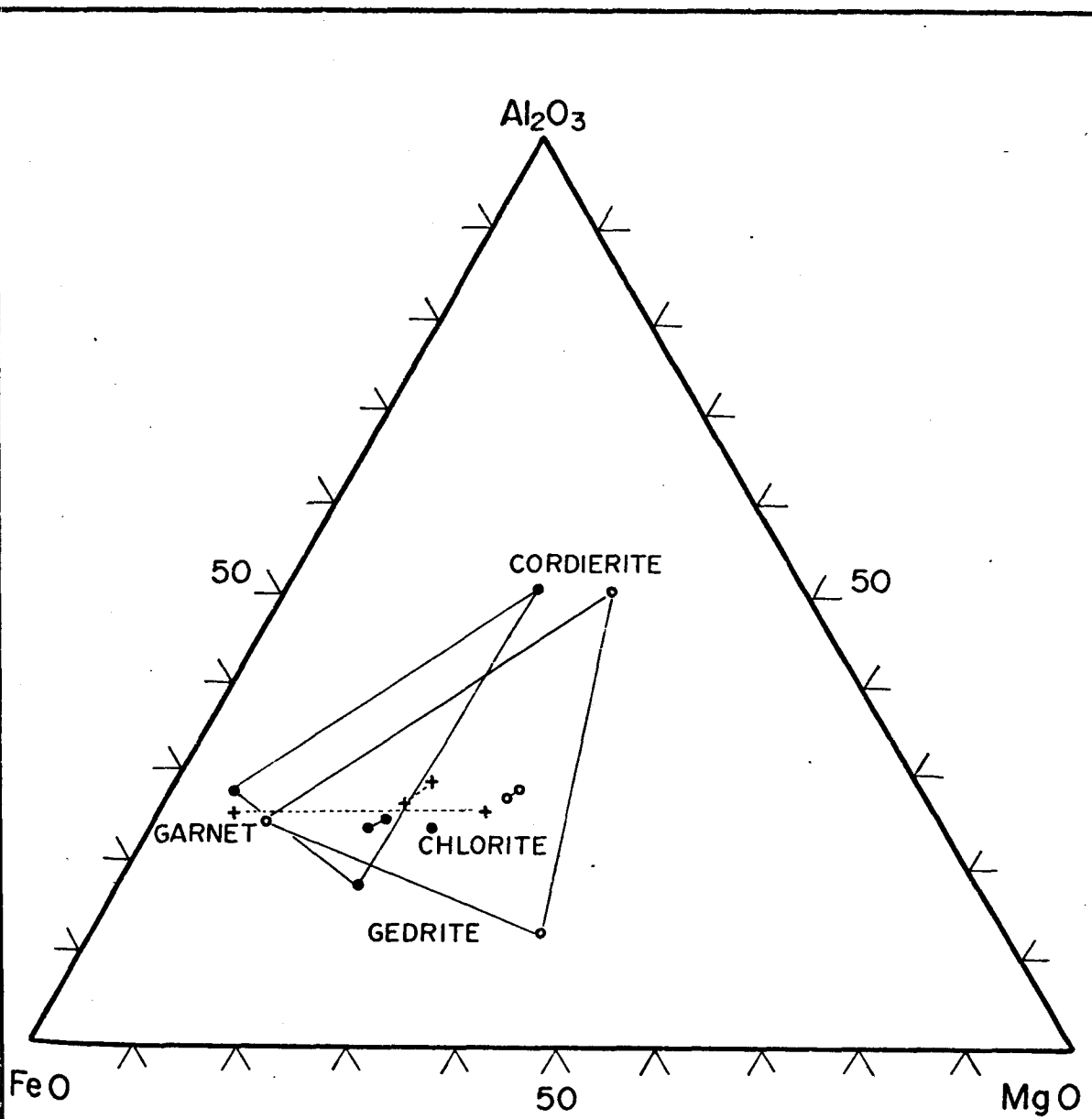


FIGURE 15: Molecular Al_2O_3 - FeO - MgO plot showing the chemical relationship between two cordierite - gedrite - garnet (\pm quartz \pm chlorite) assemblages from Koolanooka W.A., and a chlorite - quartz - garnet schist from the Jervois Range area N.T. Open circles: sample 892; filled circles: sample 891, (W.A.); crosses: sample 886 (N.T.). Closely spaced, tied symbols represent the variation in bulk rock composition owing to possible oxidation of minor magnetite, as discussed in the text.

6.5 Geochemistry

The major and trace element, bulk-rock analyses of 11 chlorite-quartz⁺-garnet schists from the Jervois Range area are presented in appendix table 8. In addition, an analysis of a staurolite- and andalusite-bearing chlorite-garnet-quartz schist (sample 827) appears in appendix table 3. The means, ranges and the half-matrix of linear correlation coefficients for the major elements of these 12 samples are presented in table 26.

Sample 884, which is cut by fine veinlets of quartz-fluorite⁺-calcite up to 2 mm thick, contains 1.31% CaO, and sample 886 contains 1.21% Na₂O. With these exceptions, each of the components CaO, Na₂O, and K₂O is less than 1% by weight in each rock. Hence, for practical purposes, the silicate assemblages fall within the system SiO₂-Al₂O₃-FeO-MgO-(MnO-TiO₂), and the oxide assemblages fall within the system FeO-Fe₂O₃-TiO₂. Within the compositional range shown by these 12 samples, the interdependence of the full 12 components is given by the perfectly defined multiple regression equation at the foot of table 26.

Most of the numerically moderate to high major element correlations may be explained by the simple mineral assemblages of these rocks. The negative correlations of silica with Al, Fe³⁺, Fe²⁺, Mg, and H₂O⁺ are a consequence of closure. Since the minerals chlorite, magnetite and garnet (and, in sample 827, staurolite and andalusite) between them contain all these components in any one rock, as the amount of modal quartz rises, so these latter minerals must decrease

BULK-ROCK GEOCHEMICAL DATA - JERVOIS RANGE AREA CHLORITE - QUARTZ ± GARNET SCHISTS

	mean	std. dev.	lowest	ampl.	highest	ampl.
SiO ₂	41.04	13.22	21.31	(881)	64.76	(888)
TiO ₂	.88	.56	.07	(888)	1.71	(879)
Al ₂ O ₃	16.31	3.26	11.24	(888)	20.48	(886)
Fe ₂ O ₃	7.70	4.77	2.13	(888)	19.45	(879)
FeO	19.59	5.56	13.04	(888)	31.47	(809)
MnO	.70	.49	.10	(883)	1.94	(880)
MgO	6.13	2.17	3.10	(827)	10.78	(881)
CaO	.40	.35	.08	(882)	1.31	(884)
Na ₂ O	.28	.38	.02	(880,5,9)	1.21	(886)
K ₂ O	.27	.36	.00	(886)	.95	(884)
P ₂ O ₅	.12	.05	.03	(888)	.19	(881,7)
H ₂ O ⁺	6.06	2.21	2.62	(884)	9.55	(881)

HALF - MATRIX OF LINEAR CORRELATION COEFFICIENTS

	SiO ₂	TiO ₂	Al ₂ O ₃	Fe ₂ O ₃	FeO	MnO	MgO	CaO	Na ₂ O	K ₂ O	P ₂ O ₅	H ₂ O ⁺	Totl.
SiO ₂	1	-.22	-.65	-.69	-.79	.00	-.76	.11	-.07	.39	-.41	-.73	.14
TiO ₂		1	-.18	.54	-.28	-.06	.53	-.10	-.37	-.45	.19	.45	-.06
Al ₂ O ₃			1	.07	.71	.07	.22	.25	.27	.00	.61	.16	-.24
Fe ₂ O ₃				1	.19	-.02	.66	-.38	.12	-.44	.08	.67	.09
FeO					1	-.04	.40	.17	.05	-.05	.35	.40	-.23
MnO						1	-.12	.48	.12	.00	-.12	-.24	-.38
MgO							1	-.45	-.21	-.63	.26	.91	.01
CaO								1	-.06	.51	.12	-.56	-.59
Na ₂ O									1	-.06	-.39	-.25	-.21
K ₂ O										1	.22	-.74	-.09
P ₂ O ₅											1	.24	.12
H ₂ O ⁺												1	.29
Totl.													1

Bulk - rock total = 3.086SiO₂ - 3.261TiO₂ + 2.115Al₂O₃ + 3.747Fe₂O₃ + 3.107FeO
- 0.093MnO + 4.877MgO + 10.247CaO + 2.255Na₂O - 11.657K₂O + 71.357P₂O₅ - 0.215H₂O⁺
- 187.249 (R = 1.000)

TABLE 26: Bulk - rock geochemical data for 12 chlorite-quartz-garnet schists from the Jervois Range area. These samples are listed in appendix table 8, and one also containing staurolite and andalusite (sample 827) is listed in appendix table 3.

in volume, together with the Al, Fe^{3+} , Fe^{2+} , Mg and H_2O^+ content of the rock. Within this group of components, the high positive correlation of Mg with H_2O^+ is explained by the fact that Mg is strongly partitioned into chlorite, essentially the only hydrous phase present. Since both garnet and chlorite are high in Al and Fe^{2+} , but differ slightly in Fe^{2+}/Al ratios, the correlation of Fe^{2+} with Al is moderate. If sample 827 is not included, $r_{\text{Al-Fe}^{2+}}$ rises to 0.91, as both staurolite and andalusite have much lower Fe^{2+}/Al ratios than do chlorite and garnet.

The abundance and behaviour of trace elements within these rocks may be differentiated into four groups. (i) The first of these contains Zn and Ga, the concentrations of which follow moderately well those of total iron and aluminium respectively ($r_{\text{Zn-Fe}^{\text{TOTAL}}} = r_{\text{Ga-Al}} = 0.78$), and do not correlate well with any other trace element analysed. The range and average zinc content of these rocks are 187 to 622 and 423 ppm respectively. Although these are high compared with marine and fresh-water shales, the high values are expected from the sedimentary equivalents of the Jervois Range rocks (quartz-chlorite-iron oxides) since zinc in pelitic sediments is concentrated in chlorite and iron oxides (Wedepohl, 1970, 30-K-4). The range and average gallium content of these rocks are 15 to 34 and 26 ppm respectively. These values are normal for both shales of comparable aluminium content and their metamorphic equivalents, as there is little if any differentiation of gallium and aluminium during sedimentation and isochemical metamorphism (Wedepohl, 1970, 31-K-1 and -2).

(ii) The second group contains Ba, Rb, Sr and Cu, none of which appear to correlate with any major or trace element analysed. Strontium contents all fall below 10 ppm, but the approximate values listed cannot be used for meaningful correlation with (admittedly low) calcium. Barium contents range from 365 ppm to below the detection limit, and do not correlate with potassium. Apart from sample 884, in which rubidium may have been hydrothermally introduced, the range of rubidium values is 142 ppm to below the detection limit; like barium, rubidium does not correlate with potassium. Excepting sample 884, the range of K/Rb ratios is 54 to 116, well below the mean value of 270 for Precambrian pelitic sediments from Alberta and British Columbia (Leask, 1967). For younger shales, the ratio average is closer to 150. The significance of these differences will be discussed in the next section. Copper contents range from 14 ppm to over 0.5%, but, since much of this is contained in chalcopyrite blebs which are not uniformly distributed (some rocks of this type contain up to 2% Cu by weight), an average figure is of little value.

(iii) The third group contains Zr, Y, and Nb, which behave coherently ($r_{\text{Zr-Nb}} = 0.86$, $r_{\text{Zr-Y}} = 0.81$ and $r_{\text{Nb-Y}} = 0.79$). This group also contains Th, U, and Pb, but correlation is weaker, and many values fall below the detection limit. The ranges are as follows:

Zr	253	-	61 ppm
Y	112	-	8 ppm
Nb	20	-	3 ppm
U	16	-	below detection limit
Th	165	-	below detection limit
Pb	74	-	below detection limit

The correlations suggest that a large part of each of these elements is in zircon, and, as suggested by Deer, Howie and Zussman (1962), in inclusions within zircon. Most yttrium is probably contained in the xenotime end-member of zircon solid-solution (Romans et al., 1975), but correlation of Y with P would be meaningless, as the partitioning of P between xenotime and apatite is not known in any of the rocks.

(iv) The fourth group of elements, which behave antipathetically to those in group three, contains Ni, Cr, V and Sc. These elements behave coherently, and correlate well with Ti; relevant data (in ppm) and the half-matrix of correlation coefficients are given below.

	Ti	Ni	Cr	V	Sc
Ti	1	0.89	0.95	0.91	0.94
Ni		1	0.86	0.83	0.95
Cr			1	0.80	0.89
Sc				1	0.89

	mean	std. devn.	range
Ni	125	111	309 - below detection limit
Cr	247	190	518 - below detection limit
Sc	28	21	61 - below detection limit
V	155	135	476 - 61

The high values of these elements exceed the range in "normal" (i.e. non-pelagic, non-ferruginous) shales, yet the lower values fall below the same range, even in rocks of similar bulk composition (e.g. 879 versus 886). The twelve rocks may thus be divided, on

the basis of their trace elements alone, by their content of group three and group four elements as follows:

high group 4	879	to		low group 4	886 to 888
low group 3	885			high group 3	and (889).

The lack of bulk-chemical control on these trace elements will be discussed in the following section.

6.6 Origin of Chlorite-Quartz⁺Garnet⁺Magnetite Schists

As shown in table 19, the chlorite-quartz⁺garnet schists from the Jervois Range area are not unique either geographically or mineralogically. At higher metamorphic grades, their bulk-compositional equivalents are cordierite-gedrite⁺garnet⁺quartz and cordierite-hypersthene⁺garnet⁺orthoamphibole assemblages. Although many of these rock-types are found in Precambrian basements, Palaeozoic and Mesozoic occurrences have been reported from the Alps (D. W. Durney, pers. comm.).

As shown in figure 16, the bulk-compositions of chlorite-quartz⁺garnet rocks and their higher-grade equivalents are also not unique. They are part of a continuum of rocks, the bulk-compositions of which lie essentially within the system $\text{SiO}_2\text{-Al}_2\text{O}_3\text{-FeO-MgO-(Fe}_2\text{O}_3\text{-MnO)}$, all with Na_2O , K_2O and CaO less than 1% by weight. Within this restricted compositional range, the more "extreme" bulk-compositions are relatively well documented. In figure 16, certain metamorphosed silicate iron-formations plot near the FeO apex (e.g. Immega and Klein, 1976; Klein, 1966, 1974; Bayley and James, 1973), whereas the

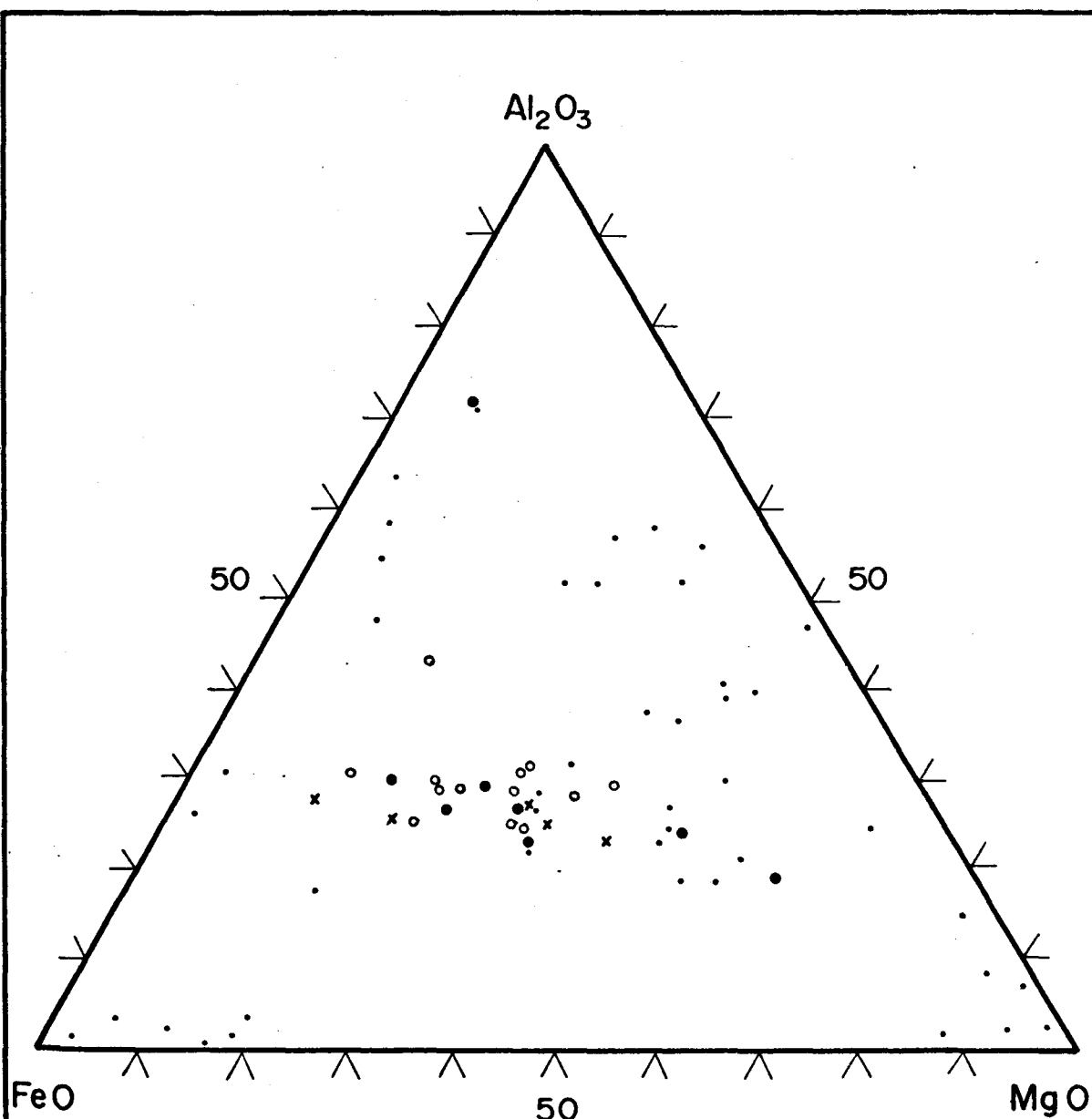


FIGURE 16: Molecular Al_2O_3 - FeO - MgO plot of bulk compositions of metamorphic rocks, each of which commonly contains less than 1% of each of the components CaO , Na_2O and K_2O . Open circles: chlorite - quartz \pm garnet - magnetite schists from the Jervois Range area; crosses: chlorite - quartz \pm garnet - magnetite assemblages from Italy, Western Australia and New South Wales, analysed as part of this work; filled circles: chlorite-rich rocks from the literature; dots: high-grade, chlorite-free assemblages from the literature. For references, see text and table 19.

MgO apex is occupied by metamorphosed low-Ca serpentinites and dunites (e.g. Irving and Ashley, 1976; Hancock et al., 1971). Metamorphosed (and reduced) laterites and bauxites plot near the Al_2O_3 apex on the FeO side (e.g. Iwao, 1973; Seki, 1954; Uruno and Kanisawa, 1965), leaving just two compositional groups, the origins of which are problematical. The first of these contain high-alumina rocks with high MgO, low silica, and only minor FeO. These rocks give rise to assemblages such as cordierite-sapphirine-spinel⁺ corundum or sillimanite, and have bulk-compositions with Al/Si much greater than those formed by any simple combination of clay minerals (e.g. Woodford and Wilson, 1976a; Warren, 1975; G. S. Teale, pers. comm.). Gibbsite, diasporite or boehmite must have been part of the pre-metamorphic assemblages of such rocks, assuming they all represent isochemically metamorphosed sediments. This problem is currently being studied by the author, and will not be dealt with here in further detail.

The second poorly understood bulk-compositional group having no chemical counterparts among common sedimentary or igneous rocks contains the chlorite-quartz⁺-garnet schists and their higher-grade equivalents. As shown in figure 16, these require subequal amounts of Al_2O_3 , FeO and MgO.

One way of deriving appropriate bulk-compositions for these rocks is by invoking metasomatic removal of K, Na and Ca from more "normal" igneous or sedimentary rocks during metamorphism, possibly with the simultaneous addition of Mg and/or Fe. This type of origin has been invoked by several workers to explain the

composition of the chlorite-garnet schist (e.g. sample 893) in the Thackaringa-Pinnacles Retrograde Shear Zone near Broken Hill, N.S.W., discussed previously. While retrogression from lower granulite and upper amphibolite facies to lower amphibolite and upper greenschist facies has undoubtedly taken place in this Zone (Vernon, 1969; Vernon and Ransom, 1971; Chenhall, 1973), this need not imply the metasomatic addition or removal of any component other than H_2O and CO_2 . Much work needs to be done before the origin of this particular occurrence can be reliably ascertained.

Another mechanism that may produce the appropriate bulk-compositions from more common sedimentary protoliths involves the partial melting of assemblages such as K-felspar-plagioclase-biotite-sillimanite-quartz. Removal of an alkali-enriched anatectic melt from its site of formation would leave behind an alkali-depleted residuum ("restite") enriched in FeO , MgO and Al_2O_3 . This type of mechanism has been proposed by Grant (1968) to explain the origin of high-grade cordierite-anthophyllite assemblages, and by Nixon et al. (1973) and Clifford et al. (1975) to account for the composition of sapphirine-bearing granulites. However, such a process cannot be invoked for the origin of lower-amphibolite facies chlorite-rich rocks in the Jervois Range area. In addition, experimental work by Green (1976) on an "average" pelitic rock has shown that, at pressures up to 10 kb, biotite and plagioclase form a significant part of the refractory residua coexisting with a granitic melt. Such residua would thus contain K_2O and CaO in excess of 1%, so that the process proposed above is restricted in

applicability to at least those pelitic sediments already deficient in K_2O , Na_2O and CaO .

Field and petrographic evidence presented in part one of this chapter strongly suggest a non-metasomatic origin for the Jervois Range chlorite-rich rocks. Several possible pre-metamorphic origins will now be examined, each of which is capable of producing appropriate bulk compositions, that would yield chlorite-quartz⁺-garnet rocks on isochemical metamorphism.

1: Hydrothermal Alteration of Mafic Rocks

The best documented geological processes that yield the appropriate bulk compositions are those of hydrothermal alteration of mafic or intermediate igneous rocks during low-grade burial metamorphism or during the late stages of magmatic activity. These processes have been inferred by Vallance (1967), Chinner and Fox (1974) and Irving and Ashley (1976) from studies of chlorite- and gedrite-cordierite-rich rocks in contact aureoles. In a regional metamorphic environment, a study of relic pyroxenes in low-grade chlorite-quartz-spessartine rocks (Barron, 1976, see also appendix table 9) has demonstrated the igneous origin of these assemblages. An appropriate alteration sequence in an unmetamorphosed environment has been documented by Kristmannsdottir (1975). His studies of the alteration of basaltic rocks in the Icelandic geothermal fields have shown the development of three zones:

- (i) a smectite-zeolite zone, at temperatures below $200^{\circ}C$, the smectite being an iron-rich saponite;

- (ii) a mixed-layer clay zone, between temperatures of 200 and 230°C, composed predominantly of clay minerals;
- (iii) a chlorite-epidote zone at temperatures above 230°C.

An analysis of the alteration "clay" (see appendix table 11) shows that, apart from $\text{Na}_2\text{O} = 1.08\%$, this alteration product fulfils the bulk-compositional requirements of chlorite-quartz rocks.

The origin of some chlorite-quartz rocks adjacent to base metal sulphide deposits has often been ascribed to "hydrothermal wall-rock alteration" during the emplacement of the ore bodies. As an example, the metamorphosed chlorite-quartz rocks in the Louvem copper deposits, Quebec, were formed in this way from massive and pyroclastic rhyodacites and dacites (Spitz and Darling, 1975; see also appendix table 11). However, in other deposits (such as the copper-zinc lodes at Noranda, Quebec) the alteration to chlorite+quartz (or their metamorphic equivalent) was contemporaneous with syngenetic ore formation (Rosen-Spence, 1969; Chinner and Fox, 1974).

The gradation of cordierite-gedrite-garnet-chlorite-quartz and cordierite-authophyllite-garnet-quartz assemblages on a regional scale into amphibolites with relict igneous textures at Koolanooka, W.A., demonstrates that these assemblages were derived by the alteration of basaltic rocks. As a consequence, these rocks are relatively rich in Ti, Ni, Cr, V and Sc, and poor in Zr, Y, Nb, U, Th and Ba (see analyses 891 and 892, appendix table 9). However, it must be stated that as yet there is no evidence at Koolanooka against chemical redistribution during metamorphism, and it is

also possible that the alteration may have taken place at near-surface temperatures.

2: Halmyrolysis of Pyroclastic Rocks

In terms of bulk-composition, the sedimentary equivalents of chlorite-quartz schists and hornfelses may be derived by the sub-aqueous alteration of pyroclastic rocks, or sediments with a high content of fine-grained, volcanically-derived material. Since pyroclastic rocks with a high glass (or volcanic ash) content are both metastable in aqueous environments and have a large surface area per unit volume, they react far more rapidly than the relatively coarse-grained clastic sediments in the same chemical environment. Partly for this reason, these reactions have been studied experimentally. They are inferred to take place soon after deposition, and may be broadly referred to as early diagenetic or "halmyrolytic" (Hummel, 1922; see also Millot, 1970).

The most common products of this type of halmyrolysis are the montmorillonites (smectites), but kaolinite, palygorskite, illite, mixed-layer clays and zeolites are not uncommon. The following points are relevant to this discussion:

- (i) Many montmorillonites low in Ca, Na and K content and high in Mg, Fe and Al have been reported (Weaver and Pollard, 1973, chapter 5).
- (ii) Most of the iron in Recent montmorillonites is in the ferric state (Weaver and Pollard, 1973).
- (iii) Montmorillonites rich in Ni, Cr, Cu, Ti, V, Mn and Zn

(sauconite) have been described (Weaver and Pollard, 1973, p.83-86).

- (iv) For the formation of montmorillonite in (i) above, halmyrolysis involves not only the depletion of the source-rock in Ca, Na and K, and the subsequent enrichment of the "residue" in Fe and Al, but may also involve the addition of Mg from sea water to the residual montmorillonite.
- (v) Montmorillonite is sensitive to later diagenetic processes, and usually reacts to chlorite-rich assemblages before the onset of low-grade metamorphism in its most commonly accepted sense (Millot, 1970). However, montmorillonite- and palygorskite-rich sediments of Jurassic and Cretaceous age have been preserved, and their derivation from pyroclastic rocks established (Couture, 1977; Bradshaw, 1975).
- (vi) Halmyrolysis in a marine environment can produce montmorillonite from pyroclastic rocks as siliceous as rhyolite (Höllner et al., 1976; Wirsching, 1976), or as mafic as basalt (Millot, 1970).

No analyses of montmorillonite-rich sediments fulfilling all the appropriate chemical constraints simultaneously have yet been found by the author, although samples differing in the content of only one component do exist. However, the trend towards depletion in alkalis and enrichment in Al and Mg is demonstrated by some of the samples analysed by Donnelly and Nalli (1973, hole 146-23-2).

Assemblages of palygorskite-sepiolite-kaolinite-quartz, derived by halmyrolysis, have been described by Rex (1970). Although these

are somewhat deficient in iron content, such an assemblage with siderite (common elsewhere in altered pyroclastic rocks) would yield the appropriate chlorite-quartz assemblages on metamorphism. As they are, their composition is appropriate to Mg-rich chlorite-quartz or cordierite-anthophyllite-quartz rocks.

The reduction of Fe^{3+} -Al-Mg-rich montmorillonites during diagenesis (and metamorphism) could produce the bulk-compositions being sought. Reduction on this scale has been inferred by Iwao (1973) to explain the derivation of staurolite-rich aluminous rocks from lateritic sediments. The relatively large size of the Fe^{2+} ion (divalent ionic radius of 78 nm for octahedral coordination) compared with the smaller sizes of the Mg^{2+} and Al^{3+} ions has been quoted to explain the absence of montmorillonite rich in ferrous ion. However, the existence of zinc- and manganese-rich montmorillonites indicates that ionic size is not the determining factor, since the divalent ionic radii of zinc and manganese are 74 and 83 nm, respectively. Two possibilities remain:

- (i) Ferrous montmorillonite does exist, but has not been recorded, or the physico-chemical environment required for its formation is very restricted.
- (ii) The stability field of ferrous montmorillonite is so small that more stable, diagenetic equivalents such as chlorite are observed in its place.

A halmyrolytic origin of the Jervois Range chlorite-rich rocks is consistent with field evidence. Finely-banded (4 mm) melanocratic rocks, with alternating layers rich in chlorite, epidote,

muscovite + biotite, spessartine garnet, plagioclase and quartz could also have been formed by the co-sedimentation of silica and volcanic ash of varying composition. Massive, conformable metarhyolites, metatascanites and metadacites also occur in the area (though these points do not prove that halmyrolysis has taken place).

Point (vi), page 171, indicates that the major element bulk-composition of the chlorite-rich rocks could have been formed from, say, rhyodacitic and andesitic pyroclastic material. If samples 886 to 889 were derived from the rhyodacitic material, this would explain the relatively low concentrations of Ti, Ni, Cr, V, and Sc, compared with the rest of the samples derived from the andesitic material, in which these elements are more concentrated.

Halmyrolysis could also explain the relatively low K/Rb ratios of the chlorite-rich rocks (and also many of the metapelitic rocks), compared with the higher values of average Precambrian shales, as documented by Leask (1967). During halmyrolysis, potassium and rubidium are removed from the source rocks (Millet, 1970). However, the larger ionic size of Rb^+ results in a higher sorptive capacity (Goldschmidt, 1954), so that Rb is preferentially retained by adsorption on to the newly-formed montmorillonite. This results in the enrichment of Rb relative to K, yielding lower K/Rb ratios than found in clastic rocks in which there is relatively little removal of K or Rb.

Such chemical considerations suggest, but do not prove, that the bulk-compositions of the Jervois Range chlorite-rich rocks may have

been derived initially from the halmyrolysis of pyroclastic material of a wide compositional range, together with the co-sedimentation of silica and the possible precipitation of an iron-oxide phase. Many of the Jervois Range rocks, especially the magnetite-quartz-spessartine rocks, have compositional similarities to the spessartine-chlorite-quartzites in the Venn-Stavelot Massif (see analysis 10, appendix table 10). These rocks, together with iron-silicate-rich slates, have been shown to have been formed initially by halmyrolysis of tuffs (Kramm, 1976).

3: Formation of Authigenic Chamosite

The bulk-composition of the chlorite-rich rocks cannot be derived from any simple combination of clastic (detrital) minerals so far recorded. As an example, to ensure a low potassium content, illite and sericite would have to be replaced with kaolinite as a source of aluminium. The co-precipitation of iron oxides or siderite could act as a source of iron, but this still leaves a source of magnesium to be found. High magnesium in sediments is usually associated with dolomite, but on decarbonation this mineral would yield too much calcium, in which the chlorite-rich rocks are notably deficient. In theory, magnesite could provide the magnesium, as could montmorillonite, but these minerals are not found as large components of clastic sediments. The only suitable mineral combination would be chlorite, with lesser amounts of kaolinite, ⁺ silica ⁺ iron oxides/carbonate, without appreciable illite or sericite, calcite or dolomite or any other Na, K- or Ca-rich mineral. Such a

clastic assemblage has not been recorded to date.

However, authigenic "chlorite" may be precipitated directly from solutions sufficiently high in Al, Fe, Mg and Si (the so-called "neof ormation" of Millot, 1970). "Chlorites" formed in this way have structural units with $d_{001} = 7\text{\AA}$, and are referred to as "septe chlorites" to distinguish them from their higher-temperature (metamorphic) polymorphs. Septe chlorites show a larger compositional range than chlorites, and include greenalite ($\text{Fe}_6\text{Si}_4\text{O}_{10}(\text{OH})_8$), which has no polymorphic equivalent. By definition, chamosite (or "berthierine") is $\text{Fe}_4\text{Al}_4\text{Si}_2\text{O}_{10}(\text{OH})_8$, but in common usage contains varying amounts of greenalite, amesite ($\text{Mg}_4\text{Al}_4\text{Si}_2\text{O}_{10}(\text{OH})_8$), and cronstedtite ($\text{Fe}_4^{2+}\text{Fe}_4^{3+}\text{Si}_2\text{O}_{10}(\text{OH})_8$) end members (Deer, Howie and Zussman, 1962).

In a model Fe-free system, Helgeson and Mackenzie (1970) have shown that chlorite is the dominant equilibrium solid phase in sea water at 25°C with $\text{pH} > 8$ and $f_{\text{CO}_2} < 10^{-4}$. They also inferred that Precambrian marine sediments were richer in montmorillonite, chlorite and aluminosilicate than Palaeozoic sediments. It is likely that, before the buildup of oxygen in the oceans and atmosphere, the activity of Fe^{2+} would have been greater and, as a consequence, aluminous ferromagnesian silicates may also have been equilibrium phases in Precambrian marine environments.

Recent sediments containing chamosite have been found off the Orinoco and Niger deltas (Porrenga, 1965) and in Loch Etive, Scotland (Rohrlich et al., 1969). Both the Nigerian and Scottish chamosites are oolitic, with nuclei of quartz grains or fecal

pellets, and both contain sufficient magnesium to be considered as possible source material for chlorite-quartz rocks. Trend lines indicating the compositions of the analysed chamosites and the Nigerian clay matrix ($K_2O = 1.5\%$, CaO and Na_2O both less than 0.8%) are shown in figure 17. The analyses report only total iron, so the trend towards the Al_2O_3 - MgO join indicates increasing oxidation ratios. However, it is evident that different proportions of chamosite and kaolinitic matrix will yield bulk-compositions appropriate to chlorite-quartz⁺ garnet rocks.

Rohrlich et al. (1969) have pointed out that winnowing and sorting of the chamositic oolites may result in the formation of oolitic "ironstones". Chamositic ironstones and their metamorphic equivalents, the silicate iron formations, are found throughout geologic time, but are especially common in Precambrian terrains. The occurrence of chamositic ironstones within and adjacent to iron formations explains why, in Western Australia, for example, chlorite-rich and chlorite-quartz⁺-garnet rocks are relatively common in areas containing metamorphosed iron formations (M. J. Gole, pers. comm.; see also sample 890, appendix table 9).

Cochrane and Edwards (1960) have analysed a septechlorite-rich "shale" which fulfils all the chemical criteria for metamorphism into a chlorite-quartz-garnet rock. This "shale" occurs in a sequence of Precambrian rocks, rich in magnetite and greenalite, in the Roper Bar area, Northern Territory (Corchoran and Baker, 1960; see also appendix table 11). A chamosite-rich parent-rock has also been inferred for the assemblage olivine-cordierite-garnet-gedrite.

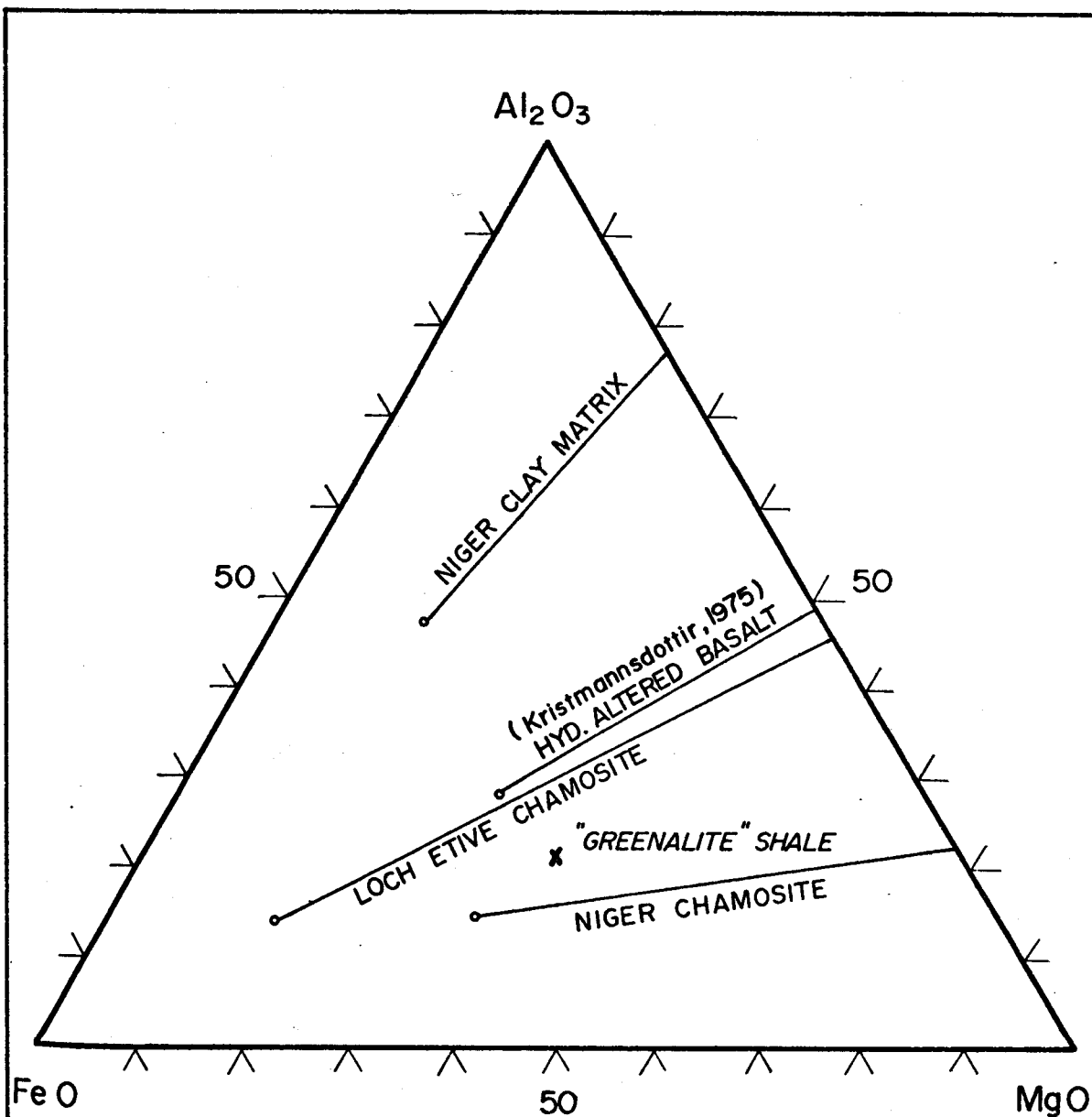


FIGURE 17: Molecular Al_2O_3 - FeO - MgO plot of sedimentary minerals and rocks from which many of the rocks depicted in figure 16 could be derived by essentially isochemical metamorphism. The lines represent variable oxidation ratios, (since only total iron is cited in the published analyses) with all iron in the ferrous state at the open circles (O.R. = 0), and all iron in the ferric state on the Al_2O_3 - MgO join (O.R. = 100). Note the large range of bulk compositions that may be produced by varying the ratio of chamosite to clay matrix, as well as varying the oxidation ratio. The bulk composition of the "greenalite" shale is very similar to those of many chlorite - quartz - garnet - magnetite assemblages. Niger Delta data: Porrenga 1965; Loch Etive data: Rohrlach et al. 1969; "greenalite" shale from the Northern Territory: Cochrane and Edwards, 1960; see also appendix table 11.

(Abraham and Schreyer, 1974), and samples plotting towards the iron end of the join $\text{FeO-Al}_2\text{O}_3$ in figure 16 may be inferred to share this origin.

The relatively high manganese content of many of the Jervois Range chlorite-quartz⁺-garnet rocks ($\bar{x} = 0.7\% \text{ MnO}$) may be the result of co-precipitation of manganese with oxides of iron (James, 1966), and/or substitution of manganese for iron in the chamosite structure (e.g. the Loch Etive chamosite contains 1.7% MnO according to Rohrllich et al., 1969). Manganese may equally well be retained or concentrated during halmyrolysis (up to 8% MnO; Kramm, 1976). Similarly, the range of phosphorus contents of these rocks ($\bar{x} = 0.12\% \text{ P}_2\text{O}_5$) may be derived by halmyrolysis (up to 0.3% P_2O_5 ; Kramm, 1976) or by co-precipitation of phosphorus with iron oxides and/or chamosite (up to 5% P_2O_5 ; James, 1966). Unfortunately, accurate trace-element data for chamosite-rich rocks are almost non-existent, and comparison may best be made with the calculated values of Rohrllich. However, these values are insufficient as a basis for genetic arguments.

The abundance of magnetite-rich metapelites and Mn- and P-rich magnetite-quartzites in the Jervois Range area is consistent with the formation of chlorite-quartz⁺-garnet rocks from chamosite-rich sediments. However, in the absence of conclusive field and chemical evidence, and bearing in mind that halmyrolysis and chamosite-formation may both form similar bulk compositions, neither mode of origin is preferable, on the basis of presently available data.

CHAPTER 7: MAGNESIAN CORDIERITE-RICH ENCLAVES IN PHLOGOPITE-SCHIST
FROM THE VALLEY BORE AREA, EASTERN HARTS RANGE, N.T.

7.1 Field Occurrence and Petrography

In the Valley Bore area, the predominantly felspathic Entia Gneiss contains several lenses of mica-schist (see chapter 2.5). One of these occurs in the northeastern part of the area, within a fine-grained, leucocratic quartz-plagioclase-gedrite-garnet gneiss (see map accompanying this thesis), and has been studied in detail as a representative occurrence.

This particular lens, about 60 m wide and 110 m long, is a phlogopite-schist, which in some places contains elongate porphyroblasts of kyanite up to 18 cm long, and, in others, "books" of bladed gedrite up to 30 cm long and 12 cm wide. Minor amounts of quartz commonly occur with the gedrite, but quartz is absent from the kyanite-bearing domains. In some of these domains, the kyanite is deep blue in colour, and locally, distorted hexagonal prisms of pink corundum up to 6 mm wide and 20 mm long may also be present. Domains containing both gedrite and kyanite, with or without quartz, have not been observed in the schist to date. However, they may have escaped detection, owing to the extensive weathering of the outcrop.

A relatively quartz-rich "pocket" occurs in the central part of the schist outcrop. This pocket is 8 m long and 1.5 m wide, is vertically dipping, and contains essentially two types of "pods" or

enclaves rich in cordierite.

- (i) Enclaves of the first type are ovoid porphyroblasts of cordierite up to 22 cm wide and 35 cm long. Though fractured, the cordierite is almost optically continuous, and contains single-phase and polyphase inclusions. The single-phase inclusions consist of gedrite, quartz, paragonite and albite, and, less commonly, kyanite, rutile, zircon, and rare, blue corundum. None of these single-phase inclusions exceed 5 mm in maximum dimension, and rutile and zircon are usually less than 1.5 mm long. Polyphase inclusions are more common, consisting of varying proportions of subangular quartz and albite, idioblastic gedrite and laths of paragonite. The grain-size within these aggregates is variable, the largest being that of gedrite (up to 14 mm long). The aggregates are generally rounded and may reach 2 cm in diameter. Patches of inclusion- and crack-free cordierite, up to 120 cm³ in volume, may be found in most enclaves of this type.
- (ii) The second type of enclave, similar in size and shape to the first, is made up of granular aggregates of cordierite, gedrite and quartz, in approximately equal proportions, with lesser amounts of phlogopite, paragonite and albite. Individual grains may exceed 1 cm in length or diameter, and larger patches of blue, inclusion-free cordierite, up to 8 cm³ in volume, have also been observed. Kyanite

inclusions in this type of enclave are less common than in those of the first type, and corundum is limited to isolated, spindle-shaped inclusions within some paragonite idiomorphs.

The idiomorphic paragonite referred to above (and the paragonite of parageneses (67) and (68) to be described in the next section) is inferred to be prograde from petrographic evidence. The relatively coarse-grained idiomorphic prograde paragonite contrasts strongly with the very fine-grained retrograde paragonite that occurs in intergrowths with (retrograde) chlorite. The inferred time relation between the crystallization of the two generations of paragonite is best illustrated by several samples in which prograde paragonite idiomorphs are partly replaced by retrograde paragonite-chlorite intergrowths that also replace adjacent cordierite and gedrite, as described below.

The retrograde alteration of cordierite, and the other aluminous minerals, to chlorite and chlorite-paragonite intergrowths, is common in both types of enclave.

- (i) In the first type, the alteration is most common around the edges of polyphase inclusions, and in cracks (in the cordierite) that radiate from these inclusions. Retrograde alteration also occurs around single-phase inclusions. Several polyphase inclusions have been extensively altered, with only a few ragged grains of kyanite (with or without gedrite and quartz) still preserved in the alteration products. From these examples,

it is inferred that other patches, comprised of paragonite-rich alteration products alone, represent the retrograde equivalents of kyanite-rich polyphase inclusions.

- (ii) The pattern of alteration in the second type of enclave is similar, except that it is not as localized, being common along many cordierite grain boundaries. The widths of these alteration zones generally do not exceed 5 mm. However, a few larger patches of alteration products also occur, and, as before, these are inferred to be the retrograde equivalents of kyanite-rich domains.

A faintly green chlorite is the dominant alteration product in a few domains inferred to have been gedrite-rich. More commonly, the alteration products are masses of radiating, highly birefringent laths strongly resembling pyrophyllite or talc. However, microprobe analyses of these radiating flakes show that they contain up to 6.2% Na_2O (and subordinate K_2O in type-two enclaves) and up to 18% MgO . From this it is inferred that these alteration products are microscopic retrograde intergrowths of paragonitic white mica and chlorite.

7.2 Phase Relations

The following highest-grade parageneses have been observed or inferred:

a: the Entia Gneiss

quartz-andesine-garnet-gedrite

(59)

b: in the phlogopite-schist:

phlogopite-kyanite	(60)
phlogopite-kyanite-corundum	(61)
phlogopite-gedrite	(62)
phlogopite-gedrite-quartz	(63)

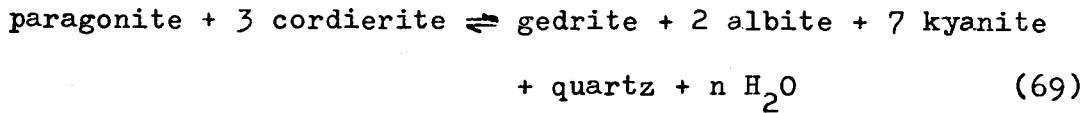
c: in the cordierite-rich enclaves:

cordierite-corundum	(64)
cordierite-gedrite ⁺ quartz	(65)
cordierite-gedrite-kyanite-quartz	(66)
cordierite-gedrite-paragonite-albite-kyanite-quartz	(67)
cordierite-gedrite-paragonite-albite-kyanite-phlogopite- quartz	(68)

Microscopic domains of cordierite enclosing single-phase inclusions of each of the minerals in assemblage (67) could be considered as independent assemblages on their own. In order to test this possibility, three domains for microprobe analysis were taken from different parts of a single, type-one enclave, the diameters of analysed circular sections being about 2 cm. The compositions of all similar single-phase inclusions within each of the three relatively unaltered "circular" domains are essentially constant. This implies a nearly constant chemical potential for each component in every phase in each of the domains, and from this it may be inferred that diffusion of some of the chemical components within the domains may have been relatively unrestricted. It follows from this that each of the five cordierite-inclusion pairs belongs to one assemblage, namely assemblage (67).

The relative invariance of phase compositions in each domain also implies that mineral compositions were controlled by an

equilibrium reaction such as the one below, which is univariant in the system $\text{SiO}_2\text{-Al}_2\text{O}_3\text{-FeO-MgO-Na}_2\text{O-H}_2\text{O}$:



For simplicity, gedrite is taken as $(\text{FeMg})_6\text{Al}_2\text{Si}_7\text{O}_{22}(\text{OH})_2$.

In addition, the range of mineral compositions between domains is quite small. As examples, the maximum variation in cordierite Mg is from 89.27 to 93.85; for gedrite Mg it is from 71.80 to 75.13; and for plagioclase $\text{Na}/(\text{Na}+\text{Ca})$ it is 87.20 to 93.56. These small variations may be explained by mosaic equilibrium, but they may also be accounted for by other components such as Ca and Ti not diffusing between domains, and making reaction (69) strictly multivariant. Corundum inclusions in cordierite have not been observed to occur closer than 1.4 mm from any quartz-bearing inclusion. This implies that the diffusion of Al and/or Si has also been relatively restricted.

7.3 Temperature-Pressure Conditions of Formation

The occurrence of cordierite + kyanite is not common, and, because of the constraints of the particular bulk-composition, that of cordierite + kyanite + paragonite + quartz is less so. Figure 18 depicts stability fields and reaction curves relevant to these assemblages.

The stability field of pure Mg-cordierite (Seifert and Schreyer, 1970; Newton, 1972) intersects the kyanite stability field at about 620°C at 5 or 6.2 kb $P_{\text{H}_2\text{O}}$, depending on whether the data of Richardson

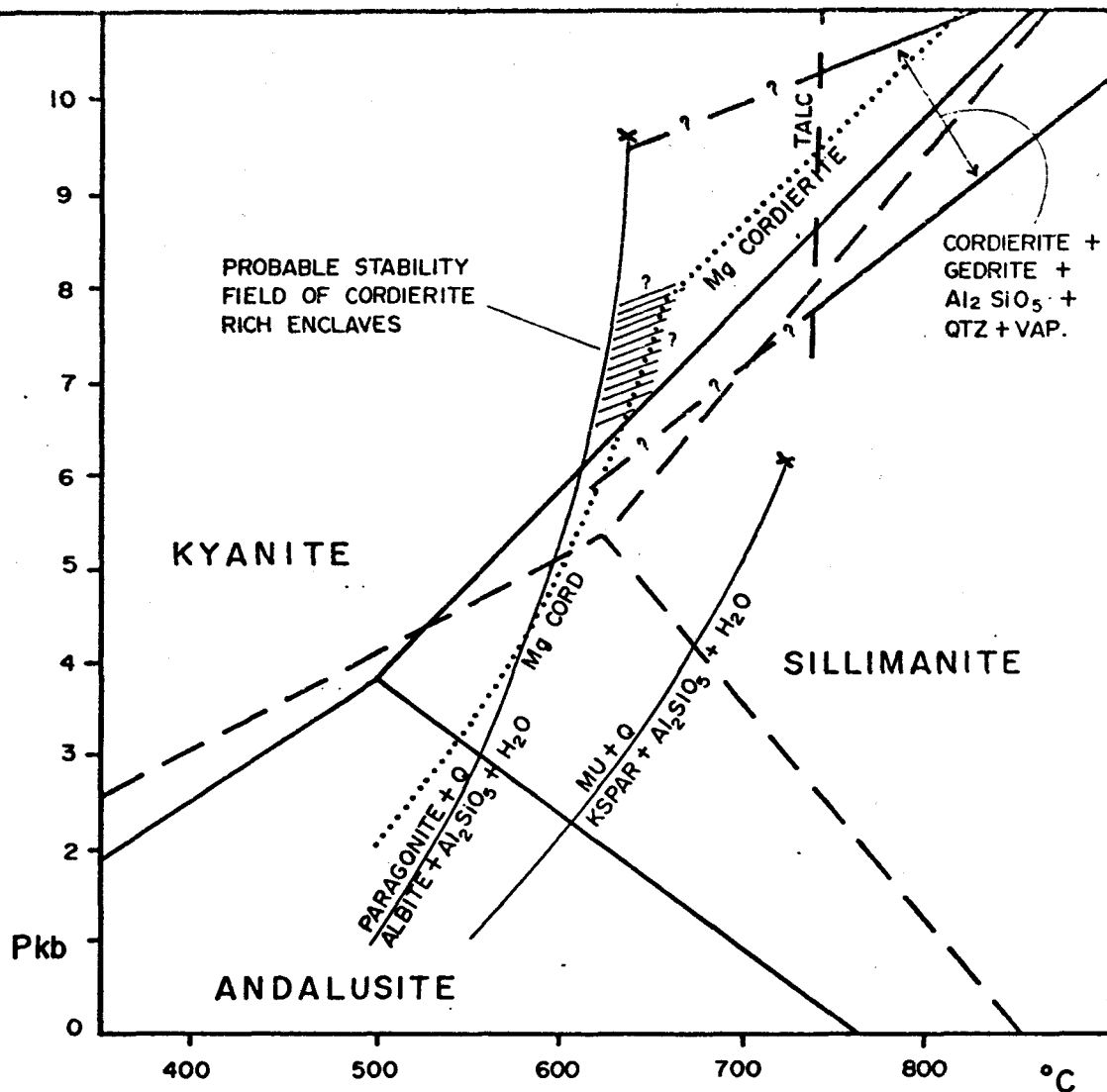


FIGURE 18: Probable stability field of the cordierite - rich enclaves in the Valley Dore area (ruled), in relation to experimentally derived reaction curves. Crosses terminating the mica breakdown curves represent the formation of melts. For further explanation, see text. Al_2SiO_5 stability fields: solid lines; Holdaway, 1971; dashed lines; Richardson et al., 1969; breakdown of white mica in the presence of quartz in the muscovite - paragonite system: Chatterjee and Froese, 1975; stability field of Mg cordierite at lower vapour pressures: Seifert and Schreyer, 1970; at higher vapour pressures: Newton, 1972; divariant stability field of cordierite + gedrite + kyanite + quartz + vapour for a bulk composition of $\text{Mg} = 87$, and the appearance of talc for this composition: Green and Vernon, 1974.

et al. (1969) or those of Holdaway (1971) are used. The data of Holdaway (1971) are preferred by the author, since Holdaway accounted for the effects of grinding strain, disequilibrium Al-Si disorder in sillimanite, and the inclusion of very fine-grained sillimanite in the starting materials. Recent experiments using oxide-melt solution calorimetry have lent support to the data of Holdaway (Anderson et al., 1977).

The experimentally-determined upper temperature-pressure stability of synthetic Mg-cordierite in the range 8 to 10 kb P_{H_2O} (Newton, 1972) is lower than that determined on naturally-occurring cordierite with $Mg = 93$ (Green and Vernon, 1974); see fig. 18. Apart from experimental errors, the discrepancy may be due to structural differences between synthetic and naturally-occurring cordierites (see section 3), and to compositional factors, such as the Na content of the naturally-occurring cordierite (Vernon, 1972). If this is correct, then the lower-pressure cordierite stability curve may also be extended to slightly lower temperatures, since most naturally-occurring cordierites contain significant sodium, as well as other "excess" elements (Leake, 1960; see also the analyses of Lepezin and Melenevsky, 1977).

The stability of cordierite + gedrite + kyanite + quartz (66) under high-pressure, hydrous conditions was inferred by Vernon (1972) and the position of this stability field, for a magnesium-rich system, was determined experimentally by Green and Vernon (1974). The projection of these stability field boundaries to lower temperatures overlaps the P-T region inferred for the formation of the Valley Bore

enclaves (fig. 18). However, in the experiments, talc occurs at 700°C for $P_{H_2O} > 8$ kb (Green and Vernon, 1974). Talc may be metastable, or, strictly, may belong to the di- or trivalent equilibrium assemblage, cordierite-kyanite-gedrite-quartz-talc, since minor amounts of Na occur in both gedrite and cordierite, and gedrite may also contain some Ca. The same conclusion with respect to Na in gedrite has been made in a similar, natural system (Schreyer and Abraham, 1976).

The reaction $\text{gedrite} + \text{kyanite} \rightarrow \text{cordierite} + \text{corundum} + H_2O$ may be inferred for silica-deficient, Fe-free domains in rocks from Sar e Sang, Afghanistan, described by Schreyer and Abraham (1976). Other domains in these rocks from Sar e Sang contain the assemblages paragonite + quartz and cordierite + talc, and also relict kyanite that has been partly converted to sillimanite. Pressure-temperature conditions inferred for the final stage of metamorphism of these Sar e Sang rocks (using the Al_2SiO_5 data of Richardson et al., 1969) are 640°C, 5-6 kb (Schreyer and Abraham, 1976). The use of the Al_2SiO_5 data of Holdaway (1971) increases the above stability field to a maximum pressure of 7 kb at 650°C. Holdaway's data also permit a much lower pressure minimum for the stability of sillimanite at 640°C. However, the Sar e Sang assemblages are none the less restricted to the higher pressures listed above, since the P-T conditions for the final (third) stage of metamorphism did not vary greatly from those of the second, kyanite-producing stage (Schreyer and Abraham, 1976).

Other assemblages containing cordierite + gedrite + quartz + kyanite or sillimanite, without talc, have been described (e.g.

Robinson and Jaffe, 1969; Gable and Sims, 1967). Those with kyanite in a magnesium-rich system must have formed either under conditions inferred for the prograde metamorphism of the Valley Bore enclaves (shaded area, fig. 18), or under conditions falling within the stability field determined by Green and Vernon (1974) (see fig. 18).

Within the Valley Bore enclaves, the inferred stability of prograde paragonite + albite + quartz does not imply univariant equilibrium conditions, since both paragonite and albite contain some potassium, albite contains calcium, and paragonite may contain some fluorine and ferric iron. As shown by Chatterjee and Froese (1975), this results in a di- or multivariant stability field, in which both albite_{ss} and paragonite_{ss} may be stable in the presence of quartz. This field extends to temperatures above those of the univariant paragonite breakdown curve. However, the field is not wide, and its upper temperature boundary probably does not exceed 660°C for any vapour pressure up to the melting of paragonite_{ss} + quartz. Consequently, based on the inferred stability of prograde paragonite, the upper temperature limit for the formation of the cordierite-rich enclaves is set at 660°C.

The upper pressure limit for the formation of the enclaves is set by the stability limit of cordierite. For reasons already discussed, this value is in some doubt, so that the absolute pressure limit is set by the melting of paragonite + quartz (fig. 18). In the absence of textures attributable to melting, this absolute limit is 9.5 kb P_{H_2O} (Chatterjee and Froese, 1975).

For $P_{H_2O} \ll P_{total}$, the paragonite breakdown curve moves to

lower temperatures. Hence, it may be inferred that vapour pressure was approximately equal to total or confining pressure during the formation of the enclaves. If this were not the case, there would be no stability field in which both prograde paragonite_{ss} + quartz and cordierite could coexist.

7.4 Mineralogy of the Cordierite

The size and relative purity of the type-one cordierite porphyroblasts are unique. A similar occurrence of smaller porphyroblasts from White Well, Western Australia, has been documented by Pryce (1973). In this locality, pale blue cordierite occurs with corundum and sillimanite, in masses measuring up to 8 x 8 x 4 cm, within an enclave of phlogopite schist. Cordierite porphyroblasts, measuring up to 13 cm in maximum dimension, have been found in quartz-muscovite-biotite-sillimanite gneisses in Fremont County, Colorado (Travis, 1956). The cordierite is dark gray in colour, and is rich in inclusions of magnetite and quartz.

All the cordierite in the Valley Bore enclaves is strongly pleochroic, varying in colour from pale, smoky gray to an intense blue-violet. Inclusion-free patches of cordierite may be found in the type-one enclaves, measuring up to 5 x 3 x 2 cm in size. The cordierite in some of these patches contains trails of fluid inclusions which may reach 20 μ m in length. However, other patches, which are free of inclusions, are completely transparent and of gem quality.

One gem-quality patch was selected for intensive analysis. Electron microprobe analyses showed no detectable compositional

differences in any part of the cordierite. The sample was then crushed, and analysed by X-ray fluorescence spectrography and atomic absorption spectroscopy. The major element analysis (practically identical to cordierite in a domain in a type-two enclave) is presented in table 27. The trace element concentrations (in ppm) are as follows:

Mn	204	Ti	5	Cu, Cr, V,
Zn	36	Ba	< 20	Y, Sr, Rb,
Ga	27	K	< 10	Pb: all
Ni	10	Ca	< 1	below 4 ppm.

The sodium content of the cordierite is appreciable, but not high compared to some older tabulated values (Leake, 1960) or more recent microprobe results (Ramsay and Kamineni, 1977; Lepezin and Melenevsky, 1977). The potassium and calcium contents are negligible, and thus compare with the sodium-bearing (but iron-free) cordierite described by Schreyer and Abraham (1976). Lepezin and Melenevsky (1977) have also reported a cordierite with 1.08% Na₂O, but low in CaO and K₂O.

The water content of the cordierite is appreciable, but not excessive compared with values tabulated by Leake (1960). However, it cannot be used to infer values of P_{H₂O} at the time of cordierite crystallization, since water must have been available within the enclave during retrogression. Thus, the water content of the cordierite is more likely to reflect retrograde, rather than prograde, conditions, and its interpretation will depend on its subsequent cooling history (Lepezin and Melenevsky, 1977).

The following cell parameters have been kindly determined for the Valley Bore cordierite by I. M. Threadgold of Sydney University:

$$\begin{array}{ll} a_o & 17.0550 \text{ \AA} \\ b_o & 9.7295 \text{ \AA} \\ c_o & 9.3455 \text{ \AA} \end{array}$$

The "distortion index" calculated from the above values is 0.225, and the observed distortion index, measured by diffractometry, is 0.21. These values are comparable to the value of 0.24 calculated for the White Well cordierite from the data of Pryce (1973).

As defined by Miyashiro (1957), the distortion index is supposedly a measure of the departure of the cordierite structure from that of indialite, the high-temperature, hexagonal polymorph of cordierite with a distortion index of zero. The conventional interpretation is as follows:

- (i) The distortion index measures the degree of tetrahedral Al-Si ordering in cordierite.
- (ii) Increased ordering results in an increase in symmetry, so that "low-cordierite" is the orthorhombic polymorph of the high-temperature indialite.
- (iii) The rates of order-disorder reactions are temperature-controlled, and the amount of ordering is also controlled by elapsed time.
- (iv) By measuring the structural state (amount of ordering) of cordierite, the distortion index indicates the cooling history of cordierite.

Following the conventional approach, the Valley Bore cordierite is

"subdistortional", indicating that it was formed under metamorphic conditions characterized by slow heating and slow cooling. As pointed out by Stout (1975), the distortion index is uniquely defined by the values of cordierite d_{131} , d_{421} , d_{511} , which in turn are defined by the cell parameters. Any change in the values of the cell parameters, which results in a change in the cordierite axial ratios, will result in a change in the distortion index. Hence the distortion index is not uniquely a measure of Al-Si ordering in cordierite, but is also a function of any change, chemical or structural, which results in changing axial ratios (Stout, 1975; Goldman et al., 1977).

Since changes in the water content, oxidation ratio, composition or content of "channel ions" in cordierite will change the axial ratios, the distortion index cannot be used to infer conditions of formation in any but the broadest sense. Even in a single area, variations in the distortion index between many cordierites may be difficult to interpret with any certainty (Kamineneni, 1974).

7.5 The Distribution of Mg and Fe between Coexisting Minerals in the Cordierite-Rich Enclaves

The compositions of coexisting minerals within a single polymineralic domain from a type-two enclave are presented in table 27. These analyses are representative of most domains within both types of enclaves. The Fe-Mg distribution coefficients for the ferromagnesian mineral pairs are listed in table 28, together with a range of distribution coefficients from broadly similar rocks.

CORDIERITE-GEDRITE-KYANITE-CUARTZ-PARAGONITE-PHLOGOPITE ENCLAVE

	<u>CORDIERITE</u>	<u>GEDRITE</u>	<u>PHLOGOPITE</u>	<u>PARAGONITE</u>	<u>CHLORITE</u> retrograde
SiO ₂	49.51	45.85	41.11	45.73	26.66
TiO ₂	.00	.17	1.28	.00	.00
Al ₂ O ₃	33.31	16.54	18.24	40.20	23.22
Fe ₂ O ₃	.11				
FeO	1.91	12.91	6.15	.38	9.55
MnO	.026	.23	.00	.00	.18
MgO	12.37	20.48	21.49	.67	26.75
CaO	.00	.39	.00	.00	.00
Na ₂ O	.55	1.84	.68	7.32	.00
K ₂ O	.00	.00	7.36	.62	.00
H ₂ O ⁺	2.14				
H ₂ O ⁻	.05				
<u>TOTAL</u>	<u>99.98</u>	<u>98.41</u>	<u>96.31</u>	<u>94.92</u>	<u>86.36</u>
CATIONS PER No. OXYGENS	18	23	22	22	28
Si	4.9891	6.3943	5.6909	5.8718	5.2426
Ti		.0178	.1332		
Al	3.9560	2.7186	2.9758	6.0834	5.3814
Fe ³⁺	.0083				
Fe ²⁺	.1610	1.5057	.7120	.0408	1.5705
Mn	.0022	.0272			.0300
Mg	1.8582	4.2578	4.4347	.1282	7.8417
Ca		.0583			
Na	.1075	.4975	.1825	1.8223	
K			1.2996	.1016	
<u>TOTAL</u>	<u>11.0823</u>	<u>15.4772</u>	<u>15.4287</u>	<u>14.0481</u>	<u>20.0662</u>
<u>Mg</u>	92.03	73.88	86.17		83.31
Al ^{iv}		1.6057	2.3091	2.1282	2.7574
Al ^{vi}		1.1129	.6667	3.9552	2.6240

TABLE 27: Analyses of minerals in a cordierite-rich enclave. The cordierite was analysed by XRF, AAS and wet chemical methods, and is very similar to the microprobe analyses of this mineral in this enclave. All other minerals were analysed by microprobe, and all the iron is assumed to be ferrous iron for calculations.

K_D^{cd-oe} K_D^{MgFe}	K_D^{cd-bi} K_D^{MgFe}	K_D^{bi-on} K_D^{MgFe}	K_D^{cd-gt} K_D^{MgFe}	K_D^{bi-gt} K_D^{MgFe}	K_D^{on-gt} K_D^{MgFe}	K_D^{Mg} K_D^{cd}	K_D^{Mg} K_D^{bi}	K_D^{Mg} K_D^{oe}	K_D^{Mg} K_D^{gt}	X_{Al}^{vi} X_{Al}^{oe}	X_{Ca+Mn}^{viii} X_{gt}	X_{Ti}^{vi} X_{bi}	X_{Al}^{vi} X_{bi}
cordierite-gedrite-phlogopite-paragonite-kyanite-quartz Valley Fire area, this work, chapter 7													
4.08	1.85	2.20				92.0	86.2	73.9		.161		.022	.112
cordierite-gedrite-garnet-sillimanite-phlogopite-plagioclase-quartz Valley Fire area, this work, chapter 8													
(3.09)	1.94	1.60	6.74	3.47	(2.18)	82.0	70.2	59.6	40.4	.180	.045	.031	.104
cordierite-gedrite-garnet-quartz-ret.chlorite Koolanooka, W.A., this work, chapter 6, sample 891													
2.60		10.84		4.18		49.7		27.6	8.3	.153	.144		
cordierite-gedrite-garnet-biotite-trace ret.chlorite Koolanooka, W.A., this work, chapter 6, sample 892													
1.79	2.89	0.62	10.82	3.74	6.05	63.8	37.8	49.6	14.0	.159	.031	.020	.083
cordierite-orthopyroxene-biotite Quairading, Western Australia, Davidson and Mathison, 1974													
1.91						82.9	71.8					.075	.050
cordierite-orthopyroxene-biotite-quartz Quairading, Western Australia, Davidson and Mathison, 1974													
1.85						82.4	71.7					.056	.066
cordierite-orthopyroxene-biotite-plagioclase Quairading, Western Australia, Davidson and Mathison, 1974													
1.77						82.3	72.4					.051	.075
cordierite-orthopyroxene-biotite-garnet Quairading, Western Australia, Davidson and Mathison, 1974													
2.34		6.67	2.85			79.3	62.0		36.5		.041	.088	.046
cordierite-gedrite-biotite-quartz-plagioclase New Hampshire, U.S.A., Robinson and Jaffe, 1969													
2.73						83.6		65.2		.146			
cordierite-corundum-sillimanite-phlogopite White Well, Western Australia, Pryce, 1973													
0.68						96.4	97.6					.003	.193
cordierite-hypersthene-kyanite-quartz-garnet-biotite Strangways Ra., Northern Territory, Vernon, 1972													
3.59						89.8		71.0		.068			
cordierite-gedrite-garnet-quartz-biotite Fishtail Lake, Ontario, Lal and Moorhouse, 1969													
2.30	1.71	1.35	5.86	3.43	2.54	81.5	72.0	65.6	42.9	.085	.051	.024	.068
cordierite-gedrite-biotite-quartz Fishtail Lake, Ontario, Lal and Moorhouse, 1969													
3.02	1.64	1.84				82.4	74.0	60.7		.077		.020	.080
cordierite-gedrite-garnet-biotite-quartz-plagioclase Yellowknife, N.W. Territories, Canada, Kamineni, 1975													
2.83	1.59	1.77	12.20	7.66	4.32	66.9	55.9	41.7	14.2	.163	.118	.035	.159
2.89	2.11	1.37	10.47	4.96	3.62	65.3	47.1	39.4	15.2	.198	.132	.035	.154
		1.40					54.1	45.8		.122		.032	.136
3.28	2.00	1.64	11.98	5.99	3.65	66.2	49.5	37.4	14.1	.252	.130	.033	.116
2.54	1.74	1.46	12.91	7.43	5.09	66.9	53.7	44.3	13.5	.092	.136	.028	.111
2.68	2.06	1.30				68.5	51.3	44.8		.141		.031	.109
2.75	1.95	1.41				67.0	51.0	42.5		.222		.031	.088
2.77	1.90	1.46				67.9	52.6	43.3		.107		.032	.108
		1.66					51.0	38.6		.176		.034	.094
cordierite-garnet-biotite-hypersthene-sillimanite-kapariquartz Bangalore, India, Iyer and Kutty, 1975													
2.68		5.33	1.99			78.4	57.5		40.5	.033	.039	.167	
2.18		4.82	2.21			75.9	59.1		39.5	.024	.033	.154	
2.88		4.41	1.53			75.1	51.2		40.6	.003	.032	.158	
garnet-biotite-sillimanite-kapari-quartz-plagioclase Ivrea, Italy, Schmid and Wood, 1976													
		6.13				77.2		33.6		.027	.113	.033	
		5.34				66.4		27.0		.082	.114	.052	
cordierite-biotite-gedrite-quartz-relict garnet & staurolite Slave Craton, Canada, Ramsay and Kamineni, '77													
2.65	1.77	1.50				65.7	52.0	42.0		.176		.033	.116
(values based on average analyses of minerals)													
cordierite-garnet-sillimanite-biotite-quartz-kapari Front Ra., Colorado, U.S.A., Cable and Sims, 1969													
2.03		6.95	3.42			64.2	46.9		20.5		.054	.067	.151
cordierite-gedrite-kyanite-quartz experimental run at 740°C, 10.35kb, Green and Vernon, 1974													
2.19						93.4		86.6		.156			

cd: cordierite oe: orthoamphibole (gedrite) bi: biotite (or phlogopite) gt: garnet - K_D 's have been calculated as defined on page 7.

TABLE 28: Compilation of Mg-Fe distribution coefficients for cordierite- and garnet-bearing assemblages drawn from the literature for comparative purposes. Note that many of the values listed above were calculated from analyses of mineral separates, and may be in error if one or both minerals are strongly zoned.

These were calculated from data available in the literature, or from analyses carried out by the author.

The distribution coefficient for the cordierite-gedrite pair from the Valley Bore area has the highest value listed in table 28. If gedrite solid solution were ideal, this might imply that the temperature of equilibration of the assemblage was lower than those of all the other pairs listed. However, Papike and Ross (1970) have shown that Fe and Mg ions are strongly ordered in the gedrite octahedral Al sites, which results in a compositional dependence of K_D . As will be discussed in chapter 9, gedrite octahedral Al is functionally related to gedrite Mg, so that variations in gedrite Al^{vi} content will also affect the value of K_D .

The dependence of the value of K_D on gedrite composition is illustrated by the seven cordierite-gedrite pairs of Kamineni (1975), listed in table 28. All seven of these mineral pairs were taken from a single metamorphic zone, so that the temperature dependence of these K_D 's is essentially zero. Hence the variations in the values of K_D must arise mainly from compositional variations in gedrite.

An example of a relatively high value of $K_D^{cord-ged}$ derived from a high-grade metamorphic assemblage has been described from the Strangways Range area, N.T., by Vernon (1972). At this locality, the coexisting cordierite and gedrite occur in a hypersthene-bearing granulite, and have a K_D value of 3.59. This value is higher than the K_D values documented by Kamineni (1975b) for amphibolite-facies rocks from the Yellowknife area in Canada, but is lower than the

K_D value of 4.08 in the Valley Bore enclaves (see table 28). The contrasting K_D values from the two Northern Territory samples may be attributed to the differing Al contents of the gedrite, since the Mg values are similar. The gedrite in the Strangways Range granulite has an X_{Al}^{vi} value of 0.068, whereas the gedrite from the lower-grade enclaves in the Valley Bore area has an X_{Al}^{vi} value of 0.161.

As discussed in chapter 4, a similar dependence exists between biotite composition and K_D 's involving biotite. Because of this, distribution coefficients between biotite and cordierite, and biotite and orthoamphibole, are strongly dependent on mineral compositions, and may only be compared directly with compositionally identical mineral pairs.

CHAPTER 8: GARNET, GEDRITE and CORDIERITE-BEARING GNEISS IN THE VALLEY BORE AREA (IRINDINA CK)

8.1 Field Occurrence

Samples 897 to 899 were collected from a garnet-gneiss lens within the Irindina Gneiss, some 15 km west of the cordierite-rich enclave locality described in the previous chapter (see map accompanying the thesis). Bulk-rock analyses, together with petrographic descriptions, are presented in appendix table 13, et seq.

In outcrop, the garnet-gneiss lens is approximately 70 m long and over 12 m in true thickness. It dips at 35° to the northwest, and is concordant with the predominantly felspathic Irindina Gneiss. Laterally, the lens grades into garnet-free biotite-gneiss, but its upper surface is in sharp contact with phlogopite-schist. Its lower surface, where exposed, grades into a quartz-rich banded biotite gneiss.

The size and distribution of garnet within the lens is not uniform. For the most part, garnet porphyroblasts do not exceed 4 cm in diameter, and comprise less than 3% of the rock volume. However, several garnet-rich domains occur within the lens, and, in these, the garnet crystals are generally much larger, commonly occurring in clusters of porphyroblasts, in which each crystal may reach 6 cm in diameter. Smaller (≤ 1 cm) crystals may occur adjacent to these garnet clusters, and several elongate porphyro-

blasts, up to 26 cm in length, have also been observed in these garnet-rich domains.

The phlogopite schist that overlies the garnet-gneiss is extremely weathered, but appears to be lacking in quartz. Several samples of the schist were sufficiently coherent for sectioning, and yielded the assemblages listed in the next section. A metamorphosed ultramafic sill occurs within the Irindina Gneiss at this locality, and comprises cummingtonite and a faintly pleochroic hornblende.

8.2 Phase Relations

The following highest-grade parageneses have been observed at this locality.

A - in the phlogopite schist:

phlogopite-corundum	(70)
phlogopite-garnet	(71)
phlogopite-corundum-tourmaline-kornerupine	(72)
phlogopite-gedrite-spinel-(högbohmite?)	(73)

B - in the garnet gneiss:

phlogopite-oligoclase-quartz	(74)
cordierite-phlogopite-oligoclase-quartz	(75)
cordierite-sillimanite-phlogopite-oligoclase-quartz	(76)
garnet-sillimanite-phlogopite-oligoclase-quartz	(77)
gedrite-sillimanite-phlogopite-oligoclase-quartz	(78)
cordierite-garnet-sillimanite-phlogopite-oligoclase-quartz	(79)
gedrite-cordierite-sillimanite-phlogopite-oligoclase-quartz	(80)

In order to obtain representative microprobe and bulk-rock analyses, samples were collected from a relatively fine-grained, garnet-poor horizon within the gneiss lens. In diameter, the largest

garnet crystal in these samples measures 3.2 cm, and the smallest 7 mm. Four types of mineral domains exist in these samples, and are best developed around the larger garnet porphyroblasts.

- (i) Phlogopite-rich domains mantle garnet porphyroblasts greater than 2 cm in diameter. These domains increase in width with increasing garnet crystal size, and may be up to 4 mm wide. They comprise the minerals of assemblage (77): garnet-sillimanite-phlogopite-oligoclase-quartz. Sillimanite crystals occur in contact with all the other minerals, and may also occur as inclusions within the larger garnet crystals.
- (ii) Second-type domains surround the first type described above. They are up to 2 cm in width, and comprise the minerals belonging to assemblage (75): cordierite-phlogopite-oligoclase-quartz. These domains are cordierite-rich, and relatively phlogopite-poor. The cordierite is altered along cracks and grain boundaries to fine, felted aggregates rich in white-mica, with subordinate chlorite. By analogy with similar alteration products described in chapter 5, this type of alteration in these rocks is inferred to be the result of low-temperature, retrograde hydration reactions. Several idioblastic gedrite inclusions have been observed within plagioclase grains, but no coexisting gedrite-cordierite pairs have been observed in domains of this type in the samples available.

- (iii) Third-type domains surround second-type domains and commonly comprise the minerals of assemblage (74): phlogopite-oligoclase-quartz. Less commonly, the domains may also contain minor amounts of sillimanite, and a few small grains of cordierite that have been entirely altered to aggregates of felted white-mica and chlorite. As above, this alteration is inferred to be the result of low-temperature retrograde hydration, and not the result of higher-temperature mineral reactions. Hence, another inferred paragenesis of these domains is assemblage (76): cordierite-sillimanite-phlogopite-oligoclase-quartz.
- (iv) The fourth type of mineral domain may be considered the "matrix", and represents garnet-free portions of the gneiss. Commonly, the matrix comprises the minerals of assemblage (78): gedrite-sillimanite-phlogopite-oligoclase-quartz. Less commonly, this domain may contain the minerals of assemblage (74), or, for more magnesian and aluminous bulk-compositions, those of (75) or (76).

Two points arise in connection with the succession of domains listed above.

- (i) First, in samples in which the garnet crystals are small (< 1 cm in diameter), the domains are narrow and poorly developed. In some rocks, the first domain may be completely absent, and cordierite of the second domain is inferred to be in contact with the garnet rim.

However, the actual "contact" is a zone of mica-rich alteration products extending into the cordierite.

This zone may be as narrow as 0.07 mm, or as wide as 0.6 mm. If it is assumed that the minerals in these alteration zones were derived by the retrograde hydration of the cordierite, then a mineral pair garnet-cordierite may be inferred to have been part of an equilibrium assemblage at some stage of the metamorphic episode. On the other hand, the alteration products may have been derived by the retrogression of a mineral (or minerals) between the cordierite and garnet grains. It is then possible that these two minerals were never in equilibrium with each other, since they were nowhere in contact. The second alternative does not rule out Fe-Mg equilibration by diffusion through other minerals, and the succession of domains does indicate diffusion of at least Mg and Fe over distances of several centimetres to produce the compositional domains.

The similarity of cordierite alteration in the second and third domains suggests that the above inference of former contact between cordierite and garnet is correct. Hence assemblage (79) (cordierite-garnet-phlogopite-sillimanite-oligoclase-quartz) was probably a stable paragenesis.

- (ii) Second, at the boundary between third and fourth-type domains in some samples, altered cordierite belonging to

assemblage (76) "surrounds" slightly embayed crystals of gedrite belonging to assemblage (78). It may be argued that this feature results from an ionic reaction of the type gedrite + sillimanite \rightleftharpoons cordierite + garnet. It may also be argued that only the cordierite has undergone retrograde alteration, so that the mineral pair gedrite + cordierite may have been stable.

Unfortunately, the textural evidence does not favour one alternative over the other, so that the stability of assemblage (80) is yet to be confirmed or disproved.

Although the garnet-gneiss is compositionally heterogeneous in the vicinity of large garnet porphyroblasts, fine-grained samples may be found in which all the minerals belonging to assemblages (79) and (80) may be observed in a section some 3 cm² in area. This does not imply that all the minerals are stable together, since, in the samples available, garnet has not been observed in contact with gedrite, and the mineral pairs cordierite-gedrite, and cordierite-garnet may possibly not be in equilibrium (as discussed above).

However, the phase rule permits the assemblage

garnet-cordierite-gedrite-phlogopite-sillimanite-oligoclase-
quartz-(vapour or melt) (81)

to exist in divariant equilibrium within the compositional system SiO₂-Al₂O₃-FeO-MgO-CaO-Na₂O-K₂O-H₂O (note that the gedrite contains 2.01% Na₂O; table 29). Consequently, the fact that gedrite has not been observed in contact with garnet may be explained in one of two

ways:

- (i) gedrite + garnet is stable, but appropriate bulk-compositions are lacking in the samples; or
- (ii) gedrite and garnet are not stable together, but react to give a more stable mineral assemblage.

The same two points hold for the mineral pair gedrite + cordierite, but, from the evidence available, the pair garnet + cordierite is likely to be stable (as discussed above). Unfortunately, the samples collected probably do not represent the full range of bulk-compositions available in different domains of the garnet-gneiss. It is also possible that bulk-compositions appropriate to the stability of the full 7 solid-phase assemblage (81) do not exist at this locality. These problems may be resolved, at least in part, by a program of intensive sampling planned by the author.

8.3 Temperature-Pressure Conditions of Metamorphism of the Garnet-Gneiss

Points relevant to the temperature-pressure conditions of the metamorphism of the garnet-gneiss are as follows:

- (i) None of the observed assemblages in the garnet-gneiss contain K-felspar.
- (ii) All the ferromagnesian phases are relatively Mg-rich.
- (iii) The bulk-compositions of the samples are relatively rich in Fe, Mg and Al, and poor in K compared with average pelitic sediments (Wedepohl, 1969).

In the area surrounding the garnet-gneiss:

- (iv) Most of the felspathic rocks are deficient in K-felspar.
- (v) Quartz-felspar pegmatites and veins cut most rock units in this area.
- (vi) Amphibolites are rich in cummingtonite.
- (vii) Migmatization is extensively developed 4 km to the west of this locality.

These observations are put into perspective by the work of Grant (1968, 1973). He has shown that, during high-grade metamorphism, cordierite-, gedrite- and garnet-rich rocks may be formed by the partial melting of metasedimentary rocks with compositions ranging from those of shales to those of greywackes. During anatexis, "filter-pressing" may drive off the melt, leaving behind a residue ("restite") rich in ferromagnesian and aluminous phases, and, depending on the original bulk-compositions, depleted in K-felspar.

Assemblages (74) to (81) have been observed by Lal and Moorhouse (1969) in the Fishtail Lake area, Ontario. These authors have confirmed the deductions of Grant (1968), and have inferred temperatures of 500-720°C and pressures of 4-8 kb for the metamorphic conditions producing these cordierite- and gedrite-rich rocks. Assemblages (75), (76), (78) and (79) have also been observed by Gable and Sims (1969) in the Front Range area, Colorado. These authors also infer upper-amphibolite facies conditions for the metamorphism, and substantially confirm the work of Grant (1968).

The distribution of Ti and Fe between coexisting ilmenite and magnetite pairs in the Valley Bore garnet-gneiss suggests temperatures of formation of 825°C (Buddington and Lindsley, 1964) or 800°C (Powell and Powell, 1977), with f_{O_2} equal to 10^{-14} atm. (Buddington and Lindsley, 1964). These temperatures are in agreement with those inferred for the formation of low-boron kornerupine by Seifert (1975). This is relevant to the Valley Bore area because the kornerupine in the phlogopite-schist contains, approximately, only 1.6% B_2O_3 (I. M. Threadgold, pers. comm.).

The highest geothermal gradient appropriate to the formation of the cordierite-rich enclaves of the previous chapter passed through the point 620°C, 6 kb. Hence, for the garnet-gneiss at these higher temperatures, an absolute minimum pressure of formation would be 6 kb, with a maximum of 10 kb at the sillimanite-kyanite transition boundary. This pressure range is also consistent with that inferred by Seifert (1975) for the formation of boron-poor kornerupine.

8.4 The Distribution of Elements between Phases in the Garnet-Gneiss

Representative compositions of minerals within the garnet-gneiss are presented in table 29. These analyses were obtained from a single, circular section of 2.2 cm diameter, exhibiting the polyminerale domains described in section one of this chapter.

Coexisting cordierite and garnet

As described previously, it is almost certain that cordierite-

CORDIERITE-GARNET- AND GEDRITE-BEARING GRANULITE

	<u>GARNET RIM</u>	<u>CORDIERITE</u>	<u>GEDRITE</u>	<u>PHLOGOPITE</u>
SiO ₂	38.98	48.49	42.32	38.91
TiO ₂	.00	.00	.27	1.69
Al ₂ O ₃	22.19	33.35	17.85	17.72
FeO	16.80	4.24	18.57	12.57
MnO	.69	.00	.27	.00
MgO	10.19	10.86	15.39	16.60
CaO	1.10	.00	.37	.00
Na ₂ O	.00	.49	2.01	.68
K ₂ O	.00	.00	.00	8.04
<u>TOTAL</u>	<u>99.95</u>	<u>97.43</u>	<u>97.05</u>	<u>96.21</u>
CATIONS PER No. OXYGENS	12	18	23	22
Si	2.9878	4.9550	6.1742	5.6046
Ti			.0296	.1831
Al	2.0046	4.0164	5.0692	3.0081
Fe	1.7179	.3623	2.2657	1.5141
Mn	.0448		.0334	
Mg	1.1644	1.6543	3.3427	3.5645
Ca	.0903		.0578	
Na		.0971	.5686	.1899
K				1.4773
<u>TOTAL</u>	<u>8.0098</u>	<u>11.0851</u>	<u>15.5457</u>	<u>15.5416</u>
<u>Mg</u>	40.40	82.03	59.60	70.19
X _{Fe}	56.93			
X _{Mg}	38.59			
X _{Mn}	1.48			
X _{Ca}	2.99			
Al ^{iv}			1.8258	2.3954
Al ^{vi}			3.2434	.6127

TABLE 29: Microprobe analyses of minerals in a sample of granulite from Irindina Ck. All these minerals occur in a single sample within a circular section some 2.2cm in diameter (see text). Coexisting plagioclase has the composition An_{17.94} Ab_{81.50} Or_{0.56} •

garnet-biotite-sillimanite-plagioclase-quartz represents an equilibrium assemblage within the garnet-gneiss. This enables the temperature and pressure of formation to be (approximately) derived from the compositions of the cordierite and garnet. However, five different calibrations have been proposed for the cordierite-garnet geothermometer-geobarometer. Two of these (Currie, 1971; Hutcheon et al., 1974) are at variance with the remaining three, which are broadly consistent with each other (Hensen and Green, 1971, 1972, 1973; A. Thompson, 1976; Holdaway and Lee, 1977).

The two experimentally-derived calibrations are those of Currie (1971) and Hensen and Green (1971, 1972, 1973). The most significant difference between them is that, in one, $K_D^{\text{cord-gt}}_{\text{Mg-Fe}}$ decreases with increasing temperature (Hensen and Green), whereas, in the other, K_D increases with increasing temperature (Currie). In general, for near-ideal solid-solution pairs, if K_D is formulated so that the mole fractions of the more magnesian mineral occupy the numerator, then K_D is greater than one, and decreases towards unity with increasing temperature (Mueller and Saxena, 1977). The calibration of Currie (1971, 1974) runs counter to this observation. Further confusion may arise from the fact that both experimental calibrations yield temperatures of formation around 700°C for K_D 's about 6. Since many cordierite-garnet-sillimanite-quartz-bearing assemblages are formed at about this temperature, some workers have been tempted to use the calibration of Currie, on the basis that it gives reasonable results, without realizing that this same calibration gives very unreasonable results for lower-grade rocks.

COMPARISON OF PRESSURES AND TEMPERATURES OF EQUILIBRATION DERIVED FROM THE
VARIOUS PROPOSED CORDIERITE - GARNET GEOTHERMOMETERS - GEOBAROMETERS

<u>HENSEN & GREEN</u>	<u>CURRIE</u>	<u>HUTCHEON ET AL.</u>	<u>THOMPSON</u>	<u>HOLDAWAY & LEE</u>
1973	1971	1974	1976	1977
cordierite- and garnet-bearing granulite, Valley Bore area, this work, #899				
750°C / 9.8kb	740°C / 6.5kb	550°C / 5.4kb	720°C / 7.0kb	720°C / 8.2kb
cordierite-garnet-gedrite gneiss, Colorado, Gable and Sims, 1969				
700°C / 8.5kb	750°C / 6.5kb	545°C / 4.2kb	710°C / 5.9kb	670°C / 6.7kb
cordierite-garnet-gedrite-quartz-retrograde(?) chlorite hornfels, Koolanooka, W.A., this work, #891				
548°C	859°C		556°C	583°C
cordierite-garnet-gedrite-biotite hornfels, Koolanooka, W.A., this work, #892				
548°C	859°C		556°C	584°C
cordierite-garnet-orthopyroxene-biotite granulite, W.A., Davidson & Mathison '74				
687°C	736°C		698°C	712°C
cordierite-garnet-gedrite-biotite-quartz gneiss, Ontario, Lal & Moorhouse, '69				
733°C	708°C		745°C	753°C
cordierite-garnet-gedrite-plagioclase gneiss, Yellowknife, Canada, Kamineni '75				
507 - 556°C	849 - 911°C		515 - 565°C	545 - 592°C
cordierite-garnet-hypersthene-sillimanite-Kspar granulite, Karnatka, India, Iyer & Kuttly, 1975				
769 - 849°C	651 - 688°C		782 - 864°C	785 - 856°C

The temperature-approximating equations derived from the published data are:

Hensen & Green	$T^{\circ}\text{C} = (1193 / (0.4187 + \log K_{\text{D}_{\text{Mg-Fe}}^{\text{cd-gt}}})) - 273.15$
Currie	$T^{\circ}\text{C} = (4515 / (6.37 - \ln K_{\text{D}_{\text{Mg-Fe}}^{\text{cd-gt}}})) - 273.15$
Thompson	$T^{\circ}\text{C} = (2750 / (0.933 + \ln K_{\text{D}_{\text{Mg-Fe}}^{\text{cd-gt}}})) - 273.15$
Holdaway & Lee	$T^{\circ}\text{C} = (3187 / (1.3377 + \ln K_{\text{D}_{\text{Mg-Fe}}^{\text{cd-gt}}})) - 273.15$

TABLE 30: Comparison of temperatures and pressures of equilibration derived from the five proposed cordierite-garnet geothermometers - geobarometers.

Wood (1973) attempted to reconcile the two opposing calibrations by assuming that, at any given P and T, the water content of cordierite is strongly dependent on cordierite composition. There is currently no evidence for such an assumption, and, in addition, the works of Weisbrod (1973), A. Thompson (1976), Currie (1974), Holdaway (1976) and Holdaway and Lee (1977) are inconsistent with this assumption. A more detailed examination of the differences between the two experimental calibrations has been made by Hensen (1977). Recent field studies, and calculations by A. Thompson (1976) and Holdaway and Lee (1977) clearly support the calibration of Hensen and Green (1971, 1972, 1973).

A comparison of equilibration temperature and pressure values derived from the various calibrations is presented in table 30. The cordierite-garnet-bearing samples in this table were taken from this work and from the recent literature. Assemblages, locations, references and compositional parameters are summarized in table 28.

The calibration of Currie (1971, 1974) yields temperatures of formation in excess of 850°C for the demonstrably middle-amphibolite facies gedrite-bearing rocks from Koolanooka W.A. (chapter 6, tables 24 and 25) and the Yellowknife district (Kamineni, 1975; Ramsay, 1974). These temperatures are inconsistent with the metamorphic grade, yielding further proof that the calibration of Currie (1971) is incorrect.

The theoretically-derived calibration of Hutcheon et al. (1974) yields temperatures of formation of around 550°C for the garnet-

gneisses from the Valley Bore area, and for the gedrite-bearing garnet-gneisses from the high-grade, migmatitic, Front Range area in Colorado. These temperatures are too low, and invalidate the calibration of Hutcheon et al. (1974).

The three calibrations that are broadly consistent are those of Hensen and Green (1971, 1972, 1973), A. Thompson (1976), and Holdaway and Lee (1977), but a choice between them is difficult. On the one hand, the experimental calibration of Hensen and Green requires no assumptions regarding the thermochemical parameters of cordierite and garnet. However, as pointed out by Hensen (1977), and Hensen and Green (1973), absolute pressures inside a piston-cylinder apparatus are not well known, and the temperature calibration may be somewhat in error, due to the low angle of interception of the compositional isopleths (Hensen and Green, 1973, fig. 2). On the other hand, the theoretically-derived calibrations are free of the problems of equilibration times and the determination of equilibrium compositions (Holdaway and Lee, 1977). However, these calibrations are subject to errors resulting from assumed or inferred thermochemical parameters calculated from simple experiments and natural assemblages, since the precise P-T conditions of formation of the latter are not known. Further errors may arise from the possible non-ideal behaviour of garnet solid-solutions, especially at relatively low temperatures (e.g. Ganguly and Kennedy, 1974).

The temperatures and pressures of formation of the two garnet-gneisses in table 30 fall just outside the stability field of sillimanite, if the calibration of Hensen and Green is used.

Fortunately, this departure is not great, and may be explained by errors inherent in the calibration (described above), or by possible cation-exchange reactions between cordierite and garnet and/or cordierite and biotite, at lower temperatures (Hensen, 1977).

In general, the three consistent calibrations yield temperatures of formation of 720 to 750°C for the Valley Bore garnet-gneiss, with pressures ranging from 7 to 9.8 kb. Since the assemblages within the cordierite-rich enclaves (chapter 7) indicate a relatively low geothermal gradient in the Valley Bore area ($P > 6$ kb for $T = 610^\circ\text{C}$), and since the compositions of coexisting magnetite-ilmenite indicate a high temperature of formation of the garnet gneiss ($\sim 800^\circ\text{C}$), the higher P and T values of Hensen and Green are favoured by the author.

Coexisting garnet and phlogopite

Reference to table 28 shows that, in general, high-grade, orthopyroxene-bearing gneisses have $K_{\text{D}_{\text{Mg-Fe}}}^{\text{bio-gt}}$ values as low as 1.5, whereas middle-amphibolite facies rocks have K_{D} values in the range of 5 to 7.4. However, high-grade, granulite-facies rocks may have high K_{D} 's (5.3 to 6.1; Schmid and Wood, 1976) and middle-amphibolite facies rocks may have relatively low K_{D} 's (3.74; Koolanooka W.A., this work).

As discussed in chapter 4, the overlapping of K_{D} values from rocks formed under different P-T conditions may be largely explained by the non-ideality of solid-solution in the octahedral sites of the mica, especially with respect to Ti and Al.

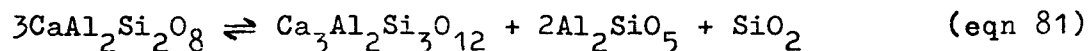
The K_D value of the garnet-gneiss from the Valley Bore area is very similar to those in the high-grade gneisses from the Fish-tail area (Lal and Moorhouse, 1969) and the Front Range area (Gable and Sims, 1969). Since the micas in these three gneisses have similar X_{Ti}^{oct} and X_{Al}^{oct} values, the similarity of the K_D values (3.47, 3.43 and 3.42 respectively) indicates similar temperatures of formation, in the range 670 to 750°C.

Coexisting cordierite-biotite and orthoamphibole-biotite

As pointed out in chapters 4 and 7, the distribution coefficient between two phases in which both Fe and Mg ions occupy octahedral sites is not very sensitive to changes in temperature. The low range of respective K_D values in table 28 supports this observation. The observed variation is, at least in part, the result of non-ideality of solid-solution in mica and orthoamphibole. Consequently, these K_D values cannot be used at this stage to indicate temperatures of formation.

Coexisting garnet and plagioclase

The grossular content of garnet and the anorthite content of coexisting plagioclase may be used to derive approximate P or T conditions of formation of rocks containing the assemblage garnet-plagioclase-sillimanite-quartz (Ghent, 1975; Kephezinskas, 1973). For this assemblage, the equilibrium reaction is as follows:



Since the activities of sillimanite and quartz are equal to unity (pure phases), the equilibrium relation appropriate to equation (81)

is:

$$(\Delta G^{\circ})_{P,T} = -RT \ln K_{81} = -RT \ln (a_{\text{gross}}^{\text{gt}} / a_{\text{an}}^{\text{plg}^3}) \quad (\text{eqn 82})$$

Equilibrium temperatures and pressures for reaction (81) have been experimentally determined by Hays (1967) and Hariya and Kennedy (1968), and the appropriate thermodynamic parameters have been derived from these studies by Ghent (1976, eqns. 1c and 2) and Schmid and Wood (1976, eqn. 7). The interaction parameters for garnet solid-solution at 700°C (Hensen et al., 1975, Schmid and Wood, 1976) have been used to derive the activity coefficient of the grossular component in the garnet in the garnet-gneiss from the Valley Bore area ($X = 2.51$). The activity coefficient for the anorthite component of the coexisting plagioclase may be taken from the work of Orville (1972), and has a value of 1.28 at 700°C.

With the above activity coefficients, equation (82) has been solved to give the following P-T combinations for the formation of the Valley Bore garnet-gneiss:

T °C	Schmid and Wood (1976, eqn. 7)	Ghent (1976, eqns. 1c, 2)
650	9.6 kb	9.1 kb
675	10.0 kb	9.6 kb
700	10.5 kb	10.1 kb
725	11.0 kb	10.6 kb
750	11.5 kb	11.1 kb

Although the above pressures are only approximate (see Ghent, 1976), with probable errors of ± 3 kb, they are consistent with P-T conditions derived from the cordierite-garnet geothermometer-geobarometer of Hensen and Green (1971, 1972, 1973), A. Thompson

(1976), and Holdaway and Lee (1977).

CHAPTER 9: CORDIERITE-GEDRITE STABILITY UNDER HIGH-PRESSURE
HYDROUS CONDITIONS--AN EVALUATION

9.1 Introduction

Green and Vernon (1974) undertook an experimental investigation of the stability field of the assemblage cordierite-aluminous anthophyllite-kyanite-quartz under high-pressure hydrous conditions, with the aim of evaluating a natural occurrence described by Vernon (1972). Their results indicate a divariant equilibrium field for the above-mentioned assemblage 2.4 kb wide at 750°C and 1.8 kb wide at 850°C; they also point out that the field width may be overestimated at lower temperatures due to incomplete reaction. By treating orthoamphibole solid-solution as a multi-site ionic solution, and making a number of assumptions, Lee and Holdaway (1976) calculated the width of the above divariant field to be 0.64 kb at 750°C and 0.7 kb at 850°C.

In this chapter, the Al-content of gedrite is examined, the Fe-Mg distribution between cordierite and gedrite is investigated, and the effect of varying the assumed parameters in the calculations of Lee and Holdaway is evaluated. Wherever possible, any assumed or inferred compositional parameters will be compared with values derived from naturally-occurring assemblages, particularly with those presented in chapters 7 and 8. This is done to determine whether there is any conclusive evidence to support Lee and Holdaway's modifications to the experimental work of Green and

Vernon (1974).

To facilitate comparison, the mathematical formulations in this chapter will be consistent with those of Lee and Holdaway (1976).

9.2 Aluminium in Gedrite

Gedrite in this chapter is taken as any non-lithian ortho-amphibole with $\text{Al}_2\text{O}_3 > 6\%$ by weight. Aluminium substitution in gedrite is believed to occur in one of two ways:

- (i) $\text{Mg}^{2+}\text{Si}^{4+} \rightleftharpoons \text{Al}^{3+}\text{Al}^{3+}$, a coupled tetrahedral-octahedral substitution which by itself would lead to the equality $\text{Al}^{\text{iv}} = \text{Al}^{\text{vi}}$.
- (ii) $\square\text{Si}^{4+} \rightleftharpoons \text{Na}^+\text{Al}^{3+}$, a substitution in which a normally vacant A site is occupied by Na^+ for every Si^{4+} substituted by Al^{3+} ; this type of substitution, added to (i) above, leads to the relation $\text{Al}^{\text{iv}} \geq \text{Al}^{\text{vi}}$.

To examine possible departures from the above substitutions in natural gedrites, and to predict octahedral to tetrahedral aluminium relations in synthetic gedrites with no "impurities" (Na^+ , K^+ , Cr^{3+} , Fe^{3+} , Ti^{4+}), fifty gedrite analyses were tested against the ideal relationships:

$$(\text{atomic}) \text{Al}^{\text{iv}} - \text{Al}^{\text{vi}} - \text{Fe}^{3+} - \text{Cr}^{3+} - 2\text{Ti}^{4+} = \text{Na}^+ + \text{K}^+ \quad (\text{eqn. 83})$$

Forty-six of the analyses were drawn from published papers (Rabbitt, 1948; Deer, Howie and Zussman, 1962; Zotov and Sidorenko, 1968; Lal and Moorhouse, 1969; Robinson, Ross and Jaffe, 1971; Kamineni, 1975; Lal and Shukla, 1975; Schreyer and Abraham, 1976). Two are presented in chapter 6 (tables 24 and 25), and one appears

in each of chapters 7 and 8 (tables 27 and 29 respectively). All contain $\leq 1\%$ of CaO, and all were recalculated on the basis of 23 oxygens to minimize the effects of incorrect H_2O determinations (Robinson, Ross and Jaffe, 1971). The analyses were first examined in three groups: microprobe analyses (9), post-1958 analyses of mineral separates (26), and pre-1958 analyses (15). There is no significant compositional difference between the two groups of wet-chemical analyses; the small difference between the microprobe analyses and the wet-chemical analyses may be explained by the assumption that all iron is Fe^{2+} , departures from which cannot be ascertained without the prior assumption that the structural formula is ideal.

Taken together, the 50 analyses show marked departures from the predicted relation (83), yielding the regression equation

$$(Al^{iv} - Al^{vi} - Fe^{3+} - Cr^{3+} - 2Ti^{4+}) = 0.574(Na^{+} + K^{+}) + 0.060 \quad (\text{eqn. 84})$$

with a low correlation coefficient $r = 0.37$. Apart from analytical errors, these departures may be interpreted as evidence of glaucophane substitution or substitution of divalent cations in the A sites (Robinson, Ross and Jaffe, 1971). Regression analysis also shows that, for gedrite free of Na^{+} , K^{+} , Ti^{4+} , Cr^{3+} and Fe^{3+} , the expected aluminium relation is $-0.14 \leq Al^{iv} - Al^{vi} \leq 0.26$ at the 99% level of confidence.

Lee and Holdaway derived a theoretical relation between gedrite Mg and X_{Al}^{M2} , the "fraction" of octahedral M2 sites in gedrite occupied by Al^{vi} ($X_{Al}^{M2} = \frac{1}{2}Al^{vi}$ based on 23 oxygens). Lee and Holdaway's plot of gedrites from Green and Vernon's experiments suggests that those gedrites occurring above the divariant field had not attained their

equilibrium X_{Al}^{M2} content as they plot predominantly below the curve calculated by Lee and Holdaway (1976). In order to derive their theoretical curve, Lee and Holdaway assumed that 11% Al_2O_3 in gedrite corresponds to gedrite $X_{Al}^{M2} = 0.43$, and further assumed that Al is equally distributed between tetrahedral and octahedral sites. However, the amount of octahedral Al^{3+} in a gedrite depends not only on the total Al_2O_3 content, but also on the amounts of all other elements present in gedrite, and hence requires a structural formula for its evaluation. As has been shown above, exactly equal distribution of Al^{3+} between the two different coordination sites in sodium-free gedrites need not be the case. The experimentally-produced gedrites of Green and Vernon (1974) lying above the divariant field generally have $Al^{iv} < Al^{vi}$, and, as a consequence, the average total M site occupancy is 97.9%. X_{Al}^{M2} values derived from the structural formulae of these synthetic gedrites cluster round a point lying above and not below Lee and Holdaway's calculated curve. Hence, in contrast to the assertion of Lee and Holdaway (1976), the experimentally-produced gedrites of Green and Vernon do not have disequilibrium Al contents.

A curve of best fit for 11 natural gedrites (curve a, fig. 19) also lies above the calculated curve (curve c, fig. 19) of Lee and Holdaway (1976). The addition of the mean Al value of the synthetic gedrites to those of the 11 natural samples gives rise to the following preferred relation between octahedral Al in gedrite and gedrite Mg (curve b, fig. 19)

$$X_{Al}^{M2} \text{ ged} = 2.4379 - 0.4456 \ln \underline{Mg} \quad (r = 0.71) \quad (85)$$

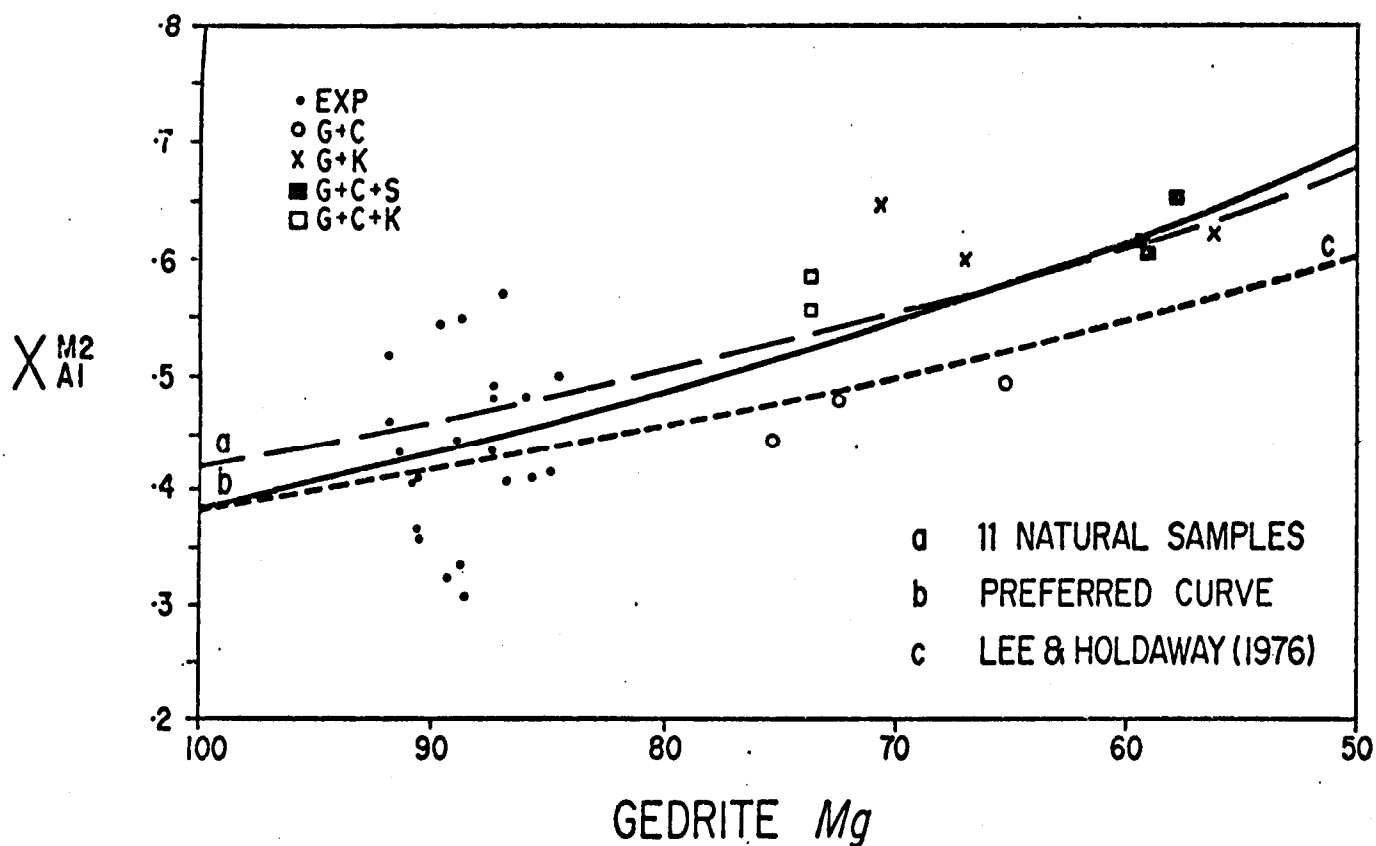


FIGURE 19: Gedrite octahedral Al^{3+} content at high pressures as a function of gedrite composition. Dots: experimentally produced gedrites; open circles: gedrite - cordierite - bearing assemblages; crosses: gedrite - kyanite - bearing assemblages; open rectangles: gedrite - cordierite - kyanite - quartz assemblages; filled rectangles: gedrite - cordierite - sillimanite - bearing assemblages.

9.3 Gedrite Site-Occupancy Relations

Gedrite has four octahedral sites (M1 to M4) with multiplicities of 2, 2, 1, 2 respectively. Based on two gedrites (001 and 002) investigated by Papike and Ross (1970), Lee and Holdaway (1976) formulated the site occupancies as follows:

$$\frac{x_{Mg}^{M1}}{x_{Fe}^{M1}} = \frac{x_{Mg}^{M2}}{x_{Fe}^{M2}} = \frac{x_{Mg}^{M3}}{x_{Fe}^{M3}} \quad (86)$$

Equation (86) implies constant \underline{Mg} values for the three sites M1, M2 and M3 for any gedrite. Substitution of the data of Papike and Ross into equation (86) yields

$$7.33 = 9 = 9 \quad (\underline{Mg}'s \ 88, 90, 90) \text{ for gedrite 001}$$

with $\underline{Mg} = 80$, and

$$2.03 = 2.56 = 1.56 \quad (\underline{Mg}'s \ 67, 72, 61) \text{ for gedrite 002}$$

with $\underline{Mg} = 56$.

Thus the site occupancies of gedrite 002 show significant departures from equation (86), and the inference, based on only two samples, that magnesian gedrites have three identical x_{Mg}^M values may be a potential source of error in all calculations utilizing equation (86). The equations

$$x_{Mg}^{M2} + x_{Fe}^{M2} + x_{Al}^{M2} = 1 \quad (87)$$

$$x_{Al}^{M1} = x_{Al}^{M3} = x_{Al}^{M4} = 0 \quad (88)$$

(Lee and Holdaway, 1976, eqns. 3 and 4) show that octahedral Al^{3+} is restricted to M2 sites.

Ordering in gedrite concentrates Fe^{2+} in M^4 relative to other sites. This concentration may be expressed by:

$$\frac{\frac{X_{\text{Mg}}^{M4}}{X_{\text{Fe}}^{M4}}}{\frac{X_{\text{Mg}}^{M1}}{X_{\text{Fe}}^{M1}}} = K_{D1} \quad (89)$$

The numerical value of K_{D1} is important in calculations to come; gedrites 001 and 002 yield K_{D1} values of 0.16 and 0.25 respectively, but Lee and Holdaway (1976) use 0.29 to allow for slight disordering at the temperatures of Green and Vernon's experiments. Unfortunately, no ordering studies are available for gedrites; data on anthophyllite-ordering kinetics cannot be applied because the blocking effects of Al in gedrite M2 sites on ordering are not known (Papike and Ross, 1970).

The value of K_{D1} as a function of temperature must, for the present, remain indeterminate. X_{Mg}^{M1} for any gedrite at high pressure is a function of $\underline{\text{Mg}}$ and K_{D1} values, and may be exactly evaluated using equations (85) to (80), bearing in mind possible errors from equation (86). Since the calculation of X_{Mg}^{M1} by hand is tedious, exactly evaluated values for $\underline{\text{Mg}} \geq 50$ and $0.1 \leq K_{D1} \leq 1$ have been fitted by least squares to yield the simple approximation:

$$X_{\text{Mg}}^{M1} \text{ ged} = 0.616 \ln \underline{\text{Mg}} - 0.057 \ln K_{D1} - 1.903 \quad (90)$$

Equation (90) is an excellent estimator, with a maximum error of 6.6% at the boundary values of $\underline{\text{Mg}}$ and K_{D1} , rapidly decreasing in error for intermediate values of the variables.

9.4 Gedrite-Cordierite Relations

$$\frac{X_{Mg}^{M1}}{X_{Fe}^{M1}} \bigg/ \frac{X_{Mg}^{cord}}{X_{Fe}^{cord}} = K_{D2} \quad (91)$$

$$\frac{X_{Mg}^{ged}}{X_{Fe}^{ged}} \bigg/ \frac{X_{Mg}^{cord}}{X_{Fe}^{cord}} = K_{DM} \quad (92)$$

The distribution of Mg^{2+} and Fe^{2+} between gedrite and cordierite may be described by equation (91) or (92); for values of K_{D1} close to unity, equations (91) and (92) are similar. As K_{D1} decreases, K_{DM} becomes increasingly dependent on gedrite composition, decreasing in value for fixed external conditions with increasing gedrite \underline{Mg} . This is a consequence of Fe^{2+} - Mg^{2+} partitioning between M4 and the other octahedral sites in gedrite. Similarly, K_{D2} must be a function of gedrite \underline{Mg} because gedrite is non-ideal with respect to Mg/Fe substitution. The behaviour of K_{D2} with T and gedrite \underline{Mg} cannot be evaluated until K_{D1} is known, at least approximately, as a function of T and X_{Al}^{M2} .

Lee and Holdaway (1976) chose equation (91) to express gedrite-cordierite relations, and, using $K_{D1} = 0.29$ and the average compositions of "coexisting" anthophyllite ($Al_2O_3 = 3.2$, $\underline{Mg} = 80$) and cordierite ($\underline{Mg} = 92.5$) from the experiments of Green and Vernon (1974), assigned $K_{D2} = 0.52$. However, Seifert and Virgo (1975) have shown that anthophyllite ($Al_2O_3 = 2\%$) is completely disordered at $720^\circ C$, so that, for the above anthophyllites at $750^\circ C$, $K_{D1} = 1.00$, giving $K_{DM} = K_{D2} = 0.32$. The use of this value of K_{D2} derived from anthophyllite-cordierite for the pair gedrite-cordierite is justified

by the fact that there is only very limited $\text{Mg}^{2+}\text{-Fe}^{2+}$ fractionation between anthophyllite and gedrite at high temperatures (Robinson, Ross and Jaffe, 1971). As an example, at the somewhat lower temperatures of the sillimanite-staurolite zone, anthophyllite $\text{Mg} = 60.4$ coexists stably with gedrite $\text{Mg} = 56.4$ (Stout, 1971).

Gedrite is the stable orthoamphibole with cordierite in the divariant field, and Green and Vernon's experimental starting mixture is probably not an equilibrium assemblage. Consequently, gedrite-cordierite $K_{D,s}$ may be taken from the natural assemblage described by Vernon (1972), giving $K_{DM} = 0.28$, and for $K_{D1} = 0.29$, $K_{D2} = 0.43$.

Making the assumption that ΔV for the Fe-Mg exchange reaction between cordierite and gedrite is insignificant, K_{DM} is a function of temperature and gedrite composition. Using the two assemblages in tables 27 and 29 of chapters 7 and 8 respectively, plus those in the recent literature, an approximate, empirical relation has been calculated for gedrite-cordierite $\text{Fe}^{2+}\text{-Mg}^{2+}$ distribution for gedrite $\text{Mg} > 40$.

$$K_{DM} = 0.3568 + 0.1870 \ln T^{\circ}\text{C} - 0.2946 \ln \text{Mg}_{\text{ged}} \quad (r=0.70) \quad (93)$$

The degree of fit of the simplified K_{DM} surface is not particularly good, and may reflect errors in the estimated values of temperature, as well as departures from the assumptions made.

However, equation (93) does indicate that K_{DM} increases with increasing temperature and decreases with increasing gedrite Mg; the value of 0.28 given for the experiments of Green and Vernon (1974) is in close agreement with the figures derived from naturally-

coexisting orthoamphibole and cordierite. In all probability, K_{DM} is a function also of other variables, but to regress a surface on more variables requires more analyses than are presently available.

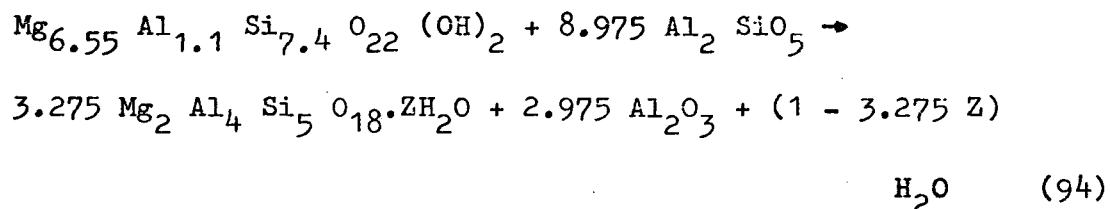
9.5 Water in Cordierite

Lee and Holdaway's calculations presuppose that cordierite breakdown is a dehydration reaction. By noting the effects of a lowered a_{H_2O} on the pressure required to crystallize gedrite, Green and Vernon (1974) demonstrated that the breakdown of their cordierite is a hydration reaction.

The presence of molecular water in cordierite has been well established; the actual amount of water, as a function of P , f_{H_2O} , T and Mg , is still subject to considerable uncertainty, due partly to the relative ease with which water enters or leaves the cordierite structure (Schreyer and Yoder, 1964). The work of Schreyer and Yoder (1964) predicts 0.7 mole H_2O per mole for the experimental cordierites of Green and Vernon (1974). Unfortunately, as pointed out by Schreyer and Yoder, there is no certainty that these values are the equilibrium water contents at the appropriate P - T conditions.

Recently, Schreyer and Abraham (1976) have shown that many reactions in high-pressure whiteschists occur in response to changing fluid phase compositions at relatively constant temperature and pressure. One of the reactions that may be attributed to decreasing a_{H_2O} is that between gedrite and kyanite to form cordierite plus corundum plus H_2O . Using the data of Schreyer and Abraham (1976), and ignoring the minor Na_2O in the system, this

reaction may be written:



Reaction (94) indicates that, under the P-T conditions of white-schist occurrence, cordierite formation as described above is a dehydration reaction so that cordierite breakdown is a hydration reaction. In addition, the maximum allowable water content per mole of cordierite in equation (94) is 0.31 mole, which is about half the value that would be predicted in Schreyer and Yoder (1964) for these conditions. Though available data indicate that cordierite breakdown at high pressures is likely to be a hydration reaction, the amount of water participating in the reaction is still indeterminate.

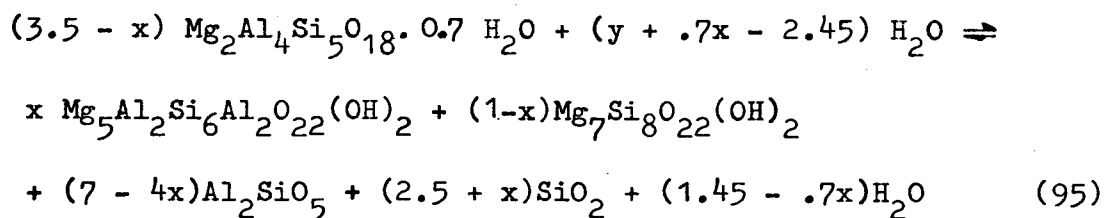
9.6 Cordierite-Gedrite-Kyanite-Quartz Divariant Stability Field

In order to carry out calculations to determine the width of the divariant stability field of cordierite and gedrite, Lee and Holdaway (1976) made the following assumptions:

- (i) Gedrite solid-solution closely approximates the multi-site ionic solution model as formulated in equations (91) and (95).
- (ii) Activity coefficients vary little for the range of pressures, temperatures and compositions used.
- (iii) Al^{3+} is equally distributed between octahedral and tetrahedral sites.

- (iv) Tetrahedral Al^{3+} ions reside near octahedral Al^{3+} to preserve short-range charge balance (based on Wood and Banno, 1973).
- (v) For the area of the divariant field, $X_{\text{Al}}^{\text{M2}}$ is insensitive to changes in pressure.
- (vi) Cordierite breakdown is a hydration reaction, and the amount of H_2O in cordierite may be determined from the work of Schreyer and Yoder (1964).

The cordierite breakdown reaction may be formulated as follows:



Reaction (95) is taken from Lee and Holdaway (1976), but has been modified to allow cordierite breakdown to be a hydration or dehydration reaction, depending on the value of y , since assumption (vi) above is unlikely to be correct. The amount of "gedrite" end-member in the orthoamphibole solid-solution in reaction (95) is fixed by the value of x , where $x = X_{\text{Al}}^{\text{M2}}$.

At the higher-pressure limit of the divariant field, the reaction is characterized by the stability of gedrite_{ss} with $\text{Mg} = 87$, because (i) this is the bulk-composition Mg value in the experiments of Green and Vernon (1974), and (ii) gedrite_{ss} is the only ferromagnesian mineral stable at pressures above the divariant field. By similar reasoning, the lower-pressure limit of the divariant field is characterized by cordierite with $\text{Mg} = 87$.

The equilibrium constant for reaction (95) is given by:

$$K = \frac{X_{Mg}^{M1^3} X_{Mg}^{M4^2} X_{Mg}^{M2(2-2x)} X_{Al}^{M2^{2x}}}{X_{Mg}^{cord(7-2x)}} \quad (96)$$

The relation

$$\frac{-\Delta V \Delta P}{RT} = \ln K \text{ (final)} - \ln K \text{ (initial)} \quad (97)$$

may be used to calculate the position and width of the divariant field relative to an "initial" reaction in the simple system at $Mg = 100$ (Lee and Holdaway, 1976).

Making the assumptions (i) to (v) above, the position and width of the divariant field in P-T space have been carried out by the writer at $K_{D2} = 0.3$ for the two unknowns in the range $0.2 \leq K_{D1} \leq 1.0$ and $-1.2 \leq y \leq 1.2$. The results are depicted graphically in figures 20 and 21.

9.7 Discussion

The relative position of the divariant field as given by figure 20 is still subject to the large error in the positioning of the $Mg = 100$ initial reaction curve (± 1 kb, Lee and Holdaway, 1976). For the present, these calculations cannot show incompatibility with the "top" of Green and Vernon's divariant field.

As the calculations and figures (20) and (21) show, the width and position of the divariant field are functions of the values of K_{D1} , K_{D2} and y . A decrease in the values of any of these parameters results in (a) a lowering of the divariant field relative to the "initial" reaction (bulk $Mg = 100$), and (b) an increase in the width of the divariant field. In addition, if equation (92) is used

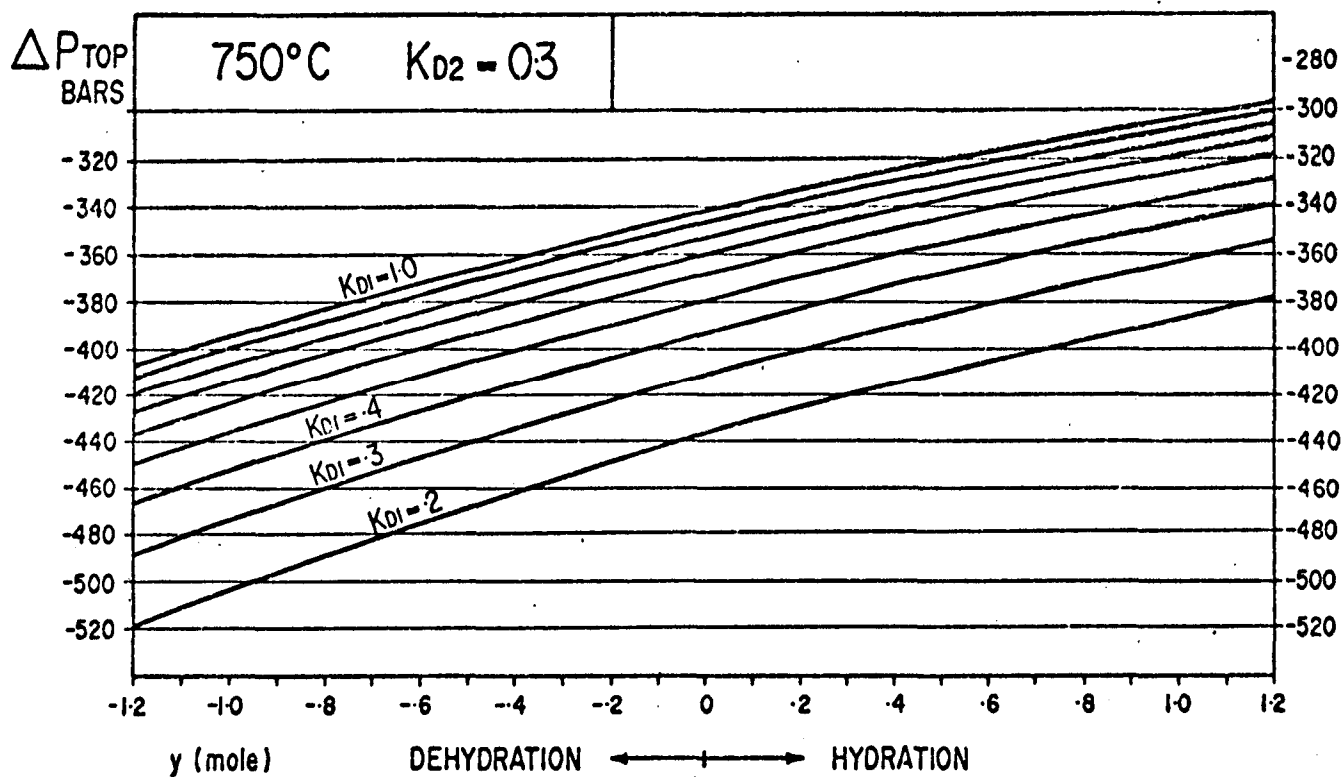


FIGURE 20: Calculated position (below the univariant $Mg = 100$ curve) of the higher - limit of the gedrite - cordierite - kyanite - quartz - vapour divariant stabil field as a function of K_{D1} (gedrite ordering) and y (the amount of H_2O in cordierite and its role in the reaction), for a bulk composition of $Mg = 8$ at 750°C for $K_{D2} = 0.3$.

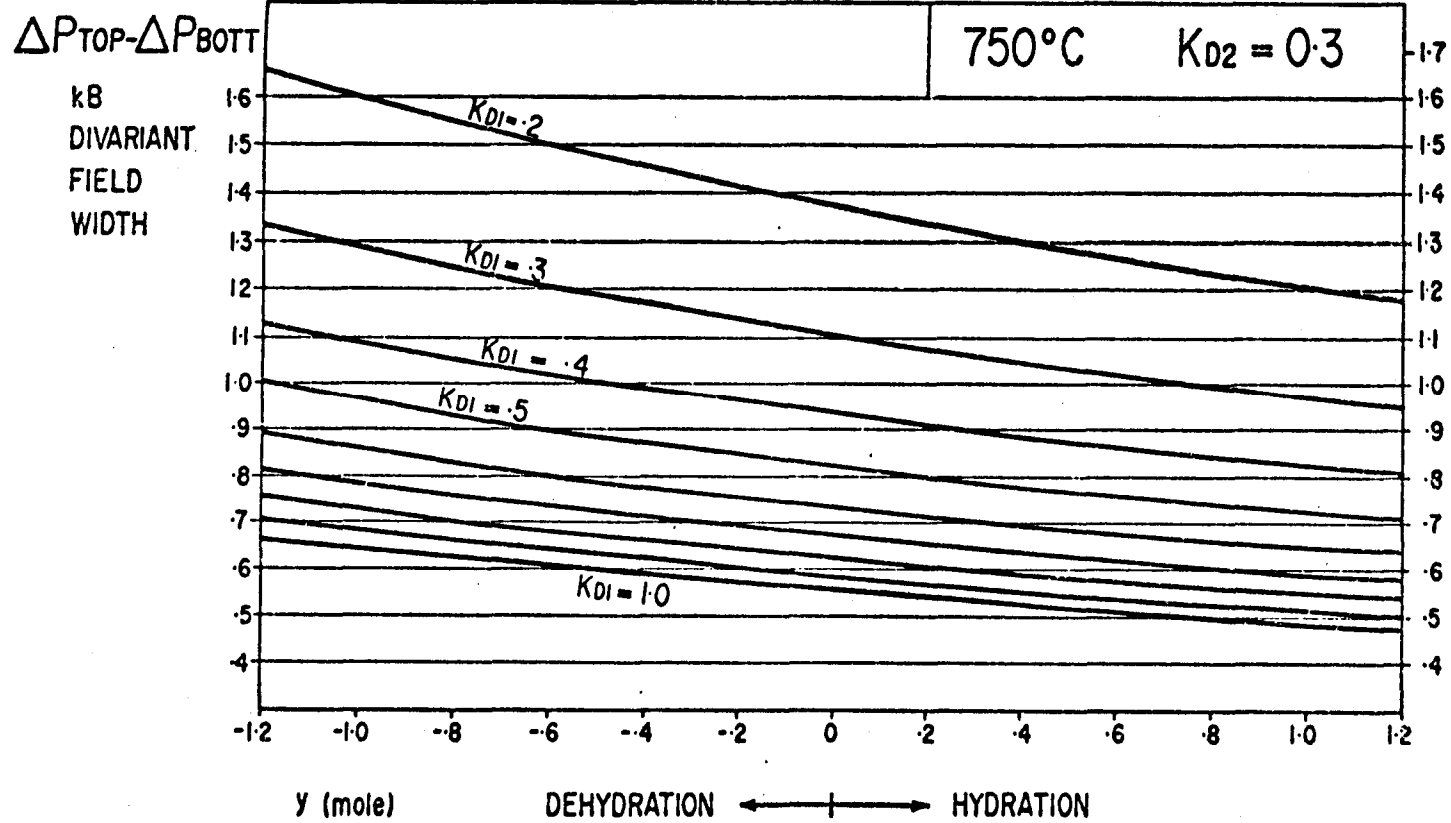


FIGURE 21: Calculated width of the gedrite - cordierite - kyanite - quartz - vapour divariant stability field as a function of K_{D1} and y , for a bulk composition of $\text{Mg} =$ at 750°C for $K_{D2} = 0.3$.

instead of equation (91) (i.e. use of the full composition of the gedrite rather than the M1-equivalent sites only), and, if the value is independent of composition, the effect is the same as a further reduction of the value of K_{D2} ; that is, the divariant field is widened.

Changing only K_{D2} to a more realistic value of 0.3 (see section 3) in Lee and Holdaway's calculations results in doubling the width of their calculated field. Use of K_{DM} instead of K_{D2} results in a field width of 1.5 kb as compared with 0.65 kb of Lee and Holdaway (1976) and 2.4 kb of Green and Vernon (1974) at 750°C. Direct comparison of these figures may be misleading as the value of $K_{D1} = 0.3$ is only assumed; should gedrite at 750°C be more disordered, the width of the field would decrease rapidly (fig. 2).

Because K_{DM} varies with gedrite Mg, equation (93) may be used to determine the following values for the top and bottom of the divariant field:

Top: $K_{DM} = .28$ cordierite Mg = 96 gedrite Mg = 87

Bottom: $K_{DM} = .34$ cordierite Mg = 87 gedrite Mg = 69

The use of these values in the foregoing equations gives a divariant field width of about 0.43 kb, and, furthermore, is almost independent of the value of K_{D1} . Unfortunately, equation (93) is only approximate, so that this figure is also open to large errors.

It has been shown that assumption (iii) need not be correct, even in gedrites free of Na^+ and Ca^{2+} . Papike and Ross (1970) have shown that Al^{3+} is unevenly distributed over three of the four tetrahedral T sites in gedrite. The validity of assumption (iv) at

750°C is questionable, since no account is taken of tetrahedral order-disorder relations in gedrite. If, as shown by Zotov and Sidorenko (1968), the Al^{3+} content of gedrites increases with decreasing pressure, assumption (v) may introduce significant errors.

The analyses of the experimentally-produced gedrites of Green and Vernon (1974) lying above the divariant field are in agreement with the Al^{3+} contents of gedrites at these P, T conditions as predicted by Lee and Holdaway (1976); see also figure 19. As the gedrites within the divariant field are at the same temperatures with only lower pressures, there is little reason to suspect that the stable orthoamphiboles have not equilibrated with respect to Al^{3+} due to temperature-controlled reaction kinetics.

The compositions of the analysed orthoamphiboles occurring with cordierite in the divariant field of Green and Vernon (1974) indicate that on the average they are aluminous anthophyllites similar to those used in the starting mix; hence they were interpreted as being relict. As pointed out by these authors, the microprobe analyses were biased towards low-Al orthoamphiboles, in order to avoid the possibility of analysing very fine intergrowths with kyanite. This analytical bias notwithstanding, several of the analyses do have much higher Al_2O_3 contents (7%). Examination of the structural formulae indicates that they are gedrites with $X_{\text{Al}}^{\text{M2}}$ values approaching those predicted by equation (85). Since the runs were not seeded with gedrite, these experimentally-produced gedrites are not relict, and represent phases approaching equilibrium

in the gedrite-cordierite divariant field.

The top of the divariant field determined by Green and Vernon (1974) is a cordierite-out reaction ($\text{Mg} \div 96$), and, within experimental error, corresponds to the upper stability limit of magnesian cordierite under hydrous conditions, as determined by Newton (1972). These two sets of experimental data are thus in agreement.

9.8 Conclusions

Examination of naturally-occurring cordierite-gedrite assemblages, experimental work, and theoretical calculations indicate that:

- (i) gedrite_{ss} is the stable orthoamphibole coexisting with cordierite + aluminosilicate + quartz under high-pressure, hydrous conditions;
- (ii) using more realistic values for the parameters in the calculations of Lee and Holdaway (1976) results in greater compatibility between experimental and theoretical methods of calculating the width of the divariant field;
- (iii) direct comparison of theoretical calculations with the experimental results of Green and Vernon (1974) cannot be made until (a) the octahedral ordering parameter used for gedrite is confirmed, (b) activity-composition data become available to determine gedrite-cordierite relations, (c) the Al^{3+} variation in gedrite as a function of pressure is known, and (d) the water content of cordierite as a function of P

and T is accurately determined.

Consequently, the calculations of Lee and Holdaway (1976) cannot be used to invalidate the experimental work of Green and Vernon (1974). Hence the experimentally-determined orthoamphibole-cordierite divariant field of Green and Vernon (1974) is the preferred stability field of the assemblage gedrite-cordierite-kyanite-quartz under high-pressure, hydrous conditions.

CHAPTER 10: ULTRAMAFIC AND CALC-SILICATE GRANULITES AT MT MARY IN THE VALLEY BORE AREA

10.1 Introduction

Mt Mary occurs within the Entia Gneiss, 8 km east-southeast of the cordierite-rich enclave locality (see enclosed map). The exposure rises about 150 m above the surrounding metapelitic rocks of the Entia Gneiss, and represents granular rocks relatively resistant to weathering and erosion.

The term "granulite" as defined by Mehnert (1972) applies only to feldspathic rocks, with or without quartz, and is thus compositionally too restrictive to include differing rock-types metamorphosed under granulite-facies conditions. The term as redefined by Winkler and Sen (1973) is less restrictive in terms of bulk-composition, but still excludes ultramafic and calc-silicate rocks. These workers proposed the term "granolite" to cover feldspar-bearing rocks with mineral assemblages characteristic of granulite-facies pressure-temperature conditions. Granulite-facies rocks having mineral assemblages that may also occur at other metamorphic grades are then termed "granoblastites" (Winkler and Sen, 1973). These terms have not yet been widely accepted, and, in this author's view, the term "granoblastite" may conceivably be applied to any rock with a granoblastic texture, irrespective of metamorphic grade.

In this thesis, the term "granulite" is retained, and applies

to rocks which (i) were metamorphosed under granulite-facies conditions, and which (ii) have granoblastic textures. (Using this definition, the macroscopically-banded garnet-gneiss of chapter 8 may be termed a garnet-cordierite-gedrite granulite.)

10.2 Phase Assemblages in the Mt Mary Granulites

The phase assemblages observed at Mt Mary are as follows:

- (i) within the ultramafic granulites
orthopyroxene-olivine-hornblende-spinel-chlorite (98)
- (ii) within the calc-silicate granulites
clinozoisite-hornblende-corundum-(margarite) (99)
clinozoisite-hornblende-anorthite (100)

Petrographic descriptions and bulk-rock analyses for the Mt Mary granulites appear in the appendix.

10.3 Mineral Compositions in the Ultramafic Granulite

The compositions of the coexisting minerals in the ultramafic granulite (sample 900 - paragenesis 98) are presented in table 31. There is no textural evidence to indicate that the chlorite is retrograde, and hence this mineral is inferred to belong to the highest-grade paragenesis.

The most magnesian phase in the paragenesis is the chlorite, which is sheridanitic with an Mg value of 86. Unlike all the other phases in paragenesis (98), the Mn content of the chlorite is below the detection limit of a wavelength-dispersive microprobe.

The next most magnesian phase in the paragenesis is hornblende, the Al^{iv} , Na+K, and $Al^{vi}+Ti$ contents of which fall in the centre

PARAGENESIS (98)

OLIVINE-ORTHOPYROXENE-HORNBLende-SPINEL-CHLORITE GRANULITE

	<u>OLIVINE</u>	<u>ORTHOPYROXENE</u>	<u>HBLD.</u>	<u>SPINEL</u>	<u>CHLORITE</u>
SiO ₂	37.32	53.85	48.44	.13	28.41
TiO ₂	.00	.00	.61	.00	.00
Al ₂ O ₃	.00	2.45	10.89	62.39	21.54
Cr ₂ O ₃	.00	.00	.00	1.17	.00
FeO	27.55	16.51	7.54	22.23	7.99
MnO	.50	.46	.19	.23	.00
ZnO	.00	.00	.00	.28	.00
NiO	.15	.00	.00	.28	.00
MgO	34.49	26.46	16.90	13.26	27.53
CaO	.00	.20	11.81	.00	.00
Na ₂ O	.00	.00	.96	.00	.00
K ₂ O	.00	.00	.13	.00	.00
<u>TOTAL</u>	<u>100.01</u>	<u>99.93</u>	<u>97.47</u>	<u>99.97</u>	<u>85.47</u>
CATIONS PER No. OXYGENS	4	3	23	4	28
Si	.9976	.9738	6.8613	.0034	5.5775
Ti			.0650		
Al		.0522	1.8179	1.9487	4.9838
Cr				.0245	
Fe	.6159	.2497	.8931	.4927	1.3118
Mn	.0113	.0070	.0228	.0052	
Zn				.0055	
Ni	.0032			.0060	
Mg	1.3744	.7133	3.5685	.5239	8.0570
Ca		.0039	1.7923		
Na			.2636		
K			.0235		
<u>TOTAL</u>	<u>3.0024</u>	<u>1.9999</u>	<u>15.3080</u>	<u>3.0099</u>	<u>19.9301</u>
<u>Mg</u>	69.05	74.07	79.98	51.53	85.00

TABLE 31: Microprobe analyses of minerals in paragenesis (98).

of the "hornblende" field as defined by Deer, Howie and Zussman (1962, vol. 2, figs. 71 and 72). The composition of the hornblende is more magnesian (80 vs. an average of 62.3) but only slightly less aluminous (19.89 vs. an average of 12.5% Al_2O_3) than those of mafic granulites in the Strangways Range area (Woodford and Wilson, 1976) which lies 100 km west of the Valley Bore area. The hornblende does not have the brown or brownish-green colour along the γ direction that characterizes many hornblendes in mafic rocks at high metamorphic grades (Miyashiro, 1958; Shido and Miyashiro, 1959; Binns, 1965). This may be explained by the relatively low Ti content of the hornblende (0.61% TiO_2), which is less than half the average Ti content of the brownish hornblendes described by Woodford and Wilson (1976).

The third most magnesian phase is orthopyroxene, corresponding to a bronzite with $\text{Mg} = 74.1$. The bronzite contains 2.45% Al_2O_3 , which, if all Fe is treated as Fe^{2+} , corresponds to $X_{\text{Al}}^{\text{iv}} = 2.62\%$ and $X_{\text{Al}}^{\text{vi}} = 2.60\%$. It is more magnesian and more aluminous (2.45 vs. an average of 2.02% Al_2O_3) than most of the orthopyroxenes described by Woodford and Wilson (1976).

The fourth most magnesian phase is olivine, with an Mg value of 69. Treating all the iron as ferrous iron yields the following divalent mole percentages: $X_{\text{Mg}} = 68.55$, $X_{\text{Fe}} = 30.72$, $X_{\text{Ni}} = 0.16$ and $X_{\text{Mn}} = 0.56$.

The most iron-rich silicate phase in the paragenesis is spinel, which is a pleonaste with $\text{Mg} = 51.5$. The pleonaste also contains 1.17% Cr_2O_3 , and minor amounts of Zn, Ni and Mn (see table 31).

The mole percentage $Mn/(Mn+Fe)$ in the coexisting phases increases in the following order: chlorite (?) < spinel (1.04) < olivine (1.81) < hornblende (2.49) < orthopyroxene (2.74). Both the mole percentages $Ni/(Ni+Mg)$ and $Ni/(Ni+Fe)$ increase in the order: olivine (0.23, 0.52) < spinel (1.13, 1.20).

10.4 Mineral Compositions in the Calc-Silicate Granulites

Clinozoisite constitutes over 65% of the volume of both parageneses (99) and (100). Its composition is virtually identical in both parageneses, and a representative analysis is presented in table 32. The clinozoisite is iron-rich, and, for the octahedral sites, the ratio $Fe^{3+}/(Fe^{3+}+Al)$ is 14.72%, if all iron is treated as ferric iron. Only 1.06% of the silicon in the ideal formula is replaced by tetrahedral Al.

Minute amounts of margarite_{ss} occur in paragenesis (99), in isolated, 0.02 mm-wide laths within cracks in clinozoisite. This mineral is probably retrograde in origin, and has a composition corresponding to 93.2% margarite and 6.8% paragonite end-members.

The amphibole in the corundum-bearing paragenesis (99) is relatively aluminous (17.28% Al_2O_3). If all iron is treated as ferrous iron, then 25.46% of the tetrahedral sites of this amphibole are occupied by Al, $Al^{vi}/(Al^{vi}+Ti+Fe+Mg+Mn) = 18.76\%$ and $Mg = 73.3$. According to figs. 71 and 72 of Deer, Howie and Zussman (1962, vol. 2), this amphibole is a pargasitic-tschermakitic hornblende. The amphibole of the plagioclase-bearing paragenesis (100) is less aluminous (9.57% Al_2O_3) and less sodic (100 vs. 1.90% Na_2O) than

PARAGENESES (99), (100)

SAMPLE 902 PARA.(100)

SAMPLE 901 PARA.(99)

	<u>CLINOZOISITE</u>	<u>HBLD.</u>	<u>HBLD.</u>	<u>MARGARITE</u> retrograde
SiO ₂	37.42	40.53	47.41	29.31
TiO ₂	.00	.89	.35	.00
Al ₂ O ₃	27.75	17.28	9.57	50.45
Fe ₂ O ₃	7.41	.00	.00	.00
FeO	.00	8.74	9.12	.36
MnO	.00	.25	.29	.00
MgO	.42	13.45	15.09	.41
CaO	23.05	12.69	12.78	13.11
Na ₂ O	.00	1.90	1.00	.53
K ₂ O	.00	.57	.64	.00
<u>TOTAL</u>	<u>96.05</u>	<u>96.30</u>	<u>96.25</u>	<u>94.17</u>
CATIONS PER No. OXYGENS	25	23	23	22
Si	5.9365	5.9633	6.9144	3.9491
Ti		.0985	.0384	
Al	5.1884	2.9964	1.6449	8.0112
Fe ³⁺	.8846			
Fe ²⁺		1.0754	1.1123	.0406
Mn		.0312	.0358	
Mg	.0993	2.9501	3.2808	.0824
Ca	3.9178	2.0004	1.9969	1.8925
Na		.5420	.2828	.1385
K		.1070	.1191	
<u>TOTAL</u>	<u>16.0266</u>	<u>15.7643</u>	<u>15.4254</u>	<u>14.1143</u>
<u>Mg</u>		73.28	74.68	

TABLE 52: Microprobe analyses of minerals in the calc - silicate granulites at Mt Mary. All iron in the clinozoisite has been assumed to be ferric, in all the other minerals, it is assumed to be ferrous. Plagioclase in sample 902 is An_{90.9} Ab_{8.3} Or_{0.8}.

that of paragenesis (99). With the same proviso as above, 13.57% of the tetrahedral sites are occupied by Al, $Al^{vi}(Al^{vi}+Ti+Fe+Mg+Mn)$ = 11.13%, and Mg = 74.68. The composition of this amphibole corresponds to that of hornblende.

The plagioclase of paragenesis (100) is composed of the following end-members: 90.0% anorthite, 8.3% albite, and 0.8% orthoclase.

10.5 Temperature-Pressure Conditions of Metamorphism at Mt Mary

The occurrence of hornblende + bronzite in the ultramafic granulite indicates that the metamorphic grade of the rocks discussed in this chapter is that of the lower granulite facies (Turner, 1968). (P_{H_2O} -T conditions as inferred from the ultramafic assemblage belong to the hornblende-granulite subfacies (Fyfe et al., 1958) or to the hornblende-orthopyroxene-plagioclase granulite subfacies (de Waard, 1965).) Unfortunately, the distribution coefficients between the phases are difficult to use as geothermometers since, with the possible exception of spinel, none of the minerals belong to ideal solid-solution series.

By considering orthopyroxene at high temperatures to be close to an ideal solid-solution, Saxena (1969a) has attempted to fit observed and experimental $K_{D_{Mg-Fe}^{opx-ol}}$ values to a regular solution model. Although the proposed tentative model (Saxena, 1969a, fig. 5) appears to give reasonable estimates of temperature for the data of Nafziger and Muan (1967) and Ramberg and De Vore (1951), the plot of the Mt Mary orthopyroxene-olivine pair falls in an area where the

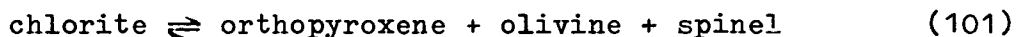
distribution curves are (i) very closely spaced, and (ii) close to an inflection point. As a consequence, this model yields very large errors in temperature for even small changes in phase compositions.

$K_{\text{D}^{\text{hbld-opx}}_{\text{Mg-Fe}}}$ for the Mt Mary granulite is 1.40, whereas, for slightly less-magnesian minerals in the Strangways Range mafic granulites, the corresponding values are 1.06 and 1.24 (Woodford and Wilson, 1976, samples 87 and 298). However, even this comparison is not conclusive of identical temperatures, since the Strangways Range amphiboles are more sodic, aluminous, and titaniferous than that at Mt Mary, and the orthopyroxenes differ in Al content.

Evans and Frost (1965) and Medaris (1975) demonstrated that Fe-Mg partitioning between olivine and spinel is sufficiently temperature-dependent to be used as a geothermometer. Correcting for the presence of Cr in spinel (Irvine, 1965), and neglecting the minor amounts of Mn, Zn and Ni in olivine and spinel, the experimentally-calibrated olivine-spinel geothermometer (Fujii, 1977) yields a temperature of equilibration of 815°C for the Mt Mary ultramafic granulite. However, this temperature can only be considered approximate (Fujii, 1977), and may be influenced by the possible presence of Fe^{3+} in spinel.

The presence of chlorite in paragenesis (98) allows some inferences to be made regarding its P-T conditions of formation. In the absence of quartz, and for relatively magnesian compositions, the breakdown of chlorite proceeds according to the divariant

reaction



The thermally most stable chlorite is the Mg-chlorite clinocllore, and the univariant Mg-end-member reaction corresponding to reaction (101) has been experimentally determined by Fawcett and Yoder (1966), McOnie et al. (1975), and Staudigel and Schreyer (1977). At pressures above 30 kb, reaction (101) is terminated by the reaction of orthopyroxene + spinel to olivine + garnet (determined experimentally in the Mg-system by MacGregor, 1964, and Staudigel and Schreyer, 1977). At pressures below 3.5 kb, reaction (101) is terminated by the reaction of orthopyroxene + spinel to olivine + cordierite (determined experimentally by Fawcett and Yoder (1966), Seifert (1974), and McOnie et al. (1975)).

Since the sheridanite in paragenesis (98) is quite magnesian ($Mg = 86$), two inferences may be made from the above data:

- (i) The pressure of formation of paragenesis (98) was above 3 kb P_{H_2O} and below 20 kb P_{H_2O} , consistent with the range of possible pressures derived for the Irindina Ck granulite in chapter 8.
- (ii) The temperature of formation of paragenesis (98) was above 700°C but below 800°C (see McOnie et al., 1975, fig. 1).

The temperature range above is consistent with a retrograde origin of margarite in paragenesis (99), since the calculated upper thermal stability of margarite is about 670°C at 9 kb P_{H_2O} (Chatterjee, 1976).

CHAPTER 11: SUMMARY AND CONCLUSIONS

11.1 Brief Summary of Major Conclusions drawn from Chapters 2 to

6--Jervois Range Area

(i) The Jervois Range area underwent a single, prograde metamorphic episode, dated at 1850 m.y. This corresponds to the age of the "Arunta Orogeny", the oldest, widespread prograde metamorphic event in the Arunta Block.

(ii) A minor "thermal event" took place at about 1700 m.y., probably caused by the emplacement of large alaskitic and pegmatitic bodies. This event probably caused the retrograde alteration of cordierite to chlorite + muscovite. The age of this event corresponds to that of the second oldest, widespread metamorphic event within the Arunta Block.

(iii) The Jervois Range area was not affected by the Carboniferous Alice Springs Orogeny, which caused widespread retrogression elsewhere in the Arunta Block.

(iv) Mafic rocks in the Jervois Range area are orthoamphibolites comprised of plagioclase (An 25 to 58) + hornblende, with or without lesser amounts of epidote, chlorite, sphene and diopside.

(v) Because of the relatively restricted bulk-compositional range of the orthoamphibolites, it is possible to predict the Mg value of hornblende from the Al content of hornblende and the anorthite content of coexisting plagioclase (eqn. 3).

- (vi) The parent-rocks for the orthoamphibolites appear to have been calc-alkaline or island-arc basalts, which were slightly to extensively altered prior to (or during) prograde metamorphism.
- (vii) Staurolite occurs in iron-rich metapelites in the Jervois Range area. Apart from micas, these rocks may contain garnet, chlorite and andalusite. Multiphase assemblages such as staurolite-garnet-chlorite-biotite-muscovite-andalusite-quartz do not violate the phase rule, and in fact are di- or trivariant if components such as Zn (in staurolite), Mn, Ca and Na are taken into account.
- (viii) In some of the staurolite-bearing rocks, primary chlorite coexists with a more magnesian biotite, implying a possible miscibility gap for some chlorite compositions. This occurrence also permits a "new" AFM topology (fig. 9).
- (ix) Chlorite + quartz in some rocks is stable, even in the presence of muscovite_{ss}, under P-T conditions of the lower-amphibolite facies. The assemblage may also be stable to temperatures marked by the first appearance of sillimanite.
- (x) In the lowest-grade rocks of the Jervois Range area, the assemblage chlorite-andalusite-muscovite-quartz is stable for chlorite Mg > 50. With a slight increase in metamorphic grade, chlorite reacts with muscovite to produce cordierite, biotite and andalusite. In naturally-occurring rocks this reaction is commonly at least divariant, and, unlike almost all similar proposed reactions, the inferred reaction in the Jervois Range rocks also produces quartz (reaction 48).

(xi) Naturally-occurring prograde reactions probably involve all the coexisting phases, and, in several (if not many) instances, differ markedly from simplified reactions used to set up Schreinemaker's multisystems grids.

(xii) The bulk-compositions of the Jervois Range metapelites represent a sequence of geosynclinal shales, many units of which are iron-rich, and may be considered silicate iron-formations in the sense of James (1966).

(xiii) Chlorite-quartz⁺-garnet schists in the Jervois Range area and at Koolanooka, W.A., are not the products of retrograde metamorphism and large-scale metasomatism. Sedimentary rocks, with bulk-compositions appropriate to chlorite-quartz⁺-garnet schists, may be formed by halmyrolysis of predominantly volcanoclastic sediments, or by the direct "precipitation" or "neoformation" of chamosite to yield iron- and magnesium-rich pelitic rocks.

(xiv) The relatively simple bulk-compositions of chlorite-quartz-garnet rocks permit the inference of several realistic garnet-forming reactions. These are characterized by the consumption of chlorite + quartz, with the remaining stable chlorite becoming more magnesian and less manganiferous as the reaction proceeds. There is relatively little change in the Al-content of the chlorite as the reaction proceeds (see reaction 57 and fig. 14).

(xv) The lower-grade equivalent of chlorite-quartz-garnet assemblages is the assemblage chlorite-quartz, and, at higher grades, chlorite-quartz-garnet rocks react to yield garnet-cordierite-

gedrite⁺-quartz⁺-chlorite assemblages.

11.2 Brief Summary of Major Conclusions drawn from Chapters 7 to

10--Valley Bore Area

- (i) Cordierite-rich enclaves, characterized by the stability of cordierite + kyanite, contain the stable paragenesis cordierite-kyanite-gedrite-phlogopite-paragonite-quartz.
- (ii) The above assemblage was metamorphosed at a temperature close to 620°, at a pressure above 6 kb, within the stability field of kyanite.
- (iii) The garnet-, cordierite-, and gedrite-bearing K-felspar-free granulite in Irindina Creek was formed from a shale or greywacke, with the removal of a K-Al-Si-rich melt during the peak of metamorphism.
- (iv) The P-T conditions of formation of the above granulite are inferred to be 700 to 750°C at confining pressures of 7 to 9.5 kb.
- (v) The bronzite-olivine-hornblende-spinel-chlorite granulite at Mt Mary was metamorphosed at between 700 and 800°C, at confining pressures comparable to the garnet-granulite in Irindina Creek.
- (vi) Naturally-occurring cordierite-garnet pairs clearly indicate that $K_D^{\text{cord-gt}}_{\text{Mg-Fe}}$ decreases with increasing temperature, as originally proposed by Hensen and Green (1971, 1972, 1973) and Hensen (1971) for the cordierite-garnet geothermometer-geobarometer. The calibration proposed by Currie (1971) is invalid, and the theoretical calculations of Hutcheon et al. (1971) do not give results

consistent with observed phase assemblages.

(vii) In the absence of appropriate thermodynamic parameters, the theoretically-derived modification (Lee and Holdaway, 1976) of the experimentally-derived stability field of cordierite-gedrite-kyanite-quartz (Green and Vernon, 1974) cannot be accepted.

11.3 Comparison of Metamorphic P-T Conditions between the Jervois Range and Valley Bore Areas

The metamorphism in the Jervois Range area is of the low-pressure andalusite-sillimanite type, with P-T conditions of about 560°C at 2.7 kb, as shown in figs. 6 and 22. These conditions are consistent with conditions inferred for the metamorphic rocks to the west of the Jervois Range area, in the northeastern part of the Arunta Block (Forman and Shaw, 1973; R. G. Warren, pers. comm.).

In the Valley Bore area, the metamorphism is of the intermediate-pressure kyanite-sillimanite type, with temperatures in the range of 620 to 800°C, and pressures of the order of 6 to 10 kb (figs. 18, 22). These conditions are similar to those inferred by Vernon (1972), Green and Vernon (1974), and Woodford and Wilson (1976) for rocks in the Strangways Range area, 100 km west of Valley Bore. It is tentatively suggested that there is a "belt" of intermediate-pressure metamorphism extending from the Valley Bore area to at least as far west as the Strangways Range area.

Reference to fig. 22 shows that the two metamorphic domains (or "baric types", Miyashiro, 1973) are unlikely to have been formed by one inflected geothermal gradient. It is far more realistic to

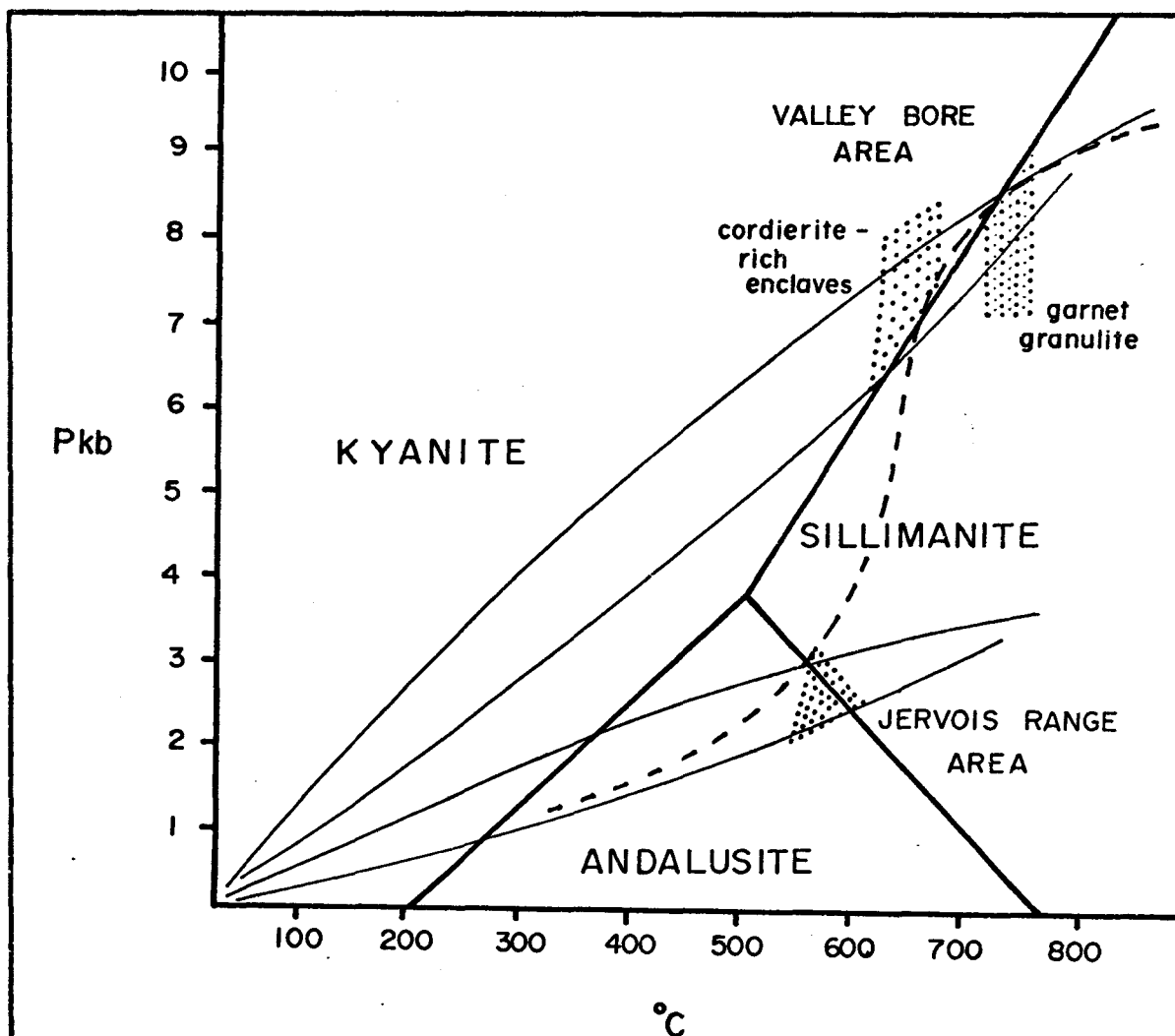


FIGURE 22: P - T domains for metamorphic assemblages from the Jervois Range and Valley areas, and possible geothermal gradients. The existence of the dashed geothermal gradient is extremely unlikely (contrast with Turner, 1968 fig. 8-4), so that the metamorphic assemblages in the Jervois Range and Valley Bore areas represent two different baric types. Note that the cordierite-rich enclave and garnet granulite localities are 15km apart, and the Jervois Range and Valley Bore areas are separated by 100 km. The aluminosilicate stability fields are those of Holdaway (1971).

assume two contrasting metamorphic gradients, as shown in fig. 22. With the data presently available, it is not known whether there is a gradation of geothermal gradients between the two areas, or whether the two geothermal gradients are discrete, and spatially separated by the effects of tectonic activity. It is tempting to assume that the two areas belong to different parts of a paired metamorphic belt (Miyashiro, 1973a). Unfortunately these problems cannot be presently resolved.

Further work is required

- (i) in the Valley Bore area, to confirm the conclusions of chapters 7, 8 and 10, and to see if there is any evidence for polymetamorphism as proposed by Woodford and Wilson (1976) for rocks from the Strangways Range area; this will be attempted by the author;
- (ii) in the Harts Range area, between the Valley Bore and Strangways Range areas, to confirm the continuity of the intermediate-pressure metamorphic "belts";
- (iii) between the Jervois Range and Valley Bore areas, to determine the P-T relationships between the two sets of contrasting geothermal gradients proposed in fig. 22.

BIBLIOGRAPHY

- Abraham, K., Schreyer, W., 1973. Petrology of a ferruginous hornfels from Riekensglück, Harz Mountains, Germany. *Contr. Mineral. and Petrol.* 40, 275-292.
- Akella, J., Winkler, H. G. F., 1966. Orthorhombic amphibole in some metamorphic reactions. *Contr. Mineral. and Petrol.* 12, 1-12.
- Albee, A. L., 1965a. Phase equilibria in three assemblages of kyanite-zone pelitic schists, Lincoln Mountain Quadrangle, Central Vermont. *Jour. Petrol.* 6, 246-301.
- Albee, A. L., 1965b. A petrogenetic grid for the Fe-Mg silicates of pelitic schists. *Amer. Jour. Sci.* 263, 512-536.
- Albee, A. L., 1965c. Distribution of Fe, Mg and Mn between garnet and biotite in natural mineral assemblages. *Jour. Geol.* 73, 155-164.
- Albee, A. L., 1968. Metamorphic zones in Northern Vermont, in E-An Zen et al., eds., "Studies of Appalachian Geology", Interscience (John Wiley & Sons), New York.
- Albee, A. L., 1972. Metamorphism of pelitic schists: reaction relations of chloritoid and staurolite. *Geol. Soc. Amer. Bull.* 83, 3249-3268.
- Anderson, A. T., 1968. The oxygen fugacity of alkaline basalt and related magmas, Tristan da Cunha. *Amer. Jour. Sci.* 266, 704-727.
- Anderson, P. A. M., Newton, R. C., Kleppa, O. J., 1977. The enthalpy change of the andalusite-sillimanite reaction and the Al_2SiO_5 diagram. *Amer. Jour. Sci.* 277, 585-593.
- Appel, P. U., 1974. On an unmetamorphosed iron-formation in the Early Precambrian of South-West Greenland. *Mineral. Deposita* 9, 75-82.
- Armstrong, R. L., Stewart, A. J., 1975. Rubidium-strontium dates and extraneous argon in the Arltunga Nappe Complex, Northern Territory. *Jour. Geol. Soc. Austr.* 22, 103-115.
- Bancroft, G. M., Maddock, A. G., Burns, R. G., 1967. Applications of the Mossbauer effect to silicate mineralogy. I. Iron silicates of known crystal structure. *Geochim. Cosmochim. Acta* 31, 2219-2246.

- Baragar, W. R. A., Goodwin, A. M., 1969. Andesites and Archaean volcanism of the Canadian Shield. Oreg. Dep. Geol. Mineral. Ind. Bull. 65, 121-142.
- Bard, J. P., 1970. Composition of hornblendes formed during the Hercynian progressive metamorphism of the Aracena metamorphic belt (SW Spain). Contr. Mineral. and Petrol. 28, 117-134.
- Barron, B. J., 1976. Recognition of the original volcanic suite in altered mafic volcanic rocks at Sofala, New South Wales. Amer. Jour. Sci. 276, 604-636.
- Bayley, R. W., James, H. L., 1973. Precambrian iron-formations of the United States. Econ. Geol. 68, 934-959.
- Binns, R. A., 1965. The mineralogy of metamorphosed basic rocks from the Willyama Complex, Broken Hill district, New South Wales. Part 1. Hornblendes. Min. Mag. 270, 306-326.
- Black, L. P., 1975. Present status of geochronological research in the Arunta Block. Abstr. First Austr. Geol. Conv. "Proterozoic Geology" Adelaide, 1975. Geol. Soc. Austr.
- Black, L. P., in Marjoribanks, R. W., Black, L. P., 1974. Geology and geochronology of the Arunta Complex, north of Ormiston Gorge, Central Australia. Jour. Geol. Soc. Austr. 21, 291-299.
- Bonatti, E., Honnorez, J., Kirst, P., Radicati, F., 1975. Metagabbros from the Mid-Atlantic Ridge at 06°N: contact-hydrothermal-dynamic metamorphism beneath the axial valley. Jour. Geol. 83, 61-78.
- Bradshaw, M. J., 1975. Origin of montmorillonite bands in the Middle Jurassic of eastern England. Earth Planet. Sci. Letters 26, 245-252.
- Buddington, A. F., Lindsley, D. H., 1964. Iron-titanium oxide minerals and synthetic equivalents. Jour. Petrol. 5, 310-357.
- Carmichael, D. M., 1969. On the mechanism of prograde metamorphic reactions in quartz-bearing pelitic rocks. Contr. Mineral. and Petrol. 20, 244-267.
- Carmichael, D. M., 1970. Intersecting isograds in the Whetstone Lake area, Ontario. Jour. Petrol. 11, 147-181.
- Caruba, C., Baumer, A., Turcc, G., 1975. Etude mineralogique du grenat de Sarvengude dans les series metamorphiques de Collobrières (Maures, France). Bull. Soc. Fr. Mineral. Cristallogr. 98, 159-165.

- Catley, D. E., 1965. Summary of investigations, Jervois Range copper-lead prospect, N. T. Rept. 9/1965 to New Consolidated Gold Fields A/Asia P. L. (unpubl.).
- Chappell, B. W., White, A. J. R., 1974. Two contrasting granite types. *Pacific Geology* 8, 173-174.
- Chatterjee, N. D., 1976. Margarite stability and compatibility relations in the system $\text{CaO-Al}_2\text{O}_3\text{-SiO}_2\text{-H}_2\text{O}$ as a pressure-temperature indicator. *Amer. Mineralogist* 61, 699-709.
- Chatterjee, N. D., Froese, E., 1975. A thermodynamic study of the pseudo binary join muscovite-paragonite in the system $\text{KAlSi}_3\text{O}_8\text{-NaAlSi}_3\text{O}_8\text{-Al}_2\text{O}_3\text{-SiO}_2\text{-H}_2\text{O}$. *Amer. Mineralogist* 60, 985-993.
- Chenhall, B. E., 1973. Some aspects of prograde and retrograde metamorphism at Broken Hill. Unpubl. Ph.D. thesis, University of Sydney.
- Chernosky, J. V. Jr., 1975. The stability of the assemblage clinochlore + quartz at low pressure (abstr). *Trans. Amer. Geophys. Union* 56, 466.
- Chinner, G. A., Fox, J. S., 1974. The origin of cordierite-anthophyllite rocks in the Land's End aureole. *Geol. Mag.* 111, 397-408.
- Chinner, G. A., Sweatman, T. R., 1968. A former association of enstatite and kyanite. *Mineral. Mag.* 36, 1052-1061.
- Clifford, T. N., Stumpfl, E. F., McIver, J. R., 1975. A sapphirine-cordierite-bronzite-phlogopite paragenesis from Namaqualand, South Africa. *Mineral. Mag.* 40, 347-356.
- Cochrane, G. W., Edwards, A. B., 1960. Roper River oolitic iron-stone formations. *Sci. ind. Resch. Org. Melbourne, mineragraphic Inv. Rept.* 22.
- Condie, K. C., 1976. Trace-element geochemistry of Archaean greenstone belts. *Earth-Sci. Rev.* 12, 393-417.
- Couture, R. A., 1977. Composition and origin of palygorskite-rich and montmorillonite-rich zeolite-containing sediments from the Pacific Ocean. *Chem. Geol.* 19, 113-130.
- Currie, K. L., 1971. The reaction $3 \text{ cordierite} = 2 \text{ garnet} + 4 \text{ sillimanite} + 5 \text{ quartz}$ as a geological thermometer in the Opinicon Lake Region, Ontario. *Contr. Mineral. and Petrol.* 33, 215-226.

- Currie, K. L., 1974. A note on the calibration of the garnet-cordierite geothermometer and geobarometer. *Contr. Mineral. and Petrol.* 44, 35-44.
- Dallmeyer, R. D., 1974. The role of crystal structure in controlling the partitioning of Mg and Fe^{2+} between co-existing garnet and biotite. *Amer. Mineralogist* 59, 201-203.
- Davidson, L. R., Mathison, C. I., 1974. Aluminous orthopyroxenes and associated cordierites, garnets and biotites from granulites of the Quairading district, Western Australia. *Neues Jb. Miner. Mh.* 1974, 272-287.
- Deb, M., Saxena, S. K., 1976. A method of appraisal of chemical equilibrium-application to terrestrial and lunar rocks. *Lithos* 9, 225-234.
- de Bethune, P., Laudron, D., Bocquet, J., 1975. Diffusion processes in resorbed garnets. *Contr. Mineral. and Petrol.* 50, 197-204.
- Deer, W. A., Howie, R. A., Zussman, J., 1962. "Rock Forming Minerals", vols. 1-5, Longmans, London.
- de Rosen-Spence, A., 1969. Genèse des roches à cordierite-anthophyllite des gisements cupro-zincifères de la région de Rouyn-Noranda, Quebec, Canada. *Can. Jour. Earth Sci.* 6, 1339-1345.
- de Waard, D., 1965. The occurrence of garnet in the granulite-facies terrane of the Adirondack Highlands. *Jour. Petrol.* 6, 165-191.
- Donnelly, T. W., Nalli, G., 1973. Mineralogy and chemistry of Caribbean sediments. Deep-Sea Drilling Program, N.S.F. Spec. Publ. 15, 27, 929-962.
- Emiliani, F., Venturelli, G., 1972. Sharp compositional zoning in an almandine garnet. *Can. Mineralogist* 11, 464-472.
- Engel, A. E. J., Engel, C. G., 1962. Hornblendes formed during progressive metamorphism of amphibolites, northwest Adirondack Mountains, New York. *Bull. Geol. Soc. Amer.* 73, 1499-1514.
- Engel, A. E. J., Engel, C. G., Havens, R. G., 1965. Chemical characteristics of oceanic basalts and the upper mantle. *Bull. Geol. Soc. Amer.* 76, 719-734.
- Evans, B. W., Frost, B. R., 1975. Chrome spinel in progressive metamorphism--a preliminary analysis. *Geochim. Cosmochim. Acta.* 39, 959-972.

- Fawcett, J. J., Yoder, H. S. Jr., 1966. Phase relationships of chlorites in the system $\text{MgO-Al}_2\text{O}_3\text{-SiO}_2\text{-H}_2\text{O}$. *Amer. Mineralogist* 51, 353-380.
- Fisher, G. W., 1970. The application of ionic equilibria to metamorphic differentiation: an example. *Contr. Mineral. and Petrol.* 29, 91-103.
- Fleming, P. D., Fawcett, J. J., 1976. Upper stability of chlorite + quartz in the system $\text{MgO-FeO-Al}_2\text{O}_3\text{-SiO}_2\text{-H}_2\text{O}$ at 2 kb water pressure. *Amer. Mineralogist* 61, 1175-1193.
- Flood, R. H., Shaw, S. E., 1977. Two "S-type" granite suites with low initial $^{87}\text{Sr}/^{86}\text{Sr}$ ratios from the New England Batholith, Australia. *Contr. Mineral. and Petrol.* 61, 163-173.
- Floyd, P. A., Winchester, J. A., 1975. Magma type and tectonic setting discrimination using immobile elements. *Earth Planet. Sci. Letters* 27, 211-218.
- Fontijn, L. A., Bok, A. B., Kornet, J. G., 1969. The TPD electron probe X-ray micro analyser, in Mollenstadt, G., Baulker, K. H. (eds.). 5th Int. Cong. X-ray Optics and Micro Analysis, p. 261-268.
- Forman, D. J., Milligan, E. N., McCarthy, W. R., 1967. Regional geology and structure of the north-eastern margin of the Amadeus Basin, Northern Territory. *Bur. Min. Res. Geol. and Geophys., Canberra, Austr., Rep.* 103 /1967.
- Forman, D. J., Shaw, R. D., 1973. Deformation of the crust and mantle in central Australia. *Bur. Min. Res. Geol. and Geophys., Canberra, Austr., Bull.* 144 /1973.
- Fox, J. S., 1971. Coexisting chloritoid and staurolite and the staurolite-chlorite isograd from the Agnew Lake area, Ontario, Canada. *Geol. Mag.* 108, 205-219.
- Froese, E., Gasparrini, E., 1975. Metamorphic zones in the Snow Lake area, Manitoba. *Can. Mineralogist* 13, 162-167.
- Fron del, C., Ito, J., 1975. Zinc-rich chlorites from Franklin, New Jersey. *Neues Jb. Miner. Abh.* 123, 111-115.
- Fujii, T., 1977. Fe-Mg partitioning between olivine and spinel. *Carnegie Inst. Washington Yb.* 76, 563-569.
- Fyfe, W. S., Turner, F. J., 1966. Reappraisal of the metamorphic facies concept. *Contr. Mineral. and Petrol.* 12, 25-62.
- Fyfe, W. S., Turner, F. J., Verhoogen, J., 1958. Metamorphic reactions and metamorphic facies. *Geol. Soc. Amer. Mem.* 73, 259 pp.

- Gable, D. J., Sims, P. K., 1969. Geology and regional metamorphism of some high-grade cordierite gneisses, Front Range, Colorado. Geol. Soc. Amer. Spec. Paper No. 128, 87 pp.
- Ganguly, J., 1968. Analysis of the stabilities of chloritoid and staurolite and some equilibria in the system $\text{FeO-Al}_2\text{O}_3\text{-SiO}_2\text{-H}_2\text{O-O}_2$. Amer. Jour. Sci. 266, 277-298.
- Ganguly, S., 1972. Staurolite stability and related parageneses: theory, experiments, and applications. Jour. Petrol. 13, 335-365.
- Ganguly, J., Kennedy, G. C., 1974. The energetics of natural garnet solid solution. Contr. Mineral. and Petrol. 48, 137-148.
- Ghent, E., 1975. Temperature, pressure, and mixed-volatile equilibria attending metamorphism of staurolite-kyanite-bearing assemblages, Esplanade Range, British Columbia. Geol. Soc. Amer. Bull. 86, 1654-1660.
- Ghent, E. D., 1976. Plagioclase-garnet- Al_2SiO_5 -quartz: a potential geobarometer-geothermometer. Amer. Mineralogist 61, 710-714.
- Goldman, D. S., Rossman, G. R., Dollase, W. A., 1977. Channel constituents in cordierite. Amer. Mineralogist 62, 1144-1157.
- Goldschmidt, V. M., 1954. "Geochemistry", Oxford Univ. Press, 730 pp.
- Grant, J. A., 1973. Phase equilibria in high-grade metamorphism and partial melting of pelitic rocks. Amer. Jour. Sci. 273, 289-317.
- Grant, J. A., 1968. Partial melting of common rocks as a possible source of cordierite-anthophyllite bearing assemblages. Amer. Jour. Sci. 266, 908-931.
- Grant, J. A., Weiblen, P. W., 1971. Retrograde zoning in garnet near the second sillimanite isograd. Amer. Jour. Sci. 270, 281-296.
- Grapes, R. H., 1975. Actinolite-hornblende pairs in metamorphosed gabbros, Hidaka Mountains, Hokkaido. Contr. Mineral. and Petrol. 49, 125-140.
- Grapes, R. H., Hashimoto, S., Miyashita, S., 1977. Amphiboles of a metagabbro-amphibolite sequence, Hidaka Metamorphic Belt, Hokkaido. Jour. Petrol. 18, 285-318.
- Green, J. C., 1963. High-level metamorphism of pelitic rocks in northern New Hampshire. Amer. Mineralogist 48, 991-1023.

- Green, T. H., 1973. Petrology and geochemistry of basalts from Norfolk Island. Jour. Geol. Soc. Austr. 20, 259-272.
- Green, T. H., Vernon, R. H., 1974. Cordierite breakdown under high-pressure, hydrous conditions. Contr. Mineral. and Petrol. 46, 215-226.
- Greenwood, H. J., 1967. Mineral equilibria in the system $MgO-SiO_2-H_2O-CO_2$, in Abelson, P. H. (ed.), "Researches in Geochemistry", John Wiley & Sons, Inc., New York, 1972.
- Griffen, D. T., Ribbe, P. H., 1973. The crystal chemistry of staurolite. Amer. Jour. Sci. 273A, 479-495.
- Grover, J. E., Orville, P. M., 1969. The partitioning of cations between coexisting single- and multi-site phases with application to the assemblages orthopyroxene-clinopyroxene and orthopyroxene-olivine. Geochim. Cosmochim. Acta, 33, 205-226.
- Guggenheim, E. A., 1967. "Thermodynamics", North-Holland Publ. Co., Amsterdam, 476 pp.
- Guidotti, C. V., 1973. Compositional variation of muscovite as a function of metamorphic grade and assemblage in metapelites from N.W. Maine. Contr. Mineral. and Petrol. 42, 33-42.
- Guidotti, C. V., 1974. Transition from staurolite to sillimanite zone, Rangeley quadrangle, Maine. Geol. Soc. Amer. Bull. 85, 475-490.
- Guidotti, C. V., Cheney, J. T., Conatore, P. D., 1975a. Coexisting cordierite + biotite + chlorite from the Rumford quadrangle, Maine. Geology, March 1975, 147-148.
- Guidotti, C. V., Cheney, J. T., Conatore, P. D., 1975b. Inter-relationships between Mg/Fe ratio and octahedral Al content in biotite. Amer. Mineralogist 60, 849-853.
- Guidotti, C. V., Sassi, F. P., 1976. Muscovite as a petrogenetic indicator mineral in pelitic schists. Neues Jb. Miner. Abh. 127, 97-142.
- Hallberg, J. A., 1972. Geochemistry of Archaean volcanic belts in the eastern goldfields region of Western Australia. Jour. Petrol. 13, 45-56.
- Hancock, W., Ramsden, A. R., Taylor, G. F., Wilmshurst, J. R., 1971. Some ultramafic rocks of the Spargoville area, Western Australia. Geol. Soc. Australia Spec. Publ. No. 3, 269-280.

- Hariya, Y., Kennedy, G. C., 1968. Equilibrium study of anorthite under high pressure and high temperature. *Amer. Jour. Sci.* 266, 193-203.
- Harte, B., Graham, C. M., 1975. The graphical analysis of greenschist to amphibolite facies mineral assemblages in metabasites. *Jour. Petrol.* 16, 347-370.
- Hays, J. F., 1967. Lime-alumina-silica. *Carnegie Inst. Washington Yb.* 65, 234-239.
- Helgeson, H. C., Mackenzie, F. T., 1970. Silicate - sea water equilibria in the ocean system. *Deep-Sea Resch.* 17, 877-892.
- Hensen, B. J., 1971. Theoretical phase relations involving cordierite and garnet in the system $\text{MgO-FeO-Al}_2\text{O}_3\text{-SiO}_2$. *Contr. Mineral. and Petrol.* 33, 191-214.
- Hensen, B. J., 1977. Cordierite-garnet bearing assemblages as geothermometers and barometers in granulite facies terranes. *Tectonophysics* 43, 73-88.
- Hensen, B. J., Green, D. H., 1971. Experimental study of the stability of cordierite and garnet in pelitic compositions at high pressures and temperatures. I. Compositions with excess alumino-silicate. *Contr. Mineral. and Petrol.* 33, 309-330.
- Hensen, B. J., Green, D. H., 1972. Experimental study of the stability of cordierite and garnet in pelitic compositions at high pressures and temperatures. II. Compositions without excess alumino-silicate. *Contr. Mineral. and Petrol.* 35, 331-354.
- Hensen, B. J., Green, D. H., 1973. Experimental study of the stability of cordierite and garnet in pelitic compositions at high pressures and temperatures. III. Synthesis of experimental data and geological applications. *Contr. Mineral. and Petrol.* 38, 151-166.
- Hensen, B. J., Schmid, R., Wood, B. J., 1975. Activity composition relationships for pyrope-grossular garnet. *Contr. Mineral. and Petrol.* 51, 161-166.
- Hess, P. C., 1969. The metamorphic paragenesis of cordierite in pelitic rocks. *Contr. Mineral. and Petrol.* 24, 191-207.
- Hess, P. C., 1973. Fig. 3-9, page 81 in Miyashiro A., "Metamorphism and Metamorphic Belts", George Allen & Unwin, London.
- Hirschberg, A., Winkler, H. G. F., 1968. Stabilitätsbeziehungen zwischen Chlorit, Cordierit, und Almandin bei der Metamorphose. *Contr. Mineral. and Petrol.* 18, 17-42.

- Holdaway, M. J., 1971. Stability of andalusite and the aluminum silicate phase diagram. *Amer. Jour. Sci.* 271, 97-131.
- Holdaway, M. J., 1972. Thermal stability of Al-Fe epidote as a function of f_{O_2} and Fe content. *Contr. Mineral. and Petrol.* 37, 307-340.
- Holdaway, M. J., 1976. Mutual compatibility relations of the Fe^{2+} -Mg-Al silicates at 800°C and 3 kb. *Amer. Jour. Sci.* 276, 285-308.
- Holdaway, M. J., Lee, S. M., 1977. Fe-Mg cordierite stability in high-grade pelitic rocks based on experimental, theoretical and natural observations. *Contr. Mineral. and Petrol.* 63, 175-198.
- Hollister, L. S., 1966. Garnet zoning: an interpretation based on the Rayleigh fractionation model. *Science* 154, 1647-1651.
- Hollister, L. S., 1969a. Contact metamorphism in the Kwoiek Area of British Columbia: an end member of the metamorphic process. *Geol. Soc. Amer. Bull.* 80, 2465-2494.
- Hollister, L. S., 1969b. Metastable paragenetic sequence of andalusite, kyanite, and sillimanite, Kwoiek area, British Columbia. *Amer. Jour. Sci.* 267, 352-370.
- Höllner, Von H., Kolmer, H., Wirsching, U., 1976. Chemische Untersuchungen der Umwandlung glasiger Tuffe in montmorillonit- und kaolinit-Mineralen. *Neues Jb. Miner. Mh.* 1976, 456-466.
- Hoschek, G., 1969. The stability of staurolite and chloritoid and their significance in metamorphism of pelitic rocks. *Contr. Mineral. and Petrol.* 22, 208-232.
- Hsu, L. C., 1968. Selected phase relations in the system Al-Mn-Fe-Si-O-H: a mode for garnet equilibria. *Jour. Petrol.* 9, 40-83.
- Hsu, L. C., Burnham, C. W., 1969. Phase relationships in the system $Fe_3Al_2Si_3O_{12}$ - $Mg_3Al_2Si_3O_{12}$ - H_2O at 2.0 kilobars. *Bull. Geol. Soc. Amer.* 80, 2393-2408.
- Hummel, K., 1922. Die Entstehung eisenreicher Gesteine durch Halmyrolyse (=submarine) Gesteinszersetzung. *Geol. Rundsch.* 13, 40-81; 97-136.
- Hurley, P. M., Fisher, N. H., Fairbairn, H. W., Pinson, W. H., 1961. Geochronology of Proterozoic granites in Northern Territory. *Bull. Geol. Soc. Amer.* 72, 653-662.

- Hutcheon, I., Froese, E., Gordon, T. M., 1974. The assemblage quartz-sillimanite-garnet-cordierite as an indicator of metamorphic conditions in the Daly Bay Complex N.W.T. Contr. Mineral. and Petrol. 44, 29-34.
- Immega, I. P., Klein, C. Jr., 1976. Mineralogy and petrology of some metamorphic Precambrian iron-formations in southwestern Montana. Amer. Mineralogist 61, 1117-1144.
- Irvine, T. N., 1965. Chromian spinel as a petrogenetic indicator. Pt 1. Theory. Can. Jour. Earth Sci. 2, 648-674.
- Irving, A. J., Ashley, P. M., 1976. Amphibole-olivine-spinel, cordierite-anthophyllite and related hornfelses associated with metamorphosed serpentinites in the Goobarragandra District, near Tumut, New South Wales. Jour. Geol. Soc. Austr. 23, 19-44.
- Iyer, G. V. A., Kutty, T. R. N., 1975. Petrology of garnetiferous cordierite gneisses from the vicinity of the Closepet Granite. Indian Jnl. Earth. Sci. 2, 125-141.
- Iwao, S., 1973. Chemical compositions of aluminous metamorphic rocks from the Kitakami Mountains, northeast Japan. Jour. Fac. Sci. Univ. Tokyo; Sec. II, 18, 455-474.
- Jakes, P., Gill, J. B., 1970. Rare earth elements and island arc tholeiitic series. Earth Planet. Sci. Letters 9, 17-28.
- Jakes, P., White, A. J. R., 1971. Composition of island arcs and continental growth. Earth and Planet. Sci. Letters 12, 224-230.
- Jakes, P., White, A. J. R., 1972. Major and trace-element abundances in volcanic rocks of orogenic areas. Bull. Geol. Soc. Amer. 83, 29-40.
- James, H. L., 1966. Chemistry of the iron-rich sedimentary rocks. Chpt. W in Data of Geochemistry, U.S. Geol. Surv. Prof. Paper 440-W.
- James, R. S., Turnock, A. C., Fawcett, J. J., 1976. The stability and phase relations of iron chlorite below 8.5 kb P_{H_2O} . Contr. Mineral. and Petrol. 56, 1-25.
- Joklik, G. F., 1955. The geology and mica-fields of the Harts Range, Central Australia. Bur. Miner. Res. Austr. Bull. 26, 226 p.
- Jolly, W. T., 1972. Degradation (hydration)-aggradation (dehydration) and low-rank metamorphism of mafic volcanic sequences. Rept. 24th Int. Geol. Cong. 1972.

- Jolly, W. T., Smith, R. E., 1972. Degradation and metamorphic differentiation of the Keweenaw tholeiitic lavas of northern Michigan. *Jour. Petrol.* 13, 273, 309.
- Juurinen, A., 1956. Composition and properties of staurolite. *Ann. Acad. Sci. Fennicae, ser. A III*, no. 47, 1-53.
- Kaminen, D. C., 1974. Variation in the distortion index of cordierite east of the Sparrow Lake granite pluton, District of MacKenzie. *Can. Mineralogist* 12, 419-421.
- Kaminen, D. C., 1975. Chemical mineralogy of some cordierite-bearing rocks near Yellowknife, Northwest Territories, Canada. *Contr. Mineral. and Petrol.* 53, 293-310.
- Kaminen, D. C., 1976. Coexisting garnet and chlorite in crystalline rocks. *Neues Jb. Miner. Mh.* 1976, 174-185.
- Kepezhinskas, K. B., 1973. Pressure variability during medium-temperature metamorphism of meta-pelites. *Lithos* 6, 145-158.
- Kepezhinskas, K. B., Khlestov, V. V., 1977. The petrogenetic grid and subfacies for middle-temperature metapelites. *Jour. Petrol.* 18, 114-143.
- Klein, C. Jr., 1966. Mineralogy and petrology of the metamorphosed Wabash Iron Formation, southwestern Labrador. *Jour. Petrol.* 7, 246-305.
- Klein, C. Jr., 1974. Greenalite, stilpnomelane, minnesotaite, crocidolite and carbonates in a very low-grade metamorphic Precambrian iron-formation. *Can. Mineralogist* 12, 475-498.
- Korzhinskii, D. S., 1959. Physicochemical basis of the analysis of the paragenesis of minerals. Moscow: Acad. Sci. trans. New York Consultants Bureau 1959.
- Kramm, U., 1976. The coticule rocks (spessartine quartzites) of the Venn-Stavelot Massif, Ardennes, a volcanoclastic meta-sediment? *Contr. Mineral. and Petrol.* 56, 135-155.
- Kretz, R., 1959. Chemical study of garnet, biotite and hornblende from gneisses of southwestern Quebec, with emphasis on distribution of elements in coexisting minerals. *Jour. Geol.* 67, 371-402.
- Kretz, R., 1961. Some applications of thermodynamics to coexisting minerals of variable composition. Examples: orthopyroxene-clinopyroxene and orthopyroxene-garnet. *Jour. Geol.* 69, 361-387.

- Kretz, R., 1973. Kinetics of crystallization of garnet at two localities near Yellowknife. *Can. Mineralogist* 12, 1-20.
- Kretz, R., 1974. Some models for the rate of crystallization of garnet in metamorphic rocks. *Lithos* 7, 123-131.
- Kristmannsdottir, H., 1975. Clay minerals formed by hydrothermal alteration of basaltic rocks in Icelandic geothermal fields. *Geologiska Foreningens i Stockholm Forhandlingar* 97, 289-292.
- Lal, R. K., Moorhouse, W. W., 1969. Cordierite-gedrite rocks and associated gneisses of Fishtail Lake, Harcourt Township, Ontario. *Can. Jour. Earth. Sci.* 6, 145-165.
- Lal, R. K., Shukla, R. S., 1975. Genesis of cordierite-gedrite-cummingtonite rocks of the northern portion of the Khetri Copper Belt, Rajasthan, India. *Lithos* 8, 175-186.
- Leake, B. E., 1960. Compilation of chemical analyses and physical constants of natural cordierites. *Amer. Mineralogist* 45, 282-298.
- Leake, B. E., 1965. The relationship between composition of calciferous amphiboles and grade of metamorphism, in Pitcher, W. S. and Flinn, G., "Controls of Metamorphism". Oliver and Boyd, Edinb., pp.299-318.
- Leake, B. E., 1971. On aluminous and edenitic hornblendes. *Mineral. Mag.* 38, 389-407.
- Leask, D. M., 1967. The geochemistry of Precambrian argillites: Purcell system of Southern Alberta and British Columbia. Unpubl. M.Sc. thesis, Univ. of Calgary.
- Lee, S. M., Holdaway, M. J., 1976. Cordierite breakdown under high-pressure hydrous conditions: a comment. *Contr. Mineral. and Petrol.* 56, 289-295.
- Lepezin, G. G., Melenevsky, V. N., 1977. On the problem of water diffusion in the cordierites. *Lithos* 10, 49-57.
- Liou, J. G., 1973. Synthesis and stability relations of epidote, $\text{Ca}_2\text{Al}_2\text{FeSi}_3\text{O}_{12}(\text{OH})$. *Jour. Petrol.* 14, 381-413.
- Liou, J. G., Kuniyoshi, S., Ito, K., 1974. Experimental studies of the phase relations between greenschist and amphibolite in a basaltic system. *Amer. Jour. Sci.* 274, 613-632.
- Loomis, T. P., 1975. Reaction of zoning of garnet. *Contr. Mineral. and Petrol.* 52, 283-305.

- MacGregor, I. D., 1964. The reaction 4 enstatite + spinel = forsterite + pyrope. Carnegie Inst. Washington Yb. 63, 157-162.
- McOnie, A. W., Fawcett, J. J., James, R. S., 1975. The stability of intermediate chlorites of the clinocllore-daphnite series at 2 kb P_{H_2O} . Amer. Mineralogist 60, 1047-1062.
- Medaris, L. G., 1975. Coexisting spinel and silicates in alpine peridotites of the granulite facies. Geochim. Cosmochim. Acta 39, 947-958.
- Mehnert, K. R., 1972. Granulites. Results of a discussion: II. Neues Jb. Mineral. Mh. 1972, 139-152.
- Millot, G., 1970. "Geology of Clays". Springer-Verlag, 429 pp.
- Miyashiro, A., 1957. Cordierite-indialite relations. Amer. Jnl. Sci. 255, 53-62.
- Miyashiro, A., 1958. Regional metamorphism of the Gosaisyo-Takanuki district in the central Abukuma Plateau. Jour. Fac. Sci. Univ. Tokyo, sec II, 11, 219-272.
- Miyashiro, A., 1961. Evolution of metamorphic belts. Jour. Petrol. 2, 227-311.
- Miyashiro, A., 1973. "Metamorphism and Metamorphic Belts". George Allen and Unwin, London, 492 pp.
- Miyashiro, A., 1973a. Paired and unpaired metamorphic belts. Tectonophysics 17, 241-254.
- Miyashiro, A., 1974. Volcanic rock series in island arcs and active continental margins. Am. Jour. Sci. 274, 321-355.
- Miyashiro, A., Shido, F., 1975. Tholeiitic and calcalkaline series in relation to the behaviors of titanium, vanadium, chromium and nickel. Am. Jour. Sci. 275, 265-277.
- Moorbath, S., 1972. Measuring geological time, in Gass, I. G., Smith, P. J., Wilson, R. C. L. (eds.) "Understanding the Earth". Artemis Press, Sussex, 383 pp.
- Morgan, W. R., 1959. The petrology of the Jervois Range mining area. Bur. Min. Res. Geol. and Geophys. Canberra Austr. Rec 1959/ 109 (unpubl.).
- Mueller, R. F., 1960. Compositional characteristics and equilibrium relations in mineral assemblages of a metamorphosed iron formation. Amer. Jour. Sci. 258, 449-497.

- Mueller, R. F., 1961. Analysis of relations among Mg, Fe Mn in certain metamorphic minerals. *Geochim. Cosmochim. Acta* 25, 267-296.
- Mueller, R. F., 1972. Stability of biotite: a discussion. *Amer. Mineralogist* 57, 300-316.
- Mueller, R. F., Saxena, S. K., 1977. "Chemical Petrology". Springer-Verlag, New York Inc., 394 pp.
- Mueller, G., Schneider, A., 1971. Chemistry and genesis of garnets in metamorphic rocks. *Contr. Mineral. and Petrol.* 31, 178-200.
- Nafziger, R. H., Muan, A., 1967. Equilibrium phase compositions and thermodynamic properties of olivines and pyroxenes in the system $\text{MgO}-\text{FeO}-\text{SiO}_2$. *Amer. Mineralogist* 52, 1364-1385.
- Newton, R. C., 1972. An experimental determination of the high-pressure stability limits of magnesian cordierite under wet and dry conditions. *Jour. Geol.* 80, 398-420.
- Nixon, P. H., Reedman, A. J., Burns, L. K., 1973. Sapphirine-bearing granulites from Labwor, Uganda. *Mineral. Mag.* 39, 420-428.
- Nockolds, S. R., 1954. Average chemical composition of some igneous rocks. *Bull. Geol. Soc. Amer.* 65, 1007-1032.
- Norrish, K., Hutton, J. T., 1969. An accurate X-ray spectrographic method for the analysis of a wide range of geological samples. *Geochim. Cosmochim. Acta* 33, 431-453.
- Oliver, R. L., Jones, J. B., 1965. A chlorite-corundum rock from Mount Painter, South Australia. *Mineral. Mag.* 35, 140-145.
- Orville, P. M., 1972. Plagioclase cation exchange equilibria with aqueous chloride solution at 700°C and 2000 bars in the presence of quartz. *Amer. Jour. Sci.* 272, 234-272.
- Papike, J. J., Ross, M., 1970. Gedrites: crystal structures and intracrystalline cation distributions. *Amer. Mineralogist* 55, 1945-1972.
- Pearce, J. A., 1975. Basalt geochemistry used to investigate past tectonic environment on Cyprus. *Tectonophysics* 25, 41-67.
- Pearce, J. A., Cann, J. R., 1971. Ophiolite origin investigated by discriminant analysis using Ti, Zr and Y. *Earth Planet. Sci. Letters* 12, 339-349.

- Pearce, T. H., Gorman, G. E., Birkett, T. C., 1975. The TiO_2 - K_2O - P_2O_5 diagram: a method of discriminating between oceanic and non-oceanic basalts. Earth Planet. Sci. Letters 24, 419-426.
- Pettijohn, F. J., 1963. Chemical composition of sandstones--excluding carbonate and volcanic sands. Chpt. S in Fleischer, M. (ed.), "Data of Geochemistry". U.S. Geol. Surv. Prof. Paper 440-S.
- Petrov, B. V., 1969. Conditions of chloritoid and staurolite formation in metapelites of Paton Upland. Doklady AN SSSR 188, 201-204.
- Porrenga, D. H., 1965. Chamosite in Recent sediments of the Niger and Orinoco deltas. Geologie en Minjbouw 44, 400-403.
- Powell, R., Powell, M., 1977. Geothermometry and oxygen barometry using coexisting iron-titanium oxides: a reappraisal. Mineral. Mag. 41, 257-263.
- Pryce, M. W., 1973. Low iron cordierite in phlogopite schist from White Well, Western Australia. Mineral. Mag. 39, 241-243.
- Raase, P., 1974. Al and Ti contents of hornblende, indicators of pressure and temperature of regional metamorphism. Contr. Mineral. and Petrol. 45, 231-236.
- Rabbitt, J. C., 1948. A new study of the anthophyllite series. Amer. Mineralogist 33, 263-323.
- Raheim, A., Green, D. H., 1974. Talc-kyanite-quartz schist from an eclogite-bearing terrane, Western Tasmania. Contr. Mineral. and Petrol. 43, 223-231.
- Ramberg, H., De Vore, G., 1951. The distribution of Fe^{++} and Mg^{++} in coexisting olivines and pyroxenes. Jour. Geol. 59, 193-210.
- Ramdohr, P., 1969. The ore minerals and their intergrowths. Pergamon Press, 1174 pp.
- Ramsay, C. R., 1974. The cordierite isograd in Archaean meta-sediments near Yellowknife N.W.T. Canada - Variations on an experimentally established reaction. Contr. Mineral. and Petrol. 47, 27-40.
- Ramsay, C. R., Kamineni, D. C., 1977. Petrology and evolution of an Archaean metamorphic aureole in the Slave Craton, Canada. Jour. Petrol. 18, 460-486.
- Reed, S. J. B., Ware, N. G., 1975. Quantitative electron microprobe analysis of silicates using energy-dispersive X-ray spectrometry. Jour. Petrol. 16, 499-519.

- Rex, R. W., 1970. X-ray mineralogical studies - Leg 2. Deep-Sea Drilling Program, N.S.F.P. Spec. Publ. 2, 2, 329-346.
- Richardson, S. W., 1968. Staurolite stability in a part of the system Fe-Al-Si-O-H. Jour. Petrol. 9, 467-488.
- Richardson, S. W., Gilbert, M. C., Bell, P. M., 1969. Experimental determination of kyanite-andalusite and andalusite-sillimanite equilibria: the aluminum silicate triple point. Amer. Jour. Sci. 267, 259-272.
- Ringwood, A. E., 1974. The petrological evolution of island arc systems. Jl. Geol. Soc. Lond. 130, 183-204.
- Robertson, W. A., 1959. The Jervois Range copper mines. Bur. Min. Res. Geol. and Geophys. Canberra Austr. Rec 1959/ 103 (unpubl.).
- Robinson, P., Jaffe, H. W., 1969. Aluminous enclaves in gedrite-cordierite gneiss from southwestern New Hampshire. Amer. Jour. Sci. 267, 389-421.
- Robinson, P., Ross, M., Jaffe, H. W., 1971. Composition of the anthophyllite-gedrite series, comparisons of gedrite and hornblende, and the anthophyllite-gedrite solvus. Amer. Mineralogist 56, 1005-1041.
- Rorhlich, V., Price, N. B., Calvert, S. W., 1969. Chamosite in the Recent sediments of Loch Etive, Scotland. Jour. Sed. Petrol. 39, 624-631.
- Romans, P. A., Brown, L. L., White, J. C., 1975. An electron microprobe study of yttrium, rare earth, and phosphorus distribution in zoned and ordinary zircon. Amer. Mineralogist 60, 475-480.
- Rumble, D. III, 1970. Chloritoid-staurolite quartzites from the Moosilauke quadrangle, New Hampshire. Carnegie Inst. Washington Yb. 69, 290-294.
- Rumble, D. III, 1973. Fe-Ti oxide minerals from regionally metamorphosed quartzites of western New Hampshire. Contr. Mineral. and Petrol. 42, 181-195.
- Saxena, S. K., 1968a. Crystal-chemical aspects of distribution of elements among certain coexisting rock-forming silicates. Neues Jb. Mineral. Abh. 108, 292-323.
- Saxena, S. K., 1968b. Distribution of elements between coexisting minerals and the nature of solid solution in garnet. Amer. Mineralogist 53, 994-1014.

- Saxena, S. K., 1969b. Silicate solid solution and geothermometry 3. Distribution of Fe and Mg between coexisting garnet and biotite. *Contr. Mineral. and Petrol.* 22, 259-267.
- Saxena, S. K., 1969a. Silicate solid solutions and geothermometry 2: Distribution of Fe^{2+} and Mg^{2+} between coexisting olivine and pyroxene. *Contr. Mineral. and Petrol.* 22, 147-156.
- Saxena, S. K., 1973. "Thermodynamics of Rock-forming Crystalline Solutions", Springer-Verlag, Berlin, 188 pp.
- Saxena, S. K., Hollander, N. B., 1969. Distribution of iron and magnesium in coexisting biotite, garnet and cordierite. *Amer. Jour. Sci.* 267, 210-216.
- Schmid, R., Wood, B. J., 1976. Phase relations in granulitic metapelites from the Ivrea-Verbano Zone (northern Italy). *Contr. Mineral. and Petrol.* 54, 255-279.
- Schreyer, W., Abraham, K., 1976. Three-stage metamorphic history of a whiteschist from Sar e Sang, Afghanistan, as part of a former evaporite deposit. *Contr. Mineral. and Petrol.* 59, 111-130.
- Schreyer, W., Chinner, G. A., 1966. Staurolite-quartzite bands in kyanite quartzite at Big Rock, Rio Arriba County, New Mexico. *Contr. Mineral. and Petrol.* 12, 233-244.
- Schreyer, W., Yoder, H. S. Jnr., 1964. The system Mg-cordierite- H_2O and related rocks. *Neues Jb. Miner. Abh.* 101, 271-342.
- Seifert, F., 1975. Boron-free kornerupine: a high-pressure phase. *Amer. Jour. Sci.* 275, 57-87.
- Seifert, F., 1974. Stability of sapphirine: a study of the aluminous part of the system $\text{MgO-Al}_2\text{O}_3\text{-SiO}_2\text{-H}_2\text{O}$. *Jour. Geol.* 82, 173-204.
- Seifert, F., Schreyer, W., 1970. Lower temperature stability of Mg cordierite in the range 1-7 kb water pressure: a redetermination. *Contr. Mineral. and Petrol.* 27, 225-238.
- Seifert, F. A., Virgo, D., 1975. Kinetics of the Fe^{2+} -Mg order-disorder reaction in anthophyllites: quantitative cooling rates. *Science* 188, 1107-1109.
- Seki, Y., 1954. On chloritoid rocks in the Kitakami Median Metamorphic Zone, northeastern Japan. *Sci. Rept. Saitama Univ. Ser. B* 1, 223-262.
- Seki, Y., 1961. Calcareous hornfelses in the Arisu district of the Kitakami Mountains, northeastern Japan. *Jap. Jour. Geol. and Geog.* 32, 55-78.

- Selley, R. C., 1970. "Ancient Sedimentary Environments", Chapman and Hall, London, 237 pp.
- Sen, S. K., Chakraborty, K. R., 1968. Magnesium-iron exchange equilibrium in garnet-biotite and metamorphic grade. Neues Jb. Miner. Abh. 108, 181-207.
- Shaw, D. M., 1956. Geochemistry of pelitic rocks. Part III: Major elements and general geochemistry. Bull. Geol. Soc. Amer. 67, 919-934.
- Shaw, D. M., 1972. The origin of the Apsley Gneiss, Ontario. Can. Jour. Earth Sci. 9, 18-35.
- Shaw, R. D., Milligan, E. N. (Comp.), 1969. 1:250,000 Geological Series Explanatory Notes: Illogwa Creek, N.T. Sheet SF/53-15 International Index. Bur. Min. Res. Geol. Geophys. (Canberra) Austr.
- Shaw, R. D., Stewart, A. J., 1973. Regional geology of the Precambrian Arunta Block. Bureau Min. Res. Geol. Geophys. (Canberra) Austr. Rec. 1973/94.
- Shaw, R. D., Stewart, A. J., 1975. Arunta Block - Regional Geology, in Knight, C. L. (ed.) "Economic Geology of Australia and Papua - New Guinea". 1. Metals. Monograph Ser. 5. Australasian Institute of Mining and Metallurgy.
- Shido, F., 1958. Plutonic and metamorphic rocks of the Nakoso and Iritono districts in the central Abukuma Plateau. Jour. Fac. Sci. Univ. Tokyo Sec. II, 11, 131-217.
- Shido, F., Miyashiro, A., 1959. Hornblendes of basic metamorphic rocks. Jour. Fac. Sci. Univ. Tokyo Sec. II, 12, 85-102.
- Shiraki, K., 1971. Metamorphic basement rocks of Yap Islands, western Pacific: possible oceanic crust beneath an island-arc. Earth Planet. Sci. Letters 13, 167-174.
- Smith, K. G. (Comp.), 1963. 1:250,000 Geological Series Explanatory Notes: Huckitta, N.T. Sheet SF/53-11 International Index. Bur. Min. Res. Geol. and Geophys. (Canberra) Austr.
- Smith, R. E., 1968. Redistribution of major elements in the alteration of some basic lavas during burial metamorphism. Jour. Petrol. 9, 191-219.
- Smith, R. E., Smith, S. E., 1976. Comments on the use of Ti, Zr, Sr, K, P and Nb in classification of basaltic magmas. Earth Planet. Sci. Letters 32, 114-120.

- Sobolev, V. S. (ed.), 1972. "The Facies of Metamorphism". Australian National University, Canberra, 417 pp.
- Spitz, G., Darling, R., 1975. The petrochemistry of altered volcanic rocks surrounding the Louvem copper deposit, Val d'Or, Quebec. Can. Jour. Earth Sci. 12, 1820-1849.
- Spry, A., 1963. Precambrian rocks of Tasmania, part V, petrology and structure of the Frenchmans Cap area. Papers and Proc. Roy. Soc. Tas. 97, 105-127.
- Staudigel, H., Schreyer, W., 1977. The upper thermal stability of clinocllore, $\text{Mg}_5\text{Al AlSi}_3\text{O}_{10}(\text{OH})_8$ at 10-35 kb $\text{P}_{\text{H}_2\text{O}}$. Contr. Mineral. and Petrol. 61, 187-198.
- Stewart, A. J., 1971. K-Ar dates from the Arltunga Nappe Complex, Northern Territory. Jour. Geol. Soc. Austr. 17, 205-211.
- Stout, J. H., 1971. Four coexisting amphiboles from Telemark, Norway. Amer. Mineralogist 56, 212-224.
- Stout, J. H., 1972. Phase petrology and mineral chemistry of coexisting amphiboles from Telemark, Norway. Jour. Petrol. 13, 99-145.
- Stout, J. H., 1975. Apparent effects of molecular water on the lattice geometry of cordierite. Amer. Mineralogist 60, 229-234.
- Streckeisen, S. L. and Committee, 1973. Plutonic rocks: classification and nomenclature recommended by the I.U.G.S. Sub-commission on the systematics of igneous rocks. Geotimes 18, 26-30.
- Thompson, A. B., 1976. Mineral reactions in pelitic rocks: I. Prediction of P-T-X (Fe-Mg) phase relations II. Calculations of some P-T-X (Fe-Mg) phase relations. Amer. Jour. Sci. 276, 401-454.
- Thompson, J. B. Jr., 1955. The thermodynamic basis for the mineral facies concept. Amer. Jour. Sci. 253, 65-103.
- Thompson, J. B. Jr., 1957. The graphical analysis of mineral assemblages in pelitic schists. Amer. Mineralogist 42, 842-858.
- Thompson, J. B. Jr., Norton, S. A., 1968. Paleozoic regional metamorphism in New England and adjacent areas, in E-An Zen et al., eds., "Studies of Appalachian Geology". Interscience (John Wiley & Sons), New York.

- Travis, R. B., 1956. Note on large cordierite porphyroblasts, Fremont County, Colorado. *Amer. Mineralogist* 41, 796-799.
- Turekian, K. K., Wedepohl, K. H., 1961. Distribution of the elements in some major units of the earth's crust. *Geol. Soc. Amer. Bull.* 72, 175-192.
- Turner, F. J., 1968. "Metamorphic Petrology: Mineralogical and Field Aspects". McGraw-Hill, New York, 403 pp.
- Turnock, A. C., 1960. The stability of iron chlorites. *Carnegie Inst. Washington Yb.* 59, 98-103.
- Uruno, K., Kanisawa, S., 1965. Staurolite-bearing rocks in the Abukuma metamorphic belt, Japan. *Earth Sci.* 81, 1-12.
- Vallance, T. G., 1965. On the chemistry of pillow lavas and the the origin of spilites. *Mineral. Mag.* 34, 471-481.
- Vallance, T. G., 1967. Mafic rock alteration and isochemical development of some cordierite-anthophyllite rocks. *Jour. Petrol.* 8, 84-96.
- Vallance, T. G., 1969. Spilites again: some consequences of the degradation of basalts. *Proc. Linn. Soc. N.S.W.* 94, 8-51.
- Vallance, T. G., 1974. Spilitic degradation of a tholeiitic basalt. *Jour. Petrol.* 15, 79-96.
- Velde, B., 1973. Phase equilibria in the system $MgO-Al_2O_3-SiO_2-H_2O$: chlorites and associated minerals. *Mineral. Mag.* 39, 297-312.
- Vernon, R. H., 1969. The Willyama Complex, Broken Hill Area, in Packham, G. H. (ed.), "The Geology of New South Wales". *Jour. Geol. Soc. Austr.* 16, 654 pp.
- Vernon, R. H., 1972. Reactions involving hydration of cordierite and hypersthene. *Contr. Mineral. and Petrol.* 35, 125-137.
- Vernon, R. H., 1976. "Metamorphic Processes. Reactions and Microstructure Development". Murby - George Allen & Unwin, London, 247 pp.
- Vernon, R. H., 1977. Relationships between microstructures and metamorphic assemblages. *Tectonophysics* 39, 439-452.
- Vernon, R. H., Ransom, D. M., 1971. Retrograde schists of the amphibolite facies at Broken Hill, New South Wales. *Jour. Geol. Soc. Austr.* 18, 267-277.

- Ware, N. G., Reed, S. J. B., 1973. Background corrections for quantitative electron microprobe analysis using a lithium-drifted silicon X-ray detector. Jour. Phys. E6, 286-288.
- Warren, R. G., 1975. A metamorphosed regolith from the Arunta Block, Central Australia (abstr.). Abstrs. 1st Austr. Geol. Conv., Geol. Soc. Austr. May 1975, p.86.
- Warren, R. G., Stewart, A. J., Shaw, R. D., 1975. Arunta Block--Mineralization, in Knight, C. L. (ed.) "Economic Geology of Australia and Papua - New Guinea". 1. Metals. Monograph Ser. 5. Australasian Institute of Mining and Metallurgy.
- Watson, D. P., 1975. Atuttra copper, lead and scheelite zone--Jervois Range, in Knight, C. L. (ed.) "Economic Geology of Australia and Papua - New Guinea". 1. Metals. Monograph Ser. 5. Australasian Institute of Mining and Metallurgy.
- Weaver, C. E., Pollard, L. D., 1973. "The Chemistry of Clay Minerals". Elsevier, Amsterdam, 213 pp.
- Wedepohl, K. H., 1969, 1970, 1972, 1947. Exec. ed. "Handbook of Geochemistry", Springer-Verlag, Heidelberg (5 vols.)
- Wedepohl, K. H., 1969. Composition and abundance of common sedimentary rocks, in Wedepohl, K. H. (ed.) "Handbook of Geochemistry", vol. 1. Springer-Verlag, Berlin, 442 pp.
- Weisbrod, A., 1973. The problem of water in cordierite. Carnegie Inst. Washington Yb. 72, 521-523.
- White, A. J. R., Chappell, B. W., 1976. Ultrametamorphism and granitoid genesis. Abstr. 25th Int. Geol. Cong. Sydney, p. 674.
- Wilson, A. F., 1975. Aspects of the geochemistry and petrology of the mafic granulites of the Arunta, Musgrave and Fraser blocks. Abs. First Austr. Geol. Conv., Adelaide, May 1975, Geol. Soc. Austr.
- Wilson, A. F., Compston, W., Jeffery, P. M., Riley, G. H., 1960. Radioactive ages from the Precambrian rocks of Australia. Jour. Geol. Soc. Austr. 6, 179-196.
- Winkler, H. G. F., 1967. "Petrogenesis of Metamorphic Rocks" (2nd ed.). Springer-Verlag, New York Inc., 237 pp.
- Winkler, H. G. F., 1976. "Petrogenesis of Metamorphic Rocks" (4th ed.). Springer-Verlag, New York Inc., 334 pp.

- Winkler, H. G. F., Sen, S. K., 1973. Nomenclature of granulites and other high grade metamorphic rocks. Neues Jb. Mineral. Mh. 1973, 393-402.
- Wirsching, U., 1976. Experiments on hydrothermal alteration processes of rhyolitic glass in closed and "open" system. Neues Jb. Miner. Mh. 1976, 203-213.
- Wood, B. J., 1973. Fe^{2+} - Mg^{2+} partition between coexisting cordierite and garnet - a discussion of the experimental data. Contr. Mineral. and Petrol. 40, 253-258.
- Wood, B. J., 1975. The application of thermodynamics to some subsolidus equilibria involving solid solutions. Fortschr. Miner. 52, 21-45, Spec. Issue: IMA Papers, 9th Meeting, 1974.
- Wood, B. J., Banno, S., 1973. Garnet-orthopyroxene and orthopyroxene-clinopyroxene relationships in simple and complex systems. Contr. Mineral. and Petrol. 42, 109-124.
- Woodford, P. J., Wilson, A. F., 1976. Chemistry of coexisting pyroxenes, hornblendes and plagioclases in mafic granulites, Strangways Range, central Australia. Neues Jb. Miner. Abh. 128, 1-40.
- Woodford, P. J., Wilson, A. F., 1976a. Sapphirine, hognomite, kornerupine, and surinamite from aluminous granulites, northeastern Strangways Range, Central Australia. Neues Jb. Miner. Mh. 1976, 15-35.
- Zotov, I. A., Sidorenko, G. A., 1968. Magnesian gedrite from the southwestern Pamiro. Doklady Akad. Nauk. SSSR 180, 138-141.

APPENDIX

Facies Classification Used in this Thesis

This author agrees with Turner (1968) that attempting to force individual metamorphic assemblages and metamorphic gradients into subfacies and a few standardized facies series serves to distort rather than clarify P-T relationships within metamorphic terrains.

On the one hand, to cover even the more common metamorphic assemblages requires the formulation of a multitude of subfacies. In addition, many assemblages do not easily fit into the appropriate subfacies.

On the other hand, the complete abolishment of the facies (as well as the subfacies) scheme, and its replacement with just four metamorphic grades, as proposed by Winkler (e.g. 1976), results in too general a classification, with the consequent loss of much useful detail. The facies scheme of Turner (1968, p.366) is widely used and understood by most metamorphic petrologists. This scheme logically subdivides the P-T grid, and is based on naturally-occurring parageneses. It seems pointless to this author to abandon such a scheme in favour of the one proposed by Winkler (1976). Therefore, the facies nomenclature used in this thesis is that of Turner (1968), with one modification.

Turner (1968, p.308) states that many metapelitic rocks belonging to the amphibolite facies are characterized by "assemblages in which micas are associated with almandine, staurolite, kyanite or sillimanite, but never with andalusite or cordierite". According to these criteria, the metamorphic rocks in the Jervois Range area cannot belong to the amphibolite facies, but must belong to the hornblende-hornfels facies. However, much petrographic and experimental data, not available to Turner in 1968, have become available in the past decade.

It has been shown by many workers that cordierite- and/or andalusite-bearing rocks are common in the amphibolite facies of many relatively low-pressure regional metamorphic terrains (e.g. the Abukuma-type facies series of Winkler, 1967). Hence, this author has retained the use of the amphibolite facies to cover the rocks in the Jervois Range area, in part to emphasize the regional nature of the metamorphism in that region. This usage is also compatible with amphibolite facies conditions as tentatively proposed by Turner in figure 8-6 (1968, p.366).

The problem of nomenclature is largely resolved if it is understood that the amphibolite facies, as defined by Turner (1968), refers to the upper- or high-pressure portion of the amphibolite facies P-T field as depicted in figure 8-6 of Turner (1968, p.336), whereas the amphibolite facies, as applied to the Jervois Range rocks,

refers to the low-pressure portion of the amphibolite facies P-T field.

Analytical Methods

(i) Minerals

Most of the mineral analyses were carried out at the Research School of Earth Sciences, The Australian National University, Canberra, on a TPD energy-dispersive electron-microprobe (Fontijn et al., 1969), fitted with a lithium drifted silicon detector. The analytical and correction procedures used were those of Reed and Ware (1973) and Ware and Reed (1973).

Apart from somewhat higher detection limits, compared with wavelength-dispersive microprobes, energy-dispersive microprobes have two minor limitations relevant to the analyses in this thesis:

(i) Concentrations of elements below 0.2%, but above the theoretical detection limit, may sometimes not be recorded, owing to minor errors in peak-stripping and background corrections. In addition, a low, but spurious, concentration of one element may be recorded in a mineral if there is a high concentration of a second element adjacent to the first element in atomic number. An example of this is the spurious Na content of Zn-free, Mg-rich chlorite. In this thesis, mineral formulae were recalculated to exclude Na in chlorite.

(ii) Interference of minor or trace-element L peaks with major-element K peaks is a possible source of error. This may be detected during analysis by a visual examination of the X-ray spectrum. A typical example of this is the appearance of Zn (L_{α} - 1.01 keV) as Na (K_{α} - 1.04 keV) in staurolite analyses. An empirical correction formula (N. G. Ware, pers. comm.) has been used to yield the approximate ZnO values listed in the staurolite analyses.

A number of mineral analyses were carried out on the recently commissioned ETEC wavelength-dispersive electron microprobe at Macquarie University. In addition, this instrument was used to confirm the absence of Na in both Zn-free and Zn-bearing chlorites, and the absence of Na and the presence of Zn in staurolite.

(ii) Bulk-Rock Compositions

Selected rock-samples were trimmed on a diamond wheel to eliminate (where possible) any oxidized domains and veining, followed by crushing in a Tema disc mill (with a tungsten-carbide barrel) for 60 seconds. The resultant rock powders were analysed

in duplicate by X-ray fluorescence spectrography following the method of Norrish and Chappell (1967) and using the inter-element matrix corrections of Norrish and Hutton (1969). The equipment used was a Siemens SRS Spectrometer with a Siemens Kristalloflex 4kW generator and standard counting rack. These instruments have been fully automated by S. E. Shaw and R. H. Flood, and the analyses are computer-corrected for detector dead-time, counting statistics, background, L.O.I. and Na, and inter-element matrix effects. The analyses were standardized using United States Geological Survey standards G-2, W-1, DTS-1, AGV-1, and PCC-1, and background corrections were checked with spectrographic-pure SiO_2 run with each batch of samples. Accuracy is within $\pm 2\%$ for major elements in concentration in excess of 3%.

Sodium was determined by atomic-absorption spectroscopy, H_2O^+ by the Penfield method, and Fe^{2+} by volumetric analysis of 0.2 g samples dissolved in HF/HClO_4 .

Trace-elements were determined in duplicate on pressed-pellets of rock powder, by XRF. Practical detection limits are 2 ppm for U, Th and Pb, and 8 ppm for the other elements listed in the appendix tables. Since near the detection-limit the concentrations of the elements are strongly dependent on counting errors and the background correction factor used, element values lower than the limits above have been included to allow for possible errors in correction. In general, concentrations of U, Th and Pb below 5 ppm, Ba below 30 ppm, and other elements below 15 ppm are approximate, and values only slightly higher than these figures may be in error by as much as $\pm 15\%$.

Spl.	<u>801</u>	<u>803</u>	<u>804</u>	<u>805</u>	<u>806</u>	<u>807</u>	<u>808</u>	<u>809</u>
SiO ₂	67.51	60.38	70.41	77.15	73.06	73.72	74.30	58.40
TiO ₂	.48	.85	.45	.08	.01	.01	.19	.72
Al ₂ O ₃	14.90	17.51	12.69	11.84	14.62	14.14	13.56	19.28
Fe ₂ O ₃	1.30	2.58	1.39	.88	.08	.01	.62	3.96
FeO	3.39	3.31	3.27	.45	.16	.24	1.03	3.69
MnO	.08	.07	.09	.01	.01	.12	.02	.10
MgO	1.34	2.31	.65	.30	.15	.25	.52	3.27
CaO	2.45	5.15	2.18	.52	.42	.66	1.57	.51
Na ₂ O	3.45	3.59	2.82	3.24	3.25	4.02	3.52	.57
K ₂ O	3.83	2.03	4.71	5.00	6.46	5.75	4.00	6.38
P ₂ O ₅	.17	.26	.11	.01	.31	.11	.04	.21
H ₂ O ⁺	1.01	1.24	.71	.39	.72	.12	.53	2.57
H ₂ O ⁻	.05	.05	.05	.09	.05	.04	.08	.15
TOTAL	99.96	99.33	99.53	99.96	99.31	99.19	99.98	99.81
Y ppm	62	9	114	121	5	4	27	26
Sr "	117	291	90	25	25	69	90	40
Zr "	244	426	308	130	5	27	152	133
U "	4	2	3	3	*	10	11	3
Rb "	207	135	197	281	1208	538	211	280
Th "	19	3	28	28	*	*	32	15
Pb "	24	10	16	16	6	34	112	11
Ga "	19	26	21	23	17	13	18	31
Zn "	61	79	83	33	8	13	31	112
Cu "	7	37	8	5	*	27	12	8
Ni "	14	18	5	5	*	*	4	49
Cr "	14	31	*	*	*	*	*	103
V "	30	70	12	*	*	*	11	90
Ba "	611	204	957	531	138	173	561	762
O.R.	25.65	41.22	27.67	63.76	31.03	3.61	35.13	49.13
Mg	41.34	55.44	26.16	54.30	62.56	65.00	47.37	61.24
Na/K (atomic)	1.37	2.69	.91	.98	.76	1.06	1.34	.14

APPENDIX TABLE 1: Chemical analyses of samples used in radiometric age determinations in the Jervois Range area.

- 801: biotite-granodiorite ("Jervois Granite"), 6 km south of Jervois Mine; in thin section, feldspars contain fine muscovite aggregates representing recrystallized feldspar alteration products; minor amounts of epidote commonly occur adjacent to altered biotite laths; biotite $Mg = 28\%$, bulk rock mol. $Al_2O_3/(Na_2O + K_2O + CaO) = 1.04$; normative corundum = 1.03%.
- 803: slightly foliated biotite-granodiorite, 7 km north-northeast of Bonya Mine; abundant magnetite, in places rimmed by ilmenite, giving an equilibration temperature of $740^\circ C$ at $f_{O_2} = 10^{-16}$ atm. (Buddington and Lindsley, 1964; Powell and Powell, 1977); abundant magnetite has raised biotite Mg to a high value of 53%; biotite commonly altered to muscovite and chlorite, large feldspar grains commonly contain recrystallized muscovite aggregates; bulk rock mol. $Al_2O_3/(Na_2O + K_2O + CaO) = 2.00$, normative corundum = 0.67%.
- 804: lineated hornblende-biotite-granite, 9 km north of Bonya Mine, contains pargasitic hornblende $Mg = 12\%$, biotite (in places altering to chlorite), minor magnetite, traces of epidote and muscovite, some large euhedral zircon crystals; bulk composition mol. $Al_2O_3/(Na_2O + K_2O + CaO) = 0.93$, normative diopside = 1.73%.
- 805: alaskite, 5 km north of Jervois Mine, very minor biotite (almost completely altered to chlorite), primary muscovite commonly adjacent to grains of haematite, feldspars relatively unaltered; quartz appears in stringers and shows evidence of deformation; bulk composition mol. $Al_2O_3/(Na_2O + K_2O + CaO) = 1.01$, normative corundum = 0.18 %.
- 806: slightly deformed muscovite-plagioclase-microcline-quartz pegmatite containing minor amounts of fine-grained tourmaline.
- 807: fine-grained microcline-plagioclase-quartz pegmatite containing very minor amounts of muscovite and tourmaline.
- 808: biotite-microgranite dyke cutting metagabbro, 7 km southwest of Jervois Mine; all biotite grains partly altered to chlorite; some small muscovite flakes; minor epidote; bulk composition mol. $Al_2O_3/(Na_2O + K_2O + CaO) = 1.05$, normative corundum = 0.68%.
- 809: quartz-muscovite-biotite-magnetite schist; contains trace amounts of fine-grained tourmaline and garnet.

Sample	810	811	812	813	814	815	816	817	818	1	2	3	4	5
SiO ₂	48.39	49.81	49.37	46.85	46.90	53.75	49.91	51.73	49.89	49.7	49.8	51.1	50.2	50.3
TiO ₂	1.82	.41	1.12	.69	.71	1.97	1.75	1.58	.36	1.0	1.5	.83	1.0	2.2
Al ₂ O ₃	14.72	22.36	14.27	16.43	16.77	13.71	13.86	15.47	18.36	14.9	16.0	16.1	17.7	14.3
Fe ₂ O ₃	3.78	1.11	4.04	2.45	3.08	5.42	3.83	3.90	1.81	2.6	2.0	3.0	3.9	3.5
FeO	9.81	4.46	9.06	6.90	7.42	10.48	11.32	9.45	5.27	8.8	7.5	7.3	6.3	9.3
MnO	.27	.11	.22	.10	.26	.22	.21	.33	.20					
MgO	5.52	4.29	6.98	7.76	9.41	3.28	4.28	3.44	7.61	6.3	7.5	5.1	5.4	5.9
CaO	10.79	12.97	11.38	11.86	8.93	6.51	7.64	8.44	9.53	9.4	11.2	10.8	9.8	9.7
Na ₂ O	2.67	2.32	1.30	1.08	1.01	3.84	3.77	3.77	1.22	2.1	2.8	2.0	2.7	2.5
K ₂ O	.90	.52	.39	1.75	2.39	.89	1.12	.67	3.14	.32	.14	.30	.9	.8
P ₂ O ₅	.26	.01	.11	.06	.09	.32	.19	.15	.08					
H ₂ O ⁺	.96	1.35	1.04	2.91	2.08	1.34	1.59	.71	2.43					
H ₂ O ⁻	.08	.07	.10	.18	.07	.07	.02	.11	.12					
TOTAL	99.97	99.79	99.38	99.02	99.12	101.80	99.49	99.75	100.02					
Y ppm	32	14	31	17	16	63	46	41		15	30	20	23	30
Sr "	242	168	111	60	80	221	299	165		165	135	225	300	350
Zr "	94	29	69	37	45	202	201	204		100	100	60	100	200
U "	.	.	.	3	.	9	5	10						
Rb "	42	28	15	153	163	52	79	32		10	1	5	10	30
Th "	.	.	.	6	.	11	.	24						
Pb "	7	9	11	28	8	94	57	12						
Ga "	20	23	18	16	17	23	23	25						
Zn "	178	47	116	48	185	188	184	72	104	100	75	80	80	90
Cu "	29	50	212	77	167	119	158	144	46	110	70	88	80	100
Ni "	76	49	80	131	281	32	52	55	84	100	100	25	50	100
Cr "	336	95	288	415	405	21	40	46	178	175	300	50	50	100
V "	222	119	282	199	157	220	358	273	180					
Ba "	81	144	104	384	50	398	216	392	323	90	11	60	100	200
Mg	50.08	63.16	57.87	66.72	69.33	35.81	40.26	39.35	72.02	56.07	64.06	55.46	60.44	53.07
mol MgO	54.82	65.88	63.21	70.47	73.54	42.10	44.29	44.35	75.28	59.54	66.95	60.44	67.93	57.65
FeO-Fe ₂ O ₃ +MgO														
O.R.	25.75	18.30	28.63	24.21	27.19	31.76	23.34	27.08	23.61	21.00	19.35	27.00	35.77	25.30
wt% Na ₂ O+K ₂ O	.074	.057	.034	.060	.073	.088	.098	.086	.087	.049	.059	.045	.072	.066
SiO ₂														
wt% K/Rb	178	154	216	95	122	142	118	174		350	1200	700	350	300
wt% Rb/Sr	.17	.17	.14	2.55	2.04	.24	.26	.19		.08	.01	.02	.03	.09
wt% K/Na	.27	.25	.34	1.81	2.65	.26	.33	.20	2.88	.17	.06	.17	.37	.36

1 Average "enriched" Archaean tholeiite (enriched in light rare-earth and large-ion-lithophile elements with respect to "depleted" Archaean tholeiite); Condie, (1976)

2 Average modern ocean-rise tholeiite; Condie, (1976)

3 Average modern island-arc tholeiite; Condie, (1976)

4 Average modern calc-alkali tholeiite; Condie, (1976)

5 Average modern continental tholeiite; Condie, (1976)

APPENDIX TABLE 2: Major and trace-element analyses of amphibolites from the Jervois Range area (810-818).

The average compositions of enriched Archaean tholeiites and four modern tholeiite types serve for comparison.

- 810: plagioclase-hornblende-sphene metagabbro: amphibole occurs as subidioblastic grains up to 4 mm in length, commonly surrounded by finer-grained idioblastic hornblende; plagioclase appears in granular aggregates with minor quartz and varying amounts of idioblastic hornblende; average grain size within these felsic aggregates is 0.5 mm; most of the feldspar has been replaced by fine, white mica-rich aggregates ("sericite") and larger laths of muscovite—as a result, only about 10% of the total feldspar is optically clear; sphene occurs as scattered granular aggregates up to 4 mm across.
- 811: massive metagabbro; relict, twinned labradorite crystals (up to 6 mm in length) contain small epidote inclusions; epidote also occurs, together with quartz, along feldspar-feldspar grain boundaries; plagioclase contains scattered flakes of white-mica; individual pyroxene crystals and larger pyroxene aggregates have been totally replaced by acicular actinolite, aligned parallel to pre-existing exsolution lamellae; exsolved opaque minerals are locally preserved; many of the actinolite pseudomorphs have narrow rims of a more strongly pleochroic hornblende; minute hornblende crystals (< 0.08 mm) project from these rims into plagioclase, and may in turn be partly surrounded by small, rounded epidote grains or fine chlorite laths.
- 812: fine-grained, schistose, "spotted" amphibolite; hornblende-plagioclase assemblage with minor quartz and scattered, twinned and zoned plagioclase relics.
- 813: massive, altered metadolerite; plagioclase is extensively altered to white-mica aggregates, which contain larger flakes up to 0.5 mm in size; epidote and amphibole appear as inclusions in what remains of the relict feldspar, and are interpreted as being due to the replacement of plagioclase; blastophitic amphibole encloses smaller laths of relatively unaltered plagioclase; fine-grained amphibole and altered feldspar aggregates occur between large grains of amphibole and plagioclase.
- 814: altered metagabbro; similar to 813, except that relict plagioclase is commonly anhedral; some smaller, euhedral, unaltered and twinned feldspar grains are also present.
- 815: fine-grained, weakly schistose amphibolite; the assemblage is plagioclase-hornblende-quartz with minor magnetite, epidote, chlorite and biotite; epidote occurs as small ($< .2$ mm), idioblastic to subidioblastic grains adjacent to felted aggregates of chlorite, which commonly occur in and around partly skeletal magnetite grains scattered through the rock;

epidote also occurs, together with minute biotite laths, in granular, quartz- and feldspar-rich areas.

- 816: weakly foliated, fine-grained amphibolite; andesine occurs as small (< 0.1 mm) grains in granoblastic aggregates with quartz; locally, these contain minute, randomly oriented laths of biotite and hornblende, occurring along grain boundaries and as inclusions within the quartz and andesine; subidioblastic to poikiloblastic hornblende grains, up to 0.6 mm in length, contain inclusions of quartz and feldspar; idioblastic chlorite, up to 0.6 mm in length, is a minor constituent occurring throughout the rock; minor amounts of magnetite, ilmenite, granular calcite, and rare, rounded grains of epidote, are also present.
- 817: "spotted" amphibolite; consisting of relict plagioclase set in a fine-grained, hornblende-rich matrix; the relict plagioclase grains, commonly in clusters up to 12 mm across, contain white mica-rich domains; inclusions of fine-grained hornblende-epidote, chlorite and biotite are also common in relict plagioclase; the matrix consists of subidioblastic hornblende and smaller amounts of granular quartz, unaltered plagioclase, magnetite and ilmenite; the average matrix grain size is 0.07 mm.
- 818: altered metagabbro; plagioclase is intensely "sericitized" and rich in white-mica laths, commonly oriented along relict cleavage directions; the amphibole pseudomorphs, as in sample 811, are actinolitic, with narrow rims of more strongly pleochroic hornblende; epidote, chlorite and magnetite are absent.

Spl.	<u>826</u>	<u>827</u>	<u>828</u>	<u>829</u>	<u>830</u>	<u>831</u>	<u>832</u>
SiO ₂	29.96	51.24	71.12	67.63	56.84	69.08	64.86
TiO ₂	.85	.82	.14	.32	.69	.42	.40
Al ₂ O ₃	23.24	20.00	8.69	16.52	16.27	9.97	8.88
Fe ₂ O ₃	8.84	4.06	5.34	3.11	8.08	6.98	8.58
FeO	21.55	14.65	9.83	4.87	9.31	8.48	9.91
MnO	.37	.75	.59	.21	.40	.31	.48
MgO	6.26	3.10	1.09	.47	1.63	1.26	.94
CaO	.41	.53	.32	.19	.26	.09	.10
Na ₂ O	.60	.69	.42	.26	.20	.30	2.82
K ₂ O	3.44	.50	1.13	4.01	3.75	1.16	1.18
P ₂ O ₅	.30	.18	.02	.08	.15	.05	.07
H ₂ O ⁺	3.94	3.00	1.14	1.62	1.63	1.52	1.66
H ₂ O ⁻	.18	.12	.06	.08	.05	.15	.29
<u>TOTAL</u>	<u>99.94</u>	<u>99.63</u>	<u>99.89</u>	<u>99.37</u>	<u>99.26</u>	<u>99.77</u>	<u>99.17</u>
Y ppm	16	27	23	49	30	13	14
Sr "	8	4	14	15	15	28	*
Zr "	157	151	117	266	218	114	102
U "	*	3	19	13	4	*	*
Rb "	625	53	221	235	716	199	35
Th "	17	19	13	14	24	21	12
Pb "	19	11	37	17	52	129	21
Ga "	51	31	16	28	27	22	21
Zn "	1699	526	252	203	218	644	926
Cu "	303	17	880	183	136	2062	274
Ni "	49	46	8	6	44	17	35
Cr "	132	133	7	11	95	63	56
Sc "	19	18					
V "	116	102	15	34	86	41	43
Ba "	461	175	76	870	743	133	*
Nb "	18	15					
<u>Mg</u>	<u>34.12</u>	<u>27.39</u>	<u>16.50</u>	<u>14.68</u>	<u>23.79</u>	<u>20.94</u>	<u>14.46</u>
<u>Mg corr.</u>	<u>38.84</u>	<u>30.12</u>	<u>20.74</u>	<u>19.45</u>	<u>33.86</u>	<u>29.61</u>	<u>21.69</u>
O.R.	26.96	19.96	32.83	36.49	43.85	42.55	43.79

APPENDIX TABLE 3: Chemical analyses of staurolite-bearing samples from the Jervois Range area.

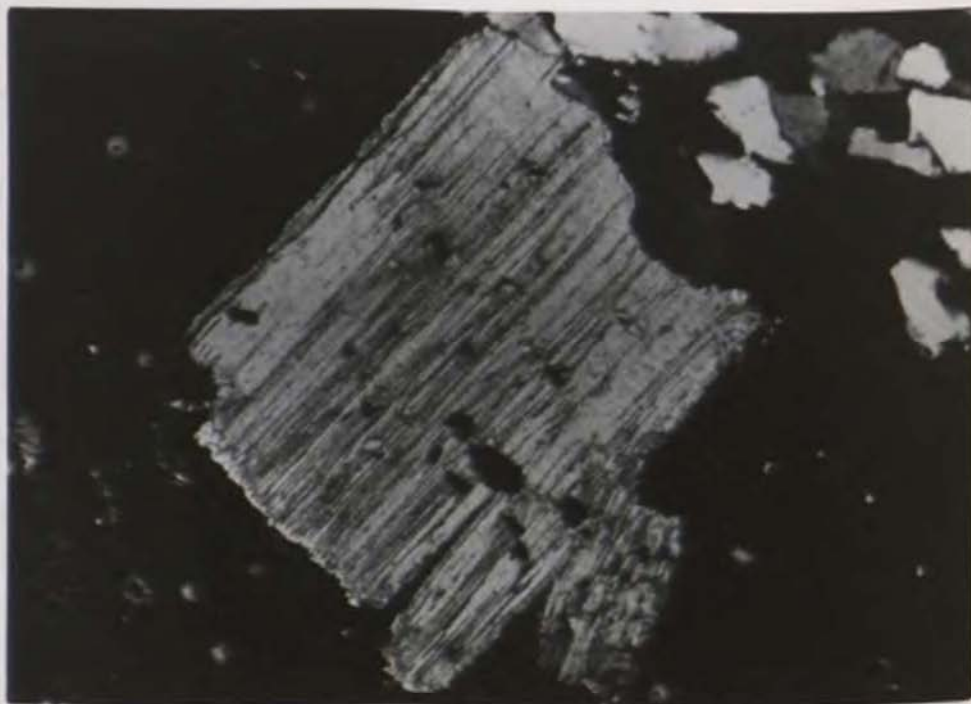
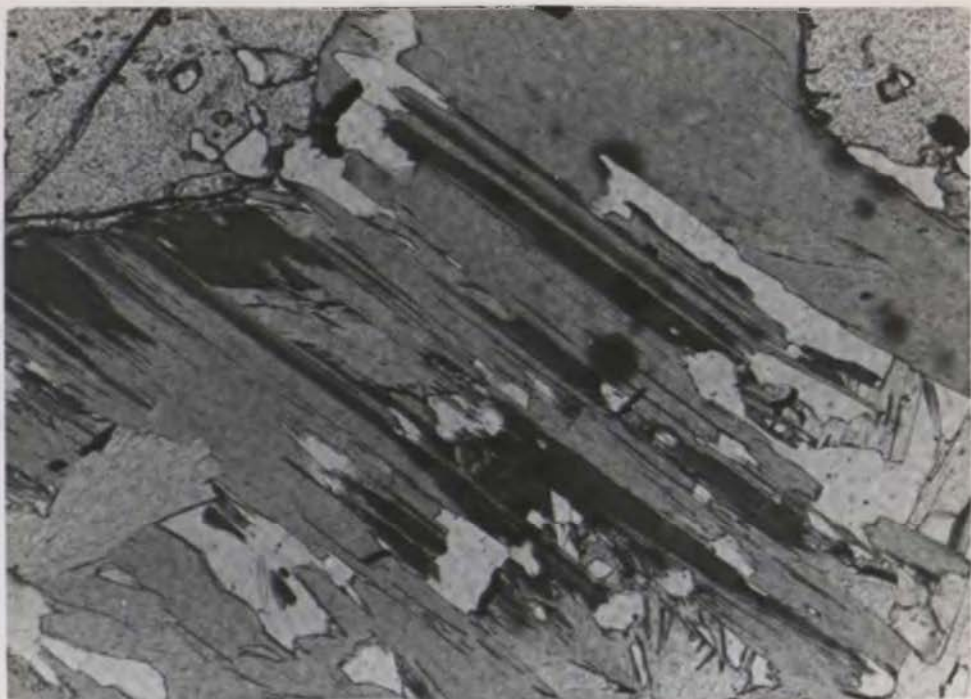
- 826: almandine-staurolite-biotite-chlorite-magnetite schist with minor muscovite, andalusite, and quartz; slightly elongated almandine porphyroblasts occur, up to 6 mm in length, together with staurolite porphyroblasts of slightly smaller size; both these minerals contain inclusions of quartz, magnetite, biotite and chlorite, and, in addition, have cracks filled with the same minerals; a few grains of andalusite, up to 4 mm in diameter, are present, and in places are partly to completely altered to muscovite-rich aggregates; all the porphyroblasts are set in a matrix of alternating chlorite- and biotite-rich bands, each of which contains magnetite octahedra, together with smaller amounts of muscovite and quartz; idioblastic chlorite and biotite crystals attain lengths of 2 mm, and are commonly aligned in a schistosity; in some domains, biotite and chlorite occur as decussate aggregates, which may contain small garnet or staurolite grains; chlorite is commonly intergrown with biotite along (001); such intergrowths (see photographs) are large and well defined, with the contact between the two minerals microscopically sharp, viewed perpendicular to (001); such intergrowths do not resemble those resulting from the replacement of biotite by lenticular chlorite aggregates parallel to (001) of biotite, observed in hydrothermally altered granitic rocks; allanite inclusions in chlorite are locally abundant, and also occur in biotite, staurolite and garnet; there is no unequivocal textural evidence to indicate the replacement of biotite by chlorite, and, as a consequence, the assemblage is considered stable by the author.
- 827: almandine-staurolite-andalusite-chlorite-quartz-magnetite gneiss with trace amounts of biotite and muscovite; rounded, poikiloblastic garnet and elongate staurolite grains are up to 6 mm in length, with inclusions of quartz and magnetite; sieve-textured andalusite occurs in ovoid masses up to 12 mm in length, and encloses quartz (average grainsize 0.1 mm), chlorite, magnetite, and somewhat larger subidioblastic garnet and staurolite; all of these large grains are set in a matrix of quartz, chlorite and magnetite, with an average grainsize of 0.2 mm; within the matrix, individual quartz grains tend to be polygonal; slightly-sutured quartz-quartz grain boundaries commonly meet the corners of chlorite laths, or meet quartz-chlorite (001) interfaces at high angles; individual chlorite laths between quartz grains define a weak foliation, though large, randomly oriented chlorite idioblasts also occur; locally chlorite occurs in parallel intergrowths along (001) with trace amounts of biotite; although some biotite laths are truncated by laths of chlorite, there is no unequivocal textural evidence to indicate that chlorite is an alteration product of biotite; chlorite also occurs in parallel intergrowths with trace amounts of muscovite in a microscopically narrow zone within the rock.

- 828: quartz-rich garnet-staurolite-biotite-muscovite-magnetite gneiss with trace chlorite; granuloblastic quartz grains vary in size from 0.1 to 3 mm, with an average of 1 mm; xenoblastic garnet and staurolite occur in ragged, granular "chains" resembling poorly developed atoll structures; lepidoblastic biotite and muscovite occur in layers rich in magnetite, though the latter mineral is also common adjacent to staurolite and garnet in quartz-rich areas; individual chlorite laths "cut" biotite laths, and also occur in ragged, spindle-shaped grains replacing biotite; hence chlorite is not part of the highest-grade paragenesis.
- 829: quartz-muscovite-garnet-staurolite-magnetite schist with minor chlorite and altered biotite; crenulated quartz-muscovite-magnetite schist, with quartz-rich layers containing poikiloblastic garnet and staurolite grains up to 2.5 mm in diameter; chlorite occurs as (i) an alteration product replacing biotite in muscovite-rich layers, (ii) as large (2.0 mm), radiating aggregates in muscovite-rich layers, and (iii) as alteration products of garnet, in narrow rims and filling cracks; the highest-grade stable assemblage is thus quartz-muscovite-biotite-garnet-staurolite-magnetite.
- 830: quartz-andalusite-muscovite-biotite-garnet-staurolite-magnetite schist, with trace amounts of chlorite; ovoid, poikiloblastic andalusite occurs in grains up to 10 mm in length, and encloses magnetite, biotite, quartz and garnet; smaller, poikiloblastic biotite laths, up to 4 mm in length, enclose quartz, magnetite and garnet; scattered, ragged, poikiloblastic staurolite grains occur in quartz-rich layers; these larger grains are set in a schistose matrix of granular quartz, magnetite, lepidoblastic muscovite and biotite, and "trails" of subidioblastic garnet grains up to 0.6 mm in diameter; locally, chlorite occurs in small, radiating aggregates cutting biotite, and in somewhat spindle-shaped intergrowths with biotite; although textural evidence is again equivocal, it is probable that chlorite has formed as a result of biotite alteration or breakdown.
- 831: quartz-rich andalusite-garnet-staurolite-biotite-muscovite-magnetite gneiss with trace amounts of chlorite; narrow, elongated "trails" of sieve-textured andalusite and staurolite, up to 12 mm in length, are set in a matrix of fine-grained, granular quartz, magnetite, rounded subidioblastic garnet and lepidoblastic muscovite and biotite; locally, trace amounts of spindle-shaped chlorite replaces biotite.
- 832: identical to 831, except that the rock is somewhat richer in mica, poorer in staurolite and garnet, and contain small, quartz- and albite-rich bands.



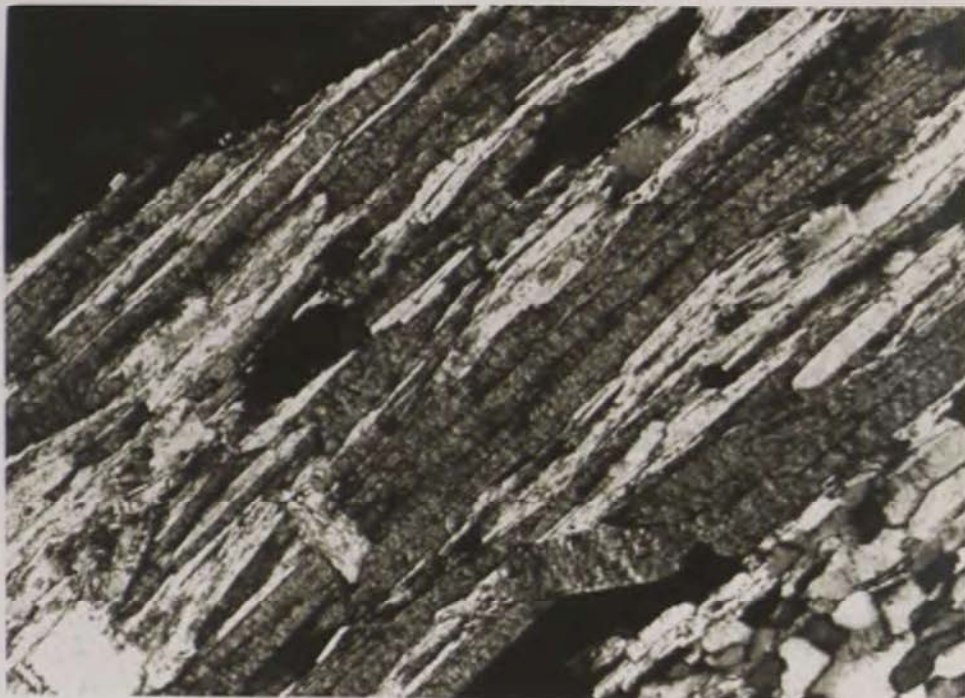
Biotite - chlorite relations, sample 826. Crossed nicols; field of view approximately 1.8 x 1.3 mm. From this texture, it cannot be ascertained whether the chlorite (darker, "smooth" laths) is replacing biotite (lighter, mottled laths), or whether both biotite and chlorite are in textural equilibrium.

Biotite - chlorite relations, sample 826. Crossed nicols; field of view approximately 1.8 x 1.3mm. Although chlorite encloses several laths of biotite, this is not unequivocal proof that chlorite is replacing biotite. It is also possible that the biotite laths extend to the edges of chlorite grains in the third dimension, so that this texture may result from an equilibrium intergrowth of biotite and chlorite.



Biotite - chlorite intergrowths, sample 827. Partly crossed nicols oriented at 45^0 ; field of view approximately $1.8 \times 1.3\text{mm}$. The biotite laths (dark) may be concentrated at the ends of chlorite grains (light), as in the top left hand corner of the photomicrograph, adjacent to a garnet crystal. In other domains, biotite laths form only parallel intergrowths with chlorite, similar to the parallel-sided laths of biotite in the top central portion of the photomicrograph.

Biotite - chlorite relations, sample 887. Crossed nicols; field of view approximately $4.7 \times 3.3\text{mm}$. A single crystal of biotite is surrounded by large grains of chlorite (at extinction). This chlorite is inferred to be primary, and has a deep blue - purple interference colour; it has an Mg value of 59.34 (table 21). The chlorite does not form intergrowths with biotite. The biotite crystal is partly replaced by secondary or retrograde chlorite. This chlorite has a steel gray interference colour, and has an Mg value of 18.64; it occurs only within biotite, and may completely pseudomorph smaller biotite grains.



Muscovite - biotite intergrowths, muscovite-biotite-quartz schist from Broken Hill, N.S.W. Crossed nicols; field of view approximately 0.7×0.5 mm. The relation of muscovite to biotite in this photomicrograph is similar to some chlorite - biotite relations. Although many workers would interpret chlorite in the same textural environment as the muscovite to be secondary, there is no evidence to suggest that the muscovite is retrograde. Hence this muscovite - biotite intergrowth may indicate that similar intergrowths of chlorite with biotite need not automatically be the result of retrograde reactions.

Muscovite - biotite intergrowths, same sample as above. Crossed nicols; field of view approximately 0.11×0.08 mm. There is no evidence to suggest that the muscovite is necessarily replacing biotite, yet many workers would interpret chlorite in the same textural environment as the muscovite to be secondary. Such textures are not conclusive by themselves, and should be interpreted with caution.

Muscovite - biotite intergrowths, muscovite-biotite-quartz schist from Broken Hill, N.S.W. Crossed nicols; field of view approximately 0.7 x 0.5 mm. The relation of muscovite to biotite in this photomicrograph is similar to some chlorite - biotite relations. Although many workers would interpret chlorite in the same textural environment as the muscovite to be secondary, there is no evidence to suggest that the muscovite is retrograde. Hence this muscovite - biotite intergrowth may indicate that similar intergrowths of chlorite with biotite need not automatically be the result of retrograde reactions.

Muscovite - biotite intergrowths, same sample as above. Crossed nicols; field of view approximately 0.11 x 0.08 mm. There is no evidence to suggest that the muscovite is necessarily replacing biotite, yet many workers would interpret chlorite in the same textural environment as the muscovite to be secondary. Such textures are not conclusive by themselves, and should be interpreted with caution.

	834	835	836	838	839	841	842	843	844	845	846	847	848	849
SiO ₂	59.34	55.13	55.32	56.36	57.58	50.00	56.36	57.99	43.56	58.11	61.06	44.32	56.57	44.38
TiO ₂	.76	.65	.74	.81	.80	.43	.66	.66	.47	.51	.35	.32	.76	.24
Al ₂ O ₃	17.94	16.10	17.74	20.19	19.55	9.70	15.00	16.36	11.90	11.91	7.22	6.95	17.00	5.27
Fe ₂ O ₃	6.60	9.12	6.02	6.63	6.21	17.64	9.79	8.64	19.51	10.83	14.10	25.51	7.46	27.57
FeO	2.08	3.38	2.31	3.10	2.97	10.45	6.11	5.28	9.57	8.23	8.93	11.69	5.20	9.32
MnO	.21	.35	.17	.13	.09	.66	.38	.29	.89	.61	.56	2.03	.26	.49
MgO	2.67	4.07	2.90	1.81	2.34	3.27	2.95	2.01	5.14	2.95	2.36	3.60	2.50	2.88
CaO	.28	.25	.21	.60	.94	1.73	.37	.28	1.51	.51	.86	1.74	.22	3.50
Na ₂ O	.35	.25	.23	.72	1.04	.16	.40	.33	.10	.19	.27	.22	.19	1.18
K ₂ O	5.35	4.44	5.37	5.54	4.92	3.01	3.99	4.46	1.61	2.68	.87	.02	4.69	1.44
P ₂ O ₅	.13	.13	.13	.13	.13	1.11	.18	.11	.61	.27	.45	.54	.13	1.20
H ₂ O ⁺	3.32	4.70	8.37	3.10	3.17	1.84	3.09	2.99	5.15	3.01	2.11	2.49	5.09	2.22
H ₂ O ⁻	.19	.59	.25	.24	.17	.10	.13	.15	.12	.11	.09	.06	.09	.08
TOTAL	99.22	99.16	99.76	99.36	99.91	100.10	99.41	99.55	100.14	99.92	99.23	99.49	100.16	99.77
Y ppm	32	39	32	34	36	31	21	23	82	23	18	21	27	27
Sr "	44	30	27	76	119	25	32	50	13	20	18	*	29	15
Zr "	146	135	154	164	164	106	145	141	105	126	83	62	156	45
U "	*	31	4	5	*	*	4	9	*	*	*	15	6	*
Rb "	385	351	345	364	383	375	333	260	171	238	78	*	406	79
Th "	19	32	29	13	35	3	13	9	11	17	5	15	12	4
Pb "	11	61	19	78	87	32	34	58	78	54	40	47	83	45
Ga "	24	23	31	34	31	16	19	24	20	22	8	15	32	15
Zn "	216	324	192	215	134	502	494	305 > 10000	521	512	728	387	714	
Cu "	19	546	89	14	24	43	43	56	72	23	112 > 10000	46	133	
Ni "	52	44	44	47	48	54	54	40	56	65	31	*	47	44
Cr "	105	109	115	116	123	64	95	106	80	70	53	45	121	44
V "	87	91	82	105	96	61	68	70	62	75	33	52	92	47
Ba "	640	333	493	982	789	185	649	1067	106	383	201	*	1969	92
Mg	69.59	66.22	69.12	51.00	58.41	35.81	46.26	40.43	48.91	38.99	32.02	35.44	46.15	35.52
Mg corr	122.98	111.07	108.35	96.50	95.95	69.87	75.51	72.01	92.04	61.03	61.93	96.79	70.74	250.44
O.R.	74.06	70.83	70.10	65.81	65.29	60.30	59.05	59.55	64.72	54.21	58.69	66.26	56.35	72.69

In this and other appendix tables, the following conventions are used:

* below the detection limit

Mg corr is equal to $\text{mol}(\text{MgO}/(\text{FeO} - \text{Fe}_2\text{O}_3 + \text{MgO}))$; this is an attempt to obtain the bulk-rock silicate Mg by correcting for magnetite content. Note that where some or all magnetite has been oxidized or weathered, the Mg corr value is too high. If the silicate minerals contain no appreciable Fe^{3+} , then the bulk-rock silicate Mg lies between Mg and Mg corr.

APPENDIX TABLE 4: Bulk-rock analyses of group one (high-iron) metapelitic rocks from the Jervois Range area. All the samples listed in appendix table 5, plus samples 828, 830, 831 and 832 (appendix table 3) also belong to this group.

	850	853	854	855	856	857	858	859	860	861	862	863	864	877
SiO ₂	56.52	63.73	58.43	56.33	58.99	57.56	44.63	58.65	65.00	59.95	35.29	67.22	36.28	61.38
TiO ₂	.70	.58	.78	.77	.83	.81	.43	.73	.33	.43	.13	.47	.13	.67
Al ₂ O ₃	15.59	13.70	18.27	19.00	19.16	19.34	10.91	16.89	10.26	11.14	2.65	7.63	3.30	14.52
Fe ₂ O ₃	9.38	8.08	7.92	1.37	3.40	7.13	20.45	7.73	5.06	7.61	52.54	6.16	48.53	8.09
FeO	5.03	6.26	2.23	7.98	7.61	2.63	11.02	3.12	10.95	10.95	2.91	5.30	4.90	8.43
MnO	.32	.46	.11	.21	.25	.14	.21	.13	1.26	.75	2.76	5.37	3.32	.18
MgO	2.50	.82	2.40	5.58	3.45	1.93	3.70	2.74	2.32	3.07	.45	2.75	.49	1.98
CaO	1.18	.15	.69	.19	.22	1.60	2.09	.20	.47	.26	.97	1.53	.79	.68
Na ₂ O	.74	.44	1.10	.78	.22	1.41	.87	.13	.69	.10	.01	.03	.01	.35
K ₂ O	5.05	3.56	4.52	3.74	3.72	4.11	2.34	4.99	1.62	2.61	.11	.07	.12	2.39
P ₂ O ₅	.31	.10	.16	.14	.15	.15	.92	.15	.07	.08	.62	.14	.50	.17
H ₂ O ⁺	2.64	1.87	3.32	3.38	1.28	2.96	1.96	3.80	1.45	2.10	.56	2.16	.66	.99
H ₂ O ⁻	.09	.07	.19	.14	.11	.23	.11	.31	.12	.12	.08	.23	.06	.04
TOTAL	100.05	99.82	100.12	99.61	99.59	100.00	99.64	99.56	99.60	99.17	99.08	99.05	99.09	99.27
Y ppm	24	6	23	30	30	33	38	33		14	28	11	27	
Sr "	26	11	69	6	"	147	119	30		6	89	"	112	
Zr "	140	177	165	153	178	160	92	162		69	28	97	33	
U "	3	10	5	"	5	5	8	22		5	"	43	"	
Rb "	291	1286	358	433	215	261	363	373		178	49	"	52	
Th "	28	3	9	4	26	7	10	11		3	26	100	38	
Pb "	41	48	13	5	9	47	53	10		1043	775	2536	503	
Ga "	26	21	32	30	29	28	30	29		28	16	24	15	
Zn "	349	754	180	170	170	121	406	209		2842	425	2946	589	
Cu "	32	129	18	12	17	9	36	302		1298	156	3132	217	
Ni "	50	31	55	54	54	38	71	43		37	41	47	34	
Cr "	110	78	102	114	129	116	61	99		58	18	71	14	
V "	70	67	85	93	105	90	127	92		61	38	80	34	
Ba "	712	344	825	733	739	981	339	1357		894	158	193	192	
Mg	46.98	18.93	64.74	55.49	44.69	56.68	37.44	61.02	27.41	33.32	21.61	48.08	15.13	29.51
Mg corr	84.62	35.77	145.27	57.46	50.28	120.19	78.38	107.90	32.29	42.10	-4.03	65.97	-5.44	42.42
O.R.	62.66	53.73	76.17	13.38	28.67	70.93	62.54	69.03	29.37	38.47	94.20	51.12	89.91	67.35

APPENDIX TABLE 5: Bulk-rock analyses of group one (high-iron) metapelitic rocks from the Jervois Range area. All the samples listed in appendix table 4, plus samples 828, 830, 831 and 832 (appendix table 3) also belong to this group.

	833	837	840	851	852	865	866	867	868	869	870	871	872	873
SiO ₂	61.59	58.36	57.76	57.21	59.92	44.41	58.40	59.80	61.02	61.42	57.84	57.30	56.63	57.19
TiO ₂	.85	.75	.77	.77	.80	.40	.72	.67	.74	.68	.68	.52	.64	.57
Al ₂ O ₃	19.55	17.11	18.16	18.25	18.78	32.95	19.28	19.92	19.42	17.93	20.06	21.81	20.00	22.55
Fe ₂ O ₃	5.21	4.25	5.30	5.42	3.66	2.62	3.96	4.00	3.58	3.52	5.41	4.89	2.80	2.27
FeO	1.77	4.16	3.18	4.12	4.92	.47	3.69	3.98	2.47	4.10	4.04	3.19	3.16	4.28
MnO	.04	.24	.19	.39	2.17	.37	.10	.07	.18	.08	.18	.18	.03	.04
MgO	1.50	2.93	3.02	3.08	1.10	.84	3.27	2.88	2.62	3.56	2.77	1.99	2.93	2.21
CaO	.15	2.71	1.22	.32	.39	1.57	.51	.83	.38	1.79	.15	.16	5.34	.75
Na ₂ O	.40	2.96	.94	.94	.13	1.26	.57	.92	.54	2.16	.44	.64	.30	1.21
K ₂ O	5.02	2.64	5.30	5.51	5.31	8.74	6.38	3.90	5.48	3.65	3.98	6.11	4.77	5.41
P ₂ O ₅	.15	.11	.13	.14	.13	1.19	.21	.14	.12	.11	.11	.03	.11	.04
H ₂ O ⁺	3.34	2.92	3.27	3.12	2.34	4.48	2.57	2.10	3.02	1.99	3.69	2.76	3.00	3.51
H ₂ O ⁻	.14	.30	.29	.10	.06	.12	.15	.15	.16	.08	.03	.03	.06	.07
TOTAL	99.71	99.44	99.53	99.37	99.72	99.42	99.81	99.36	99.73	101.07	99.38	99.61	99.77	100.10
Y ppm	31	37	26	33	34		26	32		31	30			33
Sr "	66	178	62	33	42		40	60		130	79			30
Zr "	167	160	161	170	164		133	129		150	149			141
U "	9	17	15	8	19		3	4		8	6			4
Rb "	273	398	347	351	335		280	222		199	261			176
Th "	11	10	15	20	33		15	12		15	24			23
Pb "	39	125	78	37	77		11	22		17	26			15
Ga "	31	26	28	28	28		31	31		26	30			32
Zn "	80	454	554	306	271		112	108		171	105			9
Cu "	19	417	11	16	213		8	55		86	65			15
Ni "	42	59	55	60	36		49	48		45	43			46
Cr "	106	117	107	114	126		103	103		93	87			113
V "	95	88	84	89	98		90	82		77	74			95
Ba "	1264	476	592	678	5227		762	659		1507	672			1159
Mg	60.17	55.66	62.87	57.13	28.50	76.11	61.24	56.33	65.41	60.75	48.21	52.65	62.30	47.93
Mg corr	127.34	69.91	87.13	76.55	37.46	189.87	75.34	70.19	84.46	71.61	70.08	78.18	73.32	54.73
O.R.	72.59	47.90	59.99	54.21	40.10	83.38	49.13	47.49	56.60	43.58	54.65	57.97	44.36	32.31

APPENDIX TABLE 6: Bulk-rock analyses of group two metapelitic rocks from the Jervois Range area.

	<u>874</u>	<u>875</u>	<u>876</u>	<u>878</u>	<u>1</u>	<u>2</u>	<u>3</u>
SiO ₂	57.52	58.26	60.86	62.73	58.9	50.7	54.9
TiO ₂	.56	.66	.75	.55	.78	.78	.78
Al ₂ O ₃	21.83	20.76	18.37	15.11	16.7	15.5	16.6
Fe ₂ O ₃	3.43	4.65	2.47	2.91	2.8	4.4	7.7
FeO	5.02	3.07	3.92	3.59	3.7	2.1	
MnO	.18	.19	.13	.19	.09	.08	12.01
MgO	2.15	2.00	2.84	2.61	2.6	3.3	3.4
CaO	.16	.10	4.63	8.21	2.2	7.2	.72
Na ₂ O	.47	.47	1.50	1.14	1.6	.8	1.3
K ₂ O	4.97	6.65	3.02	1.99	3.6	3.5	2.7
P ₂ O ₅	.14	.05	.15	.08	.16	.10	.72
H ₂ O ⁺	3.26	2.48	.99	.86	5.0	5.0	19.21
H ₂ O ⁻	.08	.04	.02	.04			
<u>TCTAL</u>	<u>99.77</u>	<u>99.48</u>	<u>99.65</u>	<u>100.01</u>			
<u>Mg</u>	43.29	53.73	56.36	56.45	55.61	73.69	
<u>Mg</u> corr	52.43	78.47	64.32	67.10	65.51	97.99	
O.R.	38.07	57.68	36.18	42.18	40.51	65.34	

APPENDIX TABLE 7: Bulk - rock analyses of metapelitic rocks from the Jervois Range area (874 - 878). Analyses 1 to 3 are average geosynclinal shale, platform shale, and pelagic clay, taken from the compilation of Wedepohl (1969).

- 833: andalusite-biotite-muscovite-quartz-magnetite schist; andalusite occurs in elongate, poikiloblastic grains up to 8 mm long, containing inclusions of quartz and lesser amounts of magnetite; the andalusite is partly or completely altered to fine-grained white-mica ("sericite"); biotite occurs in laths up to 3 mm long, with the cleavage directions at high angles to the schistosity defined by the muscovite; all the biotite crystals have been partly or completely replaced by retrograde chlorite.
- 834: crenulated cordierite-andalusite-muscovite-biotite-quartz-magnetite schist; "cordierite" occurs in xenoblastic grains up to 8 mm in maximum dimension; the cordierite is entirely altered to fine-grained aggregates of white-mica and chlorite ("pinite"), and biotite inclusions within these grains may be partly altered to chlorite; andalusite occurs in xenoblastic poikiloblasts up to 6 mm in maximum dimension, and contains inclusions of biotite and quartz; biotite occurs in the matrix in laths up to 3 mm long; some of these laths have been partly replaced by retrograde chlorite; trace amounts of garnet occur in the rock, in idiomorphs up to 0.3 mm in diameter; most of these have been partly pseudomorphed by iron oxides.
- 835: cordierite-muscovite-biotite-quartz-magnetite schist; "cordierite" occurs in rounded grains up to 5 mm in maximum dimension; all these grains have been altered to chlorite-rich aggregates ("pinite"); biotite occurs in laths up to 4 mm long; most of the biotite is pseudomorphed by retrograde chlorite; this rock is strongly weathered, and contains abundant oxides of iron along grain boundaries.
- 836: muscovite-rich cordierite-garnet-biotite-quartz-magnetite schist; "cordierite" occurs in rounded grains up to 1 cm in diameter, and contains abundant inclusions of quartz and lesser amounts of biotite; all the cordierite has been replaced by chlorite-rich alteration products, and most biotite inclusions have been replaced by retrograde chlorite; biotite occurs in the matrix in laths up to 1 mm long, and most of these have been altered to chlorite; garnet idiomorphs occur up to 0.8 mm in diameter, and most are partly pseudomorphed by chlorite.
- 837: quartz-rich cordierite-biotite-muscovite-plagioclase-magnetite schist; "cordierite" occurs in rounded poikiloblasts up to 11 mm in diameter, and contains inclusions of quartz, with lesser amounts of biotite and magnetite; the cordierite has been completely replaced by a pale-green alteration product; the biotite inclusions in some of these "cordierite" grains have been partly replaced by retrograde chlorite, whereas, in other grains, there is no visual evidence of the alteration of biotite inclusions; the biotite laths in the matrix are

unaltered; the average grainsize of both the quartz and plagioclase in the matrix is 0.2 mm in maximum dimension.

- 838: cordierite-biotite-muscovite-quartz-magnetite schist; "cordierite" occurs in elongate poikiloblasts up to 20 mm long, and contains inclusions of quartz, biotite and magnetite; the cordierite has been completely altered to "pinite", and some of the biotite inclusions have been partly replaced or rimmed by retrograde chlorite; other biotite inclusions show no visible alteration; minor amounts of biotite in the matrix occur in laths up to 1 mm long, and almost all of these have been replaced by retrograde chlorite.
- 839: cordierite-biotite-muscovite-quartz-magnetite schist; similar to sample 838 above, but contains more biotite, and has a larger proportion of unaltered biotite in the matrix.
- 840: fine-grained, banded schist; this rock contains bands up to 10 mm in thickness, with assemblages comprising quartz-K-felspar-muscovite-magnetite; quartz-chlorite-muscovite-magnetite⁺ garnet; quartz-chlorite-garnet-magnetite; quartz-biotite-muscovite⁺ garnet⁺ magnetite; epidote-quartz-garnet-magnetite; the rock is veined by calcite, and, adjacent to these veins, some biotite has been partly or completely replaced by retrograde chlorite, which differs optically from the inferred primary chlorite elsewhere in this sample.
- 841: fine-grained, magnetite-rich quartz-biotite-garnet-chlorite-muscovite schist; the largest grains in this rock are those of idioblastic garnet, up to 0.3 mm in diameter; muscovite occurs in fine-grained, sericite-like aggregates up to 0.1 mm in maximum dimension; primary chlorite occurs in minor amounts, and the rock also contains veins of (secondary) chlorite (adjacent to which some biotite grains are also altered to chlorite); trace amounts of retrogressed cordierite also occur in some domains of this rock.
- 842: cordierite-biotite-muscovite-quartz-magnetite schist, with minor amounts of garnet; this rock is similar to sample 838, except that "biotite" (retrograde chlorite) laths in the matrix may reach 10 mm in maximum dimension; biotite inclusions in "cordierite" have been entirely replaced by chlorite; and the sample contains garnet idioblasts up to 0.7 mm in diameter.
- 843: cordierite-biotite-muscovite-quartz-magnetite schist with minor amounts of garnet; identical to sample 842 above.
- 844: "chloritized" cordierite-biotite-muscovite-quartz-magnetite schist with minor amounts of garnet and apatite; this rock has been intensely altered, with chlorite replacing biotite (in porphyroblasts up to 8 mm in maximum dimension) and partly

replacing garnet (idioblasts up to 0.7 mm in diameter); cordierite has been replaced by chlorite-white mica aggregates; white-mica occurs in laths within the altered biotite, and a few laths occur along quartz/quartz grain boundaries; the rock is cut by veins of chlorite and adularia.

- 845: altered cordierite-andalusite-biotite-muscovite-quartz-magnetite schist, with minor garnet; sieve-textured andalusite occurs up to 12 mm in maximum dimension, with inclusions of quartz, magnetite, garnet and altered biotite; xenoblastic cordierite (up to 6 mm in maximum dimension) has been replaced by chlorite-white-mica aggregates ("pinite"); biotite laths (up to 6 mm in maximum dimension) have been replaced by retrograde chlorite having a purplish interference colour; smaller radiating aggregates of chlorite also occur in the rock, in places as "inclusions" within altered biotite; this chlorite has a brown interference colour, and may have been part of the (stable) highest-grade paragenesis, though the textural evidence is not conclusive; garnet occurs in idioblasts up to 0.5 mm in diameter, and some crystals have been partly pseudomorphed by chlorite with a purple interference colour.
- 846: fine-grained chlorite-garnet-biotite-muscovite-quartz-magnetite schist; garnet idioblasts occur up to 0.4 mm in diameter, and have the largest grain size of all the minerals in this rock; primary chlorite occurs in laths up to 0.3 mm long, and has a brownish-gray interference colour; some biotite occurs in intergrowths with this chlorite (as described in chapter 4), but other biotite grains, in chlorite-poor domains within the rock, are partly replaced by retrograde chlorite (spindle-shaped laths with a purple-blue interference colour); muscovite occurs in sericite-like aggregates, possibly replacing K-felspar grains.
- 847: "chloritized" garnet-biotite-chlorite-magnetite-quartz schist; this rock is rich in magnetite and garnet idioblasts; the garnet crystals occur up to 0.3 mm in diameter, and, in some domains, are partly pseudomorphed by chlorite; "biotite" is subordinate in volume, occurring in laths up to 2 mm long--these have commonly been replaced by chlorite with a purple-blue interference colour, but traces of spindle-shaped biotite laths remain in the pseudomorphs in some domains; minor amounts of chlorite occur in garnet-rich domains within the rock; this chlorite shows no textural evidence of retrograde origin, and has a brownish-gray interference colour--it is inferred to be primary (see table 17 for analyses of the two different chlorites).
- 848: "chloritized" cordierite-biotite-muscovite-quartz-magnetite schist with minor garnet and possible pseudomorphs after andalusite; this rock is similar to sample 844 with two exceptions:

(i) several "sericite"-rich aggregates occur up to 6 mm in maximum dimension, and possibly represent pseudomorphs after andalusite; (ii) this sample contains more primary matrix muscovite than sample 844.

- 849: magnetite-rich chlorite-quartz-muscovite schist with trace amounts of garnet and 2 cm-wide bands rich in apatite; magnetite is the most abundant mineral, occurring in octahedra up to 0.2 mm in maximum dimension; the magnetite is partly martitized; garnet idiomorphs occur up to 0.4 mm in diameter, but are almost completely pseudomorphed by retrograde chlorite (purple interference colour); matrix chlorite occurs in sub-idiomorphic grains up to 0.1 mm long; there is no textural evidence to suggest a secondary origin for the matrix chlorite; muscovite occurs in "sericite"-like aggregates, possibly replacing detrital feldspar.
- 850: muscovite-rich biotite-quartz-magnetite schist with trace amounts of primary chlorite, garnet and allanite; biotite laths (up to 1 mm long) completely altered to retrograde chlorite (purple interference colour); relatively unaltered garnet idiomorphs occur up to 0.2 mm in diameter; primary chlorite laths are brownish in interference colour; (see table 11 for analyses of the two different chlorites).
- 851: cordierite-biotite-muscovite-quartz-magnetite schist with minor garnet; "cordierite" occurs in ovoid porphyroblasts up to 6 mm in maximum dimension; the cordierite is completely altered to chlorite-rich aggregates; biotite in the matrix (up to 0.8 mm long) is partly altered to chlorite; garnet occurs in idiomorphs up to 0.5 mm in diameter, and may be partly altered to chlorite; the sample is cut by chlorite-calcite and chlorite-adularia veins.
- 852: garnet-muscovite-quartz-magnetite schist with minor biotite altered to chlorite; numerous spessartine-rich garnet idiomorphs occur up to 0.3 mm in diameter; the rock is rich in muscovite, occurring in laths up to 1 mm long; retrograde chlorite almost completely replaces biotite, and occurs in laths up to 0.4 mm long.
- 853: garnet-muscovite-biotite-quartz-magnetite schist, garnet occurs in idiomorphs up to 1 mm in diameter, and may be partly or completely pseudomorphed by retrograde chlorite; biotite laths occur up to 2 mm in maximum dimension, and most of these are partly or completely altered to retrograde chlorite, one 4 mm-wide layer in this rock contains trace amounts of elongate andalusite (?) crystals (up to 2 mm long), but these have been partly pseudomorphed by a dark brown, serpentine-like alteration product.

- 854: cordierite-biotite-muscovite-quartz-magnetite schist with possible primary chlorite; completely altered cordierite poikiloblasts occur in ovoid grains up to 8 mm in maximum dimension; these contain numerous rounded inclusions of quartz, and lesser amounts of altered magnetite and some muscovite laths; "biotite" flakes occur throughout the rock in crystals up to 5 mm in maximum dimension; these commonly lie with their (001) direction at high angles to the foliation defined by the matrix muscovite; all these biotite crystals are partly or completely (?) altered to retrograde chlorite and spindle-shaped laths of retrograde muscovite; smaller grains of chlorite, containing rounded inclusions of quartz similar to those found in the altered biotite, also occur throughout the rock; these grains show no direct evidence of retrograde origin, but their interference colours are similar to those chlorites demonstrably replacing biotite, suggesting that they may also be retrograde in origin; (see analyses of altered "biotite" and possible primary chlorite in table 14).
- 855: porphyroblastic andalusite-cordierite-biotite-muscovite-quartz-magnetite schist; large sieve-textured andalusite grains occur up to 18 mm in maximum dimension, though smaller grains with relatively few inclusions also occur; the majority of inclusions in andalusite are quartz grains, with lesser amounts of magnetite, biotite and ilmenite; cordierite occurs in irregular-shaped grain aggregates up to 11 mm in maximum dimension, and although much of the cordierite is altered along grain boundaries, unaltered cordierite is relatively abundant; these contain inclusions of quartz, altered biotite and muscovite-chlorite intergrowths; biotite occurs in subidioblastic grains up to 10 mm in maximum dimension, and contain inclusions of quartz; a few "trails" of chlorite laths occur in the rock, and these commonly cut through, or extend partly into, biotite; the replacement of biotite by chlorite indicates that the chlorite is retrograde in origin.
- 856: deformed, coarse-grained andalusite-biotite-garnet-quartz-magnetite schist, with minor muscovite; andalusite occurs in sheared, sieve-textured grains up to 40 mm in maximum dimension, containing inclusions of quartz, and lesser amounts of magnetite and small biotite laths (up to 0.8 mm long); biotite occurs in deformed grains up to 18 mm in maximum dimension, and contains inclusions of idioblastic garnet (up to 1.8 mm in diameter), rounded and ovoid quartz grains (average maximum dimension of 0.1 mm) and a few laths of muscovite up to 0.7 mm long; small muscovite laths also occur along some biotite/biotite grain boundaries; several radiating aggregates of retrograde chlorite (in laths up to 2 mm long) have replaced parts of some biotite grains.

- 857: deformed cordierite-biotite-muscovite-quartz-magnetite schist with trace amounts of primary chlorite; similar to sample 854 except that "cordierite" occurs in elongate grains up to 22 mm in length, and the inferred primary chlorite shares no textural characteristics with retrograde chlorite pseudo-morphing large biotite flakes; the primary chlorite occurs in small laths in muscovite-rich domains of the rock, and has a gray interference colour unlike retrograde chlorite which has a greenish-brown interference colour; the rock is also veined by relatively iron-rich chlorite; (see table 15 for analyses of primary and vein chlorite, and chlorite replacing biotite and cordierite).
- 858: magnetite-rich quartz-biotite schist with minor muscovite, altered cordierite (?) and retrograde chlorite; magnetite octahedra occur up to 0.7 mm in maximum dimension; sieve-textured cordierite (?) has been replaced by white-mica-rich aggregates; some biotite has been replaced by retrograde chlorite laths up to 1.2 mm in length; primary muscovite occurs in laths up to 0.8 mm long.
- 859: crenulated porphyroblastic cordierite-biotite-muscovite-quartz-magnetite schist, with inferred primary chlorite; "cordierite" occurs in elongate poikiloblasts measuring up to 24 mm in maximum dimension; the cordierite is altered to fine-grained, chlorite-rich aggregates, and contains numerous small inclusions of quartz, and lesser amounts of muscovite, biotite, magnetite, and iron oxides; "biotite" occurs in subidioblastic grains up to 5 mm in maximum dimension, and has been partly altered to thin, spindle-shaped, elongate laths of retrograde chlorite having a brownish-gray to purple interference colour; coarse-grained radiating aggregates of chlorite occur in both the "biotite" grains, and in biotite-free, muscovite-rich domains; this chlorite has a steel-gray interference colour, and laths of this mineral may be parallel, or at high angles, to both foliation in muscovite and cleavage direction in altered biotite; although some laths of this coarse-grained chlorite appear as though they replace both biotite and its spindle-shaped retrograde chlorite alteration product, similar laths of coarse-grained chlorite in muscovite do not replace biotite; it is thus inferred that the coarse-grained chlorite is primary, and laths of this mineral penetrating "biotite" parallel to the biotite (001) direction represent primary biotite-chlorite intergrowths as described in chapter 4.
- 860-864: These are the remaining samples from the set collected by W. A. Robertson (1959), and described by W. R. Morgan (1959). Since only minute amounts of sample were available, these were used for analyses, and the reader is referred to the work of Morgan (1959) for their description (sample numbers are included for reference).

- 860: garnet-biotite-quartz-magnetite schist with small amounts of biotite altered to chlorite (sample 4164, field no. JHA6).
- 861: garnet-biotite-quartz-magnetite schist (sample 4167, field no. JHA9).
- 862: garnet-quartz-magnetite schist with minor biotite (sample 4209, field no. JHA58).
- 863: garnet-magnetite-chlorite-quartz schist (sample 4214, field no. JHA101).
- 864: garnet-quartz-magnetite schist with minor biotite (no number available, but similar to sample 4209).
- 865: porphyroblastic garnet-muscovite schist, with minor apatite and tourmaline, and trace amounts of quartz; idioblastic garnet crystals occur up to 8 mm in diameter; these are almost inclusion-free, and contain only small rounded grains of quartz up to 0.3 mm in diameter; muscovite laths average 0.8 mm in length, and idioblastic apatite and tourmaline crystals average 0.4 mm in length.
- 866: muscovite-biotite-quartz-magnetite schist; mica laths average 0.8 mm in length, and the rock contains minor tourmaline and apatite.
- 867: crenulated andalusite-sillimanite-biotite-muscovite-quartz-magnetite schist; irregular-shaped, poikiloblastic andalusite occurs up to 10 mm in maximum dimension, and contains inclusions of quartz and lesser amounts of biotite; sillimanite (var. "fibrolite") occurs in curved trails, and appears to have preferentially replaced clusters of muscovite laths within bands of biotite; andalusite is not replaced by sillimanite.
- 868: very fine-grained chlorite-muscovite-biotite-quartz-magnetite schist; muscovite, biotite, and quartz occur in grains less than 0.02 mm in maximum dimension; magnetite octahedra are somewhat larger, and chlorite forms the largest grains, in laths up to 0.2 mm long; although single chlorite laths occur uniformly throughout the rock, they are also concentrated in clusters measuring up to 2 mm in maximum dimension, giving this rock a spotted appearance in the hand specimen.
- 869: fine-grained "spotted" andalusite-chlorite-biotite-muscovite-quartz-magnetite schist, with possible cordierite; andalusite occurs in irregular-shaped grains up to 0.8 mm in maximum dimension, rich in quartz inclusions; larger "clots" measuring up to 3 mm in maximum dimension are inferred to be cordierite aggregates; these contain numerous inclusions of micas, quartz

and magnetite, but no larger flakes of chlorite which occur in the "matrix"; matrix chlorite laths may reach 1.6 mm in length, and the rock also contains aggregates of magnetite grains measuring up to 1.5 mm in maximum dimension.

- 870: porphyroblastic andalusite-cordierite-chlorite-biotite-muscovite-quartz-magnetite schist; poikiloblastic andalusite occurs in irregular-shaped grains up to 3 cm in maximum dimension; these contain small inclusions of quartz, lesser amounts of magnetite and chlorite, and large laths of biotite measuring up to 3 mm in maximum dimension; these biotite inclusions themselves contain inclusions of quartz and chlorite, the latter in single laths or radiating aggregates; altered cordierite occurs in rounded grains up to 3 cm in diameter, and contains inclusions of quartz, magnetite and larger laths of chlorite, altered biotite and muscovite, as well as inclusions of chlorite-quartz-muscovite aggregates; the altered cordierite is zoned, with concentric chlorite-poor and chlorite-rich zones; the outermost cordierite alteration zone is rich in chlorite with a purplish interference colour; the matrix of this rock consists of fine-grained muscovite, quartz and magnetite, with larger flakes of chlorite, and relatively unaltered biotite, as well as several intergrowths of biotite and planar (not tapering) laths of chlorite; the chlorite in the matrix, in the andalusite, in the biotite inclusions in andalusite, and inclusions in the altered cordierite all have a brownish-gray interference colour; this chlorite is inferred to be primary, and part of the highest-grade paragenesis.
- 871: andalusite-muscovite-biotite-quartz-magnetite schist; andalusite occurs in several elongate grains measuring up to 1.8 mm in length, in muscovite-rich domains within this rock; a minor amount of biotite is altered to retrograde chlorite.
- 872: fine-grained chlorite-muscovite-biotite-quartz-epidote-magnetite schist with epidote and calcite veins.
- 873: chlorite-muscovite-quartz-magnetite schist with trace amounts of biotite; the matrix of this rock comprises fine-grained muscovite and quartz, with lesser amounts of magnetite and ilmenite; chlorite occurs in decussate aggregates measuring up to 7 mm in maximum dimension, and in dilatation cracks (with quartz); the decussate chlorite contains inclusions of muscovite and quartz; both these chlorites have a purplish interference colour; trace amounts of biotite occur in small laths in some quartz-rich domains, where this biotite has been altered, the resultant chlorite has a light grayish-blue interference colour; the decussate chlorite is inferred to belong to the highest-grade paragenesis muscovite-biotite-chlorite, since there is no evidence that the decussate chlorite is replacing another mineral.

- 874: chlorite-biotite-muscovite-quartz-magnetite schist; chlorite occurs as laths in this rock, of the same size as the biotite and muscovite (up to 2 mm long), and also occurs in a few decussate aggregates (up to 6 mm in maximum dimension), one of which contains a small amount of andalusite with quartz inclusions; although chlorite is never cut by laths of biotite, the chlorite does not appear to be replacing biotite.
- 875: fine-grained, crenulated muscovite-biotite-quartz-magnetite schist.
- 876: fine-grained, banded, biotite-quartz-magnetite schist with trace amounts of muscovite.
- 877: garnet-sillimanite-biotite-plagioclase-quartz-magnetite gneiss: this sample was collected in a stream bed north of the Jinka Plain, and is probably a xenolith brought to a higher level by the intrusion of granitic stocks in the Eurolly Bore area.
- 878: fine-grained biotite-quartz-magnetite schist.

	<u>879</u>	<u>880</u>	<u>881</u>	<u>882b</u>	<u>883</u>	<u>884</u>	<u>885</u>	<u>886</u>	<u>887</u>	<u>888</u>	<u>889</u>
SiO ₂	27.98	48.49	21.31	47.59	45.82	43.96	49.23	27.90	41.06	64.76	23.05
TiO ₂	1.71	1.08	1.70	1.02	1.12	.68	1.53	.12	.36	.07	.33
Al ₂ O ₃	13.93	15.09	19.93	13.42	13.96	1.69	13.45	20.48	16.22	11.24	20.29
Fe ₂ O ₃	19.45	5.70	13.03	8.21	9.14	4.00	3.51	8.76	7.41	2.13	7.01
FeO	18.40	14.55	22.72	16.32	16.08	23.61	16.87	26.41	20.96	13.04	31.47
MnO	1.07	1.94	.25	.20	.10	.80	.46	.81	.59	.58	.79
NiO	7.80	6.04	10.78	5.88	5.76	3.30	7.12	6.69	6.04	3.56	7.49
CaO	.28	.69	.12	.08	.11	1.31	.48	.37	.31	.15	.36
Na ₂ O	.56	.02	.04	.03	.10	.11	.02	1.21	.07	.51	.02
K ₂ O	.03	.07	.01	.03	.07	.95	.05	.00	.93	.53	.04
P ₂ O ₅	.09	.11	.19	.08	.13	.13	.11	.07	.19	.03	.17
H ₂ O ⁺	7.56	5.56	9.55	6.62	7.85	2.62	6.24	6.38	5.46	3.29	8.56
H ₂ O ⁻	.13	.23	.16	.13	.19	.11	.19	.41	.15	.08	.19
<u>TOTAL</u>	<u>99.54</u>	<u>99.57</u>	<u>99.79</u>	<u>99.61</u>	<u>100.43</u>	<u>99.27</u>	<u>99.26</u>	<u>99.34</u>	<u>99.75</u>	<u>99.97</u>	<u>99.77</u>
Y ppm	17	28	23	12	8	21	18	112	78	93	
Sr "	*	*	*	7	*	6	*	*	*	*	
Zr "	83	63	96	61	70	127	153	253	161	158	
U "	*	*	*	2	2	3	*	16	5	7	
Rb "	*	*	*	*	*	284	*	*	142	79	
Th "	5	33	5	*	*	11	12	165	33	30	
Pb "	12	30	10	*	23	12	27	74	29	6	
Ga "	31	15	32	20	18	28	26	32	34	18	
Zn "	546	296	542	378	378	453	225	436	490	187	622
Cu "	335	144	219	98	86	17	14	581	5263	21	395
Ni "	309	239	277	141	145	65	128	12	*	7	7
Cr "	423	393	481	289	287	115	518	16	56	5	*
V "	476	123	253	204	192	103	283	30	71	9	19
Sc "	61	37	57	42	43	13	36	7	11	*	4
Nb "	6	4	6	3	3	13	8	20	10	20	25
Ba "	*	*	365	56	27	32	*	18	139	141	52
<u>Mg</u>	43.04	42.53	45.82	39.11	38.97	19.95	42.93	31.11	33.94	32.74	29.79
<u>Mg</u> corr	59.03	47.32	53.27	45.36	46.18	21.24	45.36	34.67	37.92	34.44	32.04
O.R.	48.75	26.06	43.04	31.16	33.84	13.23	15.77	22.99	24.13	12.81	16.70

APPENDIX TABLE 8: Bulk-rock analyses of chlorite - quartz ± garnet schists from the Jervois Range area.

	890	891	892	893	894	(1)	(2)	(3)	(4)	(5)	(6)	(7)	(8)	(9)
SiO ₂	52.04	41.14	44.74	26.90	27.50	64.72	27.15	60.12	32.15	53.14	29.77	60.86	45.60	49.38
TiO ₂	1.36	1.28	.97	2.02	.71	1.21	.76	.30	.88		4.66	.68	.88	.74
Al ₂ O ₃	14.31	17.10	19.18	21.31	20.40	8.76	18.45	11.60	22.05	29.43	29.79	12.53	17.47	15.25
Fe ₂ O ₃	.99	3.25	2.18	2.45	3.84	.60	8.06	1.00	3.32	3.77	7.23	1.49	1.61	3.39
FeO	22.29	25.90	19.84	23.24	21.93	6.24	16.91	14.47	23.52	7.85	24.31	13.68	21.78	18.15
MnO	1.16	.77	.05	.71	.28	.05	1.45	.06	.26		.18	.32	.32	.25
MgO	2.92	5.65	9.57	12.16	15.09	11.35	15.23	7.00	8.72	1.11	1.06	3.25	6.74	7.61
CaO	1.63	.71	.14	1.17	.46	.36	.78	.68	.45	.09	.54	.43	.66	.66
Na ₂ O	.03	.69	.17	.61	.39	.01	.06	.16		.10	.34	.50	.44	1.00
K ₂ O	.03	.02	.73	.07	.02	.02	.04	.32		.20	.21	.04	.16	.10
P ₂ O ₅	.12	.04	.03	.23	.02	.35	.22	.07	.02			.00	.12	.06
H ₂ O ⁺	2.22	2.91	2.12	8.77	8.82	5.82	9.75	4.20	7.77	4.50	1.67	3.90	4.52	1.40
H ₂ O ⁻	.11	.09	.10	.22	.32	.04	.64	.18	.45		.10			
TOTAL	99.21	99.55	99.82	99.86	99.78	99.53	99.50	100.16	99.59	100.19	99.86	99.68	100.30	99.99
Y ppm	46	24	14											
Sr "	.	8	.											
Zr "	86	71	67											
U "	.	.	.											
Rb "	.	.	45											
Th "	9	.	8											
Pb "	28	41	62											
Ga "	16	19	22											
Zn "	135	349	154											
Cu "	72	128	23											
Ni "	142	105	170											
Cr "	231	351	168											
V "	361	301	372											
Sc "	36	41	65											
Nb "	3	6	3											
Ba "	37	.	29											
Mg	18.93	28.00	46.23	48.26	55.09									
Mg corr	19.24	29.19	47.49	49.47	57.11									
O.R.	3.84	10.15	9.00	8.66	13.61									

APPENDIX TABLE 9: Bulk-rock analyses of chlorite - quartz ± garnet rocks, and other rocks falling essentially within the compositional system SiO₂ - Al₂O₃ - FeO - MgO - H₂O - (MnO - Fe₂O₃). The first five were analysed as part of this work, the remainder are listed here for reference, and correspond to the assemblages listed in table 19.

	(10)	(11)	(12)	(13)	(14)	(15)	(16)	(17)	(18)	(19)	(20)	(21)	(22)	(23)
SiO ₂	73.65	68.54	77.25	33.6	64.9	48.09	47.09	56.6	60.1	75.4	51.71	48.25	30.83	28.73
TiO ₂	1.27	1.48	.21	2.0	.4	1.05	.33	.3	.2	.2	.04	.45	.63	.52
Al ₂ O ₃	16.43	9.05	7.95	14.3	9.8	18.75	18.43	14.4	12.6	12.2	32.49	15.09	19.66	18.02
Fe ₂ O ₃	.48	.75	.18	4.4	.1	2.04	1.75	6.6	4.9	1.7	.12	1.42	8.57	19.82
FeO	.17	11.55	5.99	38.1	10.0	17.55	18.99	13.1	10.5	2.9	.58	14.42	20.50	16.49
MnO	2.11	.16	.04	.27	.1	.53	.21	1.4	.4	tr	.01	.17	.26	.26
MgO	1.01	5.46	6.27	5.79	10.7	8.76	9.36	6.4	8.7	5.9	14.26	17.81	16.52	12.11
CaO	.26	.84	.15	.74	.9	.58	.37	.5	.4	tr	.05	.13	.32	.47
Na ₂ O	.74	.21	.43	.37	.1	.35	.56	.1	.9	.4		.16	.03	.23
K ₂ O	1.58	.25	.98	.21	.2	.29	.70	.3	.3	.6		.88	.04	.12
F ₂ O ₅	.10	.67			.1	.14	.02							
H ₂ O ⁺	2.13	.50	.63		2.3	1.59	1.97	.3	.9	.6	.87	1.46	2.80	2.68
H ₂ O [*]	.09	.08	.13			.16	.12					.00	.18	.22
TOTAL	100.02	99.54	100.21	99.78	99.6	99.88	99.90	100.0	99.9	99.9	100.26	100.24	100.54	99.69

APPENDIX TABLE 10: Bulk - rock analyses of metamorphic rocks which fall essentially within the compositional system SiO₂ - Al₂O₃ - FeO - MgO - H₂O - (MnO - Fe₂O₃). These analyses were compiled from published works, and correspond to the assemblages listed in table 19.

	<u>(24)</u>	<u>(25)</u>	<u>(26)</u>	<u>1</u>	<u>2</u>	<u>3</u>	<u>4</u>
SiO ₂	41.50	39.79	39.64	40.97	52	32	42.56
TiO ₂	.36	1.51	.65	.65	.4	.3	2.18
Al ₂ O ₃	22.71	18.29	32.04	12.03	8	15.5	19.38
Fe ₂ O ₃	2.33	3.83	9.53	6.09	20	34	21.52
FeO	5.38	14.50	8.49	26.08			
MnO	.08	.13	.08	.01	.22		
MgO	24.87	19.19	6.91	4.18	8.3	4	8.24
CaO	.09	.28	.31	.10	.5		.72
Na ₂ O	.06	.45	.07	.10	.3	.2	1.08
K ₂ O	.85	.32	.18	.50	.5	.5	.02
P ₂ O ₅	.05	.21	.01	.03			
H ₂ O ⁺	1.21	1.21	1.76	7.90	11	13.5	4.20
H ₂ O ⁻	.13	.15	.37	1.43	.4		
<u>TOTAL</u>	<u>99.62</u>	<u>99.88</u>	<u>100.04</u>	<u>100.07</u>			<u>99.90</u>

APPENDIX TABLE 11: Bulk - rock analyses of metamorphic, sedimentary and hydrothermally altered rocks which lie essentially within the compositional system SiO₂ - Al₂O₃ - FeO - MgO - H₂O - (MnO - Fe₂O₃).

Samples (24) to (26) correspond to the assemblages listed in table 19.

Sample 1 is a "greenalite" shale from the Roper Bar area, N.T. (Cochrane and Edwards, 1960).

Samples 2 and 3 are chamosite - rich separates from deltaic sediments (Porrenga, 1965).

Sample 4 is a hydrothermally altered basalt from Iceland (Kristmannsdottir, 1975).

- 879: crenulated chlorite-quartz-garnet-magnetite schist; crenulated layers of chlorite laths (up to 0.8 mm in length) containing abundant magnetite octahedra (up to 0.5 mm in maximum dimension) alternate with quartz-chlorite-garnet-magnetite layers; the garnet porphyroblasts are rounded, and occur up to 4.8 mm in diameter; garnet contains inclusions of irregularly-shaped quartz grains and grain aggregates, and smaller magnetite octahedra; in the matrix, the quartz occurs in xenoblasts up to 0.6 mm in maximum dimension; and quartz/quartz grain boundaries range from planar to strongly curvilinear; both types of layers may vary in thickness from 5 to 20 mm.
- 880: chlorite-quartz-garnet-magnetite schist; similar to sample 879 above, but richer in quartz; the chlorite-magnetite layers tend to be thinner and more discontinuous, commonly wrapping around the garnet porphyroblasts; magnetite is not as abundant as in sample 879, and the garnet crystals occur more uniformly throughout the sample; some of the garnet porphyroblasts are lacking in crystal faces, and some garnet porphyroblasts have irregular shapes.
- 881: fine-grained, crenulated chlorite-magnetite schist with trace amounts of quartz; maximum grain size is 0.4 mm (magnetite) and chlorite laths average 0.2 mm in length; quartz occurs in isolated lenses less than 1 mm in thickness; minute grains of zircon are abundant, and these have well-defined pleochroic haloes in chlorite.
- 882b: chlorite-quartz-magnetite schist; quartz commonly occurs in elongated grains up to 0.4 mm in length, and quartz grains are clustered into chlorite-poor lenses up to 3 mm in thickness; chlorite laths do not exceed 0.6 mm in length, and commonly form quartz-deficient lenses up to 5 mm in thickness and 8 cm in length; magnetite, and lesser amounts of ilmenite occur uniformly throughout the rock.
- 883: chlorite-quartz-garnet-magnetite schist; identical to sample 882 above, except that the rock contains a few garnet porphyroblasts; these are rounded, with diameters of the order of 1 cm, and may exhibit crystal faces, especially in chlorite-rich domains; the garnets contain numerous single- and polyphase inclusions of quartz and magnetite.
- 884: altered garnet-biotite-chlorite-quartz-magnetite schist; numerous garnet porphyroblasts occur in this rock, most of them less than 1 mm in diameter, but some elongate crystals reaching 3 mm in length; many garnet crystals contain numerous quartz inclusions (< 0.1 mm in maximum dimension) and many of these crystals occur in interlocking clusters; the matrix of this rock comprises biotite and quartz, with

lesser amounts of magnetite, in grains up to 1 mm in maximum dimension; many biotite laths are partly or completely replaced by spindle-shaped laths of chlorite, with or without white mica, whereas other biotite laths and unaltered biotite aggregates are cut by fan-shaped clusters of chlorite laths, the latter reaching 3 mm in length; small garnet fragments in the matrix are rimmed by chlorite, and chlorite also replaces garnet along some cracks; chlorite + quartz fill dilatation cracks in garnet; veins containing quartz, fluorite, andularia, calcite and tourmaline occur throughout the rock, and the degree of biotite alteration is related to the proximity to these veins; the observed bulk-composition of this rock has been derived, at least in part, by the metasomatic removal of K, and the addition of at least H_2O , from a garnet-biotite-quartz-magnetite rock.

- 885: crenulated chlorite-quartz-garnet-magnetite schist; elongate garnet poikiloblasts occur up to 8 mm in length, and contain numerous single- and multi-grain aggregate inclusions of quartz, with subordinate amounts of magnetite and ilmenite; many of the garnet crystals have sieve structures; the matrix comprises subangular quartz grains and chlorite laths (with maximum dimensions of 0.3 and 0.2 mm respectively), and lesser amounts of magnetite and ilmenite; trace amounts of biotite are also present (in laths up to 0.5 mm long), but these have been almost completely altered to very fine-grained aggregates rich in oxides of iron.
- 886: chlorite-garnet-magnetite schist; garnet porphyroblasts occur up to 7 mm in diameter, and some of these form interlocking clusters up to 22 mm in maximum dimension; the garnet crystals contain few inclusions, these being single grains and grain aggregates of quartz, chlorite and magnetite, with the largest aggregate inclusion measuring 0.8 mm in maximum dimension; the matrix comprises chlorite, in laths up to 2 mm long, with lesser amounts of magnetite; trace amounts of biotite occur in laths up to 10 mm long, but most of these have been replaced by spindle-shaped chlorite and white-mica grains; the matrix chlorite (primary) has a typical Berlin-blue interference colour, whereas the secondary chlorite replacing biotite has a steel-gray interference colour.
- 887: chlorite-quartz-garnet-biotite-magnetite schist; slightly elongate garnet porphyroblasts occur up to 6 mm in length; these contain inclusions comprising single grains and grain aggregates of quartz, chlorite and magnetite, with the largest aggregate inclusion measuring 0.8 mm in maximum dimension; the matrix comprises chlorite laths up to 1.2 mm long, subangular quartz grains up to 0.8 mm in maximum dimension, magnetite octahedra, and several laths of biotite up to 2 mm long; the biotite laths commonly cut the foliation defined by the matrix

chlorite, and some biotite crystals are partly or completely pseudomorphed by secondary (retrograde!) chlorite; as in sample 886 above, the chlorite replacing biotite occurs in spindle-shaped laths which are commonly parallel to the cleavage in biotite; in addition, the secondary chlorite has a steel-gray interference colour, whereas the primary matrix chlorite has a purplish Berlin-blue interference colour (see table 21 for microprobe analyses of the two types of chlorite).

- 888: chlorite-quartz-garnet-biotite-magnetite schist; similar to sample 887 above, but richer in quartz and poorer in chlorite and biotite.
- 889: crenulated chlorite-quartz-garnet-magnetite schist; garnet occurs in well-formed porphyroblasts of around 2.6 cm diameter; these contain few inclusions, comprising mainly magnetite (the largest grain being 1 mm in maximum dimension), with lesser amounts of quartz and chlorite; the matrix comprises mainly fine-grained chlorite (in laths less than 0.3 mm long), with aggregates of larger, decussate chlorite crystals (up to 1.5 mm long) occurring around clusters of magnetite octahedra and less-common aggregates of quartz grains; some of these decussate chlorite aggregates may be lens-shaped, with a thickness of 5 mm and a length of 22 mm.
- 890: chlorite-quartz-garnet-ilmenite schist from Copperfield, near Menzies, Western Australia; rounded and elongate poikiloblasts of garnet occur up to 8 mm in maximum dimension; these contain numerous inclusions of elongate quartz grains (with an average maximum dimension of 0.05 mm) and minute amounts of chlorite and ilmenite; the matrix is fine-grained, and comprises granular quartz and chlorite laths (both with an average maximum dimension of 0.1 mm) with minor amounts of ilmenite in rod-like crystals.
- 891: garnet-gedrite-cordierite-chlorite-magnetite hornfels with minor quartz, from Koolanooka, Western Australia; garnet occurs in rounded porphyroblasts up to 3 mm in diameter, and contains inclusions of quartz, plagioclase (partly "sericitized"), chlorite and magnetite; the largest inclusions are those of magnetite, reaching 0.2 mm in maximum dimension; the matrix comprises irregular-shaped grains of cordierite (up to 5 mm in maximum dimension) enclosing single crystals and radiating aggregates of idoblastic gedrite crystals (up to 3 mm long) and very minor amounts of quartz; both the gedrite and cordierite contain numerous inclusions of magnetite; the gedrite and cordierite are cut by single laths, rosettes, and fan-like aggregates of retrograde chlorite; chlorite also mantles some garnet crystals, but does not grow into garnet as it does into gedrite and cordierite.

- 892: garnet-cordierite-gedrite-biotite hornfels, from Koolanooka, Western Australia; a few garnet porphyroblasts occur in this rock (up to 3 mm in maximum dimension); these contain inclusions of chlorite laths and radiating needles of gedrite (up to 0.4 mm long); the matrix comprises a mosaic of cordierite grains (up to 1.5 mm in maximum dimension), enclosing rosettes of acicular gedrite (up to 1 mm long); minor amounts of biotite occur in subidioblastic grains (up to 0.3 mm long) in some domains within this rock; small magnetite grains are common throughout the sample.
- 893: chlorite-garnet-magnetite schist with minor labradorite and quartz, from the Thackaringa-Pinnacles Retrograde Shear Zone, Broken Hill, New South Wales; well-formed garnet porphyroblasts occur up to 25 mm in diameter; these contain a few inclusions comprising single grains and grain aggregates of quartz, chlorite and magnetite, the largest aggregate being 0.6 mm in maximum dimension; the matrix comprises chlorite, in laths up to 1 mm long, with minor amounts of idioblastic labradorite grains (up to 3 mm long), subangular quartz grains (up to 0.8 mm in maximum dimension) and magnetite; trace amounts of biotite occur in the rock, and some domains contain a few large grains of chlorite and magnetite (each up to 4 mm in maximum dimension).
- 894: chlorite-garnet schist, from Perdignano, Italy; insufficient sample available, no thin section cut; rock is the same as the one described by Emiliani and Venturelli (1972); note that the bulk-composition may be biased toward garnet or chlorite composition.

	<u>895</u>	<u>896</u>
SiO ₂	61.46	37.83
TiO ₂	.88	.44
Al ₂ O ₃	17.27	38.45
Fe ₂ O ₃	1.39	.93
FeO	3.82	2.86
MnO	.12	.02
MgO	4.87	11.38
CaO	3.75	.05
Na ₂ O	4.85	.88
K ₂ O	.14	5.48
P ₂ O ₅	.25	.01
H ₂ O ⁺	.46	.79
H ₂ O ⁻	.12	.03
<u>TOTAL</u>	<u>99.38</u>	<u>99.15</u>
Y ppm	21	7
Sr "	304	*
Zr "	81	320
U "	7	10
Rb "	*	188
Th "	*	28
Pb "	11	*
Ga "	21	20
Zn "	22	28
Cu "	9	*
Ni "	49	84
Cr "	83	14
V "	130	134
Ba "	303	1522
<u>Mg</u>	69.44	87.64
<u>Mg</u> corr	73.10	89.26
O.R.	24.67	22.64

APPENDIX TABLE 12: Bulk - rock analyses of host rocks at the cordierite-rich enclave locality.

- 895: garnet-gedrite-plagioclase-quartz-gneiss; garnet occurs as rounded and embayed porphyroblasts up to 6 mm in diameter; these contain rounded and elongate inclusions of quartz and quartz aggregates up to 1.1 mm in maximum dimension; the garnet is commonly cut by veins of secondary chlorite and opaque iron oxides; the garnet composition is $X_{Fe} = 0.60$, $X_{Mg} = 0.30$, $X_{Mn} = 0.04$, $X_{Ca} = 0.06$; gedrite occurs in idioblastic crystals up to 8 mm long, it is pleochroic (pale yellow, brownish-gray, gray) and may contain a few inclusions of quartz and biotite; gedrite contains 15.73% Al_2O_3 , and has Mg equal to 56.7, with $Al^{iv} = 1.68$ and $Al^{vi} = 1.02$ per 23 oxygens; the matrix comprises xenoblastic to subidioblastic plagioclase ($An = 29.6\%$) up to 2 mm in largest dimension, and smaller, more rounded grains of quartz up to 1.1 mm in largest dimension; the planar alignment of the gedrite imparts a weak foliation and a well-defined lineation to this rock.
- 896: kyanite-phlogopite schist; kyanite porphyroblasts occur in idioblastic to subidioblastic crystals up to 16 mm long; these may contain phlogopite inclusions in laths up to 1.2 mm long, as well as minute rods of rutile and rounded zircon grains, phlogopite occurs in idioblastic crystals, with the length of laths ranging from 0.6 to over 12 mm; the phlogopite has Mg equal to 86.1, with $Al^{iv} = 2.58$ and $Al^{vi} = 1.02$ per 22 oxygens; the subparallel alignment of both phlogopite and kyanite defines a weak schistosity and lineation; in hand specimens, the kyanite is commonly colourless, but, in some specimens, the kyanite is an intense blue in colour, with a Cr_2O_3 content of approximately 0.16%.

	<u>897</u>	<u>898</u>	<u>899</u>
SiO ₂	52.89	51.50	51.46
TiO ₂	1.31	1.22	1.40
Al ₂ O ₃	22.43	23.07	21.35
Fe ₂ O ₃	1.53	1.58	2.07
FeO	6.66	5.50	5.38
MnO	.09	.07	.04
MgO	6.66	6.87	7.33
CaO	2.37	2.11	2.27
Na ₂ O	4.97	4.31	4.38
K ₂ O	.76	2.15	2.72
P ₂ O ₅	.08	.11	.07
H ₂ O ⁺	.70	.75	1.14
H ₂ O ⁻	.08	.16	.09
<u>TOTAL</u>	<u>99.95</u>	<u>99.40</u>	<u>99.70</u>
Y ppm	44	87	64
Sr "	221	206	207
Zr "	316	211	391
U "	4	9	7
Rb "	30	96	125
Th "	32	30	17
Pb "	11	30	9
Ga "	*	31	27
Zn "	83	81	88
Cu "	*	*	*
Ni "	66	91	97
Cr "	202	189	180
V "	112	165	164
Ba "		313	399
<u>Mg</u>	66.13	69.01	70.83
<u>Mg corr</u>	68.77	71.89	74.60
O.R.	18.46	20.54	25.72

APPENDIX TABLE 13: Bulk-rock analyses of the cordierite-, garnet- and gedrite-bearing granulite from Irindina Ck.

- 897: gedrite-sillimanite-phlogopite-oligoclase-quartz granulite; single subidioblastic gedrite grains occur up to 12 mm in length, and smaller grains of gedrite commonly occur in elongate aggregates up to 8 mm in length; sillimanite occurs as trails of aligned, elongate crystals up to 2.5 mm in length; these trails cut through gedrite aggregates, and may mantle the larger, isolated gedrite crystals, but do not extend into the leucocratic matrix; sillimanite also occurs as inclusions in gedrite, and as small (< 0.1 mm long) idioblastic grains along cracks in gedrite; phlogopite occurs in idioblastic to subidioblastic laths up to 3 mm in length, uniformly distributed throughout the rock; very rare (altered?) cordierite grain aggregates occur in this sample; these are up to 2 mm in maximum dimension, and contain numerous inclusions of sillimanite, with lesser amounts of gedrite, phlogopite and allanite; although the cordierite goes to extinction under crossed nicols, it has a definite yellow interference colour (unlike other cordierite grains from cordierite-rich rocks in this locality); the cordierite has altered to minute, pale green laths that are almost isotropic along grain boundaries with phlogopite, but cordierite/gedrite and cordierite/sillimanite grain boundaries are free of these alteration products; the leucocratic matrix comprises xenoblastic grains of quartz and oligoclase, each of which may occur up to 6 mm in maximum dimension; grain boundaries between matrix minerals and gedrite, phlogopite and sillimanite tend to be planar, whereas quartz/quartz, quartz/oligoclase and oligoclase/oligoclase grain boundaries are commonly curvilinear with local concentrations of minute laths of what appear to be phlogopite; zircon, rutile and allanite are present in small amounts, but magnetite and ilmenite are rare; a weak gneissosity is defined by the sub-parallel alignment of sillimanite trails, elongate gedrite grains and the larger phlogopite laths.
- 898: gedrite-sillimanite-phlogopite-oligoclase-quartz granulite; similar to sample 897 above, but richer in phlogopite and poorer in gedrite.
- 899: garnet-cordierite-phlogopite-sillimanite-oligoclase-quartz granulite; before crushing for analysis, this sample measured approximately 8 x 8 x 10 cm, and contained a single garnet porphyroblast, 3.4 cm in diameter; in thin section, the garnet contains inclusions of phlogopite laths up to 2 mm in length, acicular sillimanite crystals of similar length, and rounded rutile grains measuring 0.8 mm in maximum dimension; in addition, the garnet is veined by retrograde chlorite and biotite, the latter having a pale green colour, unlike the brownish phlogopite; the garnet grain boundary is embayed, and several fragments of garnet (measuring up to 1 mm in maximum dimension) are isolated from the porphyroblast by

grains of quartz and oligoclase; the garnet porphyroblast is mantled by a zone measuring from 1 to 4 mm in width, rich in phlogopite laths, with minor amounts of quartz, oligoclase and sillimanite; the phlogopite-rich zone is mantled in turn by an 8 mm-wide zone rich in cordierite, with lesser amounts of quartz, oligoclase, phlogopite and very minor sillimanite; the cordierite occurs in subangular grains measuring up to 8 mm in maximum dimension, and is altered along cracks and grain boundaries to very fine-grained aggregates of white-mica and chlorite; the cordierite contains single- and polyphase inclusions of quartz, oligoclase and phlogopite, and several polyphase inclusions contain fragments of relict kyanite; some phlogopite laths, both within and adjacent to cordierite, have been partly or completely replaced by retrograde chlorite; the rest of the sample comprises quartz, oligoclase and phlogopite, with a few small (< 1 mm) gedrite idioblasts, and a few patches of chlorite- and white mica-rich alteration products (< 2 mm in diameter) that may have replaced cordierite or an aluminosilicate; small amounts of magnetite are present, accompanied by very minor ilmenite (or in several domains, by rutile), and allanite and zircon are also present in minute amounts.

	<u>900</u>	<u>901</u>	<u>902</u>
SiO ₂	45.54	38.36	40.52
TiO ₂	1.30	.36	.48
Al ₂ O ₃	8.86	28.88	27.98
Fe ₂ O ₃	2.46	7.08	6.47
FeO	12.01	.08	.48
MnO	.31	.09	.12
MgO	21.17	2.01	1.00
CaO	6.99	21.84	21.17
Na ₂ O	.59	.49	.32
K ₂ O	.06	.07	.04
P ₂ O ₅	.15	.23	.12
H ₂ O ⁺	.47	.42	.41
H ₂ O ⁻	.05	.06	.07
<u>TOTAL</u>	<u>99.96</u>	<u>99.97</u>	<u>99.18</u>
Y ppm	31	23	13
Sr "	7	1168	1550
Zr "	92	64	97
U "	*	11	15
Rb "	*	*	*
Th "	*	11	*
Pb "	5	28	27
Ga "	*	*	38
Zn "	132	9	9
Cu "	33	28	22
Ni "	679	27	18
Cr "	661	21	13
V "	211	161	199
Ba "	*	*	*
<u>Mg</u>	75.86	97.82	78.79
<u>Mg</u> corr	77.58		
O.R.	15.56	98.76	92.38

APPENDIX TABLE 14: Bulk - rock analyses of granulites at Mt Mary.

- 900: weakly gneissic bronzite-olivine-hornblende-spinel-chlorite granulite; bronzite commonly occurs in subsequent poikiloblastic grains up to 8 mm in maximum dimension, and contains inclusions of all the other minerals present in the rock; the most common inclusions are subidioblastic to idioblastic hornblende crystals up to 0.9 mm in length; the next most common inclusions are xenoblastic to subidioblastic grains of spinel, up to 0.8 mm in maximum dimension; these commonly have curved grain boundaries with orthopyroxene, but some have linear grain boundaries with inclusions of hornblende; the matrix comprises subidioblastic to idioblastic hornblende in crystals up to 6 mm long, xenoblastic olivine up to 4.5 mm in maximum dimension, lesser amounts of xenoblastic spinel up to 1 mm in maximum dimension, and minor amounts of chlorite in laths up to 1 mm long; the chlorite occurs in contact with all the other minerals in the rock, but is most common along grain boundaries between large grains of hornblende, spinel and olivine; the subparallel alignment of larger hornblende crystals in the matrix defines a weak foliation.
- 901: clinozoisite-hornblende-corundum granulite; over 70% of the volume of this rock is made up of subidioblastic to idioblastic grains of clinozoisite varying in length from 0.02 to 2 mm; hornblende occurs as porphyroblasts up to 6 mm in length; it is weakly pleochroic (colourless, light green, apple-green) and contains inclusions of clinozoisite in the same size range as in the matrix; minor amounts of corundum occur in subidioblastic grains up to 8 mm in length, and are relatively free of inclusions, trace amounts of margarite occur in laths up to 0.02 mm wide and 0.1 mm long; the margarite is found in cracks in clinozoisite and along some clinozoisite-corundum grain boundaries, and appears to be retrograde.
- 902: clinozoisite-anorthite-hornblende granulite; anorthite occurs as subidioblastic porphyroblasts up to 11 mm in length; these contain inclusions of rounded clinozoisite grains or grain aggregates up to 1 mm in maximum dimension, and subidioblastic hornblende up to 1.5 mm in length; the matrix comprises a granoblastic aggregate of largely polygonal clinozoisite grains ranging from 0.1 to 2 mm in maximum dimension; the matrix also contains minor amounts of hornblende in subidioblastic to xenoblastic grains up to 0.2 mm in maximum dimension.

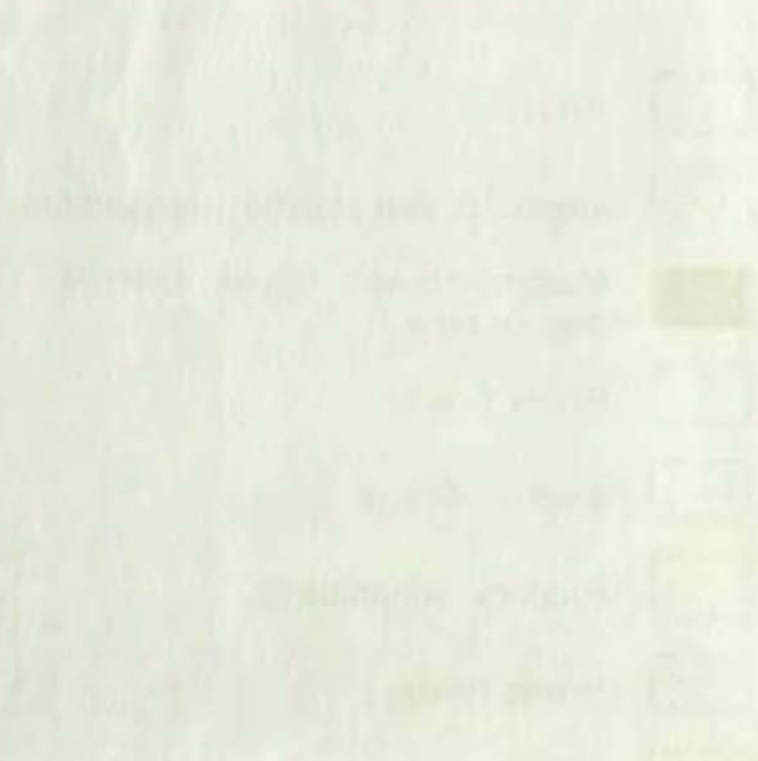
135°E

To
Alice
Springs



Geological Map of the
Valley Bore Area
(Hocking and Co.)

This map shows the geological structure of the Valley Bore area, including the Hocking River and the surrounding hills. The map is based on the work of the Hocking and Co. and is intended to show the general geological features of the area.



The map is a geological map of the Valley Bore area, showing the Hocking River and the surrounding hills. The map is based on the work of the Hocking and Co. and is intended to show the general geological features of the area.

MACQUARIE
UNIVERSITY
LIBRARY

Thesis

QE

475

.A2

.J6

and

Geological Map of the JERVOIS RANGE AREA.

BASED ON MAPPING BY GOLDFIELDS CONSOLIDATED, CENTRAL PACIFIC MINERALS
AND THIS WORK FOR LOCATION MAP - SEE FIG. 1

SAMPLE NUMBERS REFER TO ROCKS DISCUSSED IN THE TEXT.

